



## **Evolving the Landscape of Polymer Laser Powder Bed Fusion** Expanding Frontiers in Process and Materials

**Budden, Christian Leslie**

*Publication date:*  
2023

*Document Version*  
Publisher's PDF, also known as Version of record

[Link back to DTU Orbit](#)

*Citation (APA):*  
Budden, C. L. (2023). *Evolving the Landscape of Polymer Laser Powder Bed Fusion: Expanding Frontiers in Process and Materials*. Technical University of Denmark.

---

### **General rights**

Copyright and moral rights for the publications made accessible in the public portal are retained by the authors and/or other copyright owners and it is a condition of accessing publications that users recognise and abide by the legal requirements associated with these rights.

- Users may download and print one copy of any publication from the public portal for the purpose of private study or research.
- You may not further distribute the material or use it for any profit-making activity or commercial gain
- You may freely distribute the URL identifying the publication in the public portal

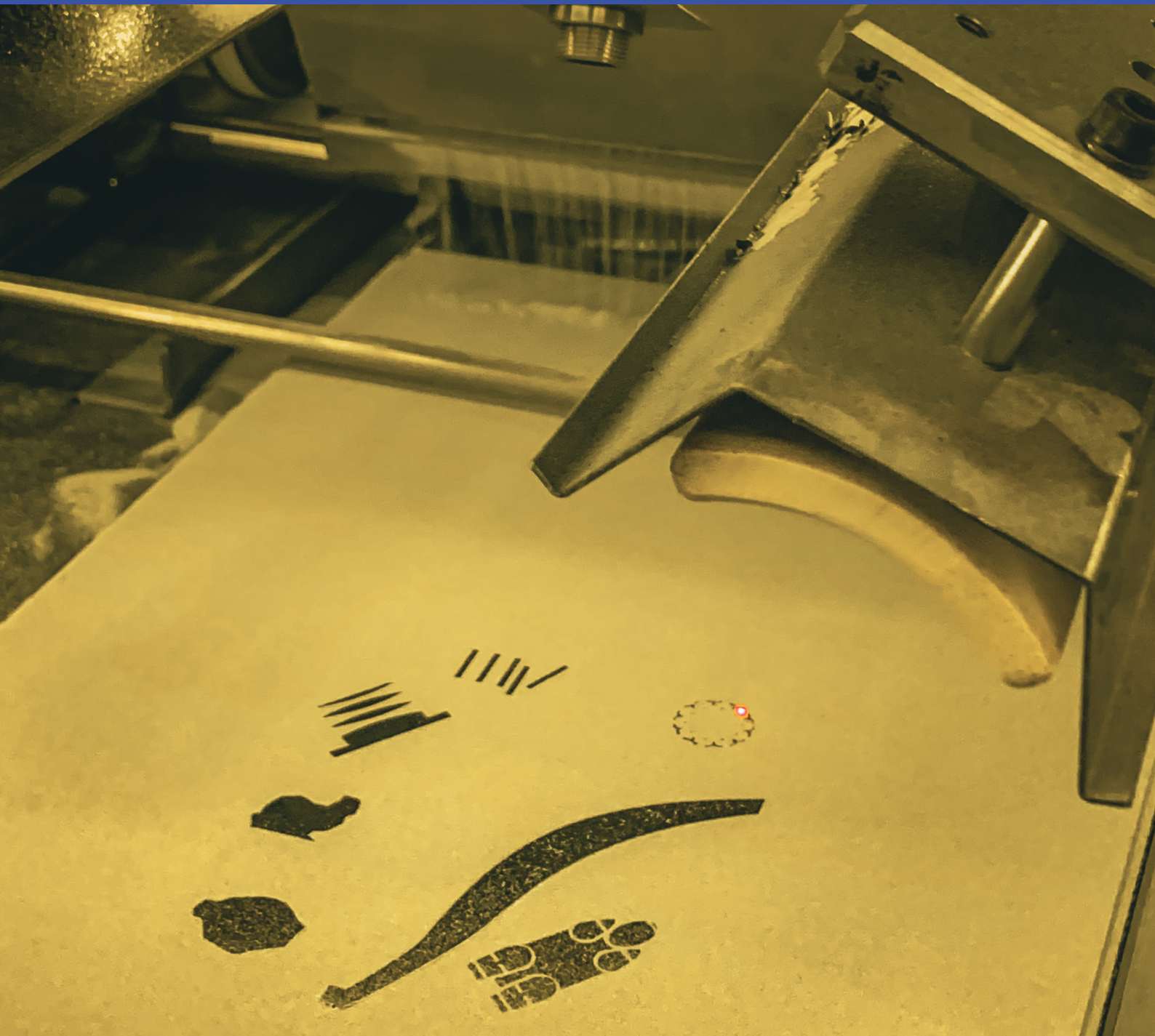
If you believe that this document breaches copyright please contact us providing details, and we will remove access to the work immediately and investigate your claim.



# Evolving the Landscape of Polymer Laser Powder Bed Fusion

Expanding Frontiers in Process and Materials

Christian Leslie Budden





## **Evolving the Landscape of Polymer Laser Powder Bed Fusion**

Expanding Frontiers in Process and Materials

PhD Thesis

August, 2023

By

Christian Leslie Budden

Supervised by

David Bue Pedersen, Senior Researcher, Department of Civil and Mechanical Engineering,  
Manufacturing Engineering, Head of Additive Manufacturing

Anders Egede Daugaard, Associate Professor, Department of Chemical and Biochemical  
Engineering, The Danish Polymer Centre

Copyright:       Reproduction of this publication in whole or in part must include the cus-  
tomary bibliographic citation, including author attribution, thesis title, etc.

Cover photo:     Christian Leslie Budden, 2023

Published by:    DTU Civil and Mechanical Engineering  
Section of Manufacturing  
Koppels allé 404  
2800 Kongens Lyngby  
Denmark  
[www.construct.dtu.dk](http://www.construct.dtu.dk)

ISBN:             [978-87-7475-762-7]



## Preface

The work presented in this PhD dissertation has been carried out to fulfil the requirements for obtaining the PhD degree. The work was conducted from May 2020 until August 2023. Throughout these three years, the research has been grounded within the Additive Manufacturing group at the Technical University of Denmark, under the Institute of Civil and Mechanical Engineering, Section of Manufacturing Engineering. Two external visits were completed during this period, one at the University of Louisville, Kentucky, under the supervision of Associate Professor Li Yang and the other at the University of Texas, Austin, under the guidance of Dr Tim Phillips.

Senior Researcher David Bue Pedersen and Associate Professor Anders Egede Daugaard have supervised the project and related work presented herein.

Christian Leslie Budden

A handwritten signature in blue ink, appearing to read 'C. Budden', written over a horizontal dotted line.

*Signature*

the 13<sup>th</sup> of August 2023

A horizontal dotted line used as a separator for the date.

*Date*



## Abstract

Laser Based Powder Bed Fusion of Polymers (PBF-LB/P) is one of the pioneering Additive Manufacturing (AM) processes, using a laser to selectively consolidate a powder feedstock into three-dimensional (3D) components. The technique functions by depositing a thin layer of powder in the build plane of the system, laser scanning the cross-sectional area of the geometry, and repeating this cycle in a layer-by-layer fashion to fabricate a component. This allows the production of complex geometries unattainable by conventional processing while inheriting mechanical properties resembling those of traditional plastic fabrication.

Conventional PBF-LB/P systems utilise a CO<sub>2</sub> laser to consolidate the powder. This study aims to investigate the utility of a fibre laser source for processing polymer powders. The functionality of the fibre laser in the process was extensively studied through three primary investigations. The first study focuses on developing the relevant process knowledge and understanding of laser processing of polymer powders, describing the critical influential factors for developing an experiment capable of defining the fibre laser utility. The second investigation relates the critical elements of the first study, delivering an experimental infrastructure designed for testing the main hypothesis. The third and final exploration establish the functionality of the fibre laser in the process, utilising the laser source in the experimental infrastructure for producing components, which were scrutinised concerning the success of the production.

To investigate the fibre laser utility in the process, an open architecture system is constructed. The open architecture allows access to all relevant process settings and parameters. This is achieved by utilisation of the tools developed throughout the Open Additive Manufacturing Initiative, presenting the open architecture for several industrially relevant AM processes.

The main driver and hindrance for fibre laser processing of polymers is the wavelength of 1080 nm, delivered by the laser. This wavelength does not match the agitation frequency of the polymer constituent elements or compounds, leading to low energy absorption by the polymer. The wavelength, however, allows for the small spot size and considerable Rayleigh length of the laser.

A metric for the requirement of an optical absorber was examined and quantified by fibre laser processing polymer powder, utilising the experimental infrastructure. The study investigated the use of two different coloured powders of the same type of PA11 polymer, where one is the pure white type, and the other contains the optical absorption quality by being coloured black. A minimum concentration of 5% black powder in a mix of white and black is sufficient for producing high-fidelity components.

From the exploration of the utility of fibre lasers in PBF-LB/P, it is concluded that the laser source can deliver satisfactory detail resolution, comparable to what is found in the industry. The fibre laser aid the utilisation by providing key parameters not offered by the conventional CO<sub>2</sub> laser source. These are the ease of beam delivery, high beam quality, and considerable Rayleigh length, enabling the fine details achieved herein.





## Dansk Resumé

Laser Powder Bed Fusion af plastpulver er en af de originale additive fremstillingsmetoder, der bruger laser til at konsolidere pulver til et tre-dimensionelt (3D) emne. Emnet bygges lag for lag ved at udlægge et tyndt lag pulver, der efterfølgende scannes af laseren. Ved at scanne hele tværsnittet af emnet omdannes plastpulveret til et massivt emne. Processen kan fremstille komplekse geometrier, der ikke er mulige ved konventionelle fremstillingsmetoder. Ofte bruger denne proces en CO<sub>2</sub> laser til konsolidering af pulveret.

Studiet præsenteret her omhandler brugen af en fiberlaser til pulverkonsolidering. Med udgangspunkt i tre projektfaser er fiberlaseren undersøgt med henblik på at afdække anvendelsesgraden. Den indledende fase beskriver den additive fremstillingsproces med fokus på en holistisk forståelse af processen. Fase to bruger denne holistiske forståelsesramme til at udvikle et eksperiment til at belyse hovedhypotesen. Det eksperimentelle forsøg er opbygget efter en systemisk forståelsesramme. Den tredje og sidste fase af projektet gransker brugen af fiberlaseren til at konsolidere plastpulveret i det udviklede system.

Fiberlaserprocesseringen af plastpulveret er udført i et system baseret på en åben arkitektur tankegang. Systemet er udviklet med henblik på at muliggøre indstilling af alle relevante procesparametre. Ved at have fuld adgang til alle procesparametre kan processen indstilles specifikt til et bestemt materiale. Den åbne arkitektur præsenterer muligheder indenfor forskning i brugen af andre laserkilder og procesindstillinger, som ikke er fundet ved industrielle systemer. Disse procesmuligheder tilbyder ydermere en åben materialeudviklingstilgang, da systemet ikke er låst til en type eller leverandør, men i stedet har fri mulighed for forarbejdning af alle slags termoplast, der er relevante for processen.

Fiberlaseren er kendetegnet ved en bølglængde på 1080 nm. Polymerer har ikke en agitationsfrekvens, der matcher denne bølglængde, hvilket minimerer evnen til at absorbere energi fra laseren. Fordelen ved en kort bølglængde er dog, at laseren tilbyder fokuspunktsstørrelser, der er betydeligt mindre end den konventionelle CO<sub>2</sub> laser. Derudover er Rayleigh længden signifikant længere grundet bølglængden.

Absorption af fiberlaserens bølglængde er påvist gennem sammenblanding af et hvidt og et sort PA11 pulver. Studiet afdækker forskellige blandingsforhold for at afdække, hvor stor en mængde sort pulver der kræves for at opnå den ønskede effekt. Resultatet af studiet påviser brugen af et farvet pulver bestående af en hvid PA11 blandet med en sort. Det er observeret, at 5% sort pulver i blandingen udgør en tilstrækkelig mængde for laserabsorption. Dette blandingsforhold muliggør produktionen af mekanisk og geometrisk robuste emner fra det eksperimentelle system. Baseret på denne observation er en metrik for brugen af absorberingsmidler præsenteret.

Konklusionen peger på, at fiberlaserprocessering af plastpulver er muligt, og at emner fremstillet ved denne metode er sammenlignelige med emner produceret af industrielle systemer.



## Acknowledgements

First and foremost, I want to express my deepest gratitude to the love of my life. Thank you for being there every step of the way, for helping me become the person I am today, and for the unwavering support that has enabled me to accomplish what I have. You are my rock, providing love, stability, understanding, and patience. Your constant care, even in the face of my forgetfulness, has kept me grounded and maintained the perfect home we share. I am forever grateful to you, Nanna, for raising our incredible boys, Calvin and Elliot, and for being the pillar of our family. Thank you.

While the journey of a PhD is often seen as solitary, in which the candidate must find answers to the relevant questions of the field, the work contributing to a doctoral thesis can never come about by the author's hand alone. Without the indispensable assistance, sparring, and backing from several sources, this project would never have succeeded in any form of the word. This work has relied on a number of resources for research contributions in the laboratory as well as for provoking and challenging the ideas and resolutions of the author to attain the outcome presented herein.

I want to express my heartfelt gratitude to my primary Supervisor, Senior Researcher David Bue Pedersen, for continually challenging my thoughts and ideas and for enhancing and developing them further. Your assistance extends beyond the formal project supervision, as our numerous talks and chats about life and its intricacies have profoundly influenced my perspective. I am ever grateful for the support you have provided, both professionally and personally.

Secondly, I would like to express my deepest gratitude to my secondary supervisor, Associate Professor Anders Egede Daugaard. Your expansive expertise has not only elevated the quality of the work but has also greatly enhanced my skills as a researcher.

The openness and embrace of the AM group is a mindset I have never found before. To all my incredible colleagues, enormous gratitude is felt. You everyday provoke me to be a better version of myself by always being available for sparring and support. Knowing that there is always room for gaining a new perspective is an incredible experience that I will always hold dear. Thank you to all AM group members, especially Alberto, Ania, Frederik, Macarena, Sebastian, and Venkata. A special thank you goes towards Magnus; I am ever grateful for the countless discussions and for keeping me sane during our thesis writing journey. The same goes for Aakil, who has been a constant aid in challenging my process knowledge, enhancing my position as a researcher, and providing an extraordinary amount of work going into this project.

Lastly, I would like to extend my sincerest gratitude to my friends & family for helping me reach this pivotal point in my education and career.

To quote my sons:

*"Vi GJORDE DET Mormor!"* - (Calvin Leslie Hebo Budden. 3 år)

*"Far hamrer, Far skruer"* - (Elliot Leslie Hebo Budden. 2 år)

*"We DID IT, Grandma!"* - (Calvin Leslie Hebo Budden. 3 years old)

*"Dad hammering, Dad fixing"* - (Elliot Leslie Hebo Budden. 2 years old)



# Scientific Contributions

## Published Papers

Throughout the three-year PhD study, several publications have been authored or co-authored. The list below shows the extent of publications by the author during the project period and is ordered by publication date.

1. Budden, C. L., Meinert, K. Æ., Lalwani, A. R. & Pedersen, D. B. Chamber Heat Calibration by Emissivity Measurements in an Open Source SLS system in ASPE and euspen Summer Topical Meeting Volume 77 77 (Knoxville, 2022), 180-185.
2. Danielak, A., Basso, A., Budden, C., Weiss, K., López, J., Anand, G., Artemeva, M. & Pedersen, D. Enhanced Build Plate Design For Vat Photopolymerization Additive Manufacturing in 2022 ASPE and euspen Summer Topical Meeting on Advancing Precision in Additive Manufacturing (Knoxville, 2022).
3. Meinert, K., Budden, C., Lalwani, A., Kleijnen, R. & Pedersen, D. In-situ optical sensor integration in an open source L-PBF system, for correlating laser power to melt pool radiation in 2022 ASPE and euspen Summer Topical Meeting on Advancing Precision in Additive Manufacturing (Knoxville, 2022). ISBN: 9781713859192.
4. Budden, C. L., Lalwani, A. R., Meinert, K. Æ., Daugaard, A. E. & Pedersen, D. B. Process optimisation of PA11 in fiber-laser powder-bed fusion through loading of an optical absorber eng. in Proceedings of the 33rd Annual International Solid Freeform Fabrication (sff) Symposium (The University of Texas at Austin, Austin, 2022), 75-86.
5. Budden, C. L., Grønborg, F., Wolstrup, A. F., Lalwani, A. R., Zsurzsan, T. G., Daugaard, A. E. & Pedersen, D. B. Simple sensor manufacturing by Laser Powder Bed Fusion of conductive polymer blends in euspen's 23rd International Conference & Exhibition, Copenhagen, DK, June 2023 (Copenhagen, 2023).
6. Vuković, M., Budden, C. L., Calaon, M., Mazzei, D., Pedersen, D. B. & Fantoni, G. External temperature and power consumption monitoring in an Open Architecture Polymer Laser Powder Bed Fusion in Special Interest Group Meeting: Advancing Precision in Additive Manufacturing, September 2023 (Leuven, 2023).
7. Kjer, M. B., Budden, C. L., Nadimpalli, V. K. & Pedersen, D. B. Preliminary geometric tests of an open-source metal laser powder bed fusion system in Special Interest Group Meeting: Advancing Precision in Additive Manufacturing, September 2023 (Leuven, 2023).

8. Budden, C. L., Kjer, M. B., Lalwani, A. R., Nadimpalli, V. K. & Pedersen, D. B. Benchmarking of an Open Architecture Polymer Laser Powder Bed Fusion system in Special Interest Group Meeting: Advancing Precision in Additive Manufacturing, September 2023 (Leuven, 2023).

### **Papers Submitted, Under Review**

9. Kjer, M. B., Andersen, S. A., Budden, C. L., Karthik, V. N. & Pedersen, D. B. Applying Systems Engineering Principles to Develop an Open Source Laser-Based Metal Powder Bed Fusion System. Additive Manufacturing (2023).

# Contents

Preface . . . . .	iii
Abstract . . . . .	v
Dansk Resumé . . . . .	vii
Acknowledgements . . . . .	ix
Scientific Contributions . . . . .	xi
Acronyms . . . . .	xxiv
Glossary . . . . .	xxv
Thesis Structure . . . . .	xxvi
<b>1 Introduction</b>	<b>1</b>
1.1 Main Hypothesis . . . . .	2
1.2 Additive Manufacturing . . . . .	3
1.3 Open Additive Manufacturing . . . . .	7
1.4 Research Relevance . . . . .	8
1.5 Chapter Summary . . . . .	12
<b>2 Powder Bed Fusion</b>	<b>15</b>
2.1 Laser Powder Bed Fusion . . . . .	17
2.2 Materials in Laser Powder Bed Fusion . . . . .	18
2.3 Chapter Summary . . . . .	27
<b>3 State of the Industry</b>	<b>29</b>
3.1 Industrial Systems . . . . .	30
3.2 Chapter Summary . . . . .	37
<b>4 State of Research in Polymer Laser Powder Bed Fusion</b>	<b>39</b>
4.1 State of Polymer Powder Processing by Laser Irradiation . . . . .	40
4.2 State of Polymer LPBF Systems . . . . .	63
4.3 Chapter Summary . . . . .	82
<b>5 The Experimental Infrastructure</b>	<b>85</b>
5.1 Holistic System Overview . . . . .	86
5.2 Repurposing an Industrial System . . . . .	89
5.3 System Breakdown and Analysis for Repurposing . . . . .	90

5.4	System Upgrades for the Polymer LPBF Process . . . . .	98
5.5	Finalised System for Fibre Laser Polymer Processing . . . . .	127
5.6	Chapter Summary . . . . .	129
<b>6</b>	<b>Validation of the Experimental Infrastructure</b>	<b>133</b>
6.1	Heater Validation . . . . .	134
6.2	Laser validation . . . . .	148
6.3	Motion Control . . . . .	159
6.4	Build sequence execution . . . . .	166
6.5	Chapter Summary . . . . .	172
<b>7</b>	<b>Fibre Laser Utility in Polymer Powder Processing</b>	<b>175</b>
7.1	Fibre laser absorption in polymers - A recap . . . . .	176
7.2	Optical Absorbers in Polymer Fibre Laser Processing . . . . .	177
7.3	Benchmark Testing at the Optimal Level of Black . . . . .	194
7.4	Conductive Polymer Part Production by Fibre Laser . . . . .	201
7.5	System Material Processing Capabilities . . . . .	204
7.6	Chapter Summary . . . . .	211
<b>8</b>	<b>Conclusion &amp; Perspectives</b>	<b>215</b>
	<b>Bibliography</b>	<b>223</b>
	<b>Appendices</b>	<b>245</b>
<b>A</b>	<b>Technical drawings of the heaters installed in the developed system</b>	<b>247</b>
<b>B</b>	<b>Chamber Heat Calibration by Emissivity Measurements in an Open Source SLS System</b>	<b>249</b>
<b>C</b>	<b>PA11 - White BASF Ultrasint (TDS)</b>	<b>257</b>
<b>D</b>	<b>PA11 - Black BASF Ultrasint (TDS)</b>	<b>261</b>
<b>E</b>	<b>Process optimisation of PA11 in fiber-laser powder-bed fusion through loading of an optical absorber</b>	<b>265</b>
<b>F</b>	<b>Benchmarking of an Open Architecture Polymer Laser Powder Bed Fusion system</b>	<b>279</b>
<b>G</b>	<b>Simple sensor manufacturing by Laser Powder Bed Fusion of conductive polymer blends</b>	<b>283</b>



# List of Figures

1.1	Main process categories in AM . . . . .	3
1.2	Market shares of the major material categories . . . . .	6
1.3	Cost breakdown for three main categories of Polymer AM. From [25] . . . . .	7
1.4	The Open Additive Manufacturing logo . . . . .	8
1.5	Web Of Science organised articles . . . . .	9
1.6	Overview of the Web Of Science categories . . . . .	10
2.1	Powder Bed Fusion processes . . . . .	16
2.2	Additive Manufacturing process . . . . .	17
2.3	Amorphous and semi-crystalline polymer structures . . . . .	19
2.4	The specific volume vs temperature curve . . . . .	19
2.5	Repeat unit for the polymers PA11 and PA12 . . . . .	20
2.6	3D printed glasses . . . . .	21
2.7	PBF-LB/M process steps . . . . .	23
2.8	Ceramic PBF parts . . . . .	25
2.9	Composite PBF parts . . . . .	26
2.10	Types of powder composites . . . . .	27
3.1	AM systems sales growth . . . . .	29
3.2	Market analysis results . . . . .	32
4.1	DSC analysis (process window) . . . . .	40
4.2	Powder morphology . . . . .	45
4.3	Additive coverage for spherical dry coated polymer particles . . . . .	48
4.4	Processing characteristics . . . . .	49
4.5	Laser-powder: Absorption, reflection and transmission . . . . .	50
4.6	Laser-powder: Processing . . . . .	51
4.7	Oscillation modes of polymer molecules . . . . .	52
4.8	FTIR analysis of pure PA11 (a) and several other grades. From [126] . . . . .	53
4.9	Particle scan duration . . . . .	53

4.10	The laser-powder interaction . . . . .	58
4.11	Stages of Solid State Sintering . . . . .	60
4.12	PBF-LB/P processing failure . . . . .	61
4.13	Full melting behaviour . . . . .	62
4.14	Additive Manufacturing process (Reprint) . . . . .	63
4.15	PBF-LB/P system description . . . . .	64
4.16	Recoater types for PBF-LB/P . . . . .	66
4.17	Powder short feed . . . . .	69
4.18	Overflow location - one-way recoating . . . . .	70
4.19	Overflow location - two-way recoating . . . . .	70
4.20	Heating cycle of the PBF-LB/P process . . . . .	72
4.21	Quartz lamp top heater array . . . . .	73
4.22	Simple principle drawing of the function of a laser . . . . .	74
4.23	Components in a galvanometer scanner . . . . .	76
4.24	Major subsystems of PBF-LB/P . . . . .	77
4.25	Fibre laser delivery types . . . . .	78
4.26	Laser production in a doped fibre . . . . .	79
4.27	The light spectrum . . . . .	80
5.1	System diagram - Top level . . . . .	86
5.2	Definitions relevant for the system development . . . . .	87
5.3	Original system . . . . .	89
5.4	Original heating system . . . . .	92
5.5	Binder jetting machine powder feed . . . . .	92
5.6	Powder agitators for internal powder movement . . . . .	93
5.7	Dosing valve system . . . . .	93
5.8	CMY manufacturing process steps . . . . .	94
5.9	vertical-stage main components . . . . .	95
5.10	Low complexity overview of the developed system . . . . .	97
5.11	The two interfaces of the controller software . . . . .	99
5.12	Slice of a job file with multiple components in the same job . . . . .	99
5.13	Process parameters and signatures - mechanical . . . . .	100
5.14	Motion control diagram . . . . .	102
5.15	Controller system diagram . . . . .	103
5.16	Process parameters and signatures - laser source . . . . .	104
5.17	Laser from Maxphotonics installed in the system . . . . .	106

5.18	Process parameters and signatures - laser delivery . . . . .	107
5.19	Laser delivery system . . . . .	109
5.20	Laser system diagram . . . . .	110
5.21	Process parameters and signatures - heating system . . . . .	111
5.22	Heater specification. Full technical drawing found in Appendix A . . . . .	112
5.23	Heater selection guide. Adapted from: [218] . . . . .	113
5.24	Contact heating system . . . . .	114
5.25	Top heater system . . . . .	116
5.26	The heater system diagram . . . . .	117
5.27	Process parameters and signatures - recoater . . . . .	118
5.28	Recoater components and assembly . . . . .	120
5.29	Powder fluidisation . . . . .	121
5.30	Recoating system diagram . . . . .	121
5.31	Thermal camera pointed towards the build plane . . . . .	123
5.32	Thermal camera installation in the developed system . . . . .	124
5.33	Software for the thermal camera . . . . .	124
5.34	Thermal imaging system diagram . . . . .	125
5.35	IIoT dashboard . . . . .	126
5.36	IIoT system diagram . . . . .	126
5.37	Final system developed . . . . .	127
5.38	Machine comparison . . . . .	129
5.39	System diagram for the entire machine/system (part: one) . . . . .	130
5.40	System diagram for the entire machine/system (part: two) . . . . .	131
6.1	The sensor array for the K-type thermocouples . . . . .	135
6.2	Powder cake sensor integration . . . . .	136
6.3	Temperature deviation . . . . .	137
6.4	Heating curves for the process temperature definition . . . . .	138
6.5	Average temperature recorded . . . . .	139
6.6	Temperature stable processing region (The build envelope) . . . . .	140
6.7	Unadjusted heaters producing an uneven energy distribution . . . . .	141
6.8	Top heater calibration . . . . .	142
6.9	Calibrated top heaters . . . . .	143
6.10	DSC curve for safe removal temperature identification . . . . .	145
6.11	Powder cake cooling curve . . . . .	146
6.12	Laser power measurement results . . . . .	149

6.13	Laser power distribution along the build plane . . . . .	151
6.14	Laser focus identification . . . . .	153
6.15	HAZ width calibration . . . . .	154
6.16	Scan speed measuring device . . . . .	155
6.17	Measured scan speed . . . . .	156
6.18	vertical-stage measurement setup . . . . .	160
6.19	vertical-stage deviation from intended layer height . . . . .	161
6.20	Recoater speed validation . . . . .	163
6.21	Build plane quality . . . . .	164
6.22	Build Plane quality of coarse and uneven-sized powder . . . . .	165
6.23	Recoating routine in three steps . . . . .	166
6.24	PBF-LB/P Build cycle . . . . .	167
6.25	Barbell geometry . . . . .	168
6.26	PA11 White DSC curve . . . . .	169
6.27	Build Job Laser Active . . . . .	170
6.28	White parts manufactured . . . . .	170
7.1	DSC analysis of the black PA11 powder . . . . .	178
7.2	PA11 Morphologies . . . . .	180
7.3	Iterative approach for the process optimisation . . . . .	181
7.4	Tensile test exemplification . . . . .	182
7.5	Engineering Stress and strain results . . . . .	183
7.6	Surface topography comparison . . . . .	184
7.7	Surface topography, for varying mixing ratios . . . . .	185
7.8	Exemplification of the hatch rotation . . . . .	185
7.9	Partial melting behaviour (DSC) . . . . .	186
7.10	Test geometry produced . . . . .	187
7.11	Mechanical properties of the tested power levels . . . . .	189
7.12	Final results of mechanical testing . . . . .	190
7.13	95-5 part cross-section . . . . .	190
7.14	Viscoelastic behaviour of PA11 powders . . . . .	192
7.15	Viscoelastic response to temperature change PA11 . . . . .	193
7.16	Benchmark reference features . . . . .	194
7.17	Manufactured benchmark geometry . . . . .	195
7.18	CMM measurements of the benchmark . . . . .	196
7.19	PBF-LB/P Design rules (HUBS) . . . . .	198

7.20	CMM measurements of the benchmark (industrial production)	199
7.21	Comparison of benchmark parts	200
7.22	Coarse powder grain (also in Figure 6.22b)	201
7.23	SEM image of a conductive polymer network	202
7.24	SEM image of a crack in the network	203
7.25	Temperature cycle during processing	206
7.26	Powder morphology and size distribution	207
7.27	Build chamber relative humidity	209
7.28	Shear dependant viscosity	210
7.29	Shear dependant moduli	211

# List of Tables

1.1	Search terms used in the Web of Science study . . . . .	9
2.1	Commercially available powder products . . . . .	18
2.2	Comparison of datasheet values of EOS PA12 . . . . .	21
3.1	List of industrial system manufacturers . . . . .	33
3.2	List of desktop system manufacturers . . . . .	36
4.1	Process critical temperatures . . . . .	41
4.2	List of available polymer powders . . . . .	43
4.3	PBF-LB/P influential parameters . . . . .	59
4.4	Influential parameters for recoating . . . . .	68
5.1	Features of an PBF-LB/P System . . . . .	88
5.2	machine specification(original) . . . . .	90
5.3	Projet 4500 sub-system overview and the required action . . . . .	90
5.4	Mechanical motion elements . . . . .	101
5.5	Laser source selection - critical elements . . . . .	105
5.6	Laser delivery critical elements . . . . .	108
5.7	Heater critical elements . . . . .	111
5.8	Critical aspects and elements for the recoater system . . . . .	118
5.9	Critical aspects for designing the thermal imaging system . . . . .	123
6.1	Temperature deviation for each gradient map . . . . .	143
6.2	Powder cake heater guide . . . . .	148
6.3	Powder cake cooling guide . . . . .	148
6.4	Laser power delivery metrics . . . . .	152
6.5	Spot size measurements . . . . .	154
6.6	Scanning speed metrics . . . . .	157
6.7	Factors influencing the size of a manufactured part . . . . .	158
6.8	Factors influencing the geometric size of a part . . . . .	161
6.9	Recoater traverse and roller rotational velocity metrics . . . . .	164

6.10	Job file settings for the build sequence verification . . . . .	169
6.11	List of build sequences verified in the test . . . . .	171
7.1	Powder mixing ratios . . . . .	178
7.2	DSC analysis results . . . . .	179
7.3	Powder specification and sizing . . . . .	179
7.4	Process parameters for the batches of the material tested . . . . .	181
7.5	Process parameters for finding the breakdown level . . . . .	188
7.6	True power settings tested . . . . .	189
7.7	Process parameters for finding the breakdown level . . . . .	191
7.8	Benchmark shrinkage factor . . . . .	195
7.9	Stable geometrical feature sizes . . . . .	197
7.10	Critical pre-processing knowledge . . . . .	205

# Acronyms

**2.5D** Two-and-a-Half Dimensional.

**3D** three dimensional.

**AM** Additive Manufacturing.

**CAD** Computer Aided Design.

**CB** Carbon Black.

**CMM** Coordinate-Measuring Machine.

**CW** Continuous Wave.

**DED** Direct Energy Deposition.

**DSC** Differential Scanning Calorimetry.

**DTU** Technical University of Denmark.

**FDM** Fused Deposition Modelling.

**FDR** Fine Detail Resolution.

**FFF** Fused Filament Fabrication.

**fff** Filament freeform fabrication.

**FTIR** Fourier Transform Infrared.

**HAZ** Heat Affected Zone.

**HD-PE** high-density polyethylene.

**IIoT** Industrial Internet of Things.

**IP** Intellectual property.

**ITO** Indium Tin Oxide.

**LASER** Light Amplification by Stimulated Emission of Radiation.

**LOM** Light Optical Microscopy.



**LPBF** Laser Powder Bed Fusion.

**LPD** Laser Polymer Deposition.

**LVER** Linear Viscoelastic Region.

**MEX** Material Extrusion.

**MFI** Melt Flow Index.

**MFR** Melt Flow Ratio.

**MJF** Multi Jet Fusion.

**PA** Polyamide.

**PA11** Polyamide 11.

**PA12** Polyamide 12.

**PA6** Polyamide 6.

**PBF** Powder Bed Fusion.

**PBF-LB/M** Laser Based Powder Bed Fusion of Metals.

**PBF-LB/P** Laser Based Powder Bed Fusion of Polymers.

**PE** Polyethylene.

**PIF** Industrial process interface.

**POM** Polyoxymethylene.

**PP** Polypropylene.

**PS** Polystyrene.

**R&D** Research and Development.

**SEM** Scanning Electron Microscope.

**SLA** Stereolithography.

**SLS** Selective Laser Sintering.

**STL** Stereolithography.

**TPE** Thermoplastic Elastomers.

**TPU** Thermoplastic Urethane.

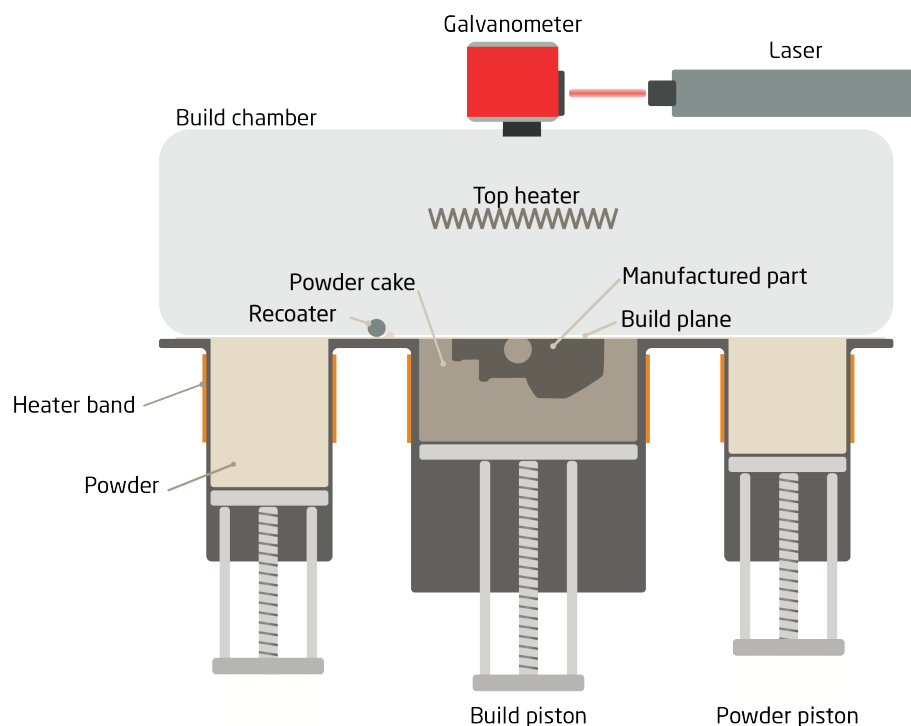
**VPP** Vat Photopolymerization.

**Yb** Ytterbium.

# Glossary

Below is a list of relevant terms for defining certain areas, system components or sub-systems of a Laser Powder Bed Fusion System. Each is found in the illustration at the bottom of the page.

Build chamber	Volume encapsulating the build plane, powder feeders, and top heaters (grey area)
Build plane	Area in which the laser irradiates the powder producing the geometry
Build piston	Chamber where the powder cake moves into during manufacturing
Galvanometer	Directs the laser in the XY plane of the build plane
Heater band	Heaters surrounding the build and powder pistons for maintaining temperature in the powder cake
Powder cake	Powder distributed in the build plane containing the manufactured part in the build piston
Powder piston	Chamber containing fresh powder for recoating
Recoater	Distributes fresh powder from the powder feeders onto the powder cake, producing the build plane
Top heater	Heater are located above the build plane, maintaining process temperature in the top layer powder
Hatch distance	Distance between two consecutive lines scanned for the inner part of a manufactured geometry



# Thesis Structure

The project is nested within a larger project funded by the Poul Due Jensen Foundation (Grant no. 2018-017), defining Open Architecture solutions for industrial additive manufacturing processes. The Open Additive Manufacturing Initiative has developed several industrially focused systems for disseminating these to a broader audience.

The thesis results from three years of work focussing on the Laser Powder Bed Fusion of Polymers process. A significant part of the thesis considers the powder bed fusion process and what happens when particles coalesce into solid objects. The methodology and theory behind powder consolidation, laser powder interaction and how to improve the results from a laser powder bed fusion of polymers process is presented within the first chapters. The work further presents the utilisation of a fibre laser in the process, developing a methodology for defining the process characteristics of this type of laser in polymer powder processing. To develop this, an open architecture platform for fibre laser processing is developed, relying on previous research within the project of Open Additive Manufacturing.

The thesis is divided into 7 main chapters and a final perspectivation, future work recommendation and conclusion.

*Chapter One* focuses on preparing the reader on the subject of additive manufacturing, with a dive into the use case of the Powder Bed Fusion process and the research discrepancy between polymers and other materials. The main hypothesis is presented here, explaining the relevance of the study.

*Chapter Two* describes the processing capabilities and workflow of Powder Bed Fusion. Here the variety of materials utilised in the process is defined. This definition aids the holistic process understanding used throughout the thesis.

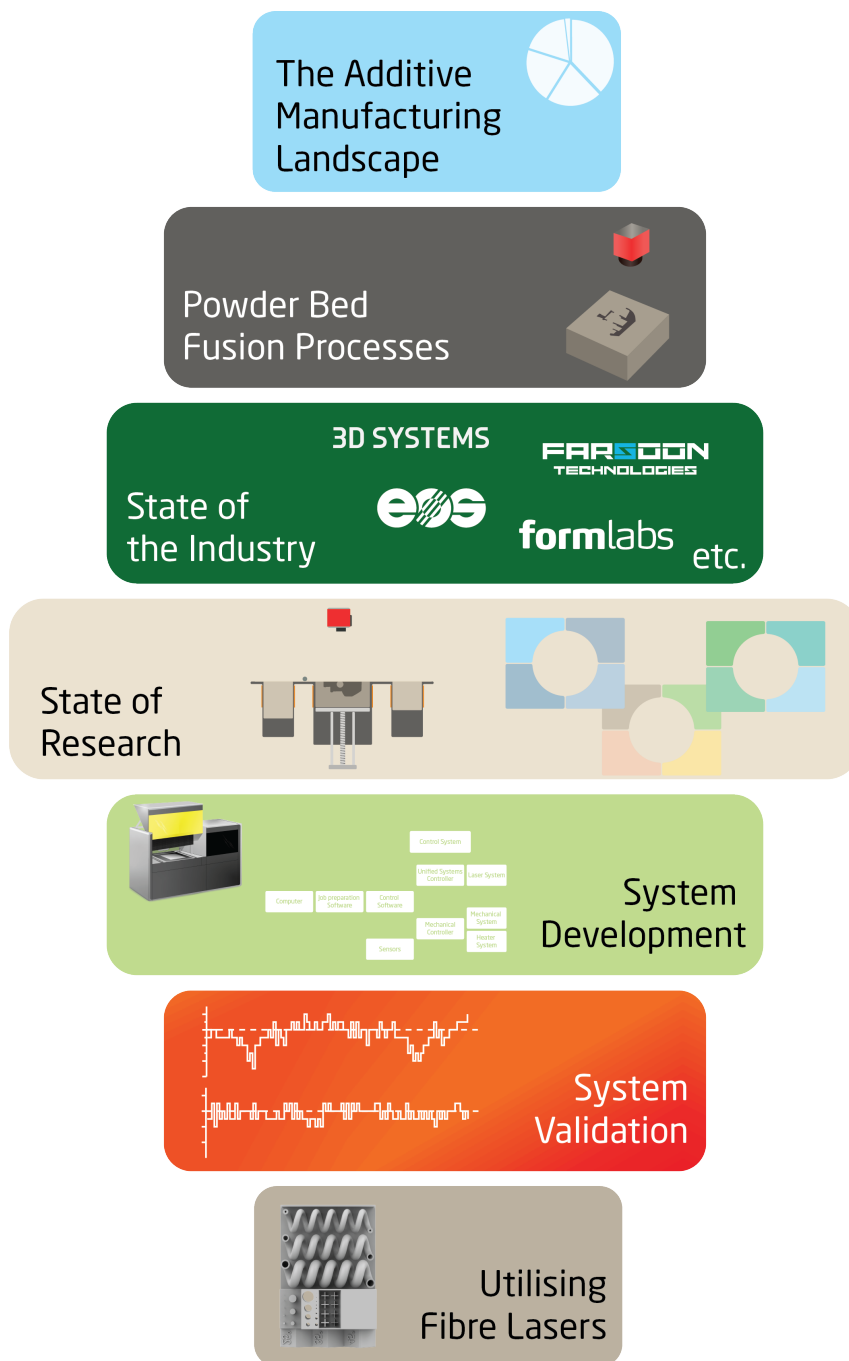
*Chapter Three* presents the state of the industry, providing a comprehensive overview of the industrial systems available for purchase within Laser Based Powder Bed Fusion of Polymers. A detailed description of the systems, including the consolidation source and processing capabilities, is provided on an individual machine level.

*Chapter Four* dives into the Laser Based Powder Bed Fusion of Polymers process. Here an in-depth analysis of the inherent material properties and the system capabilities are explored. A definition of the individual process parameters and signatures is developed concerning each individual sub-system, enabling a link to the systems development.

*Chapter Five* provide an overview of the system development based on the knowledge obtained throughout the study leading up to this point. A design guide of critical system elements and an elaboration for each of these are provided on a sub-system level, allowing in-depth process understanding.

*Chapter Six* directs the study towards the utilisation of fibre lasers in polymer powder processing, validating the critical metrics of the system. The chapter results in the overall process capability of the developed system, ensuring a stable environment for materials exploration.

*Chapter Seven* finally, introduce the fibre laser in powder processing, defining the requirements for processing polymer powder by the laser. A study of the optical absorber required for stable processing, including the functionality of the selected absorber system, is explained. Secondly, a materials investigation, focussing on conductive polymer parts, is presented, showcasing the capabilities of the system and fibre laser processing. The chapter concludes on the fibre laser and system utility, including an explanation of the polymer processing capabilities and downfalls of the developed system.





# CHAPTER 1

## Introduction

The family of Additive Manufacturing (AM) processes are not new, considering the fact that the initial patents were applied for during the 1980s. The original processes described in these patents are what is now known as Stereolithography (SLA), with its original patent filed in 1984 [1] and Selective Laser Sintering (SLS) with the patent filed in 1987 [2]. An innovation lockdown caused by these patents and the surge of patents that followed has caused a slow development of many of these additive manufacturing processes. This changed when the majority of patents expired in the middle of the 2010s. This led to the rapid development of AM systems, from limited industrial use to full-scale production capability. Today large companies rely on AM to produce parts or improve the productivity of their already developed products. Laser Based Powder Bed Fusion of Polymers (PBF-LB/P) is commonly known by the tradename SLS from the company DTM. This process is commonly used in industry today. A major use of this process is the manufacturing of speciality items as well as jigs and fixtures, which permits faster and more accurate assembly of other goods. Despite the rapid growth within the industry, little research goes into the laser processing of polymer powders compared to other AM processes. This discrepancy is the major focus of this chapter, describing the relevance of re-igniting research activities within PBF-LB/P.

## 1.1 Main Hypothesis

Laser Based Powder Bed Fusion of Polymers has been established in the industry for several years as a method of rapid prototyping of functional parts but has recently moved into serial production. Because of this, a dive into improving and revising the technology is needed. This thesis aims to inspire new research into the area of PBF-LB/P by pushing the boundaries of what is done traditionally and employing new tactics in polymer processing. The work describes the effort of repurposing and transforming an AM system previously used for binder jetting into a functional PBF-LB/P system incorporating a high-power fibre laser and an open-source framework.

Materials processing by Light Amplification by Stimulated Emission of Radiation (LASER) is a process of generating energy delivery in the form of light from a laser source to a target material. The delivered energy can be utilised for delivering high-speed communication and information or for delivering high-intensity heat in a localised area for melting or evaporation of the target. Laser-delivered energy and the wavelength of the light depend on the medium in which the laser is generated. By selection of the gain medium of the laser, a choice of possible power range, beam profile, and process capability is determined. Fibre lasers generated in a solid-state doping medium can generate high energy levels at a range of wavelengths. A common doping medium is Ytterbium (Yb), often used in fibre lasers to produce a laser beam with a 1050-1090 nm wavelength [3]. This type of laser can deliver high powers in a close to perfect Gaussian distribution of the beam, making this laser type ideal for high-fidelity materials processing.

Laser processing of polymer powders has traditionally utilised a CO<sub>2</sub> laser for producing intricate features (Table 3.1) in the PBF-LB/P process. This study aims to evolve the landscape of PBF-LB/P processing by replacing the CO<sub>2</sub> laser with a fibre laser incorporating the inherent properties of the Gaussian beam profile and high-power capabilities in the process. This allows further development within the field, enhancing the knowledge of the process and permitting the research activities to catch up with similar technologies by developing an understanding of the fundamental reactions and kinetics of new laser introduction. The desire is to investigate the use of fibre lasers in the PBF-LB/P process by utilising the framework of Open Additive Manufacturing, developing a system capable of providing answers for the usefulness of the laser source and the introduction of new materials in the process.

A genuine polytechnical engineering approach is required to study the aspects of introducing a fibre laser in the PBF-LB/P process. The study does not only rely on the physical introduction of a new consolidation source within a Powder Bed Fusion system. Instead, it takes the focus of a holistic approach. The work, therefore, includes several aspects of engineering and scientific reporting. This reaches from an analysis of the basic principles



within the PBF-LB/P process to understanding a repurposed system. It further extends to the development of this system to comprehend the new consolidation source, the functional analysis of this consolidation source, and a discussion of the utility of the system in its entirety. By incorporating all the mentioned elements, a truly holistic approach to this problem is presented.

## 1.2 Additive Manufacturing

AM has gained considerable attention within the last ten years. The process family is broadly known as 3D printing (3-Dimensional printing) and has become widely available and earned its name from the imagination of manufacturing components and products, layer-by-layer. A common explanation of 3D printing is to imagine a conventional printer that delivers information from a computer to a piece of paper. The information inscribed on the paper is left in the two-dimensional world, making it comprehensible and sharable without a digital device to decipher it. The same is true for AM. AM utilises digital information to generate a physical object. The process often occurs layer-by-layer, producing a slice of the geometry one layer at a time. A conventional 2D printer could create a printed image that can be cut out and stacked sheet by sheet, producing the 3D object. A method utilising such a process exists and is known as sheet lamination. Here a sheet of mate-

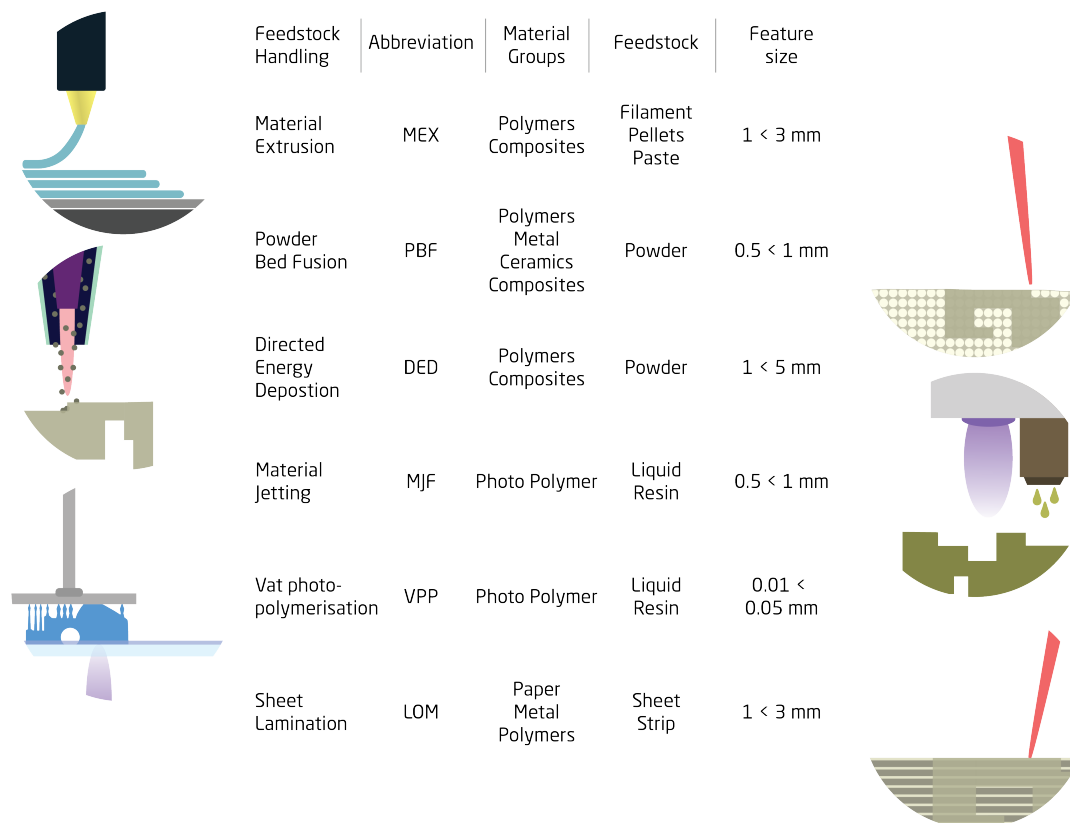


Figure 1.1: Main process categories in AM

rial is laminated onto a stack of previously laminated sheets. A cutter in the form of a laser or knife then traces the geometry perforating the boundary between the surrounding material and part. By repeating this process for the entire object, a component can be built up layer-by-layer. When finished, the whole block of laminated sheets is removed from the manufacturing system and unpacked, revealing the physical object encoded from the computer. Sheet lamination is one of the oldest techniques for AM and never gained much attention within research or industry. Still, it is a helpful case for explaining the layer-by-layer process, drawing parallels to relaying information on paper by everyday 2D printing.

The AM process contains several steps to process the raw material into the final desired shape or component. Below, each step in the process from computer designed model to physical component is exemplified.

The initial step after the design phase is to triangulate the geometry. By this, a surface mesh covering the entire geometry is produced, allowing the translation between the Computer Aided Design (CAD) software and the next step. The file type most often used when transferring this information from modelling software to the job file generator is an Stereolithography (STL) file.

The second step for AM of parts is to translate the triangulated mesh into a job file. For this, a job file generator is utilised. Here the level of detail is determined with respect to the selected manufacturing process. The file is loaded into the job file generator, which reads and translates the triangulated mesh into a list of commands designed for instructing the system in the manufacturing process. Depending on the system, these can be complex files encoded for a specific process and system. Or it can be a human-readable code format such as G-code. The programming language G-code [4] is often utilised, especially for cost-efficient systems. The encoded list of instructions contains all the relevant information in the job file. This includes the thickness of layers, which is a determining factor in the quality of the final part.

The third step considers the system executing the list of commands received from the slicing software. This is often done layer-by-layer producing the geometry.

Finally, the fourth step considers the post-processing of the components. This process is dependent on the selected processing system. It can include very little work by just removing a few support structures to a considerable effort and workload-heavy operations of surface definition and final geometrical tolerancing.

AM is governed by a group of ASTM and ISO standards. The principle is ISO 52900, which gathers the standards within AM ranging from ISO 52900 to ISO 52959. The range covers most aspects of the different processes within AM and provides a standard terminology for these processes (for example, the proprietary SLA technology name is correctly

abbreviated from vat photopolymerization to VPP). The range of processes is simplified into six main categories, as seen in Figure 1.1. The figure defines the common materials, the feedstock type and a reference frame for the typical feature and component size expected from the process. The illustrations exemplify the different processes, with most taken from one subcategory of the major process title. The figure is not comprehensive but provides an overview of the major classes and their properties. The figure is built upon the literature study. It is, therefore, a gathering of information from different works: [5–15]. All the different processes are to an extent similar but also very different. The information the figure presents is most commonly found in marketing material and literature, which is why some deviations are expected. Nevertheless, the figure produces an overview of the processes. To ensure a precise vocabulary, this work strives to follow the terminology as presented by *ISO/ASTM 52900:2021 - Additive manufacturing – General principles – Fundamentals and vocabulary* [16]. Here a standard methodology for abbreviating the long names and process descriptions utilised for these processes is explained. Another relevant international standard is the *ISO/ASTM 52911-2:2019 Additive manufacturing – Design – Part 2: Laser-based powder bed fusion of polymers* [17]. The standard describes the terminology specific for Laser Based Powder Bed Fusion of Polymers developing a reference frame for enhancing the communication of anything related to Laser Based Powder Bed Fusion of Polymers. One conflicting item between the two standards is the reference and naming convention utilised for powder bed fusion activities. A decision has therefore been made to follow the most recent naming convention presented in the ISO 52900 describing the vocabulary. The naming convention follows a rule of describing the major process (Powder Bed Fusion), the energy source utilised (Laser Based), and the material classification (Polymers) producing the abbreviation PBF-LB/P.

AM is often seen as the opposite of subtractive manufacturing. Where instead of removing material to fabricate the part from feedstock, the material is deposited in a by-layer fashion. One commonly known method is the Material Extrusion (MEX) process, referred to by many names such as; Fused Deposition Modelling (FDM), Filament freeform fabrication (fff), or Fused Filament Fabrication (FFF). The process is known for the promise of providing widespread manufacturing capabilities, making everyone capable of, for example, producing just the right spare parts for repairing close to anything, just when needed. Needless to say, this has not occurred yet, and some technical challenges are still evident before everyone's grandmother can harness the utility of the process. The material extrusion process produces components by depositing a strand of material, typically plastic, in the shape of a filament, layer-by-layer. The process utilises an extruder for heating the plastic filament above its melting point, making it malleable and sticky, ensuring adhesion between the layers. The extruder is then directed across the build plate in the horizontal plane, producing one layer before moving the desired component resolution in the vertical axis, repeating the process. The determining factor of resolution is the accuracy of the hor-

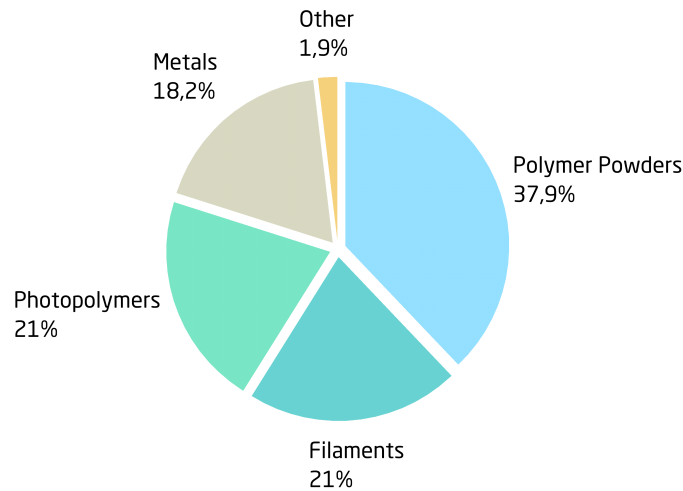


Figure 1.2: Market shares of the major material categories. Data source: The 2023 Wohlers report [19]

horizontal motion, as well as the size of the vertical movement [18]. By increasing the vertical movement, a significant increase in productivity can be gained, with the result of losing resolution and quality perceived as smooth surfaces resembling conventional manufacturing. For most AM processes, this tradeoff between speed and quality is experienced, with a large number of other determining factors influencing this.

Most types of material families are utilised in AM. A majority of the different processes use polymers, which is also clear from the material market share breakdown presented in Figure 1.2.

Polymer AM is a vast field. Different production technologies are utilised to produce parts based on thermoset or thermoplastic polymers. Thermosets are often linked with Vat Photopolymerization (VPP). This technique can produce some of the AM industry's most intricate features and finest details [20]. Current research has developed functional surfaces manufactured by VPP, allowing hydrophobicity [21]. Others have focussed on using a ceramic slurry mixed with a photopolymer resin, enabling the production of piezo elements with complex geometries [22]. According to the Wohlers report of 2023 [19], photopolymers take up 21% of the material market, making this market as big as the one for filaments. Filaments are typically used by desktop systems, manufacturing parts by Material Extrusion. The most widespread use of thermoplastic polymers is in the Laser Powder Bed Fusion (LPBF) industry. Here Polyamide (PA), often known as Nylon, is the most commonly used material. PA is mainly used for the PBF-LB/P process, but Multi Jet Fusion (MJF) also uses this material [19].

The significant usage of PA is attributed to the rapid growth of the PBF-LB/P market, with different industries adopting the technology. Another factor might also influence this, since when using polymer powders for PBF-LB/P processing, especially PA, refreshing

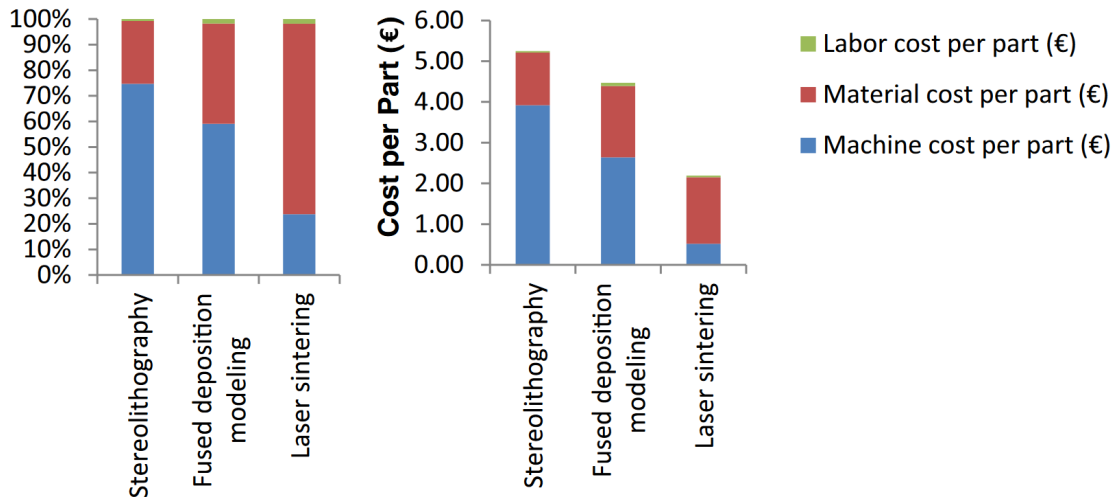


Figure 1.3: Cost breakdown for three main categories of Polymer AM. From [25]

the used material is needed before using it again. The refresh rate is typically in the range of 10% to 70% [23, 24]. This causes excessive consumption due to discarding up to 70% of the powder during manufacturing, which can skew the total amount of powder used for parts compared to the amount purchased for the process. This effect is evident in the cost breakdown for AM using different technologies by Thomas D. [25]. Here it is shown how the material price drives the cost per part produced by PBF-LB/P. However, it is also clear that parts are cheaper by a large margin when comparing the VPP, MEX, and PBF-LB/P processes as seen in Figure 1.3.

## 1.3 Open Additive Manufacturing

When investigating materials and processes, it is rarely feasible to rely on equipment or materials that the researcher cannot control in every single parameter. Unfortunately, this often occurs when material and process research is done within the field of manufacturing engineering. Research carried out on industrial systems never allows full-range process control, limiting the dissemination activities to mainly focus on the parameters perceived by the industrial users as important for adjusting during operation. This is not only the case for PBF-LB/P but is also true for other established methods such as Laser Based Powder Bed Fusion of Metals (PBF-LB/M) and VPP.

To combat this, an initiative of Open Additive Manufacturing has been explored with funding from the Poul Due Jensen Foundation (Grant no. 2018-017). The project has focussed on exploring two major parts of the AM industry, one being Vat Photopolymerization (VPP) and the other being LPBF. This work focusses on LPBF of polymer powders and the consolidation behaviour achieved when processed by a fibre laser. By building on the previous work on PBF-LB/M and utilising the tools developed, a system capable



Figure 1.4: The Open Additive Manufacturing logo

of processing polymer powders by laser radiation is developed. The developed system is meant to define the criteria for openly disseminating the tools produced previously while researching the laser powder interaction.

The Open Additive Manufacturing Initiative and the project results will be released by January 1<sup>st</sup> 2024, defining the end of the research project. The release contains several pieces of work, spanning the open architecture systems, the Unified Systems Controller, and software for the control of the systems. This work contributes to the Open Additive Manufacturing Initiative. By incorporating these platforms, this work has provided feedback and enhanced the development of the systems. Working within and utilising the Open Additive Manufacturing Initiative have provided an opportunity to rapidly develop a system capable of investigating the main hypothesis by minimising the engineering effort of these systems during this project.

To understand the powders and their use in AM, a dive into the possibilities of materials is initially carried out. Thoroughly understanding the LPBF process and the material versatility in LPBF is needed to comprehend the vast opportunities an open architecture powder processing system can provide. From this knowledge, the use of polymers in AM is further explored, developing a framework for understanding the physics and chemical complexity of the PBF-LB/P process. Based on this knowledge framework, an experimental setup is developed, utilising the Open Architecture solutions provided by the Open AM initiative. Several experiments are carried out to enhance this experimental infrastructure further, producing new findings and upgrading opportunities that are then explored.

## 1.4 Research Relevance

Research and investigation of PBF processes is not a novel idea with a considerable interest stemming from the processes' original invention, patenting, and publication. Research within PBF processes is constantly growing, as seen in Figure 1.5. To define the level of interest within the major fields of PBF, a Web of Science study was conducted. The Web of Science study was carried out for three categories considering the three main processes of Powder Bed Fusion. The search word for the independent searches is seen in Table 1.1.

The search terms are the most common, with several other denominations available for the processes mentioned. Selective Laser Melting has recently more commonly been de-

Table 1.1: Search terms used in the Web of Science study

Category	Search terms (All Fields)
Polymers	selective laser sintering <i>OR</i> sls <i>AND</i> polymer
Metals	selective laser melting <i>OR</i> slm <i>AND</i> metal
Binder Jetting	binder jetting

nominated LPBF, which is technically a term covering both metals and polymers. Based on this, it was found reasonable to utilise the search terms presented. A search for LPBF and metal yielded similar results, limited by very few publications before 2015, which is not the case in the study of metal processing, as to why the search terms were selected and found not to alter the analysis significantly.

The study indicates a rapid growth in the number of papers published, which indicates significant interest within the field of AM and PBF. In the mid-2010s, a steep growth is seen for the cumulative publication within AM. This is especially true for metal AM. This coincides with the expiration of a large group of patents, which have allowed new interest and more widespread work to be disseminated. A discrepancy between the different processes is evident, with a significant focus on Laser Powder Bed Fusion of Metals arising in the middle of the 2010s, rapidly outpacing the other processes. The primary focus of both metal and polymer powder bed fusion is materials research, indicated by the dominating categories in the Web of Science categories analysis illustrated in Figure 1.6. The Web of Science categories analysis was conducted for the past ten years (2013 - 2023) to

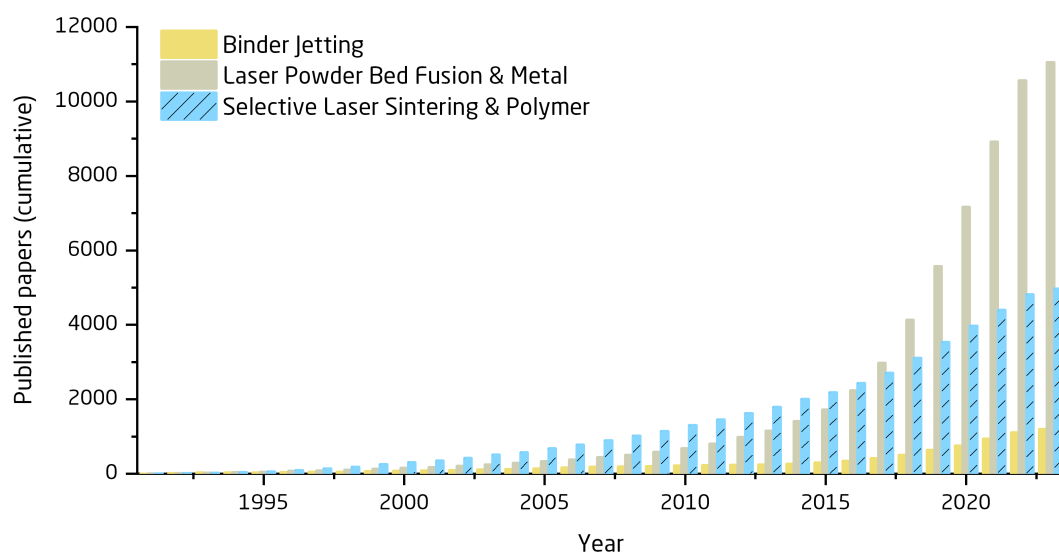


Figure 1.5: Web Of Science organised articles consider the main categories within Powder Bed Fusion



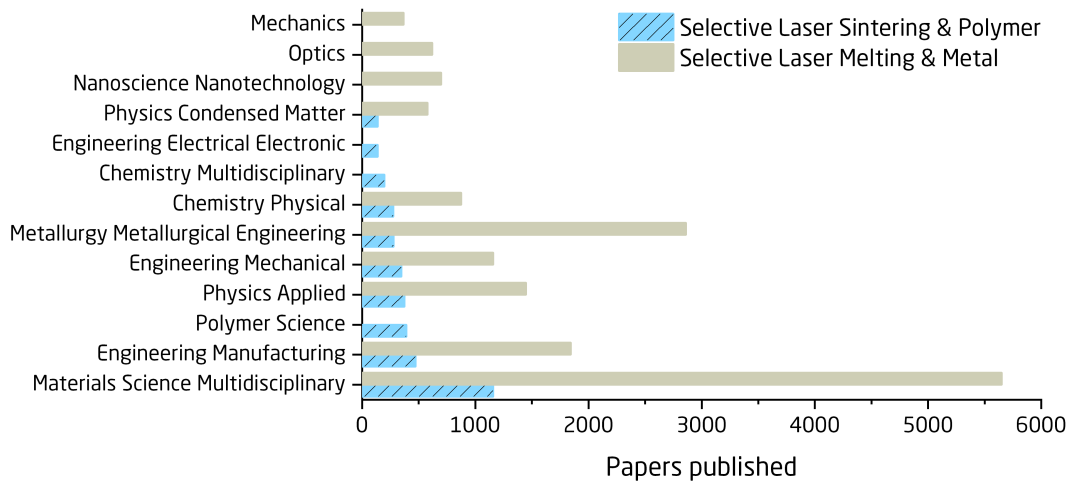


Figure 1.6: Overview of the Web Of Science categories and papers published within the last ten years

investigate the latest trends within research, utilising the same search terms as presented in Table 1.1. The plot is ordered by the most published fields within PBF-LB/P and overlaid by the categories within PBF-LB/M.

A considerable interest within research on LPBF is for material science, followed by manufacturing engineering for polymer processing and a branch of material science within metallurgy for metals is evident. Metallurgy considers, among others alloying and different post-treatments of metals, developing the properties for corrosion resistance or mechanical behaviour. The field of post-treatment of plastic components is not as expanded, leaving a gap between the two fields of study. A large gap between the two material systems is evident in the materials science category. One reason could be that the PBF-LB/P process is viewed as a prototyping and production tool used in industry but not as a process that requires large investigations. This can be based on the fact that several materials function well in the process, causing the development to plateau. Another reason can be the large investment required when open access to print parameters is desired, often limiting research institutions to utilise closed systems for research purposes. This is also the case for the systems within PBF-LB/M. Extensive efforts have more recently been put towards open-process parameter systems for metals, allowing research in the field. The trends of open access systems are not as strong for polymer systems, which hinders research and development in the field.

The field of powder bed fusion is explored in-depth in chapter 2, explaining the materials and typical use case for each category. The understanding developed for the different processing schemes and possibilities within each field are relevant for further developing the PBF-LB/P process. Having the opportunity to study the approach undertaken when processing metals, ceramics, and composites lends valuable insight when investigating the



laser processing of polymers, and a thorough explanation of the different material classes is therefore required.

Besides the limited process control, one major disadvantage when relying on industrial systems for research and development is the selection of consolidation sources. Traditionally the focus of research has relied on industrial systems and processing by CO<sub>2</sub> lasers, which are well suited for heating and melting a range of polymers. Developments in the field of lasers have enabled the manufacturing of fibre lasers at a fraction of the cost previously known, making these an interesting choice for the consolidation of polymer powders. Furthermore, fibre lasers produce a beam quality far superior to that of a CO<sub>2</sub> laser and with a much longer lifetime, power stability, and high-power capability. It is not uncommon to come across fibre lasers delivering up to 100kW laser powers, which is unheard of for CO<sub>2</sub> laser sources. The typical beam shape of a fibre laser is close to a Gaussian distribution, and the short wavelength encourages much smaller spot sizes and longer Rayleigh lengths of the focussed beam. All these factors contribute to the desire to investigate fibre lasers in the PBF-LB/P process. The capability of selecting and designing the laser source for processing powders permits research, reaching much wider than the main topic with the field of PBF-LB/P.

Chapter 3 of this work presents the industrial use of laser-based polymer powder processing equipment and to what extent these are capable of introducing new materials in the system. The chapter further introduces the laser source and the power described for the individual system. Finally, an input of the build volume of each system is presented. By doing this market research, the market understanding of PBF-LB/P showcases the lack of new material support and the deficient support for other laser sources than the CO<sub>2</sub> type. This understanding is supported by the knowledge obtained above, speaking to the fact that the research within the process is lacking behind similar processes considering other materials.

Chapter 4 introduces the relevant theory and the state of the art in the polymer powder laser processing field. Here the knowledge is developed, laying the groundwork for implementing a new laser source in this process. The chapter breaks down the essential aspects of the process to produce the framework utilised for the system development.

The experimental infrastructure is developed in chapter 5, disseminating the process of repurposing an older system for polymer powder laser processing. Several previously incorporated subsystems are utilised for the initial state of the finished system. The development of the finished system relies heavily on understanding the complex processing and the necessary subsystem development gained from previous chapters.

From the development of the system, several experiments have been conducted, gaining an understanding of the system and obtaining new ideas and knowledge for system im-

provement. The work, therefore, took on an iterative approach of designing and conducting experiments resulting in new improvement opportunities, which were implemented. Chapter 6 exhibits this iterative approach of experimentation and subsequent system development, resulting in a system which still presents several enhancement opportunities while being able to process polymer powders by fibre lasers in an efficient manner.

Based on the system and process validation, chapter 7 present the unique processing capabilities achieved by the system. Development of the fibre laser processing of polymer powders is presented, including a materials investigation and a conclusion on the reliability of the system. By this, the perspective of the work is illustrated, concluding upon the project's ability to answer the main hypothesis as described herein.

When seeking to comprehend complex problems, one must start identifying the relevant vantage points and try to define the problem from each. This will ensure a better perception of what the actual problem is. Defining this true problem based on the knowledge and vantage points from several disciplines rather than one helps confirm the relevance of this problem and the way to go about the investigation. Meeting and experiencing the vantage points of several problem identifiers, stakeholders, or disciplines allow the construction of an experimental setup that will define how the complex problem is solved. This holistic approach has tackled the problem at hand, seeking the understanding and critical aspects of the problem of introducing fibre lasers in polymer powder processing from several angles.

## 1.5 Chapter Summary

Laser powder bed fusion of polymers is one of the oldest AM techniques but has remained under slow development during the active time of the patent. These patents, along with a large group of other AM patents, have recently expired, leading to the large-scale blossom of development and research within the field. Following this, the Open Additive Manufacturing Initiative has worked on disseminating industrially relevant processes for a wider audience. This work resides with the Initiative with a focus on the interconnected system, process, and material influential factors for optimising the laser powder bed fusion of polymers process.

AM is not a new family of processes. Research and development have been on a steady incline for several years, developing new materials and enhancing processes making these relevant not just as a rapid prototyping tool but also for the actual production of parts with industrial and consumer uses. Research within PBF-LB/P is lacking behind the metal counterpart, even though the two processes are very similar. To breach this gap, new ideas and approaches are needed. This work focusses on introducing a fibre laser in the PBF-LB/P process, utilising its enhanced laser capabilities for processing polymer powders. A second leg of the work focusses on the open development and dissemination of the functionalities required for PBF-LB/P. The focus has been on disrupting what has become

a highly industrialised process, with little research activity, by utilising the Open Additive Manufacturing Initiative components developed herein. A major focus point has been utilising the Unified Systems Controller and the introduction of this into a repurposed system, demonstrating the use case of reviving older AM systems by incorporating this technology.

Investigating the main hypothesis of new laser source introduction is quantified through several fields of study. The initial approach is to understand the way PBF-LB/P systems function and to look into the state of the industry. This is to identify the relevant process capabilities that the new consolidation source must meet to become a relevant and viable solution. A dive into the knowledge produced both recently and through the historical perspective of PBF-LB/P aids the development of these processing goals further. Based on this knowledge, an experimental infrastructure is developed to encompass the new consolidation source. This experimental infrastructure has been an integral part of the process and materials development, further evolving the process of Polymer Laser Powder Bed Fusion.



## Powder Bed Fusion

Powder Bed Fusion (PBF) is a technique for fusing powder into 3D objects. The process utilises powder and a consolidation medium or source to selectively fuse particles in a layer-by-layer action [16]. PBF processes typically utilise a selectively deposited energy source or a binding medium for consolidation of the powder [26]. Figure 2.1 provides an overview of the different methods, the consolidation type, and the range of materials typically used in each process. The three processes are binder jetting, laser powder bed fusion, and electron beam melting. The present work focusses on LPBF, specifically LPBF of polymers and will be explained in the following section 2.1.

The remaining processes are binder jetting and electron beam melting. Binder jetting utilises a binder selectively deposited onto the powder bed, producing the desired geometry based on binder location and energy radiation for curing the binder [27]. Parts made by binder jetting require post-treatment in the form of sintering to initially burn off residual binder and subsequently fuse the powder grains into a dense component. The typical feature size is  $< 1\text{mm}$  and is determined by the binder chemistry and application method [28]. Electron beam melting uses a beam of electrons in a vacuum to a very low-pressure, inert chamber pumped with helium. The electron is first run in a preheating step homogenising the powder layer, and secondly, used selectively to melt a layer of metal powder [29]. Parts produced by Electron beam melting are capable of feature size  $< 0.5\text{mm}$  [30], with the part being fused and densified directly in the process.

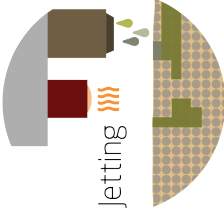
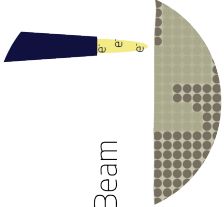
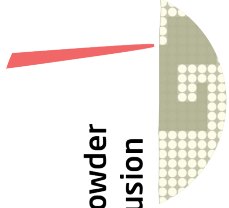
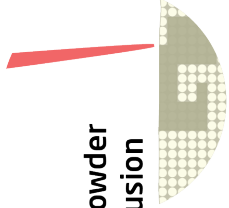
<b>Powder Bed Fusion</b>		<b>Project scope</b>
<b>Feedstock Handling</b>		
<b>Consolidation Mechanism</b>	<b>Binder Jetting</b>	<b>Electron Beam</b>
<b>Material Groups</b>		
<b>Material Groups</b>	<p><b>Polymers</b></p> <p>Metals</p> <p>Ceramics</p> <p>Composites</p>	<p><b>Polymers</b></p> <p>Metals</p> <p>Composites (conductive)</p>
<b>Feature size</b> (feedstock dependant)	<p>&lt; 0.8mm</p>	<p>&lt; 0.5mm</p>
<b>Material Composition (examples)</b>	<p>PA (6 - 11 - 12)</p> <p>TPE - TPU - PP</p> <p>No. 173</p> <p>High entropy ceramic</p> <p>No. 1</p>	<p>316L - Aluminium</p> <p>Titanium</p> <p>No. 964</p> <p>PA12 / Aluminium</p> <p>Ceramic / binder</p> <p>No. 77</p>

Figure 2.1: The Powder Bed Fusion processes, with the most common materials and possible feature size

## 2.1 Laser Powder Bed Fusion

Laser Powder Bed Fusion (LPBF) is a broad term describing powder material processing by laser radiation. These methods use a laser to selectively consolidate powder into a 3D geometry based on a Computer Aided Design (CAD) file [5, 19, 31]. The LPBF AM process has five main steps, as seen in Figure 2.2 that are carried out in a layer-by-layer method [32, 33] to produce a 3D part:

Dosing powder for new powder layer

Recoating of fresh powder layer

Scanning internal part (hatch area) of 2D cross-section for the current layer of 3D geometry

Scanning external part (contour) of 2D cross-section for the current layer of 3D geometry

Moving vertical-stage one layer height to allow for new layer recoating

The sequence of the laser scanning strategy steps can vary, depending on process, and system configuration.

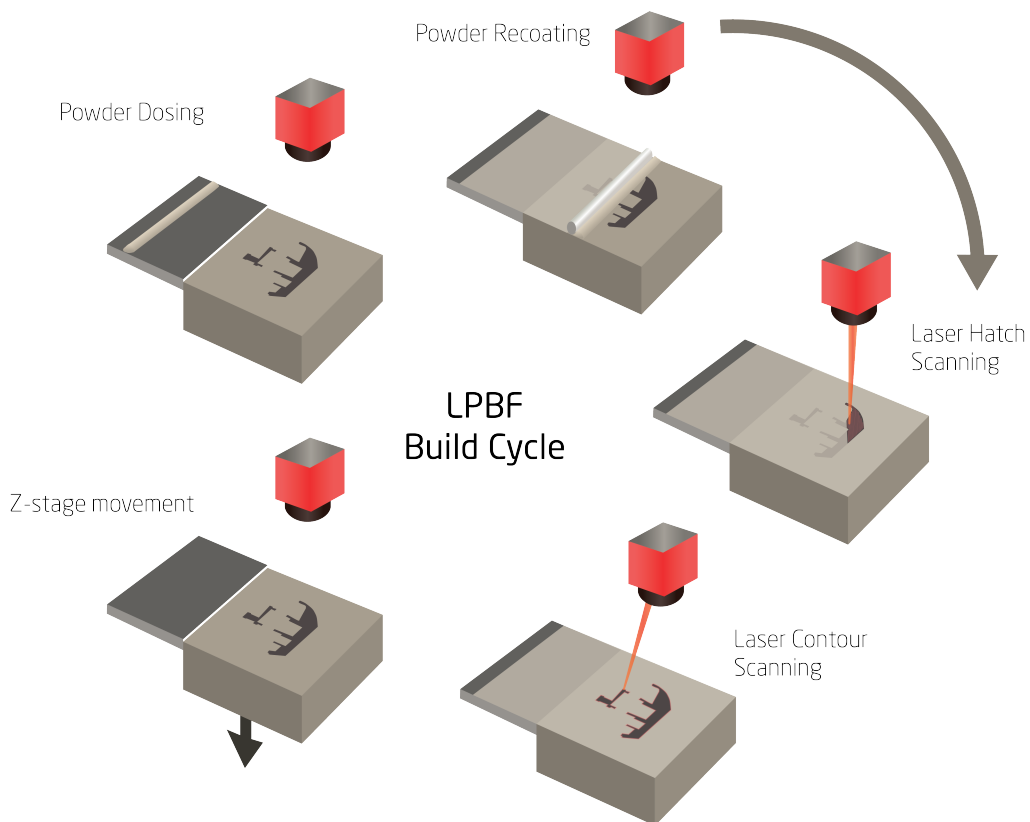


Figure 2.2: The process steps for the Additive Manufacturing cycle of Laser Powder Bed Fusion

## 2.2 Materials in Laser Powder Bed Fusion

The LPBF process can manufacture parts from close to any material. The material needs to be capable of being processed into a powder and show a distinct melting behaviour at elevated temperatures [5, 33]. Even powders that do not display this melting behaviour can still be used when a sacrificial binder is mixed with the desired material, allowing sintering of the component. Therefore, the use of LPBF is not limited to any particular material and can be applied to ceramics, metals, and polymers. Table 2.1 describes the number of commercially available materials, according to [19], with a clear dominance of different alloys represented in the PBF-LB/M market. The different material classes, their manufacturing route during LPBF, manufactured component properties, and typical uses are described in the following. New tendencies of composite materials are emerging, breaking way for even greater complexity and mechanical properties. This process can build highly complex geometries, with the two major factors for feature size being the laser and powder size [32]. Depending on the material, parts are either fastened to the build plate or built directly in the powder bed. The following is a description of the various material classes used for LPBF.

Table 2.1: Commercially available powder products. Data source the Wohlers report 2023 [19]

Powder Material Family	Commercially available products
Polymer	173
Metal	964
Composites	77
Ceramics	1
Total	1215

### 2.2.1 Polymers

The primary differentiation for thermoplastic polymers is the classification of amorphous and semi-crystalline polymers. Amorphous polymers show no polymer chain ordering, leading to an entangled polymer network with no crystal regions. On the other hand, semi-crystalline polymers show chain ordering when cooling, causing regions of crystallinity, with other regions remaining amorphous (Figure 2.3). The degree of crystallinity is influenced by the ability of the polymer chains to self-order during cooling, producing regions of folded and aligned polymer chains known as polymer crystallites [34].

These crystallites cause the two types of thermoplastic polymers to behave differently, considering mechanical properties, melting/softening behaviour, and visual appearance [36]. The focus point for processing thermoplastics in LPBF is the melting behaviour



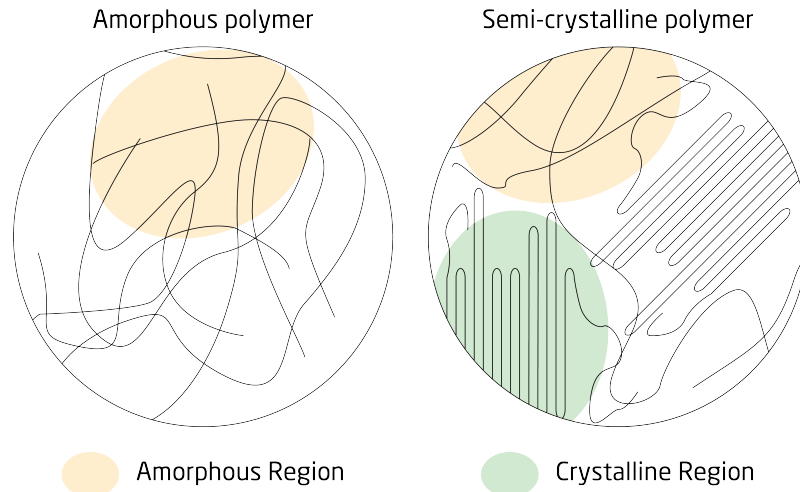


Figure 2.3: Amorphous and semi-crystalline polymer structures

and the precise definition of this point for the functionality of the process. Amorphous polymers do not exhibit a distinct melting behaviour but rather a function of softening and an increase in the polymer chain mobility over a larger temperature range. Due to the lack of a distinct melting and crystallisation point, difficulties in utilising amorphous polymers can be envisioned. The transition between rigid and soft for polymers is known as the glass transition temperature  $T_g$ . This defines the temperature where the polymer goes from displaying rigid (glass-like) properties to a rubbery and soft material with increased chain mobility. Yan C. et al. [35] investigated the use of both semi-crystalline and amorphous polymers in the LPBF process. The group reported the difficulties of processing the amorphous polymers due to their vague softening point ( $T_g$ ) relation causing instabilities in the process. This resulted in parts with very low density and deteriorated mechanical properties compared to the dense parts manufactured by conventional polymer process-

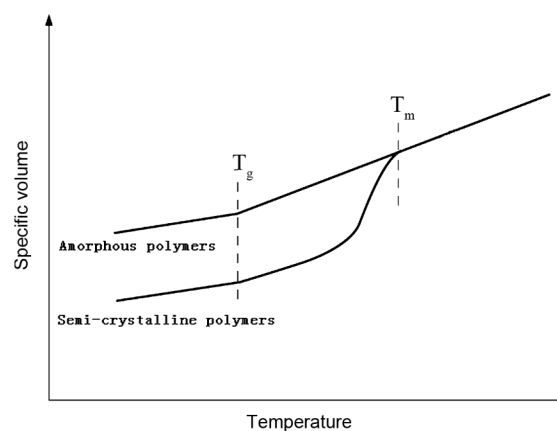


Figure 2.4: The specific volume vs temperature curve for an amorphous and a semi-crystalline polymer. From: [35]

ing, such as injection moulding. Yan C. et al. also report that semi-crystalline polymers produce higher-density components in the PBF-LB/P process with mechanical properties close to matching those of conventional processing. The work also found that amorphous polymers produce components with better dimensional accuracy. The better dimensional accuracy is attributed to the crystal regions causing shrinkage due to the self-organisation occurring during crystal growth. This behaviour of larger shrinkage is well known for semi-crystalline polymers and is exemplified in Figure 2.4.

During processing, the material is kept at elevated temperatures to mitigate the build-up of residual stresses in the part produced. For semi-crystalline polymers, a clear definition of the melting and crystallisation points is available, which is utilised for defining the process temperatures. This is not as straightforward for amorphous polymers, and the process temperatures are often defined as close to the glass transition temperature. When selecting a too-low process temperature, the polymer parts are prone to shrinkage, which can destroy the build due to uneven internal stresses between the different layers produced. Based on this, the most common materials used for LPBF of polymers are semi-crystalline.

The market for Laser Based Powder Bed Fusion of Polymers powders covers many different materials, mainly focussed on semi-crystalline polymers, with a few exceptions. The most used is Polyamide (PA) [19]. It constitutes 88% of the market, with PA12 filled and unfilled versions covering close to 50% of the total market [37]. Schmid A. [37] estimated that in 2018 more than 95% of the PBF-LB/P parts manufactured worldwide were produced from PA12 in various grades, with PA11 starting to gain momentum for replacing some of the PA12 use. PA11 was one of the original materials used for PBF-LB/P processing. Still, it was overtaken by PA12 due to a broader process window leading to greater ease of use. The two materials are very similar, with the significant difference being the chemical composition of having one  $\text{CH}_2$  unit less in the repeat unit of the poly-

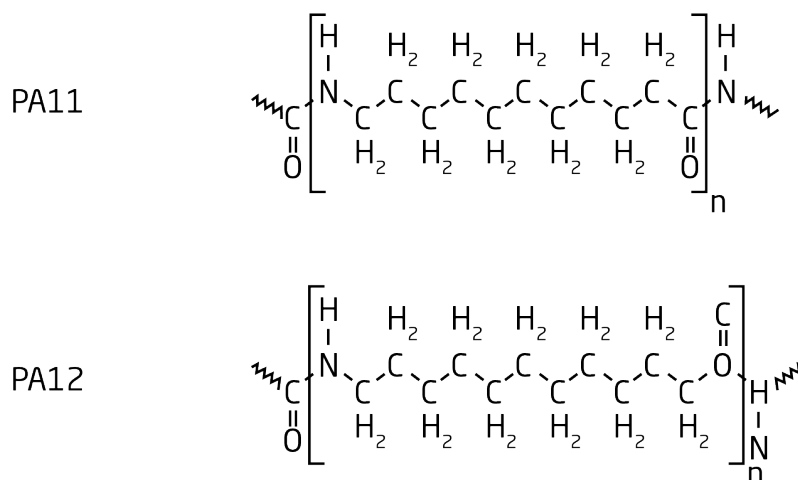


Figure 2.5: Repeat unit for the polymers PA11 and PA12

Table 2.2: Comparison of datasheet values for mechanical properties of EOS PA12 (PA2021) and PA11 (PA1101) [39]

	Tensile Strength (MPa)	Tensile Modulus (GPa)	Elongation at break (%)
PA11	48	1,6	45
PA12	48	1,7	15

mer, as seen in Figure 2.5. The polymerisation of PA depends on the monomer repeat unit structure. PA12 is produced by ring-opening polymerisation. Whereas PA11 is mainly produced by condensation polymerisation [38]. The ring-opening polymerisation is the preferred method for producing PA12 since it leads to a more stable product, useful for powder manufacturing. The two polymers are very similar considering the slight difference in the polymer structure, which infers similar mechanical properties, as seen in Table 2.2. The feedstock of the two polymers is sourced from two different methods. PA11 is a fully biobased polymer with feedstock originating in castor oil. PA12 is produced by petrochemicals, with butadiene being the initial constituent [38].

Several commercial products are produced by PBF-LB/P, ranging from fashion items such as the glasses from MONOQOOL, shown in Figure 2.6, to jigs and fixtures for industrial manufacturing.

Several other polymers are used in PBF-LB/P. Some of the most common are Thermoplastic Elastomers (TPE), Polypropylene (PP), and Polystyrene (PS) [40]. Seepersad C. et al. reports that the smallest viable feature size is  $\approx 1$  mm, with the possibility of obtaining even smaller features depending on the desired geometry [41]. PBF-LB/P are developed further in section 1.2 where the influence of the laser radiation, the system, and the material and feedstock properties is explained in-depth.

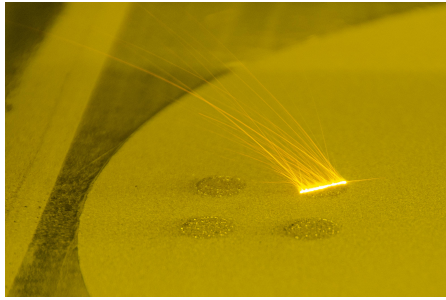


Figure 2.6: 3D printed glasses from the Danish company MONOQOOL: Reprinted with permission from MONOQOOL [42]

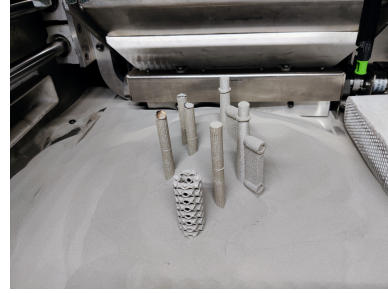
## 2.2.2 Metals

Laser Based Powder Bed Fusion of Metals of metals was discovered alongside the processing of polymers by the same research group at the University of Texas Austin [43] and is today the most common metal AM technique used [44]. The process uses a high-power fibre laser (100W - 1kW) for consolidating metal powders into the desired geometry as seen in Figure 2.7 showing the processing, unpacking and final part, manufactured on the Open Architecture PBF-LB/M system developed at the Technical University of Denmark (DTU). Parts manufactured by metal LPBF are known for high-resolution capabilities with features  $< 0.5\text{mm}$  [45]. PBF-LB/M is known for producing parts with more than 99% density [46], and mechanical properties comparable to or better than traditional manufacturing processes [47]. Several factors influence the final part density, including the scan speed, laser power, powder shape and flowability. Hoeges S. et al. [46] have shown how the density of PBF-LB/M is linked to the process settings during manufacturing by proving that water atomised powder can achieve the same density as gas atomised powders when working with 316L steels. Part density is one of the main drivers, along with the good mechanical properties and high complexity of the parts when considering PBF-LB/M. The stable production capabilities have led to a large market acceptance and adoption, shown by more than 3000 systems sold during 2022 [19]. One of the main disadvantages of PBF-LB/M is that the laser induces large thermal gradients and cooling rates experienced during processing, with cooling rates up to  $105\text{K/s}$  [44]. These have previously been shown to lead to chemical segregation causing metastable cellular structures. Another defect often seen is a rough surface finish directly after manufacturing. This is attributed to the melt pool causing neighbouring particles to adhere and partially bind without fully melting into the part. This effect is largest for the smallest particles in the powder, as reported by Sendino S. [48], due to the smaller particles being more likely to partially melt during the contour scanning of the parts. However, most parts manufactured by PBF-LB/M will be post-processed to some extent. A method often used is polishing or sandblasting, which will remove the adhered particles leaving a homogenised surface finish.

Recent research has focussed on mixing powders prior to manufacturing or during to produce parts with different alloy constitutions than the respective powder contributions or throughout the part, respectively. Valente E. et al. [50] have shown how pre-mixing two distinctive powders before LPBF processing will allow for a fully alloyed composition in the final part. The work considered a powder mix of 2.5wt%  $\text{Cr}_2\text{N}$  and 316L steel, which exhibited complete dissolution during manufacturing. Another route of mixing LPBF powders is gradually switching the composition of the manufactured part. By changing gradually, any effects of peeling or inhomogeneity in the material or the thermal properties can be mitigated. Switching over sequential layers is currently investigated for manufacturing graded structures in metal LPBF [51]. Here it is shown how gradually changing the composition of two different metal alloys can produce a component from



(a) Manufacturing process



(b) Parts during unpacking



(c) Part with no post-processing

Figure 2.7: Process steps in PBF-LB/M, shown for the open architecture machine at DTU (Credit: Magnus Bolt Kjer [49])

two materials showing material mixing and element diffusion between the two separate types, enabling the production of functionally graded components. Gökhan Demir A. [52] demonstrated this effect of gradually mixing two metals. Here steel and aluminium alloys are combined to create an inlay weld piece for welding otherwise incompatible metals. This is done by producing a transition zone where the two metals are mixed, gradually changing compositions, with either side representing the pure steel and aluminium alloy, respectively.

The significant market adoption for PBF-LB/M is driven by manufactured parts' complexity and mechanical properties. The mechanical properties are typically superior to those of traditional manufacturing [47]. With the possibility of producing specialised alloys designed for the PBF-LB/M process. Jia Q. et al. [53] have shown how a specialised aluminium alloy can significantly increase mechanical properties by utilising the rapid cooling rates during LPBF processing. The special alloy reduced the grain size by precipitation of secondary phases, enabling improved mechanical properties compared to traditional processing. Products manufactured by PBF-LB/M take advantage of the effects

of laser processing and spans over many different production areas. Some of the practical uses of PBF-LB/M is the manufacturing of topology-optimised parts, mainly used in the aerospace industry, such as critical components during spaceflight or for passenger aircraft [54]. Another use is for mould inserts used in injection moulding, incorporating conformal cooling [55] to allow shorter cycle times and less wear during manufacturing. Another use is for speciality items for the medical industry, such as bone implants [56] improving the body acceptance of implants by adhering closer to the mechanical properties of bone and surrounding tissue. It is clear how well-established the use of PBF-LB/M is, based on the numerous use cases. Another process is Ceramic LPBF, which is not as well established but still holds considerable relevance in the field. This process is described in the following.

### 2.2.3 Ceramics

As mentioned, ceramic LPBF is not as established as the other significant processes. However, ceramic LPBF is gaining interest in producing complex ceramic structures. Two methods have been the dominating processes for processing ceramic powder in LPBF. One is the indirect method, where the ceramic particles are mixed or coated with a binding agent responsible for the binding mechanism during laser processing. This binding agent is often a low-melting polymer, ensuring easy post-processing. The indirect process route includes subsequent debinding and sintering steps to produce the final part [43]. The other method is direct sintering of the ceramic powder into a part, with no extra post-processing besides what is typically expected for LPBF [57]. The direct processing route is difficult for ceramic powders due to the extremely high melting point and little to no plasticity of the material and part produced, leading to issues during the LPBF process. This is the root cause of the main issues faced when processing ceramic powders by LPBF, which is the tendency of high porosity leading to low-density parts not yielding the expected mechanical properties. Recent research has therefore focussed heavily on the development of direct manufacturing of ceramic parts by LPBF. Among others, Zhang et al. [58] have successfully demonstrated a direct manufacturing approach for two distinct ceramic powders, which have yielded promising results. Here it is shown how a high entropy ceramic can be processed by a high-power (600W) Yb laser into dense parts with minimal dislocations and large Vickers hardness. The interest in the direct manufacturing route is growing [59], with the number of ceramic material suppliers growing in the entire AM industry [19].

LPBF processing of ceramic powders has been studied heavily. Still, up to now, it has not been proven whether the binding mechanism is melting or sintering when considering the direct processing route [59]. A homogeneous part is determined by the binding mechanism, ensuring the consolidation of the powder, both in the powder-to-powder interaction and in powder to the previous layer. The consolidation behaviour is influenced by the in-





Figure 2.8: Showcase parts manufactured from ceramic Alumina powder. From Juste E. et al. [60]

teraction between powder and the energy source (typically a laser), with the spot size and geometry and the energy absorption of the material being critical factors. Understanding this powder-laser interaction is crucial for the direct manufacturing route to ensure stable production. The laser powder interaction is explained in-depth in subsection 4.1.1. One example of parts manufacturing is the production of showcase parts by Juste E. et al. [60] as shown in Figure 2.8. Here it is shown how the direct route with a laser absorbing agent can produce parts showing greater than 90% density, with no remaining absorbent in the final parts. Ceramic LPBF often follows the indirect route, with is described as a composite route since more than one material type is used during this process. The following is an introduction to composite LPBF processing, including an explanation of the various material combinations used and their purpose.

## 2.2.4 Composites

Composite systems for LPBF are described as early as 1995 by Nelson J. [61]. Composite material processing was especially of large interest before high-power lasers used for melting metals were available for a broader audience. Still, it has since developed its branch within LPBF processing. Processing two or more material-type powder mixes is used broadly in ceramic LPBF since manufacturing a green part is still less challenging than achieving complete sintering and good mechanical properties from the direct method described above. However, composite manufacturing using LPBF is now used for all the material classes mentioned above, often as a mix between them.

A study by Chuang K. et al. [62] showed how the LPBF process can manufacture a composite material. The investigation developed a method of laser sintering polyimide and short-strand carbon fibres, enabling the production of a high-thermal-stability component relevant for space exploration, as shown in Figure 2.9. The study used the LPBF process to finalise the crosslinking of a powdered thermoset polyimide, showing the crosslinking



Figure 2.9: Composite bracket developed by NASA for high-temperature capability. The composite includes Polyimide and short-strand carbon fibres. From [62]

capability, even across powder grain boundaries. A final component showing the desired thermomechanical properties was realised in the process. With the main conclusion of the paper defines how by utilising the material and method described, high-temperature components can be produced in a standard polymer LPBF system with no additional heating requirement, as is known from other high-temperature materials, such as PEEK [62].

Polymer composites are one of the significant areas of interest when considering composite materials. All material vendors provide composite materials, typically mixed with glass beads or carbon fibres. These components will increase the mechanical properties of the base polymer and produce parts with elevated mechanical properties compared to the unfilled versions [63]. As of May 2023, the EOS company provides three composite versions of their PA12 Nylon variant. EOS is one of the world leaders in polymer laser powder bed fusion and materials development for this process. The materials provided by EOS are filled with glass beads, aluminium powder, and a mix of glass beads and carbon fibres. All the filled versions show enhanced mechanical properties [15]. Parts made from composite materials often look different from natural or white coloured PBF-LB/P parts due to the filler material. Composite systems are typically divided into six different methods, as shown in Figure 2.10, with the most predominant for polymer-based composite being the base and filler system [15], shown here with glass beads in a base polymer as is done for the EOS material PA3200 GF™ [63]. Another typical filler is carbon fibres, represented in Figure 2.10. This filler system is, among others, produced by BASF for their UltraSint® PA11 Black CF material [64].

Another route of composite LPBF is presented by Chuang K. [62]. Here the LPBF processing of polyimide, a thermoset material, is presented. The thermoset resin is mixed with short-chain carbon fibres to facilitate parts manufacturing, demonstrating excellent mechanical characteristics. The parts show the homogeneous distribution of carbon fibres caused by the mixing between thermoset powder and carbon fibres and the good thermal stability achieved by the thermoset polyimide. The study also proved how the layers



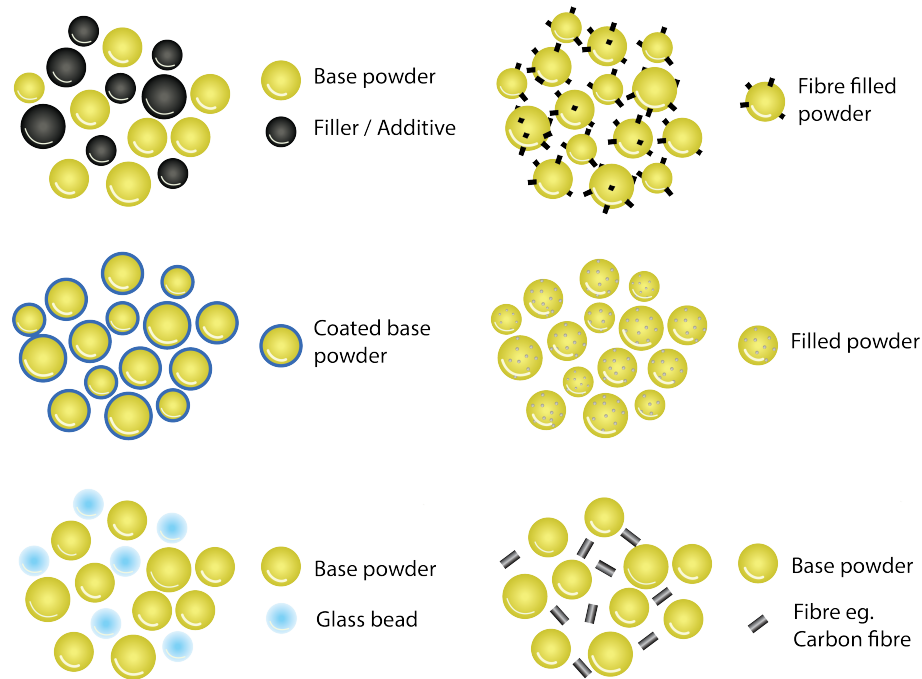


Figure 2.10: Types of composite blending for Laser Powder Bed Fusion

produced during the LPBF process could crosslink between them, gaining an isotropic crosslinked network in the components.

Current research has focussed on manufacturing conductive parts by PBF-LB/P using carbon fibres or powder to produce a conductive network in the sintered parts. Lupone F. et al. [65] have studied this effect showing how adding a carbon filler will decrease the resistivity of the polymer. Another example of composite PBF-LB/P is the increase of mechanical properties of a polymer from Chunze Y. et al. [66], showing how the introduction of nanosilica improves the properties compared to the neat Nylon. Here the nanosilica is blended into the polymer to ensure a homogeneous blend that can be handled in the LPBF process. The additive used for the composite combination was fumed silica, which is used in PBF-LB/P powders as a flow agent, ensuring an even flow during recoating [67]. This indicates that most commercial polymer powders are composite materials to some extent since most commercial suppliers will add additives to enhance and stabilise the powder and parts manufactured. Composite manufacturing by LPBF is still of research interest, and new methods for manufacturing even higher-grade parts are still being investigated.

## 2.3 Chapter Summary

Powder bed fusion is a technology relevant for producing functional components ranging in size from meso to macro scale. The diversity of materials facilitates functional components relevant to several large industries. The typical sectors utilising powder bed fusion require good accuracy and high complexity of components, which is enabled by

the powder bed fusion process. Aerospace companies often use powder bed fusion, where topology-optimised components deliver the needed complexity and weight saving [68]. Another use case is by plastic product manufacturers, where conformal cooling of the moulds decreases the cycle time by up to 40% compared to traditional mould-making techniques [69, 70]. Finally, engine manufacturers are utilising powder bed fusion to produce complex fuel nozzles, which allow lower fuel consumption by increasing fuel combustion efficiency [71].

# CHAPTER 3

## State of the Industry

The industrial utilisation of PBF-LB/P is rapidly growing. The list of new systems and systems providers continuously expands. The 2023 Wohlers report shows how the number of industrial and desktop system providers are gaining more ground with an increasing number of sales per year and a steady increase of system providers for the entire AM industry [19]. The cumulative numbers of systems sold, as reported by the 2023 Wohlers report, show how the trend of system adoption maintains a steady rate of more than ten per cent of new systems every year for the last ten years. From Figure 3.1, it is evident how the widespread adoption of AM systems continues to flood the manufacturing market. The market growth encompasses all AM processes. However, the trend depicted in the graph holds true for most of the processes, showing continuous growth.

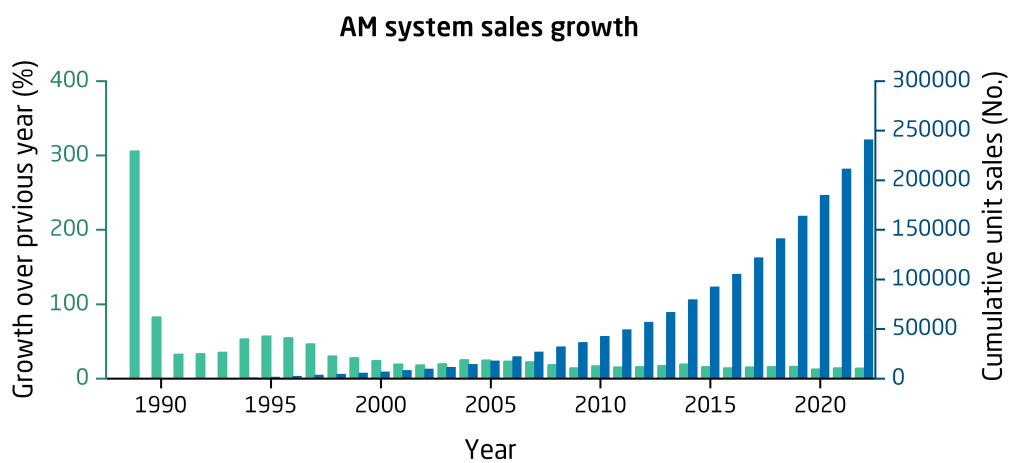


Figure 3.1: AM systems sales growth from 1988 to 2022. Data source the 2023 Wohlers report [19]

## 3.1 Industrial Systems

With the number of industrial systems expanding rapidly, an overview of the industry's current state is needed. Table 3.1 and Table 3.2 list the relevant information for the most noticeable systems in the industry. Table 3.1 focusses on systems that are developed for mass manufacturing of PBF-LB/P components and products. Large-scale manufacturing is achieved by increasing the build volume to allow more components per build cycle and increasing the scanning speed to finish each layer cycle faster. Table 3.2 focusses on smaller systems, which are aimed at Research and Development (R&D), as well as smaller production series. Typically the investment for the desktop systems is significantly smaller than for the industrial scale systems.

The lists of Table 3.1 and Table 3.2 contain information on the individual systems obtained from the marketing websites of the system manufacturers [72–91], and can be found at the end of this chapter. The lists are not comprehensive but showcase the most noticeable systems found, with the effort made for presenting the majority of the available systems on the market. The data was acquired on the 17<sup>th</sup> of June - 2023 and is indicative of the state of the industry considering the predominant manufacturers, systems, and laser sources utilised. Systems not displayed here can have been presented between the research and the publication of this study, as well as not evident during the investigation.

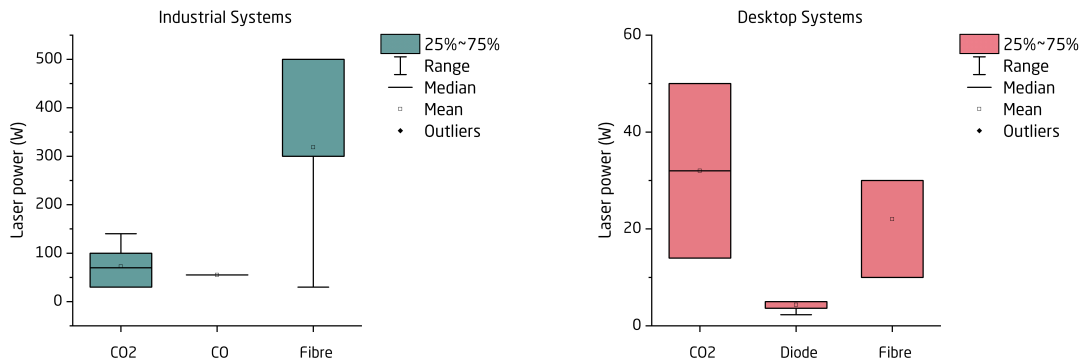
The tables presented contain relevant information for the PBF-LB/P process. Information on the laser source is presented since this influences the build speed, quality, and material range. The build volume is presented to show the limit of the individual system. The layer thickness range will influence the build speed and the possible resolution of the system, greatly affecting the final product's appearance. The feature size mentioned describes the minimum possible feature size as recommended by the manufacturer and is not presented for all the systems but only the one showcasing this information on the website or system documentation. The scan speed is the fastest scan speed allowed for the individual system, influencing the appearance and build speed. The category "Open" describes if the individual system is marketed as Open, meaning process control to an extent, allowing free selection of material. The category "Open" does not consider options of having open systems depending on investment but purely the advertised value by the manufacturer. Finally, the key feature represents the main selling point as advertised by the manufacturer, describing a feature specifically highlighted.

The industrial systems presented mainly utilise a CO<sub>2</sub> laser as the energy source for powder consolidation (40 out of 47 systems). For the desktop systems, this is more varied, with more systems utilising a low-power fibre (5 out of 11) or diode laser (4 out of 11). The desktop systems utilising fibre lasers all function with black materials, typically not offering colours other than black or grey in their material portfolios. Secondly, the ma-

majority of these systems are closed, only allowing the use of materials purchased from the system manufacturer. The material flow is often controlled by the system being connected online and RFID chips in material canisters, inhibiting the use of outside material grades. This greatly reduces the research and development capabilities of the process and mainly allows the systems to function as production equipment not relevant for process development or exploration. The Snowwhite<sup>2</sup> system is the only system that is presented as a desktop system that caters to research and development [90].

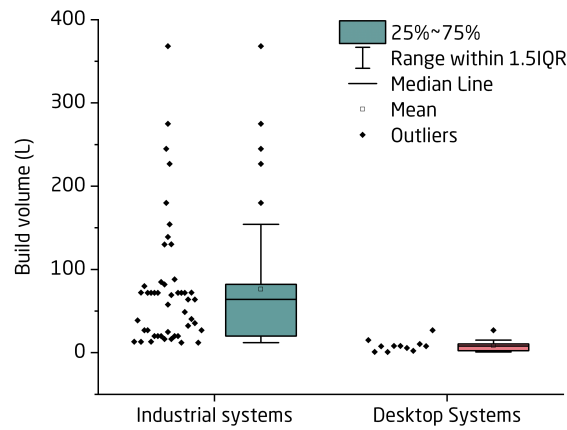
A large share of industrial systems allows for free material choice when selecting grades that can be processed with the level of process control allowed by the system. Adequate heating of the build volume is a prerequisite and process control over the laser scanning and power, ensuring a stable process is needed for the introduction of exploratory materials. Some systems present large flexibility and process adjustment opportunities, which are less prohibiting when evaluating new materials or tuning the process for a specific production. For the industrial systems, 40 utilise the conventional CO<sub>2</sub> laser, six use high-power fibre lasers, and a single system utilises a CO laser as seen in Figure 3.2b. Desktop systems generally utilise lower-power lasers and have a slower scanning speed, which is influenced by the selected scanning system. The most cost-efficient desktop systems use a gantry system for scanning the build plane, which is inherently slower than a galvo scanner due to the inertia in the system and mechanical limitations. Figure 3.2c shows the range of build volume for the industrial and desktop systems. Here it is clear that the industrial systems generally focus on large-scale production, whereas the desktop models focus on a single or few components per production run.

Increasing the productivity of a large build volume is often approached by incorporating several lasers in the same system, allowing multiple parts to be scanned simultaneously. Multiple laser sources for consolidation can be utilised by scanning in the same area while doing similar operations or scanning individual parts. To increase production stability, a recent trend found in the system survey is thermal control and balancing. This indicates not relying on single or multiple pyrometers but instead reading the temperature profile of the build plane from a thermal imaging device. A more stable process can be developed by ensuring less deviation in the temperature profile, ensuring parts with similar properties independent of the build location. Finally, a recent advance is the introduction of new laser types in the process. The high-power fibre laser systems from Farsoon are useful for increasing productivity while utilising the beam profile of the laser source [92]. EOS has introduced a CO laser which can deliver a better beam profile while introducing a larger Rayleigh length [93]. The influence of the laser is developed in subsection 4.2.1.



(a) Average laser power in industrial systems

(b) Average laser power from desktop systems



(c) Average build volume in industry and desktop systems

Figure 3.2: Results of build volume and laser source power from the market analysis

Table 3.1: List of industrial system manufacturers, their systems, and general specifications for the individual systems

Industrial / Mass manufacturing systems									
Company	Name	Laser source	Build volume (mm)	Layer thickness (mm)	Feature size (mm)	Scan speed (m/s)	Open	Key Feature	
3D systems	sPro 140	CO2 (70W)	550 x 550 x 460	0.08 - 0.15		10	no	High repeatability	
	sPro 230	CO2 (70W)	550 x 550 x 750	0.08 - 0.15		10	no	Large scale components	
	SLS 380	CO2 (100W)	381 x 330 x 460	0.08 - 0.15		12.7	no	Industrial scale production	
DediBot	DLS-250	CO2 (30W)	250 x 250 x 400	0.06 - 0.3			no	Precise thermal control	
E-Plus-3D	EP-P420	CO2 (120W)	420 x 420 x 465	0.06 - 0.2		13	yes	Temperature + stability	
EOS	Formiga P110 Velocis	CO2 (30W)	200 x 250 x 330	0.06 - 0.12	<0.5	5	no	Small footprint	
	Formiga P110 Fine Detail Resolution (FDR)	CO (55)	200 x 250 x 330	0.04	≈0.22	5	no	Fine detail resolution	
	P396	CO2 (70W)	340 x 340 x 600	0.06 - 0.18		6	no	Flexible and connectable	
	P500	CO2 (2 x 70W)	340 x 500 x 500	0.12		2 x 10	no	Fast and economical	
	P770	CO2 (2 x 70W)	700 x 380 x 580	0.06 - 0.18		2 x 10	no	Large and efficient	
	Integra P450	CO2 (120W)	420 x 420 x 500	0.1 - 0.18		12.7	yes	Open platform	
Farsoon	ST252P	CO2 (30W)	250 x 250 x 320	0.06 - 0.3		10	yes	High temperature	
	eform	CO2 (30W)	250 x 250 x 320	0.06 - 0.3		7.6	yes	Entry level	
	HT252P	CO2 (30W)	250 x 250 x 320	0.06 - 0.3		10	yes	Robust and truly open	
	HS403P	CO2 (55W)	400 x 400 x 450	0.06 - 0.3		10	yes	8 zone heating	
	SS403P	CO2 (100W)	400 x 400 x 450	0.06 - 0.3		15.2	yes	Three axis galvo	
	HT403P	CO2 (100W)	400 x 400 x 450	0.06 - 0.3		15.2	yes	High temperature	

## Industrial / Mass manufacturing systems (continued)

Company	Name	Laser source	Build volume (mm)	Layer thickness (mm)	Feature size (mm)	Scan speed (m/s)	Open	Key Feature
Farsoon	HT1001P	CO2 (2 x 100W)	1000 x 400 x 450	0.06 - 0.3		2 x 15	yes	Large scale processing
	Flight ST252P	Fibre (300W)	250 x 250 x 320	0.06 - 0.3	0.3	20	yes	Fibre laser
	Flight HT252P	Fibre (300W)	250 x 250 x 320	0.06 - 0.3	0.3	20	yes	Fibre laser
	Flight SS403P	Fibre (500W)	400 x 400 x 450	0.06 - 0.3	0.3	20	yes	Fibre laser
	Flight HT403P	Fibre (500W)	400 x 400 x 450	0.06 - 0.3	0.3	20	yes	Fibre laser
	Flight SS403P-2	Fibre (2 x 300W)	400 x 400 x 450	0.06 - 0.3	0.3	2 x 20	yes	Fibre laser
	Flight HT403P-2	Fibre (2 x 300W)	400 x 400 x 450	0.06 - 0.3	0.3	2 x 20	yes	Fibre laser
		SLS-400	CO2 (55W)	400 x 400 x 400	0.02 - 0.1		7	yes
Nexa	QLS230	CO2 (30W)	230 x 230 x 230	0.1			yes	Quick production
	QLS236	CO2 (60W)	230 x 230 x 250	0.06 - 0.3			no	Quick production
	QLS820	CO2 (4 x 100W)	350 x 350 x 400	0.05 - 0.2			yes	Multi laser function
Prodways	ProMaker P1000	CO2 (30W)	300 x 300 x 300	0.06 - 0.12		3.5	yes	Open material choice
	ProMaker P1000 S	CO2 (30W)	300 x 300 x 360	0.06 - 0.12		3.5	yes	50 Open parameters
	ProMaker P1000 X	CO2 (60W)	300 x 300 x 300	0.06 - 0.12		8	no	High thermal control
ProtoFab	PF 5300	CO2 (100W)	300 x 300 x 450	0.06 - 0.12		15,2	yes	Material open
	PF 5400	CO2 (100W)	400 x 400 x 500	0.06 - 0.12		15,2	yes	Material open
Sindoh	S100	CO2 (2 x 100W)	510 x 510 x 500	0.06 - 0.18		2 x 15	yes	Large scale + open



Industrial / Mass manufacturing systems (continued)

Company	Name	Laser source	Build volume (mm)	Layer thickness (mm)	Feature size (mm)	Scan speed (m/s)	Open	Key Feature
Sinterit	NILS	Fibre (30W)	200 x 200 x 330	0.08 - 0.18			no	Mass production
TPM3D	S320HT	CO2 (60W)	310 x 310 x 370	0.06 - 0.2		22	yes	High temperature
	P360	CO2 (60W)	350 x 350 x 590	0.06 - 0.2		15	yes	Material open
	S360	CO2 (60W)	350 x 350 x 590	0.06 - 0.2		15	yes	Material open
	S480	CO2 (100W)	470 x 470 x 590	0.06 - 0.2		21	yes	Material open
	P550DL	CO2 (2 x 140W)	540 x 540 x 840	0.06 - 0.2		22	yes	Two lasers
	S600DL	CO2 (2 x 140W)	590 x 590 x 790	0.06 - 0.2		25	yes	Two lasers
	S800QL	CO2 (4 x 125W)	790 x 790 x 590	0.06 - 0.2		25	yes	Four lasers
	Weirather	Laser Sintering 3232	CO2 (100W)	320 x 320 x 380	0.05 - 0.2		15	no
XYZ Printing	MfgPro230 xS	CO2 (30W)	230 x 230 x 230	0.08 - 0.2			no	Prototyping
	MfgPro236 xS	CO2 (30W)	230 x 230 x 250	0.06 - 0.3			yes	Functional parts
ZRapid Tech	iSLS300	CO2 (60W)	300 x 300 x 300	0.05 - 0.2		7	yes	Material open
	iSLS400	CO2 (60W)	400 x 400 x 400	0.05 - 0.2		7	yes	Material open

Laser wavelengths: CO2 laser (10.6 $\mu$ m) - CO laser (5.5 $\mu$ m) - Fibre laser (1060 - 1080nm) - 1. Diode laser (455nm) - 2. Diode Laser (808nm)

Data gathered on the 17<sup>th</sup> of June - 2023

Table 3.2: List of desktop system manufacturers, their systems, and general specifications for the individual systems

		Desktop / Prosumer systems							
Company	Name	Laser source	Build volume (mm)	Layer thickness (mm)	Feature size (mm)	Scan speed (m/s)	Open	Key Feature	
Formlabs	Fuse 1	Fibre (10W)	165 x 165 x 300	0.11			no	Fibre laser model	
	Fuse 1+	Fibre (30W)	165 x 165 x 300	0.11		12.5	no	Fibre laser model	
Red Rock 3D	SLS	Diode (5W)	180 x 180 x 180	0.1			no	Precision gantry	
	Snowwhite 2	CO2 (14W)	100 x 100 X 95	0.05		3.5	yes	Research oriented	
Sinterit	LISA	Diode <sup>2</sup> (5W)	110 x 160 x 130	0.08 - 0.1			no	Entry level system	
	LISA Pro	Diode <sup>2</sup> (5W)	150 x 200 x 260	0.08 - 0.1	0.5		no	Other materials (software)	
	LISA X	Fibre (30W)	150 x 200 x 350	0.08 - 0.1	0.5		no	Other materials (software)	
Sintratec	Sintratec Kit	Diode <sup>1</sup> (2.3 W)	100 x 100 x 100	0.1 - 0.15	0.5	0.6	yes	Assemble yourself	
	Sintratec S2	Fibre (10W)	Ø160 or 220 x 400	0.1	0.5		yes	Fibre laser model	
	Sintratec S3	Fibre (30W)	Ø160 or 220 x 400	0.1	0.5		yes	"Higher" power model	
Wematter	Gravity SLS	CO2 (50W)	300 x 300 x 300	0.1			no	System leasing	

Laser wavelengths: CO2 laser (10.6µm) - CO laser (5.5µm) - Fibre laser (1060 - 1080nm) - 1. Diode laser (455nm) - 2. Diode Laser (808nm)

Data gathered on the 17<sup>th</sup> of June - 2023

## 3.2 Chapter Summary

Dissemination of the state of the industry is limited to what information the system manufacturers provide. The list of systems is not exhaustive but shows a nuanced picture of the system landscape, the feature and layer size capabilities, the laser source, and a comment on the openness of the individual systems. The newest trends are highlighted above, where a significant focus for the system manufacturers is on the temperature gradient and thermal balancing. This will improve the build stability leading to an increase in successful build jobs and more consistent parts [14]. Another focus starting to emerge in the industry is the use of high-power fibre lasers, potentially improving part quality based on the beam quality and profile. The thermal balance and laser source are investigated in this work and will be described in detail throughout the thesis as seen in subsection 5.4.5 and subsection 6.1.2. To understand the influence of the system, the next chapter will focus on how the laser interacts with the material, the binding mechanism in the powder, and the use of polymers in PBF-LB/P.



## CHAPTER 4

# State of Research in Polymer Laser Powder Bed Fusion

By analysing the mechanisms related to a process, a framework can be constructed, aiding the system development and making sure that all sub-systems fulfil the desired objectives. The mechanism analysis of any complex process can produce an overview of the relevant parameters and signatures for the specific process. These process parameters and signatures can be further utilised to construct an experiment where certain elements are changed, causing the process to react differently. By analysing the process initially, one can ensure a more profound understanding, permitting the reconfiguration in a constructive manner.

To understand the PBF-LB/P process in-depth, this chapter focusses on the constituent mechanisms and subsequent process parameters and signatures. Defining these process relations aid the further development of the experiment as presented in chapter 5.

The chapter analysis six main topics related to the PBF-LB/P process. Initially, the chapter provides a common-ground understanding of the Laser Based Powder Bed Fusion of Polymers process. It goes into detail about the laser powder interaction and a description of the main methods of consolidation occurring during the process. The next part evolves the processing system, the main constraints and ways of setting up the processing equipment, and the influence of a change within this equipment. Finally, an elaboration of fibre lasers and a discussion of how to process polymers with fibre lasers are introduced, encapsulating the knowledge needed for systems development, is presented.

## 4.1 State of Polymer Powder Processing by Laser Irradiation

Even though the market is significantly dominated by PA-based materials for Laser Based Powder Bed Fusion of Polymers, the process allows the processing of most thermoplastic materials, with the main driver being the processing window width. The processing window for a thermoplastic material processed by PBF-LB/P is the difference in °C between the melting onset  $T_{oM}$  and crystallisation onset  $T_{oC}$  temperature. The size of this processing window determines the level of process control needed for processing a particular polymer [94]. Figure 4.1 shows the process window for a PA11. Here it is clear that the process window spans from around 170°C to 190°C. The powder cake temperature is therefore selected to 180°C to ensure the largest gap between the process critical temperatures [95, 96].

Figure 4.1 suggest a wide processing window of close to 20°C for the polymer system displayed. Differential Scanning Calorimetry (DSC) is a method for identifying the critical temperatures of materials. The method concerns the heat flow through a sample determining the changes in the molecular structure by deviation in this heat flow when changing the temperature over a defined range. The powder cake process temperature can be selected based on the processing window. Selecting an appropriate process temperature based on this ensures a significant degree of chain mobility after the laser has melted the geometry. At the same time, it minimises the degradation of the polymer caused by the extended period experienced at elevated temperatures. The process temperature must be above the defined crystallisation temperature to alleviate internal stress build-up causing warpage. Keeping the powder at this temperature can produce an isothermal process cycle, where the entire part and powder cake is left to cool and crystallise simultaneously. Drummer D.

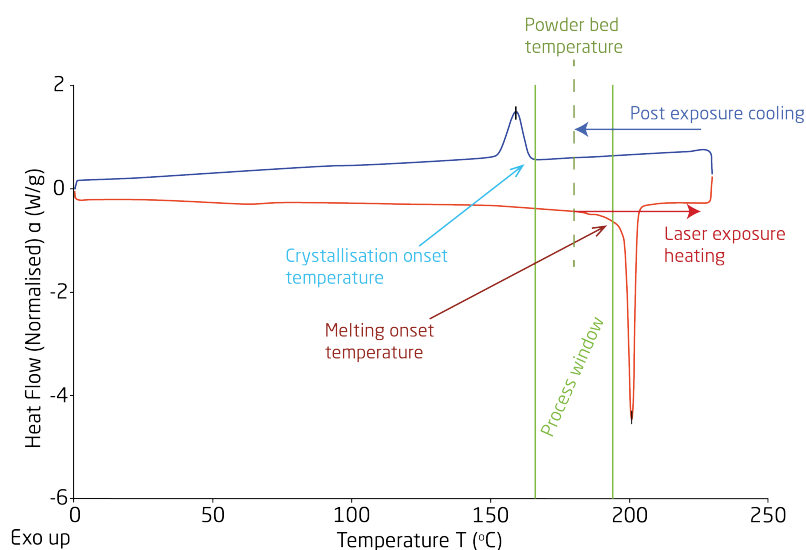


Figure 4.1: Differential Scanning Calorimetry (DSC) graph including the main attributes relevant for PBF-LB/P

Table 4.1: Process critical temperatures for the processing of polymer powders by laser radiation

Unit	Short name	Elaboration
$T_g$	Glass transition	Point where the polymer goes from exhibiting brittle to ductile behaviour when external stress is applied.
$T_{oM}$	Onset melting	Temperature at which the polymer starts to melt, as defined by the dsc analysis showing the decrease in heat flow in the sample
$T_M$	Melting	Temperature at which the polymer shows the highest degree of melting. Seen in the DSC analysis as the peak of the negative heat flow
$T_{eM}$	End melting	Temperature at which the polymer is fully molten
$T_{oC}$	Onset crystallisation	Temperature at which the polymer starts to crystallise, as defined by the dsc analysis showing the initial ramp-up in heat flow of the sample
$T_C$	Crystallisation	Temperature at which the polymer shows the largest crystallisation kinetic. Seen in the DSC analysis as the peak of the positive heat flow
$T_{eC}$	End crystallisation	Temperature at which the polymer is fully crystallised

et al. [97] showed how the processing window diminishes when maintaining an elevated temperature of the build chamber. This is due to a shift in the crystallisation temperature after melting when kept at elevated temperatures. The crystallisation temperature further rises as an effect of the low cooling rates for the PBF-LB/P process [94, 97]. This causes crystallisation to occur prior to what is expected based on the DSC analysis. Chen P. et al. [98] discovered the same kinetic for high-temperature sintering of PEEK. The complex heating and cooling of the powder cake during manufacturing are explained in subsection 4.2.1, where the entire build cycle, but also the layer cycle, is described.

For laser processing of polymer powders, seven temperatures are critical to the process's stability and success. The seven temperatures all concern the polymer's intrinsic properties and are used for describing the thermal behaviour of the polymer system. The list in Table 4.1 defines each process critical temperature, structured by when they are displayed during the DSC analysis. The table explains the temperatures relevant for semi-crystalline polymers, as this is the main focus of this work.

Polymer grades available for PBF-LB/P processing are limited by the required process window, as explained above. subsection 2.2.1 described the limitation of material selection by the required melting and crystallisation behaviour, not shown by amorphous polymers. Moreover, the process window width is not wide enough for stable processing

of many semi-crystalline polymer types. This substantially limits the selection range of suitable polymers, as seen in Table 4.2. Here a list of available polymer grades from the individual produces is shown, describing the limitations in material selection for PBF-LB/P.

There is only one producer of PA11 in the world, the French company Arkema, which makes PA11 under the tradename Rilsan B. Arkema also produces PA12 under the tradename Rilsan A. However, other companies also supply PA12. The German company Evonik produces PA12 under the tradename Vestamid, and the Schwiss company EMS-Chemie delivers another variant of PA12 under the tradename Grilamid, both used in the PBF-LB/P process [38]. Often system manufacturers will enhance the standard polymer by designing the polymer powder with additives to improve the quality of the parts produced by their specific system, based on their in-house R&D. An overview of the materials available, including the producer, is seen in Table 4.2. The list does not include variants designed by the system manufacturers or material producers but focusses on the individual polymer producers. The materials overview was published in 2021 by Wegner A. [94] providing an overview at this point in time. One of the trends while writing this thesis is polymer powder composites, introducing carbon fibres or other components for added mechanical properties. A vast difference in the polymer grades available is not expected since these composites build on the current material landscape adding new functionalities of products produced by PBF-LB/P.



Table 4.2: List of available polymer powders and their producers. Adapted from Wegner A. [94]

	AM Poly- mers	ALM	Arkema	BASF	Covestro	Diamond plastic	DSM	Evonik	Lehmann & Voss	Lubrizol	Mitsubishi chemicals	Sabic	Solvay	Victrex	Windform
PA12		X	X					X	X						
PA12 + fillers		X						X							X
PA11			X												
PA11 + fillers															
PA6	X			X								X			
PA6 + fillers				X								X			
PA612															
PA613							X	X			X				
PBT	X														
PP	X					X			X						
PE	X					X									
PS															
PC												X			
PEI												X			
PEK															
PPS															
PEKK															
PEKK + fillers			X											X	
PEEK															
TPE		X						X							
TPU	X			X					X						X

## Polymer Viscosity in LB-PBF/P

Polymers are viscoelastic materials that show temperature dependant viscosity profiles. Even when heated, polymers will typically show high viscosity and a flow behaviour resembling honey. The temperature dependant viscosity is a measure of the macromolecular mobility between other molecules. This chain mobility is for the moveability of the individual chains. Another factor is the rotation around the backbone of the polymer [99], allowing the polymer to twist and stretch. Because of this, the polymer's molecular weight and structure greatly influence the viscosity of a polymer system. Most polymer systems used in industrial plastics processing show non-newtonian flow behaviour, meaning that they often exhibit shear thinning. Shear thinning occurs due to a disentanglement and stretching of the polymer chains allowing them to move more freely when rapidly sheared [100]. For PBF-LB/P, this shear thinning behaviour cannot be utilised since no movement or shear is enforced on the build plane or powder cake during processing. This means that the polymer selected needs to exhibit low zero shear viscosity to flow and consolidate with the previous layer and surrounding particles [14]. The virgin grades of industrial polymers for the PBF-LB/P process all show low zero shear viscosity [101].

During PBF-LB/P processing, the entire build volume and powder cake especially is heated to a temperature above the crystallisation temperature of the polymer. This causes thermal degradation of the polymer, changing the powder's average molecular weight [101]. The degradation mechanics in PBF-LB/P is reported by Yang F. et al. [102] for Polyamide 12 (PA12). Here it is concluded that three dominant mechanisms are chain crosslinking, chain scission, and post-condensation. Chain crosslinking and post-condensation will both increase the average molecular weight of the polymer system. Chain scission will, on the contrary, reduce the average molecular weight. Chain scission of polyamide polymers is often caused by hydrolysis due to water vapour in the processing atmosphere. The effect on the average molecular weight of the polymer occurs due to the heated environment during processing [103]. Since the viscosity is directly influenced by the average molecular weight, refreshing the used powder with virgin powder is often implemented. This refreshing step for the powder ensures a narrower average molecular weight [101] while adding powder that has not lost flowability due to thermal processing, as described below.

Hesse N. et al. [101] have proposed a method for refreshing used PA12 powder. The method reverses the degradation mechanisms causing larger average molecular weight due to the elevated process temperatures [101]. The proposed method consists of hydrolytic reconditioning, refreshing the powder to close to virgin properties. The paper concludes that no significant change is inflicted on the powder, considering the particle size, shape or visual appearance. A minor change is seen in the width of the processing window and the isothermal crystallisation time. These are, however, not changed drastically, leading to

the reconditioned powder being accepted as a material suitable for PBF-LB/P processing.

The hydrolysis and chain scission is the opposite reaction of the polymerisation technique used for the production of PA11. The hydrolysis reaction is caused by available water in the system. By minimising the water vapour at elevated temperatures, this effect can be controlled to a minimal level. Industrial systems will often utilise an inert atmosphere to counteract the degradation mechanisms by removing the water vapour and oxygen responsible for the degradation reactions.

## Material Preparation and Production

Polymer powders are manufactured in a number of different ways. Each different method generates a product suitable for certain processes, with only some delivering the required characteristics needed in PBF-LB/P. Two distinct routes for powder manufacturing are recognised for PBF-LB/P. One route is the direct route of processing material directly into a powder of the desired shape and size, while the other is the in-direct route [104]. These are explained below, considering the material characteristics they each produce and the materials often paired with each process. An example of the shape and morphology of powder expected from each process is shown in Figure 4.2 from [104].

For the PBF-LB/P process, a spherical powder grain with a narrow size distribution between  $D_{10}10\mu\text{m}$  and  $D_{90}100\mu\text{m}$  [105] are desired. The narrow size distribution and sphericity aid the flow behaviour and packing density during the process. These two are the major goals of powder production, with the third being little to no polymer degradation caused by the processing.

Schmid M. et al. [104] mention the direct manufacturing route for polymer powders as achieving the desired particle shape and size directly from the polymerisation process. The polymerisation processes considered for this are emulsion, suspension, and solution polymerisation. Utilising one of these can provide spherical particles in a relatively narrow size distribution directly from the process if the proper conditions are applied. According to Schmid M. et al. [104], the only polymer powder commercially available processed by

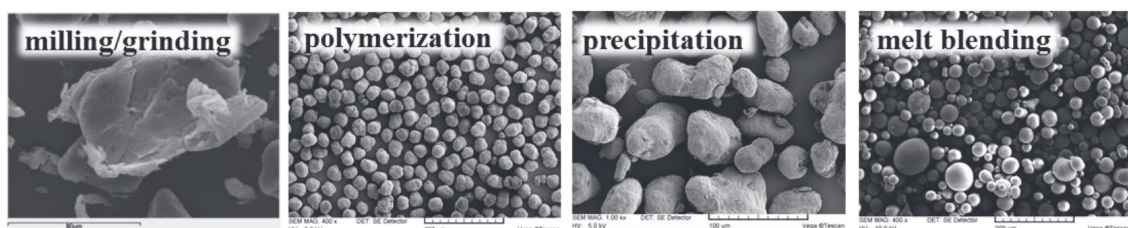


Figure 4.2: The four types of powder obtained from direct and indirect processing. The polymerisation route is the only direct, with the rest produced by the indirect route. From [104]

this route is the PA12 powder from Arkema. Several other polymers relevant to the field of PBF-LB/P can be produced in this way. These are polystyrene (PS) and polyacrylates. The direct route can produce highly spherical powders, improving the flowability and packing density of the powder bed [106]. A narrow size distribution can be achieved directly from the process by tuning the parameters. This distribution can be enhanced further by size separation. A narrow size distribution aids the packing density of the bed when coupled with spherical particles [107]. The direct manufacturing route is superior to the indirect route when considering possible output but is less used likely due to a higher manufacturing cost at scale.

The indirect route of powder manufacturing considers polymer products processed into powder after polymerisation. The most common understanding of the indirect route is the cryogenic milling of polymer pellets into a powder. The process utilises the polymer's glassy state by lowering the material's temperature with liquid nitrogen [108]. This process produces powder consisting mainly of flakes and a wide size distribution, causing the powder to be difficult to process by PBF-LB/P. Post-processing of the powder flakes is necessary, as discussed by Schmidt J. et al. [109]. The post-processing consists of heating the flaky powder above the polymer's melting point, in a downer reactor allowing the reduction of surface area. This reduction occurs due to the surface tension of the molten particles suspended in an aerosol consisting of nitrogen.

Another indirect route for powder manufacturing is the precipitation from solution [104] or solution-dissolution [110] process. Dechet M. et al. [110] show a method of liquid-liquid phase separation used for producing nearly spherical Polyoxymethylene (POM) particles suitable for PBF-LB/P processing. The powder obtained showed better flowability than cryogenic milled POM powder and was deemed useful even with no flow aids added. A similar approach is presented in another paper from the same author, showcasing the production of spherical PA11 powders from a liquid suspension [111]. The obtained PA11 powder showed good sphericity and flowability before adding flow aids. Finally, Faselow S. et al. [112] developed the same approach to encompass polyethylene (PE) producing a material qualified for the PBF-LB/P process. Common for all the studies is the conclusion that the selected emulsifier and stabiliser system consistently exert a significant influence on the success of the process, specifically with regards to the particle size distribution as concluded by Dechet M. et al. [111].

Recently a framework for the indirect manufacturing of highly spherical powders has been presented, among others, by Kleijnen R. et al. [113]. The process consists of melt blending two immiscible polymers in an extruder, with a subsequent separation step. The two polymers selected need to be immiscible. In the work by Kleijnen R. et al. [113], a water-soluble polymer is selected. Blending the desired powder polymer and the sacrificial matrix polymer allows one to obtain spherical particles, with a narrow size distribution, de-

pending on the mixing and extrusion parameters. In the work presented, a polybutylene terephthalate (PBT) polymer is selected for the powder component, with the sacrificial matrix being polyethylene glycol (PEG). It is found that the extrusion process has a negative effect on the PBT polymer due to the elevated temperature and water dissolution steps. This causes a change in the crystallisation temperature and viscosity of the final powder obtained, making the powder less suitable for the PBF-LB/P process.

The production methods for obtaining powders suitable for the PBF-LB/P process all show pros and cons. Figure 4.2 offers four variants of processed powder, which are more or less suited. The suitability is determined by the process of recoating a fine layer onto the build plane and is therefore controlled by factors other than the powder shape and size. Figure 4.2 shows four SEM images of powders produced by the methods described above. From the left is a cryogenic milled powder. The flakes and uneven sizes are problematic for good powder distribution and packing, causing this powder to be less desired in the process. The second picture shows a powder from the direct process route, promoting sphericity and narrow size distribution, making this powder ideal for the process. The third image is of a precipitation-processed powder, producing potato-shaped grains, that can prove useful in the process, especially when considering an informed decision for the recoating system, as described in subsection 4.2.1. The fourth image shows the highly spherical powder obtained by melt blending. This process has not yet been widely adopted by the industry but delivers high performance for powder fabrication. All powders presented can be processed by the PBF-LB/P process when the handling system for build plane generation is considered. The influencing factors are the dosing and recoating system, along with the flowability of the powder at elevated temperatures. The flowability is enhanced by ensuring smooth and round particles and is aided by flow-enhancing agents typically coated on the surface of the powder grains. The next section describes these flow aids, their function and their use.

## Additive Coating for Enhancing Processability

Additives used for stabilising the processing parameters are mainly focussed on flow aids. Recent publications discussing the effect of other functionalising additives show the impact of laser-absorbing agents and enhanced conductivity. The functionalising additives are discussed last in this section.

Flow aids in PBF-LB/P facilitate a better-flowing powder, producing a more homogeneous build plane. The determining factor for the flowability of powders smaller than  $100\mu\text{m}$  is the interparticle van der Waals forces, typically exceeding any other influential factors such as gravitational forces [114, 115]. This effect leads to fine powders exhibiting very high cohesive forces, which causes reduced flowability and decreasing volume-to-surface-area ratio in the powder cake and build plane. The volume-to-surface-area ratio is

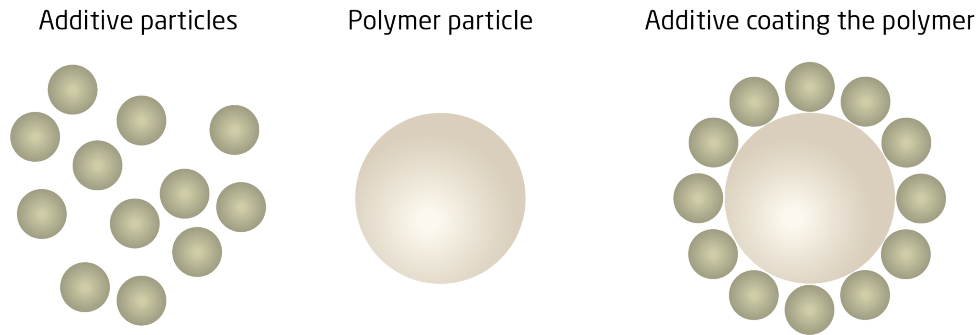


Figure 4.3: Additive coverage for spherical dry coated polymer particles

a method of describing the powder cake density by focussing on the powder's surface area and the powder cake's volume. By producing a low ratio, a low density of the powder cake is expected. The most commonly used flow aid for polymer powders is fumed silica  $SiO_2$ . The standard procedure for coating the powder is the mechanical dry coating, where the desired amount of additive and polymer powder is loaded into a tumbling or rotational vessel. Achieving complete coverage of the powder grain with minimal excess flow aid, left free in the mixture, as seen in Figure 4.3. Blümel C. et al. [116] investigated the effect of the dry coating on high-density polyethylene (HD-PE), showing how two fumed silicas, one hydrophobic, the other hydrophilic, influenced the process, build plane, and final part quality. Blümel C et al. [116] concluded that the efficiency of the flow aid is linked to the similarity in the surface chemistry between powder particle and flow aid, either showing hydrophobic or hydrophilic properties. Since the investigated HD-PE shows hydrophobic characteristics, it was concluded, based on experiments, that the hydrophobic flow aid performed superior to the hydrophilic. A reason for this is also that the hydrophilic flow aid retains moisture by adsorption, which forms capillary bridges between the powder particles, causing the cohesion in the powder to become much greater, even when compared to the uncoated polymer [115]. The correct dosing of any additive is essential, as seen from the study by Tischer F. et al. [117]. Here it is shown how an excessive amount of fumed silica deteriorates the polymer's processability due to a change in the crystallisation kinetics caused by an increased level of nucleation points developed by the nanopowder fumed silica. The effect was a diminishing of the process window, causing the processing capabilities of the polymer to decrease [115]. From this, it is clear that the minimal needed flow aid should be added for any polymer powder to ensure high processability of all parameters while still coating the powder to a functional degree. Schmidt J. et al. [115] describe close to complete coverage as 0.5wt% fumed silica for a PBT powder.

The dry coating of powder can also serve other functions besides flow aids. Depending on the additive, various properties can be enhanced or produced based on the coating medium. Xi S. et al. [118] introduced a nanoparticle Carbon Black (CB) as a dry coating for an industrial grade PA12 to enhance the flowability of a cryogenically ground powder. The



effect as a flow aid was successful. The CB caused a colour change, which lowered the needed laser power during processing. The powder showed electrical conductivity, which further aided the flow properties of the powder due to a minimisation of the tribological charging during powder motion, such as recoating [115, 118]. The dry coating process is a commonly found method for coating nano to microparticles on a powder medium. The wet coating process is a different method, where two powders are loaded in a solution producing a uniform coating [119]. The solution is then removed with the remaining powder left coated by the desired particles. Hupfeld T. et al. [120] have produced a functionalised PA12 powder by the wet coating process. By introducing an iron oxide powder to the polymer, magnetic parts could be processed by the PBF-LB/P process, maintaining the same magnetic properties as the powder mixture.

## Material Processability

The polymer chemistry, manufacturing route, and the additives used for the final product polymer powder made for PBF-LB/P all influence the powder's processability as shown in Figure 4.4. These parameters are derived from the material study presented above. All the parameters are defined by the material used and are quantified by a certain metric.

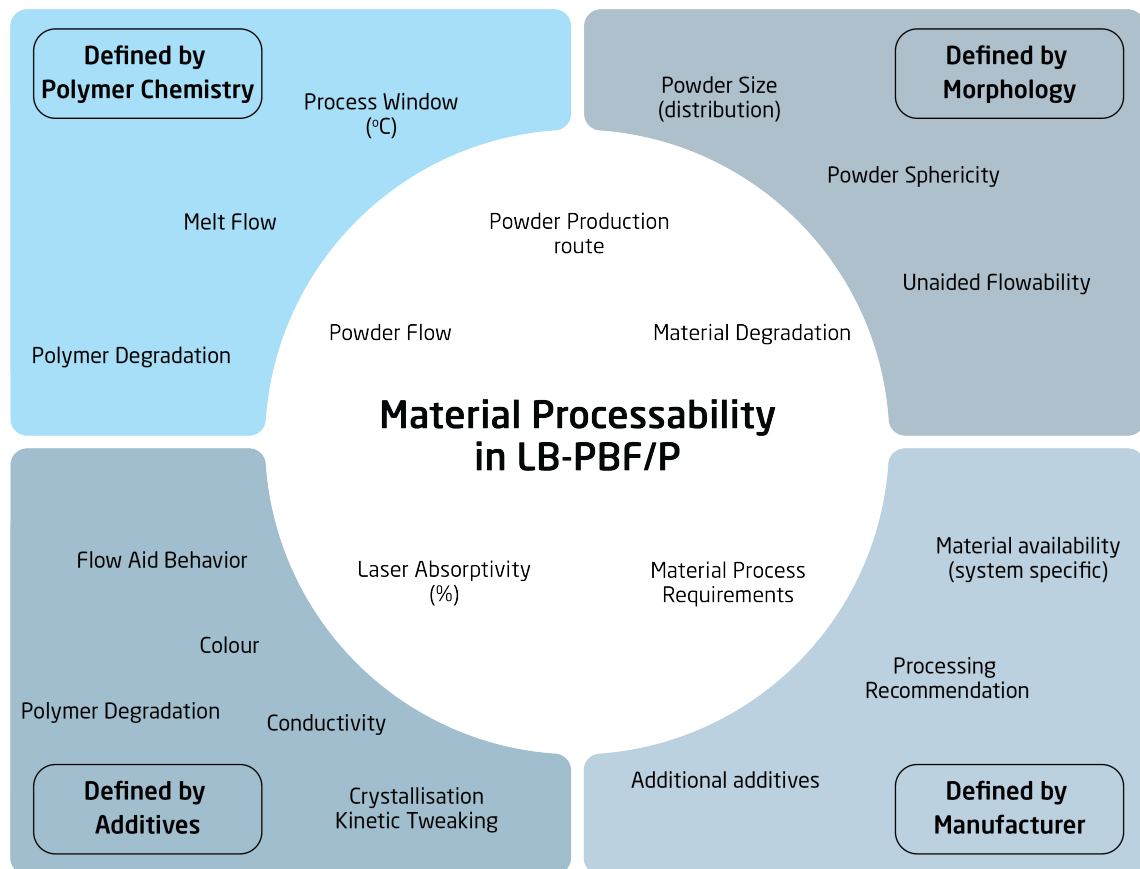


Figure 4.4: Material characteristics important to consider for processing polymer powder by laser

A last influence is mentioned in the illustration, considering the influence of the material manufacturer. This influence can be difficult to quantify fully. Considering the case of the French company Arkema, which is the only producer of PA11 worldwide. PA11 is, however, sold by most other material and system vendors. This means that some of the grades will be virtually the same polymer and additive mix. While other vendors might develop their own recipe for their material, adding certain additives to enhance the material characteristics. The additive mixtures are often company Intellectual property (IP). This means that researchers or new systems often are forced to rely on a material of which the constituents are unknown, hindering development on a broader and more open scale. Material producers and vendors will share some information, depending on the intra-company relation, but this level of access is typically only granted based on large investments.

Besides the quantifiable parameters, a range of process signatures is presented. These are the derived signatures of a combination of the parameters. All are related to the processability of polymer powder by laser irradiation, defining key considerations to be taken when designing and utilising polymer powders in laser processing. Each derived process signature is typically controlled by more than one parameter, enhancing the complexity. The diagram shown will be used for developing the methodology and requirements of materials and systems throughout this thesis.

### 4.1.1 Laser / Powder Interaction

During the LPBF process, the laser interacts with the powder bed, melting and fusing the powder grains into a solid. Three factors determine the interaction between the laser

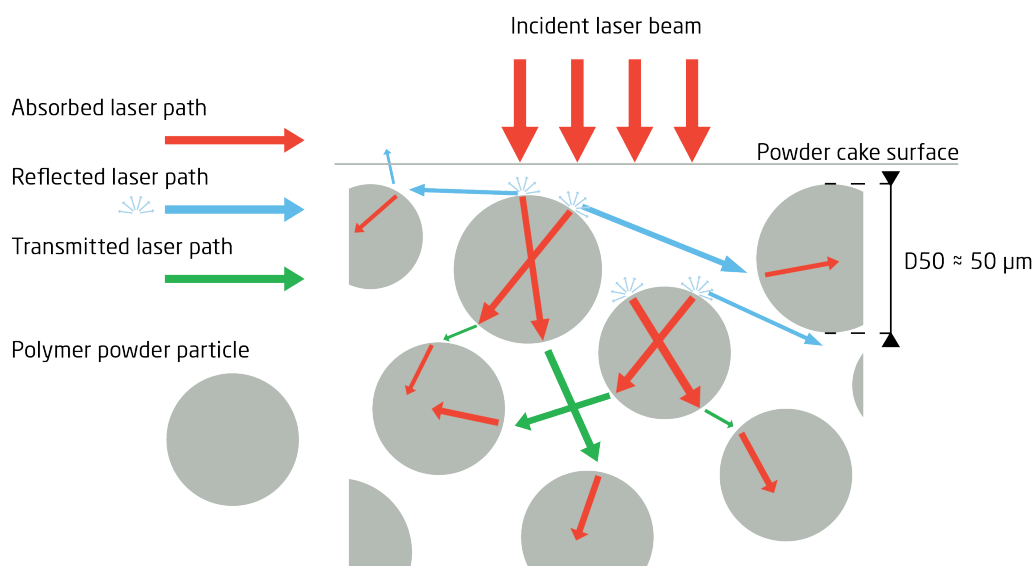


Figure 4.5: Laser-powder interaction, showing the incident laser beam, the absorption, the reflection, and the transmittance. The powder, the material, and the laser wavelength influence all these effects. Inspired from [14, 121]



light and the powder, as seen in Figure 4.5. First is reflection, the second is absorption, which is converted into heat, and the third is transmission [14, 122]. The three factors will determine how well the powder fuses into a solid. This fusion behaviour is described below in subsection 4.1.2, considering the binding mechanisms. Absorption influences heating the most, with good interaction between laser and powder material developing a greater heat output [122]. The absorption of light and, thereby, the energy input of a material is determined by the agitation frequency of the specific bonds in the compound [14].

The three interactions are affected by the state of the medium (i.e. solid, liquid, powder etc.), where powder shows a considerable interaction with laser light due to the large surface area-to-volume ratio [14, 123]. The powder size, especially the distribution, is critical when considering the laser powder interaction [121]. The larger powder will require more energy to melt based on its mass, whereas smaller powders can evaporate due to very high-power concentrations [124]. Ensuring a narrow powder size distribution aids process control and provides a more stable sintering and melting process. The melting and sintering process is depicted in Figure 4.6. In addition to energy absorption, it is worth noting that adjacent powder particles can collect transmitted energy, resulting in the heating of an entire zone instead of the localised heating of individual powder grains. Resulting in a Heat Affected Zone (HAZ) of the build plane, not limited to the exact location of the laser energy input. Moreover, the powder bed packing density influences energy absorption, with finer powders exhibiting greater effectiveness in light absorption due to their

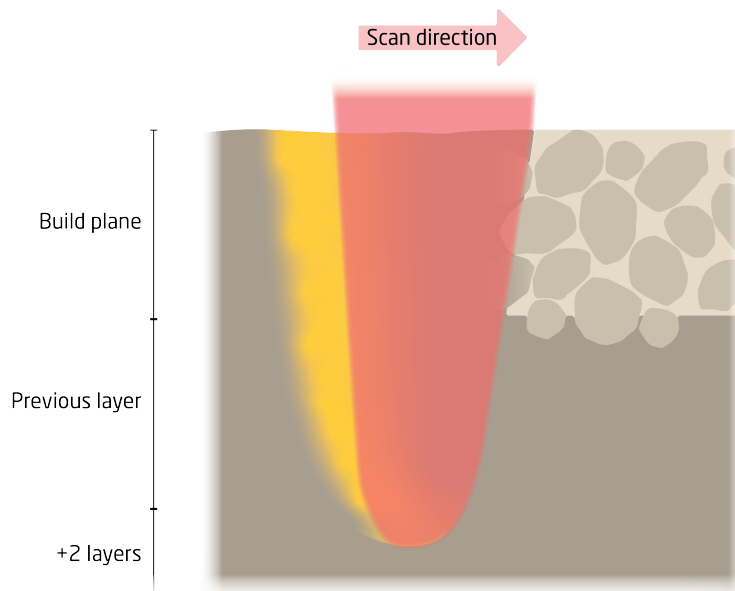


Figure 4.6: Laser-powder interaction and penetration, showing the incident laser beam and the melting behaviour. The penetration depth is determined by the laser power, powder transmission and surface area-to-volume ratio

larger surface area-to-volume ratio [123].

## Polymer Powder and Laser Interaction

Polymeric materials, such as Polyamides, are characterised by a significant presence of aliphatic Carbon-Hydrogen (C-H) bonds [125]. Another characteristic of PA's is the amide bonds, as seen in Figure 2.5. In the PBF-LB/P process, the interaction between the laser and the polymer molecules primarily involves compound agitation or vibration through bending or elongation modes [14] as seen in Figure 4.7. The molecular agitation modes are described further in subsection 4.2.4.

Figure 4.8, from [126], illustrates the frequencies of compound agitation of a PA11, describing the transmittance measured by an Fourier Transform Infrared (FTIR) analysis. The transmittance measurement is used for defining the chemical composition of a compound, by defining the wavelengths lost during light transmission. The decrease in transmission is a measure of the energy being absorbed in the sample rather than passing through it. In the PA11 sample tested, the transmittance decreases within the wavenumber range of  $700\text{ cm}^{-1}$  to  $1650\text{ cm}^{-1}$ , corresponding to the wavelengths of  $14.3\text{ }\mu\text{m}$  to  $6\text{ }\mu\text{m}$ . In PBF-LB/P, the most commonly used laser source is the  $\text{CO}_2$  laser, which typically operates at  $10.6\text{ }\mu\text{m}$  [33]. This wavelength aligns well with the aforementioned agitation frequencies, ensuring efficient and consistent energy absorption within the powder material. The efficient energy absorption is critical in PBF-LB/P when considering the very limited heating time for a powder particle during rapid laser scanning motions.

The time of scanning per powder particle ( $T_{ps}$ ) is influenced by three factors: The scanning speed  $S_S$  (mm/s), the powder particle diameter  $P_o$  (mm), and the laser spot diameter  $L_o$  (mm) with the relationship described by Equation 4.1 and in Figure 4.9, showing how the rapid scanning speeds influence the time for energy deposition in an individual powder grain. The curves show data for a sample material with a size distribution ranging from  $D_{10} = 0.022\text{ mm}$  to  $D_{90} = 0.079\text{ mm}$ , which is a common range for PBF-LB/P materials. The curves are constructed for a laser spot size =  $0.15\text{ mm}$ , similar to what is found in industrial PBF-LB/P systems, with some utilising much larger or smaller beams too.

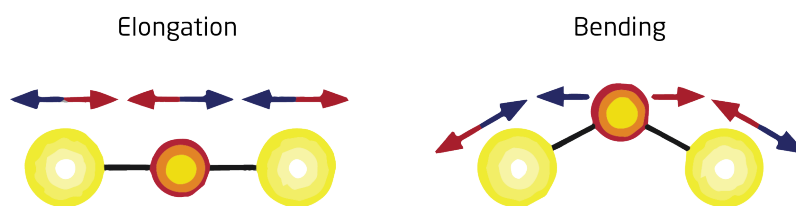


Figure 4.7: Oscillation modes of polymer molecules

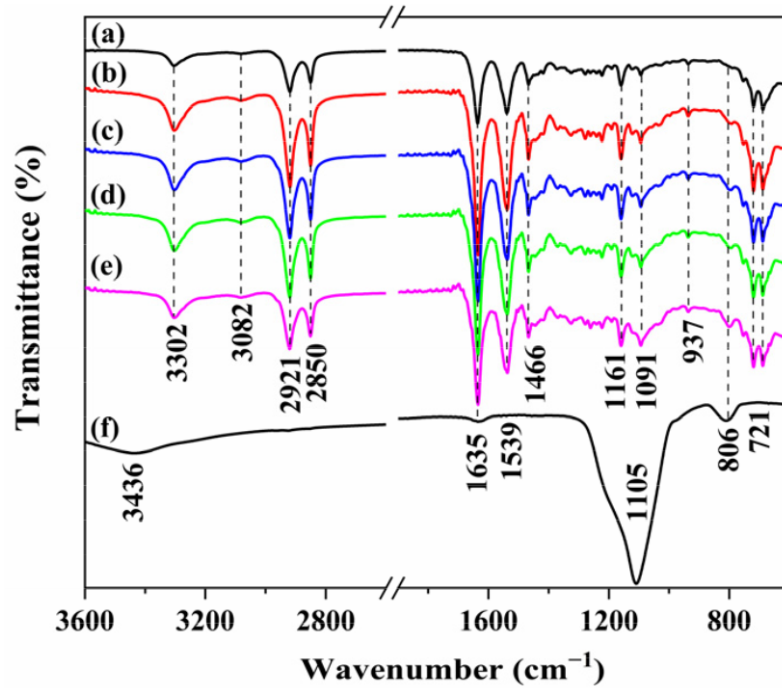


Figure 4.8: FTIR analysis of pure PA11 (a) and several other grades. From [126]

$$T_{ps} = \frac{P_o + L_o}{S_S} \quad (4.1)$$

The scanning speed plays a crucial role in energy absorption during material processing

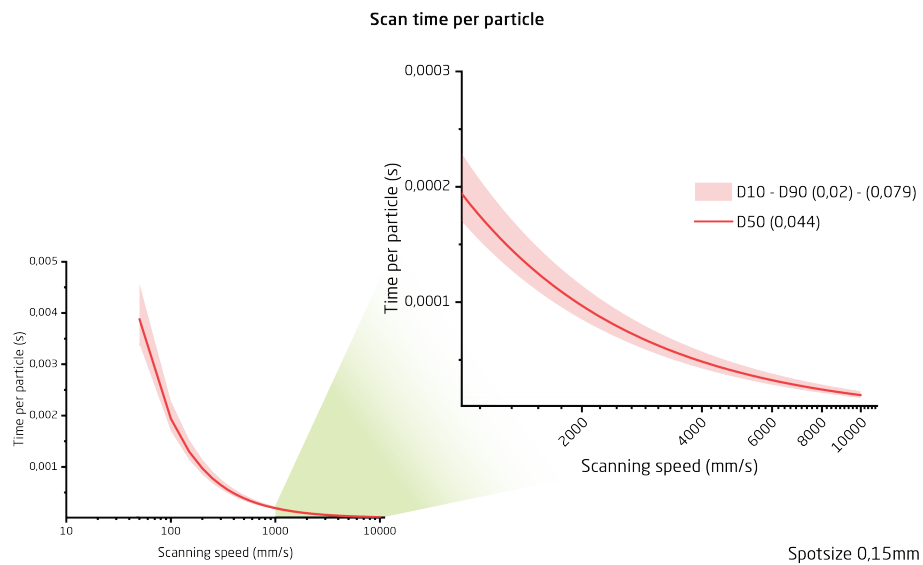


Figure 4.9: Correlation of scan speed, particle size, and laser spot size. Determining the time for an individual powder grain to absorb energy from laser radiation

and has been a significant focus of process investigations aimed at enhancing part properties [127]. The heating time for a powder particle is limited to  $64.7 \mu\text{s}$ , taking into account a median-sized particle, a scanning speed of 3 m/s, and a spot size of 0.15 mm. Considering the extremely short timeframe for energy absorption by the polymer powder, the interaction between the laser and substrate material becomes critically important. As mentioned, using a  $\text{CO}_2$  laser ensures effective absorption for polymers, particularly polyamide.

The energy absorption is rarely focussed down to a level of sintering or melting one single powder particle. The reason is the spot size and the penetration of energy in the shape of transmission and reflections, causing available energy below the top surface, as shown in Figure 4.5. Furthermore, the laser spot size in most systems is larger than any powder grain size utilised in the process, ensuring a sintering zone larger than the individual powder grains. A commonly used metric is energy density, described in detail below.

## Energy Density

Energy density, also known as the Andrew number, is one of the main parameters used in literature for conveying the energy input in the powder substrate [128, 129]. It is typically found in three variations, described in Equations 4.2, 4.3, & 4.4 [33, 130]. The three variations build upon each other, progressively developing the concept from energy density describing a line during the scanning process ( $ED_l$ ), to describing the scanned area ( $ED_a$ ), and finally expanding to encompass the volume of sintered material ( $ED_v$ ) during scanning [33, 124, 130]. All three variation includes the power  $P$  and velocity or scan speed  $v$ , which provides the line density  $ED_l$  as seen below in Equation 4.2.

$$ED_l = \frac{P}{v} \left[ \frac{\text{J}}{\text{mm}} \right] \quad (4.2)$$

Describing the energy delivery to a powder surface by one line, when considering the large area that is scanned, can lead to misjudgement of the required energy for stable material processing. To mitigate this and to normalise the value, an approach for describing the energy per area was developed [131]. For describing the area, the hatch distance ( $H_d$ ) was added to the Equation 4.3. The hatch distance can be the laser spot size  $S_S$  but is typically less due to the laser profile with less power in the sides of the laser spot when considering a Gaussian beam profile. An overlap is therefore often selected to some extent during LPBF processing [132].

$$ED_a = \frac{P}{v \cdot H_d} \left[ \frac{\text{J}}{\text{mm}^2} \right] \quad (4.3)$$

Further improvement in the transferability of the normalised energy density value is needed,

which has led to the development of the volumetric energy density. This considers the layer height ( $t$ ) deposited during processing, ensuring that the  $ED_v$  conveys the energy required for processing. This is especially helpful when considering 3D parts manufactured from powder. The  $ED_v$  is most used in scientific literature [130], proving the usefulness of this parameter. However, a one-to-one correlation between two different systems is rarely found when considering the same material and processing conditions. This is due to a large number of external influences on the processing, causing  $ED_v$  to be a metric that can be useful in conveying the needed energy for processing while not providing the entire story.

$$ED_v = \frac{P}{v \cdot H_d \cdot t} \left[ \frac{\text{J}}{\text{mm}^3} \right] \quad (4.4)$$

Another challenge associated with energy density is the existence of multiple ways to achieve the same energy density value. Since energy density is a composite metric that considers the most influential factors in the LPBF process, different approaches can yield equivalent energy densities [128]. One method involves utilising fast scanning speeds with high-power, while another involves slower scanning speeds with lower power, yielding the same energy density. Additionally, adjusting the layer thickness introduces another dimension where the same energy density can be achieved. The physical interaction of high-speed, high-power compared to low-speed, low power are very different. One will quickly force a large amount of energy into the powder bed. This can cause thermal degradation of the polymer itself, leading to lower mechanical properties and part instabilities. Whereas low power and low speed can lead to a lack of fusion and proper melting of the powder, causing unstable parts that lack mechanical properties [128, 131]. Consequently, energy density serves as a valuable metric for comparing similar experiments conducted on the same system. However, its applicability becomes uncertain when used in isolation without considering other pertinent processing parameters [123].

## True Energy Delivery to the Powder

Describing the true energy delivery in the powder differs from the energy density or the scan time per particle. A more comprehensive metric is needed since these do not consider beam shape and powder absorptivity. The energy density considers the energy delivery at the powder/atmosphere interface, lacking information on the energy absorbed in the powder causing localised heating. Gibson I. and Shi D. [132] developed a method for the fill laser power considering input needed for explaining the localised heating as seen in Equation 4.5.

$$P = \frac{v \cdot \rho \cdot L_s \cdot t \cdot [C \cdot \Delta T + L_m]}{1 - R} \quad (4.5)$$

The method by Gibson I. and Shi D. [132] considers the reflectivity  $R$ , which is the inverse of absorption, if no transmittance in the powder is assumed. It further considers  $\rho$  as density of the powder,  $C$  is the specific heat ( $\frac{J}{g \cdot ^\circ C}$ ),  $\Delta T$  is the difference between the initial and melting temperature in the process ( $^\circ C$ ),  $L_m$  is the latent heat of melting ( $\frac{J}{g}$ ). The true energy delivered to the powder is complex, with a large number of influencing factors to consider.

For metal laser welding, an approach was constructed that was later proved reliable in PBF-LB/M. This method is known as normalised enthalpy [133, 134]. The normalised enthalpy calculation defines the processing parameters for any metal powder processed by LPBF by incorporating material-dependant parameters that provide a value comparable with other materials, as seen in Equation 4.6. Any number greater than 1 for normalised enthalpy defines melting behaviour. Forien J. et al. [135] reported on the increase of normalised enthalpy and related this to a signal from a pyrometer, determining the breakdown level of the process from the pyrometer signal. This, is in good correlation with the report of Gullipalli C. et al. [136] showing increased porosity above the melt pool stability zone. Ghasemi-Tabasi H. [134] has shown for metals how three different materials, processed at similar normalised enthalpy values, produced parts with a consistent melt pool width and depth, leading to part properties expected from traditional metal processing found in PBF-LB/M. Ghasemi-Tabasi H. [134] plot the normalised melt pool depth  $\bar{d}$  (Equation 4.7) and normalised enthalpy  $\frac{\Delta H}{\Delta h}$  showing how the melt pool depth is dependent on the normalised enthalpy, proving the excellent correlation between the two.

$$\overline{\Delta H} = \frac{\Delta H}{\Delta h} = \frac{\alpha P}{\rho (C\Delta T + L_m) \sqrt{\pi\omega^3 v D}} \quad (4.6)$$

$$\bar{d} = \frac{d}{\omega} \quad (4.7)$$

In the normalised enthalpy calculation, several new terms are presented for calculating the metric comparable across LPBF systems. Here  $\alpha$  is the absorptivity of the bulk material at the laser-specific wavelength,  $\omega$  is the laser spot radius ( $mm$ ), and  $D$  is the thermal diffusivity ( $\frac{mm^2}{s}$ ). The normalised melt pool depth considers factor  $d$ , which is the melt pool depth ( $mm$ ). Equation 4.6 assumes the beam shape of a Gaussian beam producing a circular spot anywhere in the build plane. This behaviour is well established for collimated laser beams focussed by an F-theta lens typically used in LPBF systems [137]. The equation considers the absorptivity in the material, with the consideration of the energy delivered to the powder and not the powder/atmosphere interface as seen for the other methods in Equation 4.1 and Equation 4.4. The method of normalised enthalpy is generally accepted in PBF-LB/M. It is used as a metric for broadening the understanding of the desired processing parameters but is still not used as widely as the volume energy density.

The method of normalised enthalpy is not used broadly for PBF-LB/P. Starr T. et al. [138] presented a similar idea for polymers designating this as the energy-melt ratio. The energy-melt ratio considers some of the same input parameters from normalised enthalpy (Equation 4.6) as shown in Equation 4.8 for the energy-melt ratio. The major difference is the consideration of volume energy density instead of the absorbed energy. This leads to an assumption of complete laser absorption in the processed volume of the powder [139]. This assumption holds true for polymer processing by adequate laser sources, such as CO<sub>2</sub>. However, when investigating fibre lasers with limited absorption in the polymer, this metric is doubtful and does not provide a more detailed picture of the process compared to the volume energy density.

$$EMR = \frac{E_a}{E_p} = \frac{\frac{P}{y \cdot v}}{[C_p \Delta T + L_m] \cdot (\rho)(\phi) \cdot t} \quad (4.8)$$

Equation 4.8 considers the powder packing ratio needed for the correlation to volume energy density. The results presented by [138] prove that the energy-melt ratio is beneficial for structuring the dissemination of required energy for good melting and consolidation properties in the PBF-LB/P process. It is reported that, similarly to the normalised enthalpy, proper polymer processing does not occur before an energy-melt ratio of 1. The study's results show an increase in mechanical properties until an energy-melt ratio of 3 [138]. However, it is not reported for greater values, leading to a missing conclusion of the breakdown level of the energy-melt ratio for the process.

This literature survey did not find any examples of utilising normalised enthalpy for disseminating the PBF-LB/P process. This can be due to the issue in identifying the specific modes during manufacturing, differentiating between conduction and keyhole mode, which are easily identifiable in PBF-LB/M [133]. Identification of these two modes is necessary to classify the melt pool and the manufacturing mode. However, these are not the same in polymer production due to the small  $\Delta T$  supplied during production and no crystallisation due to the elevated temperature of the powder cake.

## Laser Processing of Polymer Powder

The PBF-LB/P process of laser-powder interaction is complex with several influential factors as described above. Williams J. and Deckard C. [140] developed a model for considering these factors, mainly focussing on the laser input at the powder-atmosphere interface. The issue is the lack of information concerning the laser interaction with the powder, as mentioned above.

An illustration of the influential factors for true energy delivery has been based on William J. and Deckard C.'s model on laser powder interaction. The model incorporates the laser powder interaction, ensuring a broader picture of the processing conditions as seen in



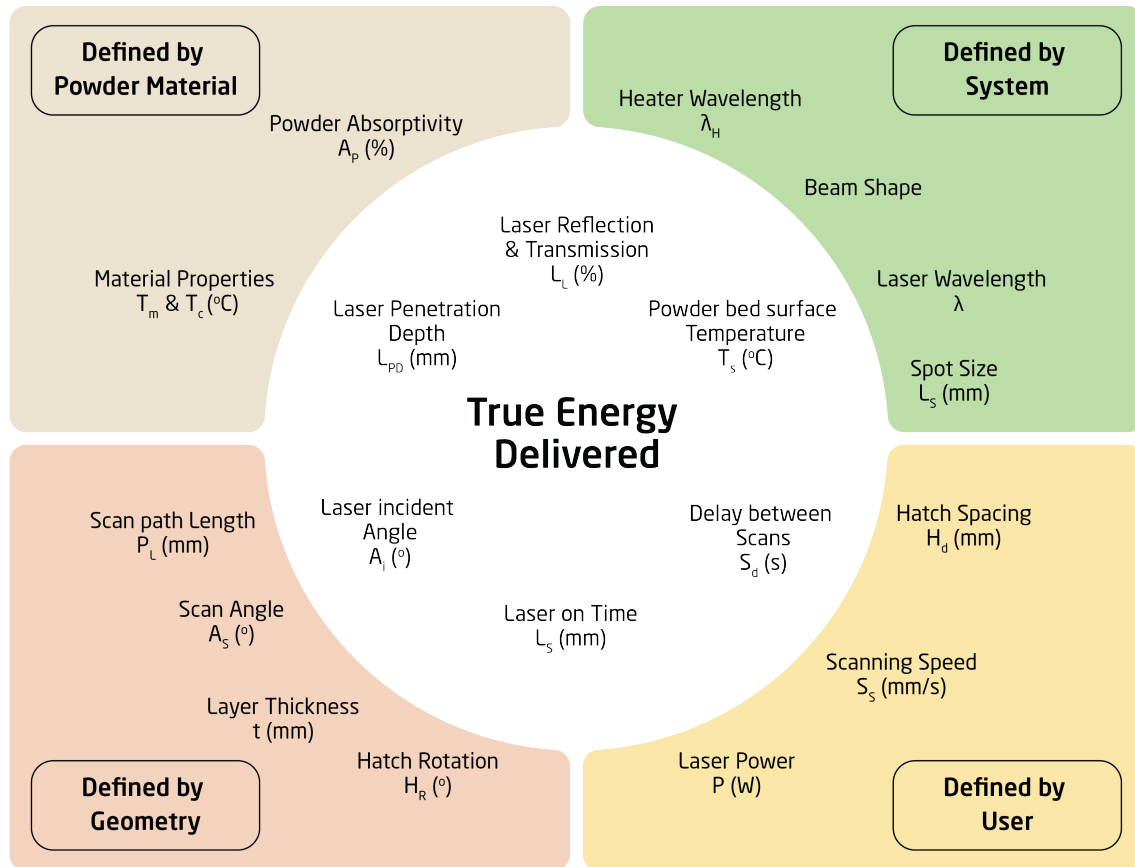


Figure 4.10: The laser-powder interaction. Considering the major influences during LPBF processing

Figure 4.10. Each corner of the model represents a system that defines the underlying factors of the laser powder interaction. Ensuring homogeneity among all aspects leads to a stable laser-powder interaction, thereby facilitating consistent powder consolidation that is beneficial for production purposes.

The individual parameters around the circle in the illustration influence different derived signatures of the process. The parameters and especially the process signatures are often considered when discussing the resulting powder processing, as seen above for the normalised enthalpy and energy density discussion. However, both of these do not convey all the relevant parameters or signatures. Therefore, each parameter and the derived process signatures are explained in Table 4.3. The quantifiable parameters and derived process signatures presented in Figure 4.10 are not an exhaustive list of the influential factors during processing but comprise an overview of the dominant factors. Goodridge R. et al. [131] reported on the different controlling parameters for stable PBF-LB/P processing. Here it is concluded that an elevated level of process control is needed for the successful implementation of the AM technology. Since the publication by Goodridge R., several improvements have been made. However, an explanation and further development are



Table 4.3: Influential parameters for the PBF-LB/P process considering the laser-powder interaction

Delay between Scans	$S_d$	The hatch profile of a geometry requires several passes to complete the entire geometry. Ensuring an appropriate time between consecutive scans is important to not let the powder cool for an extended amount of time before reprocessing.
Laser on time	$L_s$	The laser on time is critical when considering the amount of energy delivered for an entire layer during a build process.
Laser reflection and transmission	$L_L$	The amount of laser energy lost due to the reflection or transmission. Transmission of energy further into the powder bed will contain the energy but is scattered in the powder bed. Reflection is lost in the machine.
Laser incident angle	$A_I$	Depending on the scanning location and the material's absorptivity, some laser energy will travel into the powder bed. Suppose the scanning location is off-centre, considering the beam travel. In that case, it causes an incident angle which causes any energy transmitted to not go into the layer below but travel into the powder bed, depending on the geometry.
Laser penetration depth	$L_{PD}$	The laser penetration depth considers how far the laser energy will travel into the powder bed. This is a desired behaviour for layers built on top of the geometry, ensuring fusion between the new and previous layers. This is to be minimised in the empty powder bed, ensuring less part growth and bad down skin behaviour.

still needed.

The model presented will be developed throughout the study to encompass the most relevant parameters when processing polymer powders by laser. The further development relies on the physical interactions occurring in the PBF-LB/P, which is described below considering the binding mechanisms for powders.

#### 4.1.2 Binding Mechanism in Powders

A common trade between all the various materials used in LPBF is the fusing of particles by laser radiation. This binding mechanism varies between the material groups and how the processing is carried out concerning the laser irradiation, powder material, and composition. The fusion of two particles can be described by the capillary forces developing during material flow between two particles as described by Dörmann M. et al. [141]. The most prevailing binding mechanisms in LPBF are solid state sintering, chemically induced binding, liquid phase sintering, and full melting [15, 142].

## Solid State Sintering

The process of Solid State Sintering is accessed when heating a powder material to just below the melting temperature of the material, allowing the outer most surface of the powder particles to start chemical diffusion between one another [15, 142]. This diffusion behaviour is allowed by the increased mobility of molecules at elevated temperatures. The phenomenon is typically observed between the melting temperature  $T_M$  and down to half of  $T_M$ , leading to the reaction persisting for the duration of the processing. This is especially true in the case of PBF-LB/P due to the elevated temperature in the build chamber and powder cake. This effect causes uncontrolled part growth during processing, caused by the diffusion and adhering effect of the surrounding powder to the processed part [15]. Solid State Sintering cannot produce fully consolidated parts due to the thermal input, not allowing complete melting of the individual powder particles. The mechanism at the elevated temperature is diffusion controlled and does not allow low enough viscosity for the powder particles to minimise the free surface energy to a point of full coalescence. Instead, this leads to a network of particles with gaps between them, as shown in Figure 4.11. Solid State Sintering occurs by lowering the free energy by a flux of atoms or molecules replacing the void between two adjacent particles leading to neck formation and particle growth [15, 142].

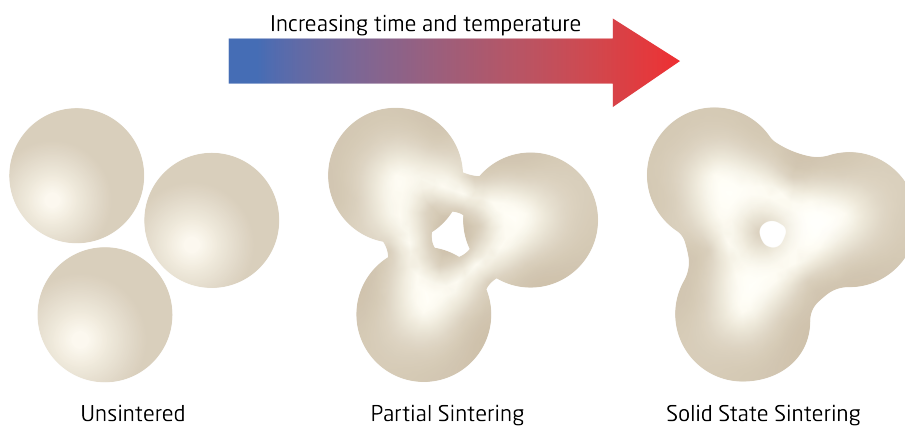


Figure 4.11: Stages of Solid State Sintering. Temperature and time increase from left to right, seeing the neck growth in the middle and the sintered particles forming a smaller porosity in the centre

## Chemically Induced Binding

Chemically induced binding is used mainly for the reaction of ceramics. Here a reaction with either the powder constituents or the processing atmosphere can introduce a new molecular structure of the original powder components. The reaction is triggered by heat, causing the powder to become one part [142]. As mentioned above, an example of direct ceramic manufacturing by chemically induced binding is by Zhang X. et al. [58]. The

research group produced a high entropy carbide ceramic proven reliable by the chemical binding of the constituent powders.

## Liquid Phase Sintering

Liquid Phase Sintering is often seen in composite systems, where a discrete binder is present for fusing particles that do not show the desired melting behaviour at the process temperature as described above [43, 142]. The binder material can be present in different stages in the powder, as seen in Figure 2.10. The binder typically has a  $T_M$  lower than the other powder constituent, allowing only one material to melt and wet the other, producing a sintered geometry. Liquid Phase Sintering is not only used for manufacturing composites for later processing, such as green parts needing subsequent debinding and sintering steps. Composite materials based on polymers with an additive component for increasing mechanical properties are also classified as Liquid Phase Sintering. The additive used is typically glass beads or carbon fibres, as mentioned above.

Another case of Liquid Phase Sintering is often attributed to PBF-LB/P. The commercial name Selective Laser Sintering (SLS) stems from this based on the outer shell of the powder grain melting and sintering to the surrounding powder but leaving a core of unmolten polymer, resembling the original crystal structure prior to sintering [142]. This can be seen in Figure 4.12, where the first peak is due to a change in the crystal structure of the polymer caused by laser sintering. While the second peak correlates with the  $T_M$  of the

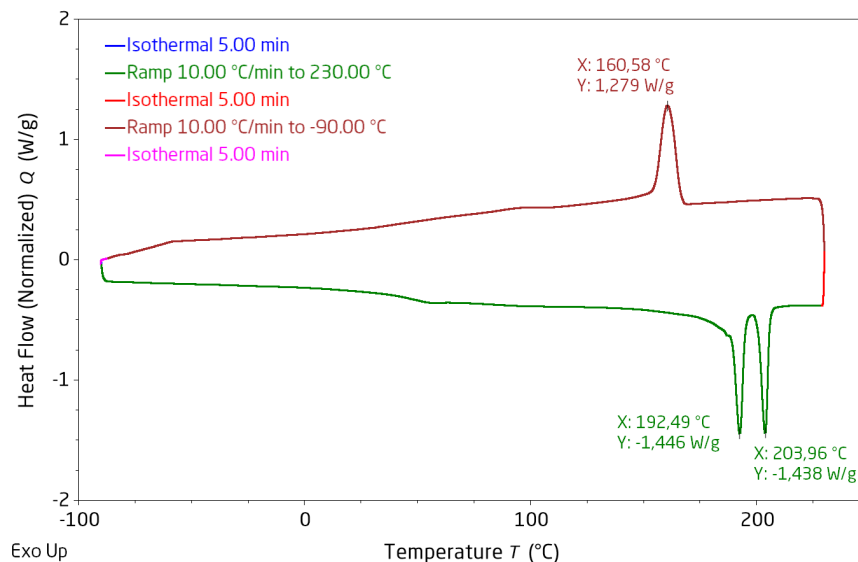


Figure 4.12: Two distinct melting peaks can be identified, one correlating with the original DSC analysis of the unsintered powder and one that shows a change in the molecular structure causing a lower melting temperature. The change in the crystal structure is evidence of prior melting from the manufacturing process of PBF-LB/P

original polymer powder as received from the manufacturer. This effect is especially evident in a combination of Solid State and Liquid Phase sintering, where powders fused to the side walls of a component experience a mix between the two methods.

## Full Melting

Full melting during LPBF processing is often associated with metal powder processing. However, polymer powders can also achieve full melting from laser processing [142]. Full melting of the manufactured part is essential when mechanical properties are the central focus. For polymers, this often incurs the need to raise the process temperature for a longer duration, inducing Solid State Sintering of the surrounding powder, as mentioned above. This causes part growth and an increase in final surface roughness. To mitigate this, a middle-ground approach is often selected [15]. This means defining the process temperature and duration that produces the desired mechanical properties with minimal part growth and surface defects. Leading to the final processing by PBF-LB/P often being a mix between Liquid Phase Sintering, Full Melting, and to an extent Solid State Sintering.

Full melting of polymer powders allows for the true interaction between the polymer molecules initially situated in the individual grains. When providing sufficient heating for an extended duration, chain mobility is increased. This increased chain mobility lowers the viscosity of the polymer significantly, allowing the powder to start flowing and coalesce. This flow and enhanced chain mobility allow the molecules to cross between the powder grain borders developing a denser component with better mechanical properties. The effect is caused by the desire to create a system of lower surface free energy by producing a larger grain with a greater surface-to-air ratio [143]. The molecular motion and diffusion are exemplified in Figure 4.13.

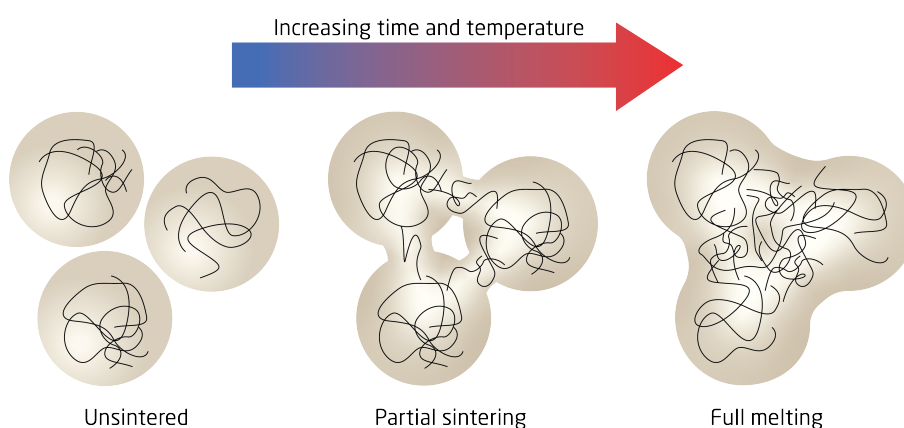


Figure 4.13: Full melting behaviour in polymers ensuring a stable network of the macromolecules due to temperature-induced mobility

## 4.2 State of Polymer LPBF Systems

The Laser Based Powder Bed Fusion of Polymers (PBF-LB/P) process was described initially as *"a three-dimensional computer output tool"* by the inventors at the University of Texas Austin [144]. The initial reference to the process can be traced back to the comprehensive exposition provided by Deckard C. and Beaman J. in their seminal work (Deckard & Beaman, 1988)[144], wherein the authors clarify the intricacies of the process. As explained in section 2.1, the process cycles through 5 steps, layer-by-layer, to produce the desired geometry in the powder bed as shown in Figure 2.2 reprinted here in Figure 4.14.

A combination of sub-systems dominates the philosophies of the commercially available PBF-LB/P systems. All allow a laser to scan the build plane of the powder cake, producing the part layer-by-layer. The difference is mainly seen in the laser source, the powder feed mechanism, and recoating system, as seen in Figure 4.15. The laser source, as mentioned in chapter 3, is commonly the CO<sub>2</sub> laser, with some variation in the industrial systems presented. The powder feed system is either a top feed or a bottom feed approach. Finally, the recoating system can be functionalised in several different ways, either by a wiper/blade, roller or a combination. The two figures 4.15a and 4.15b show two example configurations and some of the features found in industrial setups. Looking into Figure 4.15a, which shows the top feed method and a blade recoater. PBF-LB/P systems can be constructed in a variety of combinations, with the two presented as possible options. The systems illustrated are thus not comprehensive and locked to these configurations. All the individual subsystems are described below, with an explanation of their importance and impact on the final part quality.

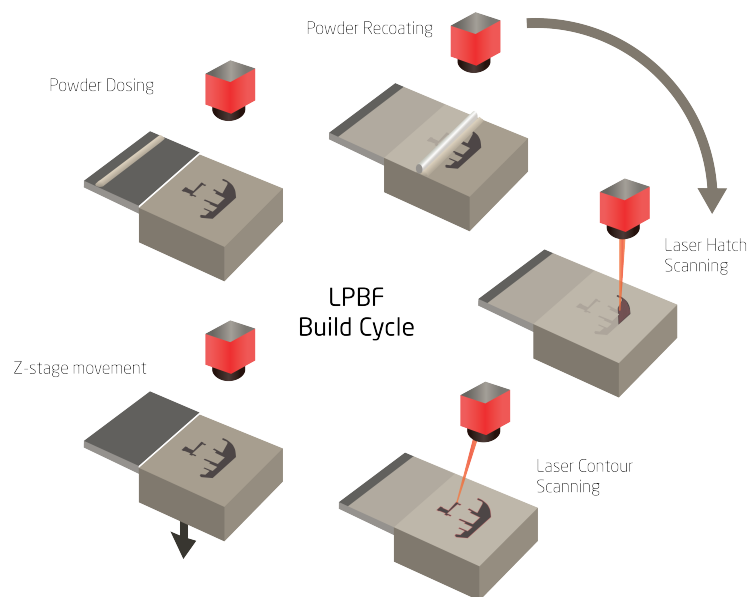
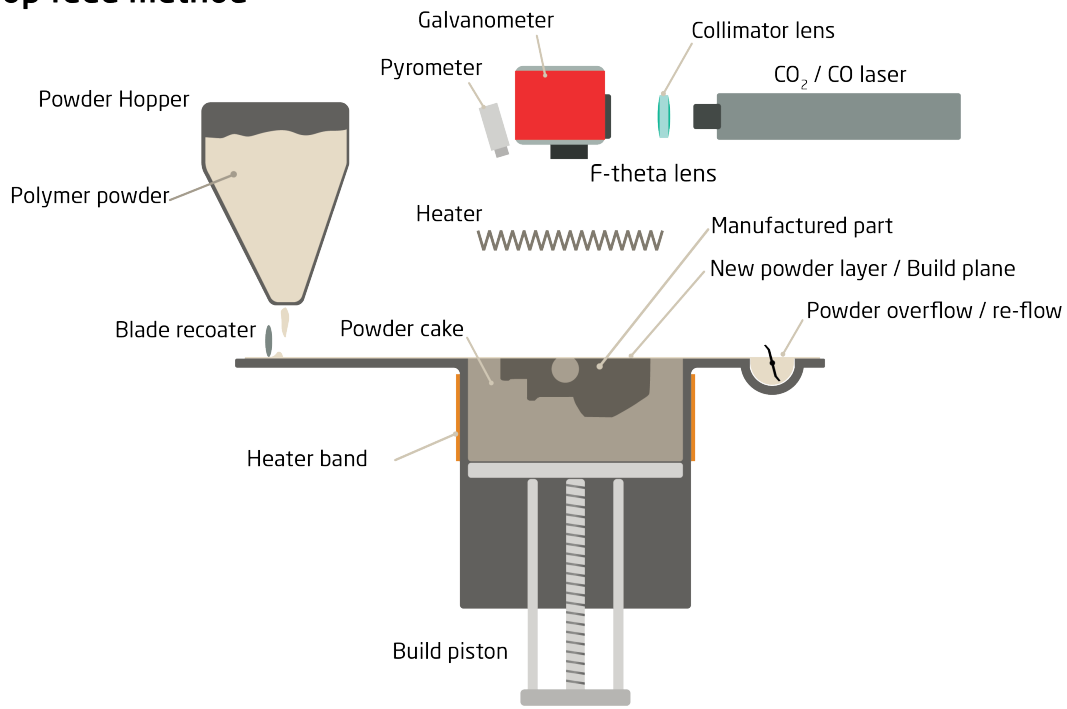


Figure 4.14: The process steps for the Additive Manufacturing cycle of Laser Powder Bed Fusion (Reprint of Figure 2.2)

### Top feed method



### Bottom feed method

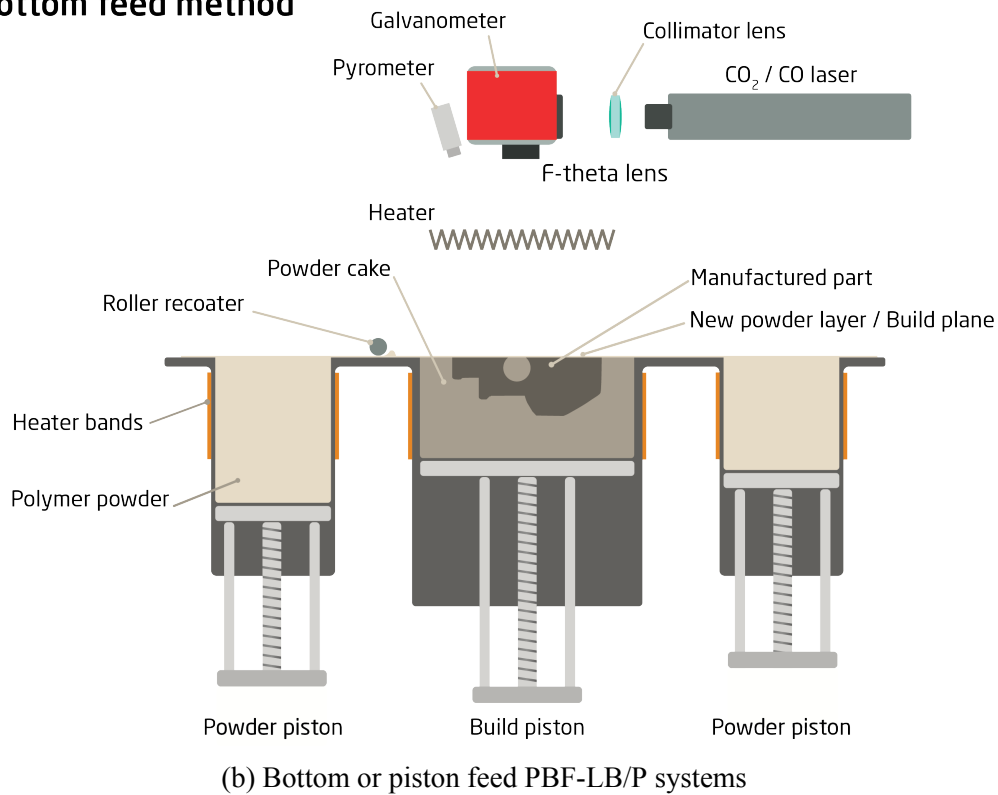


Figure 4.15: The major components in the two dominant architectures for PBF-LB/P systems

### 4.2.1 System Components and Configuration

A deep understanding of the integral systems, sub-systems, and configurations utilised in PBF-LB/P is critical for the repurposing and further development of the processing equipment when introducing a new laser source. To obtain this knowledge, an investigation of each sub-system and its influence on the final part is carried out. Below, the critical sub-system is described, presenting the state of the art for each. The in-depth knowledge and understanding are utilised for the further development of the system described in chapter 5 and on.

#### Recoater Design

Recoating systems are designed to distribute an even layer of powder onto the powder cake, producing the new build plane. The newly distributed build plane aims to cover the entire powder cake to be free from scratches, or other defect areas, typically identified by excessive surface roughness. As well as ensuring a high degree of packing, increasing the powder cake density [14]. The recoating system controls the density of packing in the powder bed, the flatness of the build plane (i.e. corner to corner/side to side), and the surface topography, which all directly influence the manufactured parts [145]. The powder material and flow properties also strongly influence the powder bed quality, so a need to consider the mechanical system and the powder feedstock is important [146, 147]. Here the major focus is on the mechanical recoater and its influence of this. The flowability and recoating-related material properties are discussed in subsection 4.1. The two dominant recoating systems are shown in Figure 4.16 with the additional types/geometries or movements for the individual types [145, 148].

A common problem during recoating is either short feed, where too little powder is dispensed, not covering the build plane or dragging of components or powder agglomerates, which scrape the surface, removing the powder from the build plane. Short feed is not within the control of the recoating system but is mainly influenced by the feed mechanism, as described below. The recoating system affects the dragging of particles or agglomerates, causing the same challenge as short feed. Both issues infer a lack of fresh powder covering the build plane, leading to double laser exposure for areas of the manufactured parts lacking powder as shown in Figure 4.17 [149]. The problem is worsened by the fact that during the next layer recoating, a double layer thickness of powder is distributed in these areas.

Figure 4.16 show the two dominant recoater configurations found in industrial and research systems for PBF-LB/P processing. Wiper recoating types utilise a stationary blade which can utilise different geometries depending on the recoating profile material and powder properties. The profile of the wiper determines the contact zone with the powder cake and build a plane, which controls the quality of the build plane post-recoating.

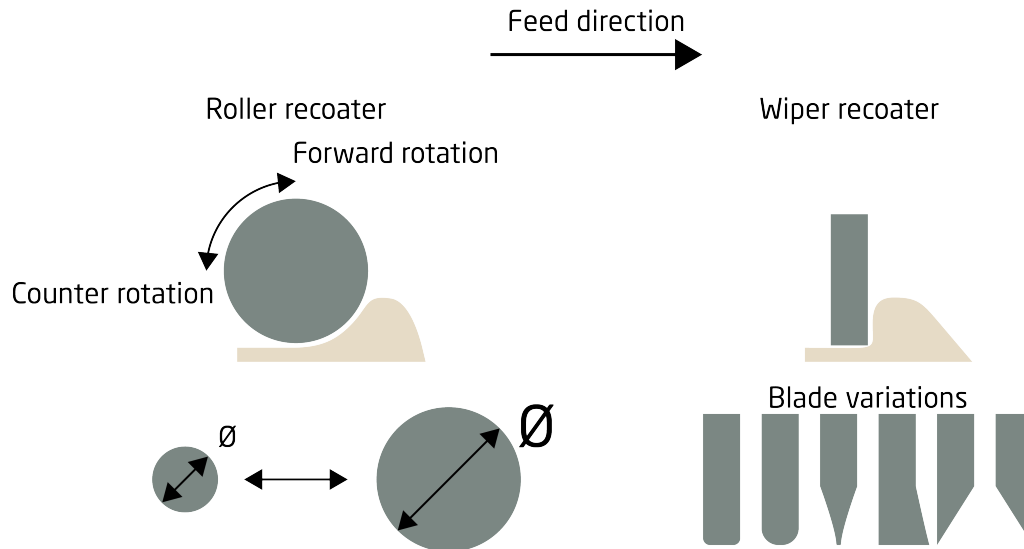


Figure 4.16: Recoater types for PBF-LB/P

Haeri S. [150] modelled the influence of the blade geometry considering three parameters determined to have the greatest impact on the build plane quality. The three geometry parameters are profile thickness, height, and shape. Considering a mixed PEEK polymer powder with a number of realistic powder shapes in the mix, a discrete element model was produced to find the optimal geometry of the blade. The optimal geometry for the modelled powder and velocity is a narrow blade with rounded edges. The blade must have a curve and a flat area to produce the highest quality build plane, as seen in the first blade variation from the left in Figure 4.16. The thickness of the blade is critical to allow for compaction, increasing the powder cake density [150]. The flat area of the wiper is further supported by Beitz S. et al. [151], proving experimentally that the larger flat area ensures even packing, a uniform surface, and a greater powder cake density. Miao G. et al. [145] conclude that wiper recoating systems are ideal for spherical powders with a narrow particle size distribution when the correct geometrical design is selected, due to the low complexity of the system, however for more complex shaped powders other methods can prove more reliable.

Roller recoaters are recoating systems that allow for a rotational motion during the traverse movement of the recoating gantry. The roller, typically a metal rod, has three modes of operation being; controlled for movement in two directions, with a third mode of being stationary (resembling a wiper blade). The roller movement can either be in the forward direction, which will compact and force the powder into the powder cake, or in the counter-rotating direction[152], which will cause an avalanche effect of the powder in front of the recoater. The diameter of the roller influences the powder cake density and packing. Zhang J. et al. [153] found by discrete element simulation that a larger roller diameter will ensure an increased density while lowering the standard deviation leading to a more stable



process. The work was done considering a counter-rotating roller and a ceramic powder. The larger diameter of the roller causes a larger compression zone with a larger number of particles, enhancing the contact forces in the powder cake and increasing the density. The avalanche effect caused by the counter-rotating roller is known for ensuring good flow in the powder before packing it into the powder cake. This assists rougher particles to produce build planes with low surface roughness, typically free of defects. This is due to the increased contact area of the counter-rotation, favouring a constant rearrangement of the powder in front of the roller. The continuous avalanche motion encountered by the counter-rotation can cause particle size segregation with more rapid deposition of the smaller particles by the counter-rotating movement, as concluded by Wang A. et al. [148].

Forward rotation recoaters have been studied by Beitz S. et al. [151], showing how initially, an increased packing density of the powder cake can be achieved. However, the forward motion incurs issues, with the spring back of the build plane caused by an elastic response in the powder cake [145]. There is also a possibility of the material sticking to the surface of the recoating roller, which drags out particles or agglomerates of the build plane, caused by the powder being sticky at elevated temperatures above the ( $T_g$ ) of the powder material [151]. This creates craters in the build plane resulting in low quality with large surface roughness. One way to improve the quality of the build plane and powder cake by forward rotation is by mixing the two modes of roller operation. This means first passing the powder cake using the counter rotation mode producing a pre-spread layer that can be post-processed. Once at the end of the build plane, the feed direction reverses, with the rotation staying the same. This will cause the forward rotation of the roller to pack the newly distributed layer to a larger degree [145]. Having multiple rollers on one gantry can complete the pre-spread and final recoat in one motion, which is typically desired in the industry to keep the productivity of a PBF-LB/P system high.

Recoating devices can also incorporate vibration modes to increase the powder cake density further than what is possible from a blade or roller. Studies have only been conducted for metal powder [145], which is why no further explanation is described in this thesis.

Studies have been reported on the build plane quality, considering the type and function of the recoater, as mentioned by Miao G. et al. [145]. Finite or discrete element modelling is the most widespread investigation method. Haeri S. et al. [154] report through discrete element modelling that the build plane is significantly improved by using a roller recoater when investigating non-spherical powders. This is related to the contact dynamics of a roller and the powder cake. The same study also concludes how the recoating traverse velocity on the build plane diminishes the build plane quality. Higher speed causes quality to deteriorate. This is supported by Chen H. et al. [152], with the experimental findings of increasing surface roughness and decreasing powder cake density for a counter-rotating roller recoater processing 316L stainless steel powder. Based on this, a lower traverse

Table 4.4: Influential parameters for recoating quality considering a roller recoater acting in the counter-rotation mode

Layer thickness	The potential powder cake density is directly linked to the layer thickness. Utilising a layer thickness close to the average powder particle size, it has been proven that the largest fraction of powder is dragged away from the powder bed leading to a lower density. However, using a layer thickness greater than twice the average powder particle size also causes deterioration in the density. Selecting an adequate layer thickness to comply with the powder particulate size is thus important and directly influences the powder cake density. This trend is true for investigations considering the multilayer approach, which is found most relevant by the author.
Rotational velocity	The rotational velocity by the counter-rotating roller drives the avalanche behaviour of the powder during recoating. Meyer L. et al. [155] developed the idea of total surface velocity, considering the effect of the recoater traverse velocity and the counter rotation in one parameter. Linking these parameters can produce greater packing densities than when considered individually.
Particle size	Particle size influences the recoating behaviour by agglomeration for very fine particles and segregating in mixes, especially during counter-rotation roller recoating.
Particle shape	The shape of the powder is important for ensuring a high-quality powder cake and build plane. The counter-rotating roller will allow even very coarse powder to be recoated due to the roller rotation, ensuring a stable avalanche motion during recoating.

velocity of the recoating system is desired. This conflicts with the interest of production speed, where a middle-ground approach of the quality of the build plane and traverse velocity is considered.

Several factors determine the powder cake density and the build plane quality, with the traverse speed being one dominating factor. The other main elements, described by Miao G. et al. [145], are presented in Table 4.4. The table concludes on the effects of a roller recoater acting in the counter-rotation mode since this configuration and operation mode is deemed the most versatile based on the findings presented above.

The majority of industrial systems include a bi-directional recoating system. This permits greater production speeds due to minimal time spent for recoating but adds complexity, especially for roller recoater systems. The complexity is dependent on the powder feed system, as described below.

## Powder Feed System

The powder feed system or dosing mechanisms shown in Figure 4.15 are the top and bottom feed versions, which are the most common configurations found in industrial machines. The primary purpose of the feed system is to ensure adequate powder dosing for each layer, to avoid short feed, where too little powder is dosed, as seen in Figure 4.17, not covering the build plane. If a short feed occurs for a layer during manufacturing, the laser will scan uncovered parts of the geometry. This causes previously sintered powder to be re-processed by the laser, causing part growth and polymer degradation due to excessive heating [149]. It can further lead to delamination in subsequent layers caused by too low volume energy density to fully consolidate the thicker layer [40].

Top dosing systems require powder to be stored above the build plane. Here a dosing mechanism release powder onto the build plane for recoating. The accuracy and the system configuration determine the level of accuracy desired for dosing. If the system has one-way recoating and a powder dump, then the required dosing accuracy is increased due to the potential material loss. If the system configuration is a two-way recoating system with a powder reflow, the dosing accuracy can be lowered since the material is maintained in the build chamber, as seen for both systems in Figure 4.15. Figure 4.18 shows a one-way recoating system with the top feed configuration. Any excess powder dosed for a layer will be discarded in the overflow to be reused during the powder refresh cycle.

The top feed powder hopper can be heated to minimise the temperature difference between the powder cake and the newly distributed build plane. Fish S. [156] describes that heating the powder minimises the temperature gradient, which decreases the residual stresses in the new layer and the final part. Pre-heating of the powder is common in the bottom-feed configuration, as seen in Figure 4.19. Here a heater band can be fitted to the powder pistons, heating the powder prior to recoating.

Bottom-feed dosing systems typically require the same level of control as the build piston. One or two powder canisters are fitted on either side of the build platform. The powder

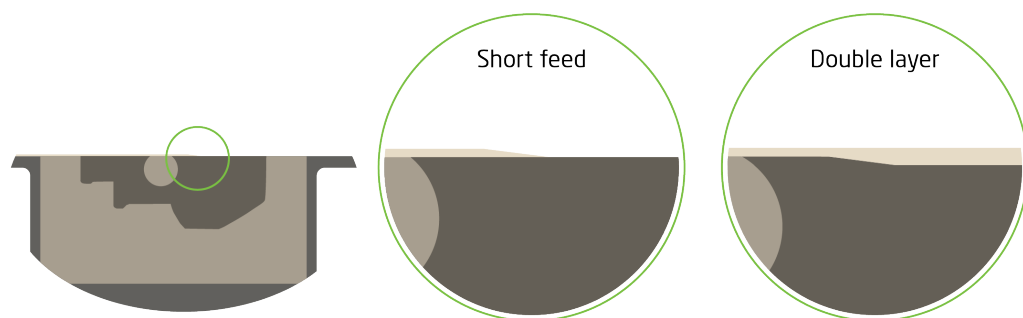


Figure 4.17: Powder short feed of a layer during production leading to double layer height in the next layer deposited

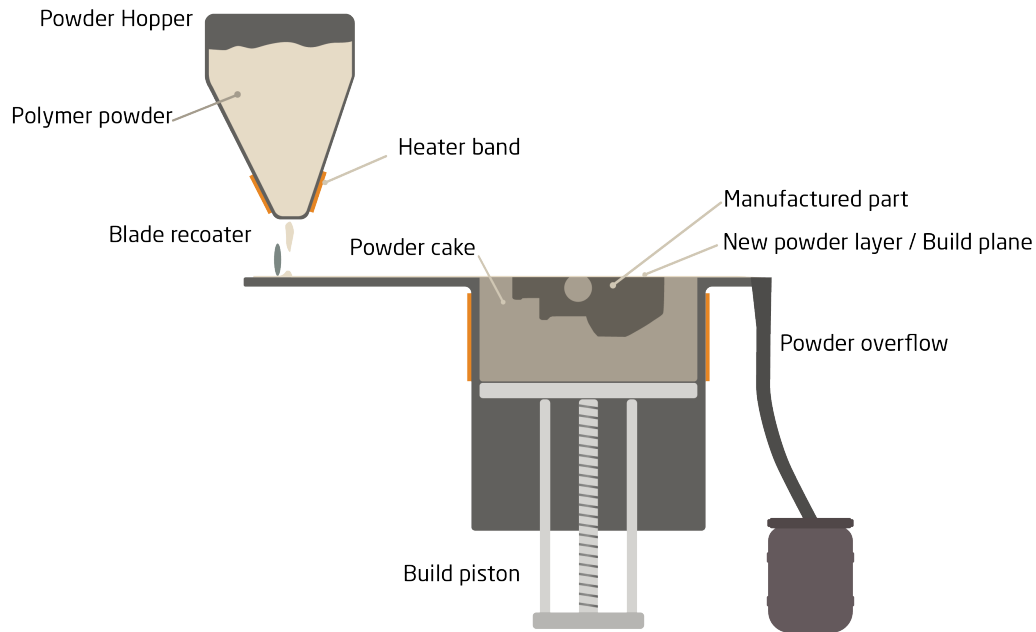


Figure 4.18: Overflow location for excess powder in one-way recoating

piston shown in Figure 4.19 moves up, exposing the volume of powder needed for recoating one layer. The recoating motion will sweep the powder across the powder cake, leaving the new build plane. After the build plane has been produced, excess material can either be collected in the opposite powder piston if the piston movement leaves a space, or the excess powder can be swept to an overflow bin. The powder piston located opposite the feed piston will have slight contamination from the build plane deposition. However, this is negligible considering the typical mixture of 50/50 new and old powder used in industry [157].

The two powder feed systems described above are examples of what most industrial systems utilise. More complex feed systems are being developed, which mix the powder feed

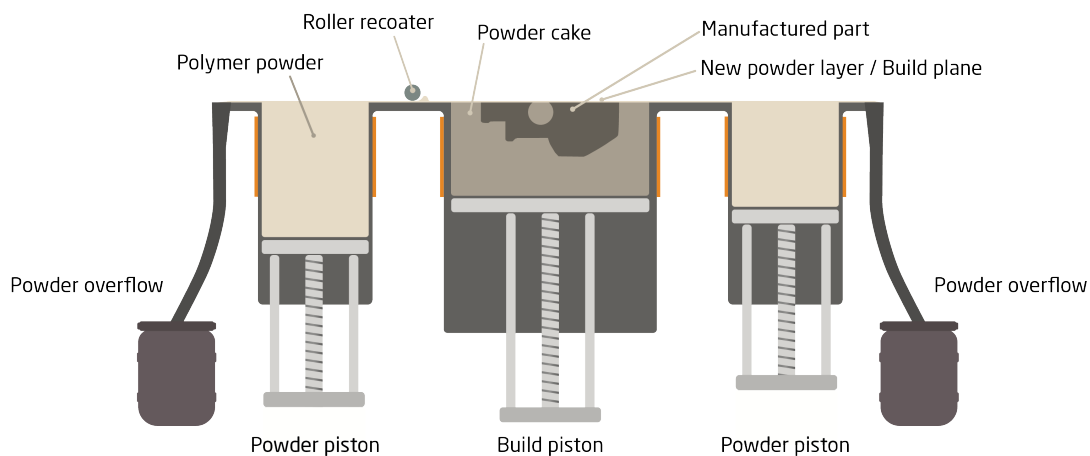


Figure 4.19: Overflow locations for excess powder in two-way recoating

and recoating system into one. Typically this is done to allow for selective deposition of powder, which can be utilised when considering multi-material productions, as shown by Tamura A. et al. [158]. This system uses a film for transferring powder particles from a carrier bin to the build plane. Then powder particles are selectively deposited on the substrate by laser irradiation from the back of the film, releasing the particles onto the substrate. Another approach is from the company Aerosint, where two or more perforated drums can deposit single powder particles in an array of pixels on the build plane [159]. The number of drums determines the number of materials possible to employ in this process, which acts as an add-on for a PBF-LB/M system where it can be implemented. The implementation is determined by the access level for modification of the system, with some industrial systems not allowing for this implementation. The focus of research by Aerosint has originally revolved around two or more component metal systems. However, the system is stated to handle most materials, including polymer powders [160]. Whitehead J. [161] developed a method dedicated for polymer powders producing multi-material components by employing a bottom-up approach and two distinct powder vats. The process resembles Stereolithography (SLA) with a vat containing one layer thickness of powder that is then compacted by a substrate, to which the first layer of a manufactured geometry adheres. The process can then incorporate several vats with different powders loaded in each one. By moving the build-substrate between the various vats, a geometry produced by more than one material can be realised. Here switching between layers in the Z direction and in the X and Y plane [161] is possible.

The recoating and powder dosing mechanisms are integral for the PBF-LB/P process, ensuring a steady flow and full build plane for consecutive layers. As previously mentioned, heating the powder before recoating can be implemented to improve the quality of the manufactured components. Another critical parameter is the build plane and powder cake heating, which hinders premature crystallisation of the polymer, thereby minimising the issue of warping and curling in the produced part. The heating configuration and control are of paramount importance for the PBF-LB/P process and are explained next.

## Heating System

The purpose of the heater system is to maintain a stable temperature during the entire build job, as depicted in Figure 4.20. This is to allow for isothermal sintering of the polymer powder by keeping the temperature above the onset crystallisation temperature  $T_{oC}$  [162]. The process and consequence of the process temperature is a vastly studied subject [144, 162–166]. This is due to the direct influence on the final part mechanical properties and surface texture. Furthermore, heating is the primary cause of polymer chain degradation during processing, which causes significant material consumption for PBF-LB/P manufacturing. The heating between  $T_{oC}$  and  $T_{oM}$  is seen in Figure 4.1, showing the processing window and typical behaviour during laser irradiation [144, 167]. Various systems

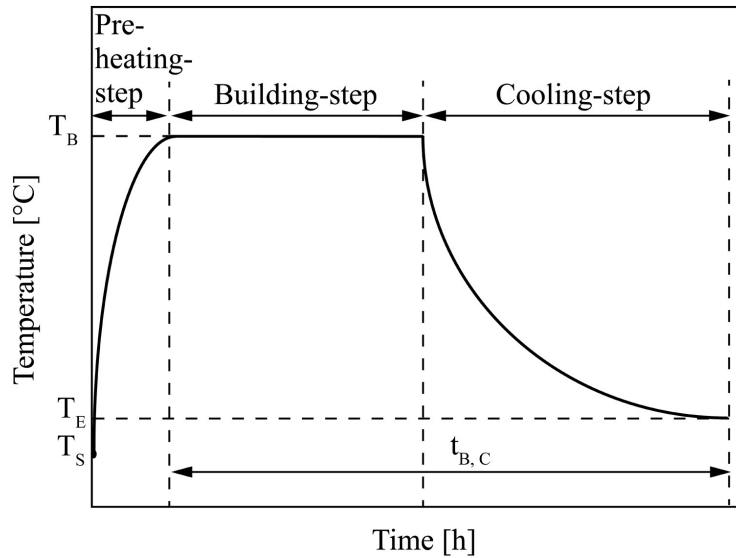


Figure 4.20: Heating cycle of the PBF-LB/P process, showing the initial heating step, the processing step at a constant temperature, and the final step of cooling to room temperature. From [162]

approach the heat input for the build piston and top heating differently. The build piston and powder cake are typically heated by contact heaters placed around the build piston as shown in Figure 4.15, where this can either be by heating elements in physical contact with the build piston outer wall or as a heated environment surrounding the build piston. The heaters for the build piston are usually set to a temperature just above the crystallisation temperature [163, 164], allowing increased mobility of the polymer chains due to the elevated temperature [168, 169]. Doing this allows pre-arrangement of the molecular chains to occur prior to cooling the powder cake and process chamber, alleviating internal stress build-up. The heating cycle for an PBF-LB/P process can be seen in Figure 4.20.

Heating from above the build plane is critical, ensuring a stable heated region with minimal thermal gradients across the build plane. Noncontact heaters are often utilised by being installed above the build plane to radiate heat onto the powder surface, maintaining a temperature below the melting point  $T_{oM}$  of the polymer. Different configurations and heater types are used. The most common are quartz lamp heaters or glow-thread heaters. Ceramic heaters are also employed in some systems. Ceramic heaters typically show longer latency of heating and cooling, making the control less precise. An example of a top heating array is seen in Figure 4.21, depicting an array of double quartz lamps situated around the laser aperture. The heating is controlled by a single point measurement of a pyrometer [164], which makes control across the build plane less accurate. Industrial systems often rely on operator knowledge for tuning the top heater settings by analysing parts produced at different locations in the build plane. By visual inspection during processing, experienced operators can tune the top heaters, minimising thermal gradients.





Figure 4.21: Double quartz lamp top heater array on the SinterStation 2000 in the AMIST centre at the University of Louisville

Studies into the influence of the final part properties have been conducted by various authors, as mentioned above. Greiner S et al. [164] concluded that the majority of final part properties are directly influenced by the top heater temperature, experienced by the powder in the build plane, and less affected by the build piston temperature. However, having no heating for the build piston and build plate causes degraded mechanical properties when investigating the elongation at break and Young's modulus of the produced parts. A model for predicting the initiation of crystallisation and how long this process is carried on has been investigated by Drummer D. et al. [162]. Here it is stated that 50% of crystallisation occurred after 22 minutes when processing at the selected conditions. It is not reported when the material is crystallised to a complete semicrystalline structure. The effect of these studies is a smaller need for build piston heating than previously expected. The conclusion is that the heating of the build plane should be homogenous, with a tendency to have less heat needed for the build piston itself. This will lower the cost of the process while running and shorten the cooling time while still producing quality parts. Heating the build plane is done by homogenous heating and laser irradiation to produce the desired geometry. The laser irradiation is described in the following.

## Laser Type

Laser light is generated in a medium that, when energised, typically by electricity, generates light at a specific wavelength depending on the medium as shown in Figure 4.22. The light generated is a parallel beam that is particularly directional, enabling precise energy delivery in a defined area. Laser is the acronym for Light Amplification by Stimulated Emission of Radiation [170]. Laser light can be produced by several active media, with

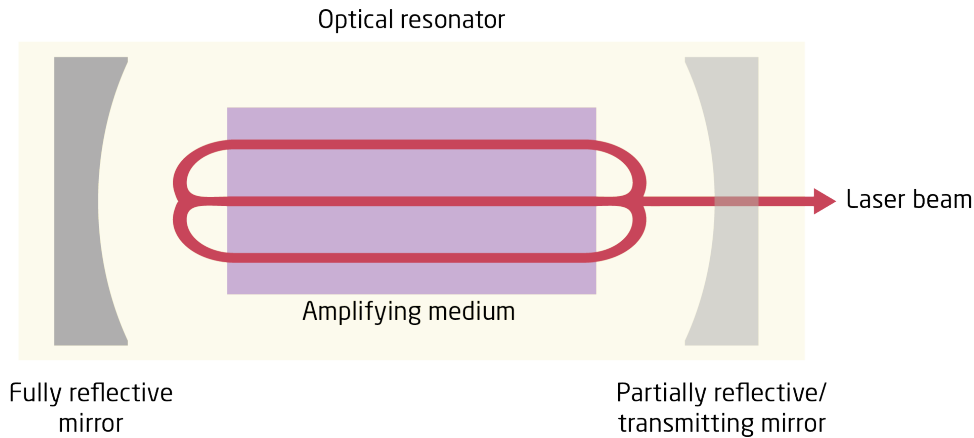


Figure 4.22: Simple principle drawing of the function of a laser

the dominating for PBF-LB/P being  $\text{CO}_2$  [171]. Deckard C. and Beaman J. [144] use this laser type in their original description of the PBF-LB/P process.  $\text{CO}_2$  lasers have been used widely ever since for powder processing, especially for polymers. The laser and powder material interaction has been explained in-depth in subsection 4.1.1. The focus here is on the different laser sources and the new development of lasers for PBF-LB/P.

$\text{CO}_2$  lasers produce radiation by energising a  $\text{CO}_2$  -  $\text{N}_2$  - H gas mixture producing a Continuous Wave (CW) beam delivering high-power as described by the inventor Kumar Patel in 1965 [172].  $\text{CO}_2$  are known as versatile and robust lasers often used in industrial settings for engraving, cutting and fusing different materials. In PBF-LB/P, the wavelength of  $10.6 \mu\text{m}$  is sublime for heating the polymer powder due to the correlation between the molecular agitation frequency and the laser wavelength, as described in subsection 4.1.1. Recently new laser types have been used for processing polymer powders. The company Farsoon has chosen a different laser source by developing a system equipped for ultra-fast scanning speeds of up to  $20\text{m/s}$  [173]. By scanning rapidly, an increased laser power can be utilised in the process. Farsoon uses a  $500\text{W}$  fibre laser to process dark-coloured polymer powder, enabling a minimum feature size of  $0.3\text{mm}$  and a layer thickness range of  $0.06$  to  $0.3\text{mm}$ , as seen in Table 3.1. The company EOS has developed the Fine Detail Resolution (FDR) technology. Here a  $55\text{W}$  CO laser is employed to produce parts with superior detail resolution and low surface roughness [174]. This technology claims to produce walls with a minimum dimension of  $220 \mu\text{m}$  and layer thickness of  $40 \mu\text{m}$ , enabling the user to produce parts with small features and fine detail resolution. The CO laser produces a wavelength of  $5.5 \mu\text{m}$  and a better beam quality than the  $\text{CO}_2$  laser [93]. Both these technologies have been released within the last three years [175, 176], proving that the market for PBF-LB/P is still growing with an increasing demand for faster manufacturing, with greater levels of details and surface finish. Utilising fibre lasers in the PBF-LB/P process causes issues with the heating and consolidation of the polymer powder due to a mismatch between the laser wavelength of  $1080 \text{nm}$  and the agitation



frequency in the polymer. This concept will be explored further in subsection 4.2.3, considering the challenges and possible gains from using fibre lasers.

The CO laser produces a laser beam similar to the CO<sub>2</sub> laser by electric excitation of the gaseous mixture. The mixture is typically CO - He - N<sub>2</sub> - Xe, producing wavelengths between 5.2 and 6.5  $\mu\text{m}$ . The wavelength can be tuned in CO lasers by varying the mixture ratio between the mentioned gasses [177]. The smaller wavelength of the CO laser allows a potential processing spot size half the size of the traditional CO<sub>2</sub> laser. This is based on the diffraction-limited spot size relating to the wavelength of the laser. Furthermore, the Rayleigh length is improved substantially by the smaller wavelength [93, 178]. The Rayleigh length is a measure of the distance between the focal point of a laser beam and the point at which this beam has increased to double this size [179]. The larger Rayleigh length produces a longer depth of focus, which facilitates an increased volume energy density in the beam and greater penetration depth of the high-energy beam while being able to cope with uneven surfaces, still ensuring focus at the build plane of the system. All these features permit the systems utilising CO laser to produce improved quality parts by ensuring better beam quality throughout the build plane and consistent volume energy density. For the laser motion traversing the build plane, a scanner system is utilised, producing the features in the desired locations. These scanning systems are described in the following.

## Scanner System

LPBF systems often use a galvanometer scanning head for traversing the laser spot across the build plane in the X (side to side) and Y (front to back) direction, producing the part. Galvanometer scanners use two mirrors to direct the laser. The mirrors are placed in an orthogonal arrangement, which directs the laser from the side of the scanner and onto the build plane. The focus at the build plane is maintained by an f-theta lens producing a flat plane focus area at the desired focal length. The components of a galvanometer scanner are depicted in Figure 4.23. The motion of the two mirrors can produce rapid movements of the spot in the focal plane of the laser, ensuring acceptable scan speed and build times for a production run. Galvanometers are a well-known technique of producing a rotational force between a rotor and a stator, depending on a current level [180]. Originally intended for the measurement of current or voltage by moving a needle along a gauge, depending on the level experienced by the galvanometer. This principle is now employed in the scanner, utilising the motion generated when a current is applied to rotate a mirror, directing the laser to the desired location. An added option is the use of a feedback loop, determining the location of the rotor to an increased degree of accuracy by comparing the current and desired position, minimising errors.

By keeping the mirror and rotor assembly as light as possible, rapid scan speeds of the

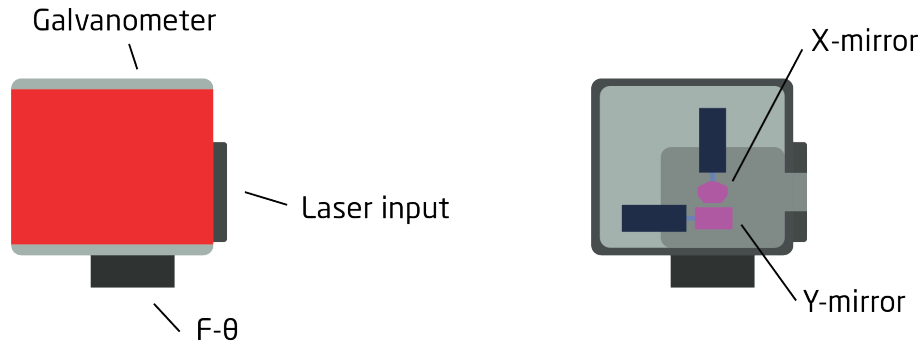


Figure 4.23: Components in a galvanometer scanner

laser spot can be achieved by the rotation of the mirrors while maintaining consistent repeatability. The scanning speeds greatly influence the final part properties. Ensuring adequate speed for not overheating the polymer while still delivering the desired amount of energy needed for particle coalescence [181]. Lexow M. et al. [182] reported a decrease in mechanical properties with increasing scanning speed while maintaining the same area energy density level. Here they conclude that a non-linear effect occurs when moving the laser spot faster while keeping the energy density at the same level. This is expected to be caused by the lack of energy dissipation into the core of the polymer particles since no difference between the sintered particles was determined by visual inspection. A two-phase system is built by not allowing heat dissipation into the core of the powder grains. This two-phase system is constructed by Liquid Phase Sintering (subsection 4.1.2), where the outer shell will bind with the surrounding particles while the inner core is kept as the virgin polymer powder, impairing the part's mechanical properties. Scanning at lower speeds can cause chain scission due to excessive heating in one region [181]. This will also cause a deterioration in the mechanical properties, as well as the surface roughness and colour of the part, due to polymer degradation and discolouring. Therefore, a correlation between the laser energy input and the scanning speed is required to obtain parts that show good mechanical properties and no polymer chain degradation.

### 4.2.2 System Capability

The aim of any system is to complete the intended function while fulfilling the requirements set up for said system. To gain an understanding based on the study presented above concerning the PBF-LB/P process, a framework depicted in Figure 4.24 has been developed. Here the major influential parameters are shown for each specific subsystem presented above. All the influential parameters link to one or more of the derived process signatures. The process signatures are quantifiable resultants, which are directly measurable in the final part quality. Some process signatures have been presented before in the previous influence and signature diagrams. This proves that each part presented above is not unique but influences and is affected by each other when considering the goal of

improving the final part quality.

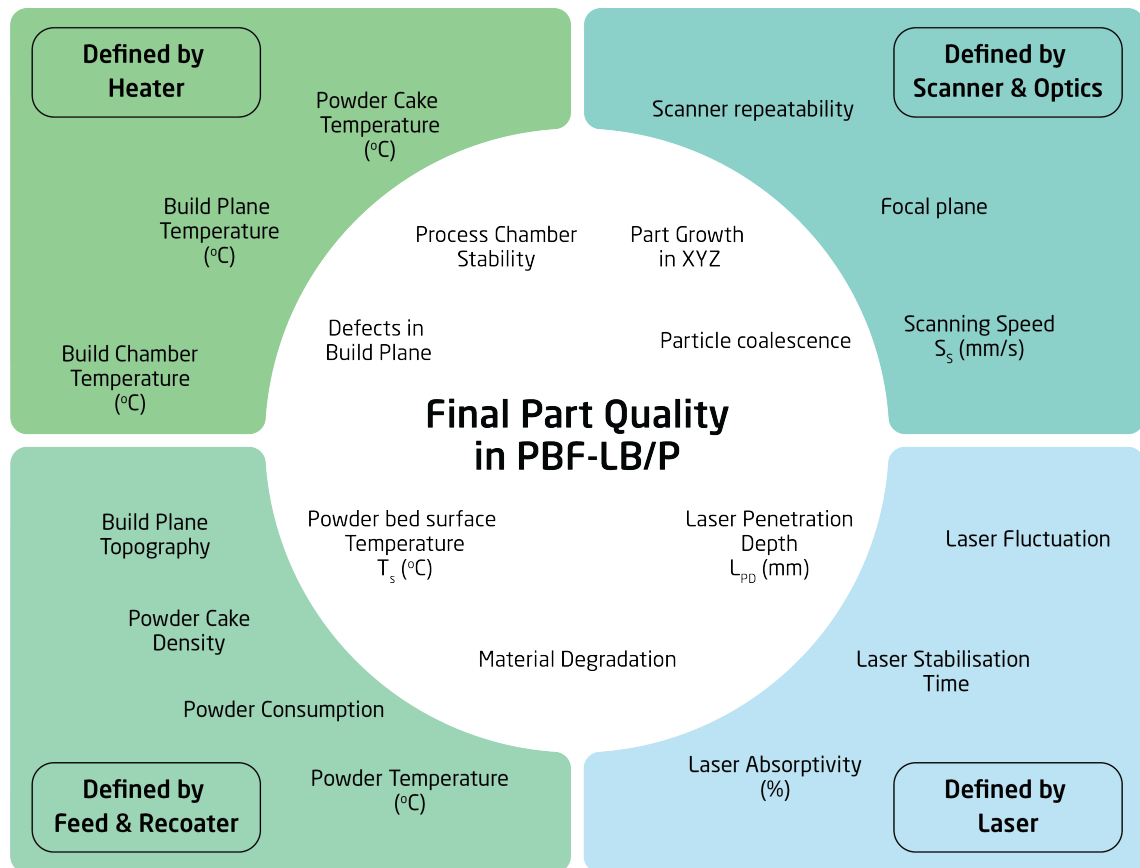


Figure 4.24: The major subsystems in PBF-LB/P, showing the process signatures of the influential parameters

### 4.2.3 Fibre Lasers

Fibre lasers have been developed over the past 50 years [183]. Several types of fibres are available, with glass fibres, polymer fibres, hollow fibres, and single-crystal fibres being among the most common. Fibre lasers are known for their robustness, excellent beam quality, and low maintenance, among others. Fibre lasers are therefore gaining ground for the choice of materials processing, such as laser cutting and welding, as well as for medical applications, such as biomedical imaging [183]. Fibre lasers utilise the fibre as the gain medium, typically in the form of rare-earth-doped glass fibre [184], used for high-power fibre lasers in the near-infrared wavelength spectrum [185]. Fibre lasers are produced in a wide variety of wavelengths and as Continuous Wave (CW) and pulsed versions. The highest power CW lasers made, as reported by Shi W. et al. [183], is a 100kW multimode fibre, with the highest power single mode diffraction-limited fibre producing a 10kW laser beam. Fibre lasers can deliver a very high-power, with the ability to guide the laser easily by positioning the fibre output [186]. The laser produced shows slight divergence, typically reporting  $M^2$  values less than 1.5.  $M^2$  is a measure of the

beam propagation and represents the beam deviation from a perfect Gaussian beam. The goal is to have a beam quality close to one, creating a fully Gaussian and diffraction-limited beam profile [186]. By achieving a low  $M^2$  value, a longer Rayleigh length can be produced, effectively increasing the depth of focus produced by a beam, as discussed for the CO vs CO<sub>2</sub> lasers in subsection 4.2.1.

Fibre lasers have traditionally operated well in the visual to the near-infrared spectrum (400 - 2000 nm), with a dominance of fibre laser for industrial use processing at 1060 - 1080 nm wavelength. The fibre core transmits these wavelengths with minimum loss ensuring no heat retention in the fibre. CO<sub>2</sub> and CO laser has traditionally not been delivered by fibre laser due to the laser transmission loss in the fibre, limiting the capabilities. Recent work by Novikov A. [187] has shown how hollow waveguides and polycrystalline infrared fibres allow for a transmission band between 3 and 18  $\mu\text{m}$  [187]. The work presents the efficacy of using these fibres for transporting and guiding CO and CO<sub>2</sub> lasers. The conclusion is that the polycrystalline infrared fibre shows greater stability in bending, not diminishing the laser output in the fibre. However, the polycrystalline infrared fibre needs a fresnel lens to introduce the laser to the fibre, leading to a loss of power for CO<sub>2</sub> lasers of up to 25% . Novikov A. et al. suggest an improvement by replacing the fresnel lens with an AR anti-reflective window, leaving this for future work. In contrast, hollow waveguides (Figure 4.25 Right) produce better transmission but endure larger losses due to the mechanical bending of the fibre, making them less desirable in a mechanical delivery device. Therefore the fibre delivery system will need to be selected based on the constraints for the delivery system of physical bending [187]. Fibre delivery of CO and CO<sub>2</sub> laser are therefore not commonly used in industrial systems.

Fibre lasers operating at 1060 - 1080 nm are common in industrial processes, with fibres capable of delivering superior laser power with minimum loss. Typical applications are welding, cutting, and marking, with laser powder bed fusion becoming a larger contributor

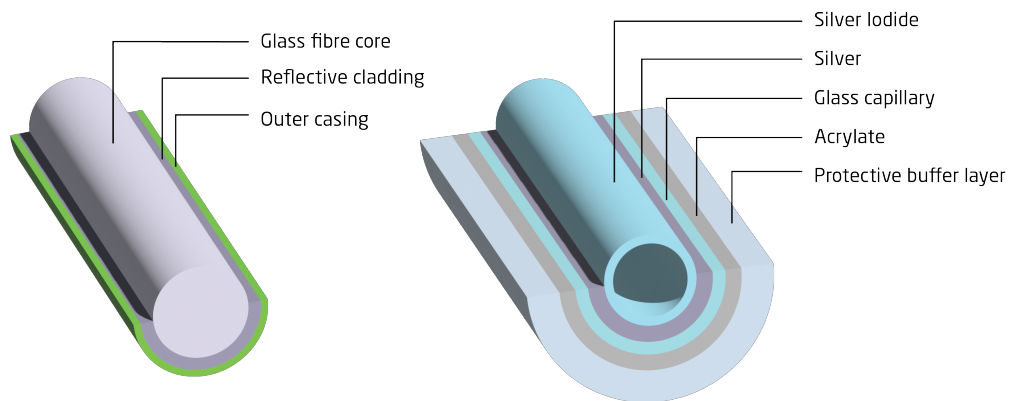


Figure 4.25: Fibre delivery types for a fibre laser at 1080 nm [188] and a CO laser at 5,5  $\mu\text{m}$  [187] wavelength

recently [186]. Fibre lasers are predominantly used in metal AM for any fusion process considering powdered metal [189]. Fibre lasers in the 1010 to 1150 nm wavelength range are based on rare earth doping medium produced by trivalent Ytterbium (Yb) [188, 190]. The Yb-based fibre lasers endure much fewer ion-ion interactions because the system only requires two excitation levels for stable laser production. This means shorter fibre lengths can produce a stable and high-power laser, which is beneficial for running the laser in pulsing mode, delivering elevated peak powers [188]. The laser is produced by pumping a diode onto the laser medium-doped fibre, allowing the intensity to build between two fibre Bragg gratings [191], only releasing the energetic laser as seen in Figure 4.26. When the laser reaches the required energy level, it is left to travel the entire distance of the fibre until the termination end. This behaviour resembles the resonant chamber for gas lasers discussed above, only changing the medium to a solid-state doped fibre.

Recent research has been focussed on developing a multi-wavelength laser capable of tuning the output wavelength to a desired level [192, 193]. The work presented by Larionov I. et al. [193, 194] presents a method for producing mid-infrared radiation by periodic pooling of a lithium niobate crystal. This work was based on the two-stage approach presented by Pandey A. et al. [195] analysing the performance of the two-stage amplifier. The periodic pooling is a conventional method for mid-infrared light generation [196], with Larionov I. et al. presenting the use of a Yb pump (1030 nm) and erbium seed (1550 nm) laser. Based on the control of temperature and pump pulsing, a 3000 nm stable idler radiation is achieved, with a power of 5.5W to 8W. The mid-infrared region can thereby be achieved by fibre laser input allowing for greater stability in organic compound processing. The potential output efficiency can theoretically be improved to close to 40%

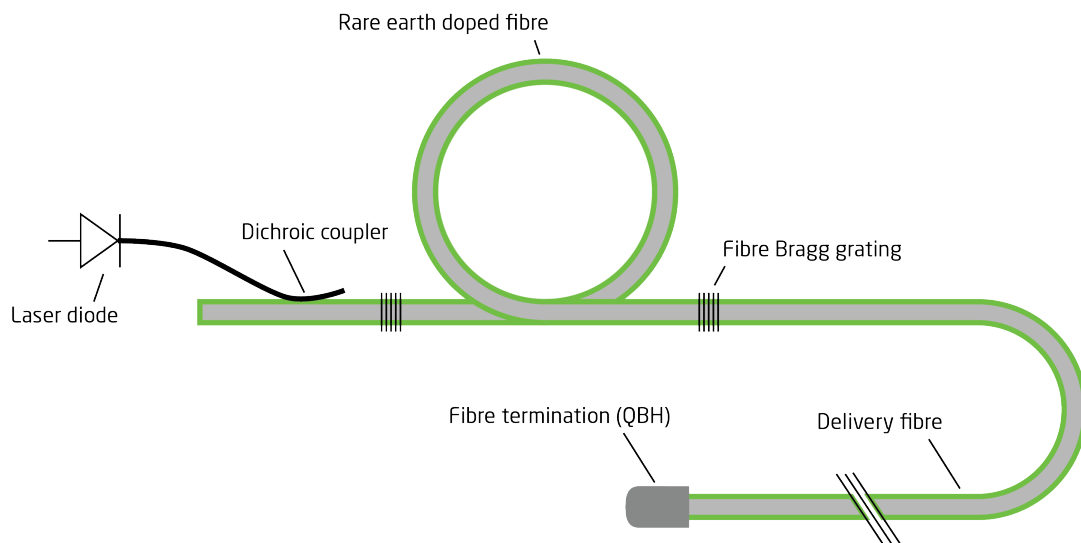


Figure 4.26: Laser production in a doped fibre, causing the resonant chamber effect between the Bragg gratings ensuring only high energy release of the laser. Inspired from: [191]

increased from the initial results of less than 20% [197, 198] with a major factor being the stage lengths of the periodic pooling crystals. Ostapiv A. et al. [199] found that the waist diameter and Rayleigh length are influenced by the pump power from the Yb laser, showing an increase in beam waist as pump power increases, making the possible processing more demanding on the optics and setup. This effect was reversed for the seed pump, which has minimum influence on the output laser properties concerning beam quality. The main focus presented above has been on processing water-containing or organic compounds, not showcasing the possibility of a 3000 nm laser for polymer processing. Utilising fibre laser for polymer processing is therefore described in the following.

#### 4.2.4 Processing Plastics with Fibre Lasers

Fibre laser processing of polymers is notoriously difficult, as mentioned previously [200, 201]. Polymers do not absorb the near-infrared light of the fibre laser, and minimal molecular agitation or electronic excitation is inflicted [14]. The issue is exemplified in Figure 4.27 showing the absorption spectra of a polymer used in laser welding [202, 203]. The figure further plots the wavelengths of the lasers mentioned herein, showing the molecular agitation caused by each individual laser type. CO<sub>2</sub> lasers traditionally used for polymer processing have a significant disadvantage in beam delivery compared to fibre lasers, which is why the investigation of fibre lasers for polymer processing is relevant.

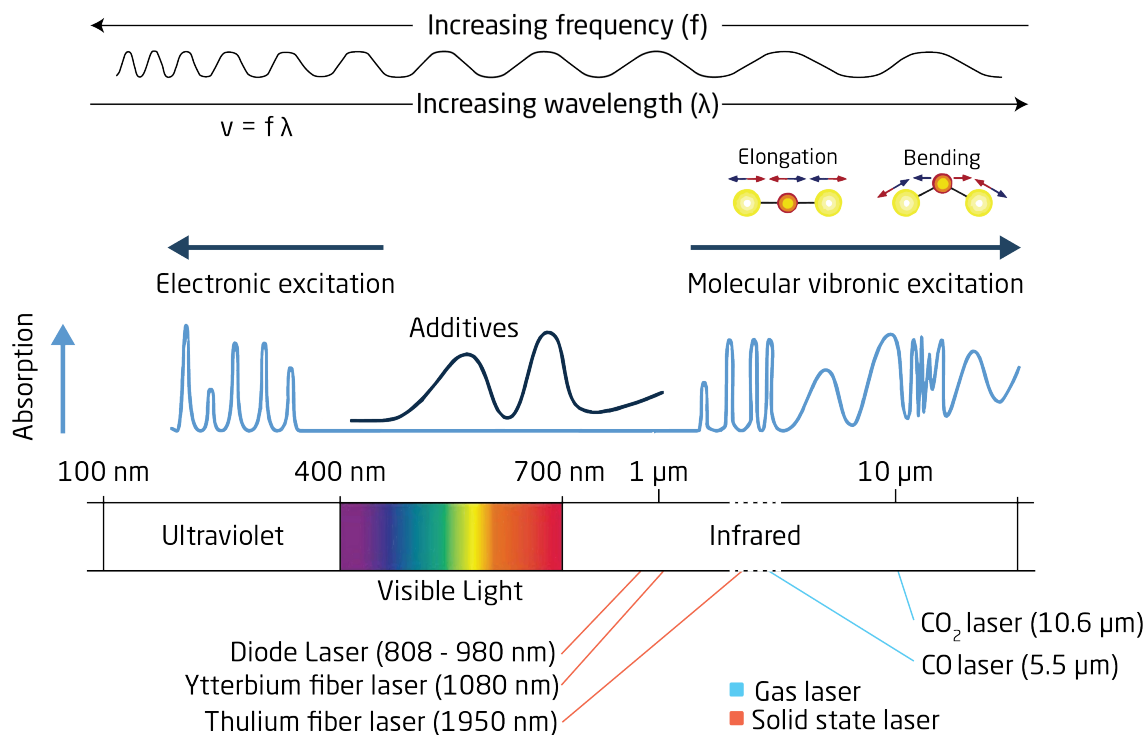


Figure 4.27: Light spectrum with the relevant laser wavelengths plotted. Inspired from [202]

Thiele M. et al. investigated the route of Direct Energy Deposition (DED) of polymers dubbed Laser Polymer Deposition (LPD). In their work, an Nd:YAG (1064 nm) pulsed laser is utilised for direct processing of a polymer powder feed onto a geometry as is known from the DED process, conventionally using metal powder. The technique allowed the production of a free-standing structure processed from polymer powder. Still, it was only possible by doping the Thermoplastic Urethane (TPU) feedstock material with carbon black ensuring the absorption of the laser. A similar approach was demonstrated by Kutlu Y. et al. [204]. Here a process of incorporating multi-walled carbon nanotubes in a pristine PA12 was shown, developing a dark material with good absorption of visible and near-infrared light. The absorptivity in the powder is accredited to the incorporation of the carbon nanotubes but enables the use of the PA12 in the process utilising a fibre laser. However, dense parts were not produced, causing deterioration in the mechanical properties of the manufactured parts. Both of the absorber systems presented cause the parts to turn black, which is not ideal for all components or products. The laser welding industry has looked into welding clear or light-coloured polymers with fibre lasers and has encountered the same issue described above.

Kumar Goyal D. et al. [205] presented a solution utilising electrolytic iron as an absorbing agent. The electrolytic iron is a good absorber of the fibre laser wavelength and therefore produces the desired heat input in the clear polymer weld. However, it is seen that the particles settle in the bubbles formed during the production, causing a decrease in the mechanical properties, as compared to a traditional welding method, due to an increase in pore size. Another research group investigated the use of Indium Tin Oxide (ITO) [206] for improving laser absorption. Here a comparison of carbon black and indium tin oxide reveals that carbon black has an advantage in laser absorption producing comparable welds at half the required energy density compared to the indium tin oxide absorber. Other additives, such as the industrially available Clearweld, allow the bonding of clear or coloured plastics by a fibre laser without influencing the colour in the weld area [207]. Adding absorbers is the most traditional way of processing polymers by fibre laser.

A new type of fibre laser has recently gained attention showing capabilities of processing polymers with no additives. The laser is a thulium-doped fibre laser producing a wavelength close to 2000 nm, which corresponds better with the vibronic frequencies of polymers, as seen in Figure 4.27. The laser is capable of welding polymers with no additives, promising no added colour to the final part [201]. Wittmann A. et al. [208] showed the capabilities of processing PA12 with additives as a film coating on a stainless steel 316L substrate. Here the process is studied concerning the scanning speed, hatch distance, laser power and substrate temperature. They proved that an adherent coating can be produced with no additives by a thulium-doped fibre laser. An initial study for the manufacturing of a 3D part is presented by Böhm S. et al. [201]. The study utilises a thulium-doped fibre



laser to process absorber and unfilled PA12 onto a Polyamide 6 (PA6) substrate, building several layers in their initial trial. The parts produced are not fully dense, and some issues with melting behaviour are identified. The main issue presented by Böhm S et al. [201] is the lack of full consolidation, which is attributed to the large layer size of 0.2 mm and insufficient process development. The study proves that thulium-doped fibre lasers can be of large interest for the PBF-LB/P process due to the easy beam delivery. Furthermore, does the thulium laser produce the laser with a beam quality comparable to that of a Yb fibre laser [209, 210].

Fibre lasers are used widely in the industry based on their ease of use and high-power capabilities. Variants of the traditional fibre laser are emerging, promising better alignment of polymer agitation frequencies, which will aid the use of fibre lasers in polymer processing. Yb fibre lasers still hold relevance but will need an optical absorber for the increase of laser energy absorption.

### 4.3 Chapter Summary

The state of the research within Polymer Laser Powder Bed Fusion has presented an array of particular challenges in processing polymer powder by laser irradiation. Throughout the chapter, an analysis focussing on the relevant process parameters and signatures has been developed. The analyses intend to ensure capable system development, delivering on the key aspects as required. The analysis of process parameters and signatures is utilised throughout the study.

The initial part of the chapter described polymers and the specific characteristics important for laser processing. Here a method for developing the process window was presented by analysing the critical temperatures of the polymer system to be processed. The study further provides knowledge on the polymers available for commercial laser processing, as well as the most common production methods for producing powder from the polymer feedstock.

A definition of the laser and polymer powder interaction is presented, relying on the state-of-the-art knowledge presented by relevant authors. Here the definition of the optical transparency between polymers and Yb fibre laser wavelengths is presented. An investigation of the critical process parameters and how these can be disseminated and related across platforms is introduced, aiming at developing other metrics than the commonly used energy density. A part conclusion as to why energy density functions well for polymers is presented, relating to the difficult process signature definition when analysing polymer parts. The study further develops the sintering mechanisms responsible for part manufacturing during the PBF-LB/P process.

Based on the process understanding developed in the previous sections, an in-depth anal-



ysis of the laser processing system is demonstrated. Here an analysis of each critical sub-system is presented, providing the basis for the system development presented in the following chapter.

The chapter concludes by investigating the fibre laser delivery and determining the qualities and pitfalls of the selection of this laser source. A possible second laser choice is presented, promising better coupling between the laser wavelength and absorption spectra of the polymer. An interesting solution is presented but deemed inappropriate considering the overall goal of the project in which this work has been conducted.



# CHAPTER 5

## The Experimental Infrastructure

This chapter presents the effort of repurposing a binder jetting system for the investigation of polymer powder processing using a fibre laser. The primary objective of this work is to examine the application of LPBF systems for materials and process investigation. The development of an experimental infrastructure is crucial for catering to the critical elements of the PBF-LB/P process (described in chapter 4).

Any LPBF system designated for materials and process investigation must consider the limitations often encountered in new material studies. These limitations are frequently linked to material availability consumption. By limiting the quantity of powder needed, exotic and experimental materials can be studied. As presented in chapter 3, industrial systems rarely exhibit full process control capabilities with even less utilising a fibre laser for the fabrication sequence. This limitation significantly hampers the research capabilities of these systems, rendering them unsuitable for the intended investigation of fibre laser utilisation in the PBF-LB/P process. Only one systems provider offers fibre laser processing and fully open process parameters in one system, as advertised in their marketing efforts. The company Farsoon provide an industrial system with the mentioned capabilities in a large-scale industry platform developed for the mass production of components.

This chapter presents the complete transformation of the system from the binder jetting machine through the repurposing and system breakdown to the sub-system development and implementation. Design and development of the system were approached in an iterative process. By developing the specific sub-systems over several iterations, a robust system and process is achieved. These iterations are done by experimental analysis and development of the sub-system functionality in the PBF-LB/P system and process. The following disseminates the results of this iterative development process by presenting the final solutions and fully developed system.

An experimental infrastructure must be designed and constructed to investigate the aforementioned main hypothesis. This infrastructure must accommodate the desired processing capabilities to verify the main hypothesis, which requires a two-fold experimental focus. Part one is the development of the physical system allowing fibre laser processing of polymer powder. For this, a systems understanding is required. Part two is utilising the laser processing system, developing the methodology for introducing fibre lasers in the PBF-LB/P process. Therefore, knowledge of the process and materials is imperative. Understanding of the manufacturing method, the system, and the process and materials have been developed in the chapters leading up to this point. This chapter's emphasis is the system's development, permitting the laser processing of the powder.

## 5.1 Holistic System Overview

The subsequent sections describe the original machine and useful components repurposed from this. Nested within the repurposed system, a new systems design and implementation phase is undertaken, developing the required elements for PBF-LB/P. The repurposing and design phase relies on the process parameter and signature analysis presented in chapter 4. Based on these analyses, a list of critical elements is developed for each sub-system, ensuring the desired process capability throughout the development phase.

A top-level diagram is constructed in Figure 5.2 to comprehend the entire system. The centre of the diagram is the focal point of the work regarding the sub-systems development. The diagram's input and output sides are further developed in the following chapters, defining the material requirements through experiments with different materials in the

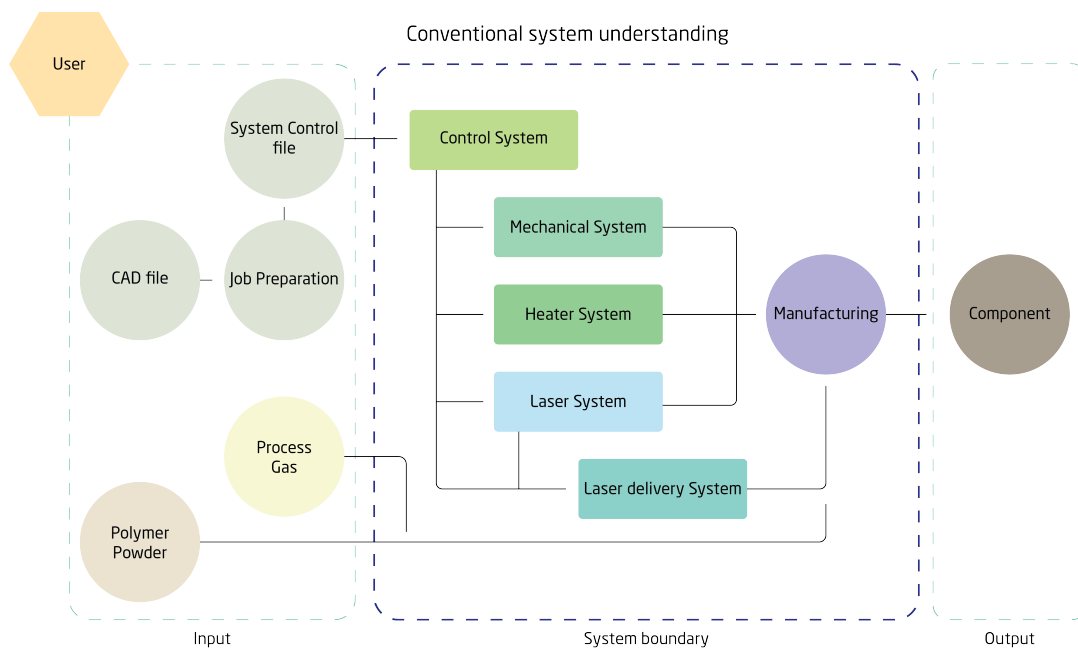


Figure 5.1: System diagram - Top level

developed system. Each sub-system described in Figure 5.2 contributes significantly to the resulting part quality. Each sub-system is presented by a systems diagram relating the critical elements to the components and process. By approaching each sub-system design or redesign similarly, attention to detail is established, which determines the success of the developed system.

An evaluation of the final part quality parameters and signatures described in Figure 4.24 contributes to the top-level system analysis and subsequent list of critical elements and features. To comprehend the relevant system capabilities, a list of the process parameters and signatures is presented in Figure 5.1. The list references the origin of the parameter or signature, which facilitates the understanding and importance of each.

The analysis produces a set of selection and design criteria for all the sub-systems, increasing the chance of success. To define the system, a list of critical system elements and features is set up, as seen in Table 5.1. The list represents the essential features and controls preferred for manufacturing parts by the PBF-LB/P process.

An approach for facilitating all the desired process capabilities could be the design and construction of a new system. The main focus of this work is not the design of a new and/or improved PBF-LB/P configuration but, instead, the application of a fibre laser in the process. A significant design, sourcing, and construction effort is needed to develop a new system. Instead, a repurposing approach was selected, minimising the necessary workload during this part of the project. For this, an older Powder Bed Fusion machine was donated to the project. Using an older unit for the project set certain boundaries and constraints for the development work and finalised system. One limitation identified early








<b>Top level System</b>	Defined by	
Scanner repeatability	<i>Scanner &amp; Optics</i>	
Scanning speed	<i>Scanner &amp; Optics</i>	
Laser Fluctuation	<i>True Energy Delivered</i>	
Powder Cake Temperature (°C) Build Plane Temperature (°C) Build Chamber Temperature (°C)	<i>Heater</i>	
Powder Cake Density	<i>Feed and Recoater</i>	
Particle coalescence Process Chamber Stability Powder bed surface Temperature $T_s$ (°C)	<i>Final Part Quality in PBF-LB/P</i>	

Figure 5.2: Definitions relevant for the system development

Table 5.1: Features of an PBF-LB/P System

<b>Critical Top-level System Elements</b>	
Critical element	Elaboration
Heat build volume to process temperature	The polymer system defines the temperature. The system will be able to process grades of PA12, PA11, and PP
Control of heating	The heaters must be controllable and preferably switched On-Off by the Unified Systems Controller
Unified control of all sub-systems	Having a single control pipeline from the computer to the system's controller streamlines the control process, minimising errors
Adequate level of mechanical motion control	Fine-tuning powder dosing, vertical-stage motion, and recoating action facilitate the processing capabilities of the system
Adequate level of laser motion control	Accurately directing the laser to a desired location with good repeatability
Fast and reliable laser power setting	Setting the laser power and the On-Off switching rapidly support consistent processing
Contain laser with adequate power	The power of the consolidation/heating source must be enough for melting the powder
Stable processing chamber	The processing chamber must be stable regarding temperature deviation. Can contain an inert gas
Produce flat build plane	The flatness of the build minimises defects in the final parts
Produce high-density powder cake	The density of the powder cake is directly reflected in the final part density
Adequate resolution of Z-axis	To ensure fine detail manufacturing with minimised Z stair stepping, a high-resolution vertical-stage is required

in the project was the impossible integration of an inert atmosphere in the build chamber. This meant that the vast build chamber was not sealed from the surrounding atmosphere. The lack of an inert atmosphere is a significant drawback of the original system since this can lead to issues such as excessive material degradation during processing. Secondly, incorporating a laser source other than a fibre-delivered laser is not possible due to the external limitations and functionalities of the system.

Repurposing and redesigning an older machine resulted in faster system development. This aided the work in producing results from an early stage of the project. The primary sub-systems reused are powder handling, the build piston, and the precision vertical-stage operation. These functionalities are included in the developed system with no significant modifications. All repurposed sub-systems are analysed for efficacy in the final system before allowing complete or partial incorporation. The utilisation and the upgrades of the original machine developing this into the PBF-LB/P system are described in the following.

## 5.2 Repurposing an Industrial System

Prior to its redesign for the new functionality, the original machine was a binder jetting system designed by the company 3D Systems (Projet 4500). The machine utilised three distinct coloured binder inks and a transparent version to produce complete CMY-coloured components, mainly focussed on prototypes for design optimisation. The two machines, including a representation of the colour capabilities of a manufactured part from the Projet 4500, are shown in Figure 5.3. Specifications of the Projet 4500 system are listed in Table 5.2.

At the beginning of the project, the Projet 4500 was granted for the repurposing efforts by an external company. It presented a unique opportunity as the first industrial platform to be retrofitted with the Unified Systems Controller, developed in the encompassing Open Additive Manufacturing Initiative. By retrofitting the platform with the Unified Systems Controller and developing a new set of sub-systems, polymer powder processing by fibre laser could be enabled. Since the original machine was designed for binder jetting onto a powder bed, the majority of the powder handling systems were suitable for exploring different polymer powders. Therefore, limited reconfiguration of the powder handling systems was required. However, a significant overhaul was necessary for most of the other sub-systems, as presented below.

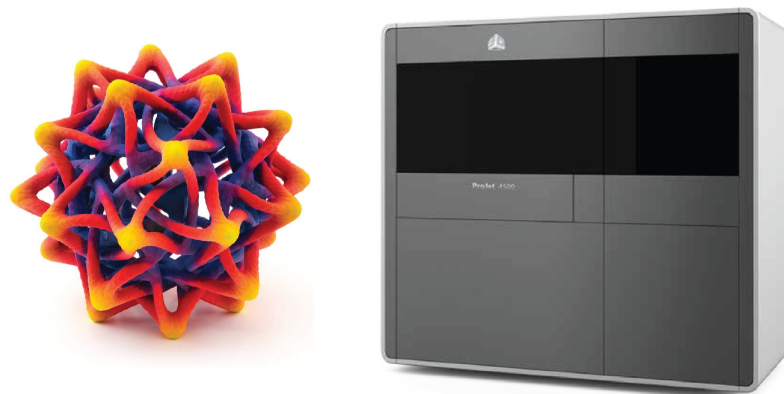


Figure 5.3: Left: Advertised colour model from 3D Systems - Right: Projet 4500

Table 5.2: The build specification of the Projet 4500 from 3D Systems

Resolution	600 dp
Colour mode	CMY + transparent binder = white to dark (never black)
Feature size	0.1 mm
Layer height	0.1 mm
Build volume (XYZ)	203 mm x 254 mm x 203 mm (10.5 L)
Material	VisiJet C4, Core (powder) and Spectrum (binder) <i>3D Systems proprietary</i>
Material Refresh rate	0% (complete material usage)

### 5.3 System Breakdown and Analysis for Repurposing

Utilising the framework of a machine that previously had a different purpose proved efficient for the development of the experimental infrastructure. Repurposing the machine entailed several elements which could be utilised for the new process. Based on the critical elements presented in Table 5.1, an analysis of the existing machine elements was carried out. Each machine element must be defined and verified for the intended use of polymer powder laser processing. Defining the level of redesign or utilisation is evaluated by considering the desired processing capabilities and level of integration.

The sub-systems installed in the machine served either as an inspiration or direct application for the experimental infrastructure developed. The specific components utilised for repurposing into the experimental setup are listed in Table 5.3. The overall frame of the machine was mostly kept intact, where only slight modifications were required. The sub-system remaining largely unchanged is the powder hopper, which only had minor optimisations. Here a load cell was removed, along with the automatic powder feed system. The most significant change occurred for the control and the binder jetting system, which was removed in its entirety. The control system was fully replaced. Easy access and installation were achieved by utilising the cleaning bay of the Projet machine (right side of the machine) for the electronics cabinet.

Table 5.3: Projet 4500 sub-system overview and the required action

Heating system	Fully redesigned
Recoater	Fully redesigned
Recoater X-gantry	Removed
Recoater drive unit	Redesigned for a stepper motor



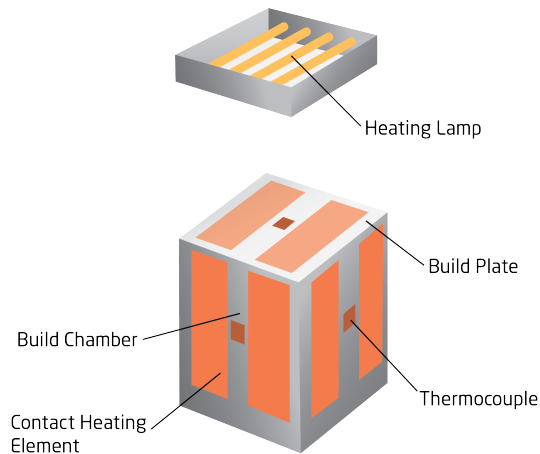
Powder hopper	Fully repurposed (including agitators, dosing unit, and all motion stages)
Powder back feed (Automatic)	Removed due to thermal degradation of the processed material
vertical-stage	Repurposed with slight reconfiguration
Build plate	Repurposed with added heating
Build volume	Repurposed with added heating
Machine frame	Repurposed with design changes
Build area machine frame	Fully redesigned
Front window	Changed for a laser safety window (300W & 1080nm)
Electronics and control systems	Fully redesigned
Wire harness	Fully redesigned

The subsequent sections detail the actions taken for individual sub-systems, which are listed in Table 5.3. Each component's or assembly's utility and the conclusions drawn for either repurposing or redesigning are comprehensively explained.

### 5.3.1 Original Heater System

In the original machine, a heating system consisting of five sets of two heating elements was placed around the build piston and on the build plate. An array of quartz heating lamps directed onto the build plane was positioned at the top of the machine. The heating lamp array consisted of four 120-volt, 300 Watt halogen lights. These lamps provided light and heat stabilisation of the build chamber during operation. The heating elements physically in contact with the build piston were silicon heating pads, with sets of two separate pads located at each of the five sides of the build piston. The heating elements were limited to  $\approx 80$  °C by a thermal switch on each element. The elements were 120 volts, 140 Watts each and were controlled by a thermocouple located in the centre of each build piston wall and on the build plate. The heating capacity of contact heaters was calculated for the installed heaters to be  $\approx 5$  W/in<sup>2</sup> or 0.78 W/cm<sup>2</sup>.

Considering the limited functionality of only heating to 80 °C, with minimal directionality of the top heating unit. A full redesign of the heater was required. The redesign effort of the heating system is developed in subsection 5.4.3.



(a) Heater location and distribution



(b) Outline of heating elements

Figure 5.4: Original heating system layout with the heater and thermocouple location exemplified

### 5.3.2 Original Powder Feed System

The powder hopper situated in the back and top of the machine allows gravity feeding of the powder onto the build plane. Before reaching the build plane, a homogenisation zone enables the powder to distribute and produce an avalanche effect in front of the roller recoater (as described in subsection 4.2.1). The powder hopper can contain  $\approx 20\text{L}$  powder, which is equivalent to the build volume, not accounting for overflow waste or spillage.

Powder drop

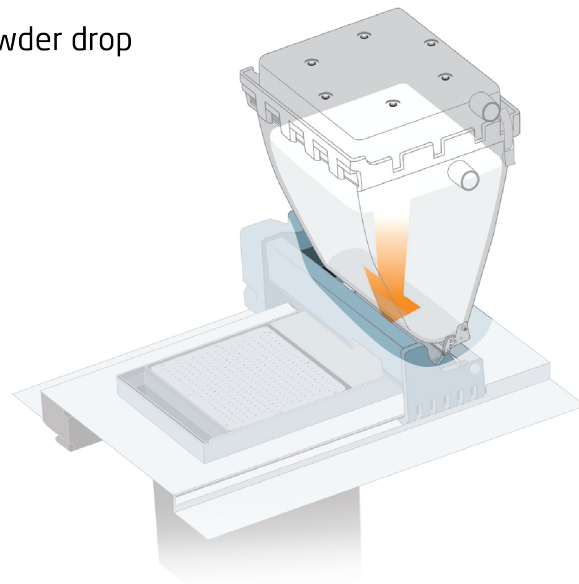


Figure 5.5: The powder canister is located behind the build plane of the machine. Adapted from: [211]

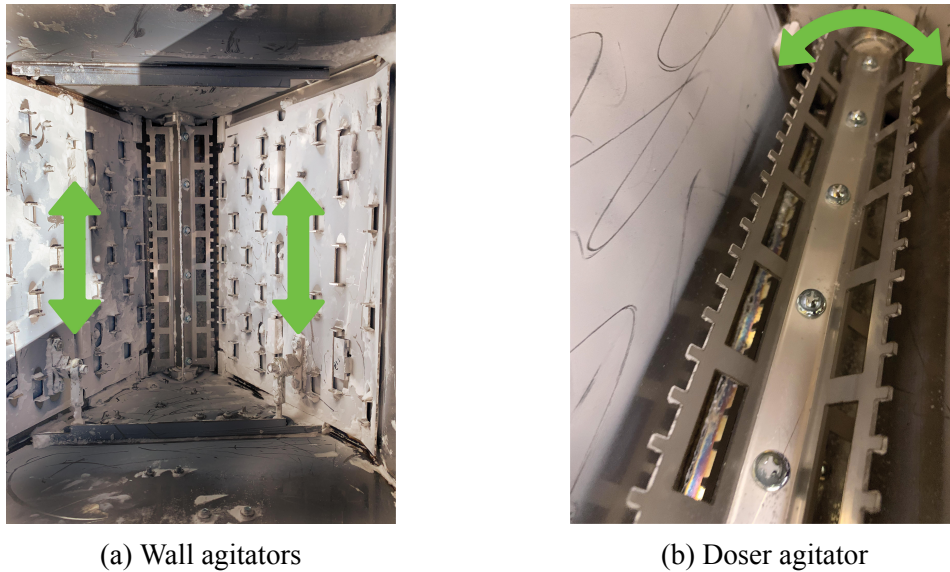


Figure 5.6: Powder agitators for internal powder movement

Inside the powder hopper, several agitation mechanisms minimise the risk of powder cavitation and caking, leading to short feed in the build plane. The agitators move the powder hopper's side walls (Figure 5.6a) and rotate in the bottom (Figure 5.6b) to distribute an even flow of powder during dosing.

At the bottom of the powder hopper, a valve ensures minimal powder leakage during operation. The valve is operated by a stepper motor and is held shut by springs. The valve and the operation are shown in Figures 5.7b & 5.7a.

Powder dosing and the entire powder hopper were not reconfigured. The motion relied on stepper motors in the original machine. Based on the analysis, only an extra wire for sensor capabilities was installed for this sub-system as a redundant option. The powder feed and dosing mechanism are tuned for every build job on the system due to dependen-



Figure 5.7: Dosing valve in the bottom of the hopper for not over-dosing powder

cies of material, temperature, and humidity, all of which influence the flowability of the powder. The system allows for accurate tuning of the dosed amount to ensure that overdosing of powder is reduced to a safe level and excessive use of powder does not occur. A recoating system is utilised to spread the powder for producing a new build plane, which is deconstructed in the following.

### 5.3.3 Original Recoater System

In the original machine, a recoating device based on a counter-rotating recoater was utilised. The recoater functioned in a single-direction approach (Y-gantry), having the powder feed in the back of the machine bringing the material forward for recoating. The recoating gantry contained the print head, which traversed the build plane (X-gantry) normal to the recoating motion for selective deposition of the binding agents. 3D Systems in [211] explains the process in-depth, which is illustrated in Figure 5.8. The system's efficiency is increased by utilising the reverse motion of the recoater for the binder jetting axis and print head motion. The build plane was lowered during the reverse motion of the recoater to ensure that the recoater does not interact with any of the newly deposited binder and powder. This means that the powder density is only compacted in one direction, packing the front of the powder cake better than the back, as seen from the inspection window.

As mentioned above, 100% of the powder could be reused due to very low degradation in the powder bed. To limit the user interaction with the powder, funnels at the front and back of the build plane were installed. These funnels transported powder from the build plane back into the powder hopper by a vacuum system. This vacuum and powder recirculation system was removed entirely due to the degradation of the polymer powder at elevated temperatures, such as those required for laser processing.

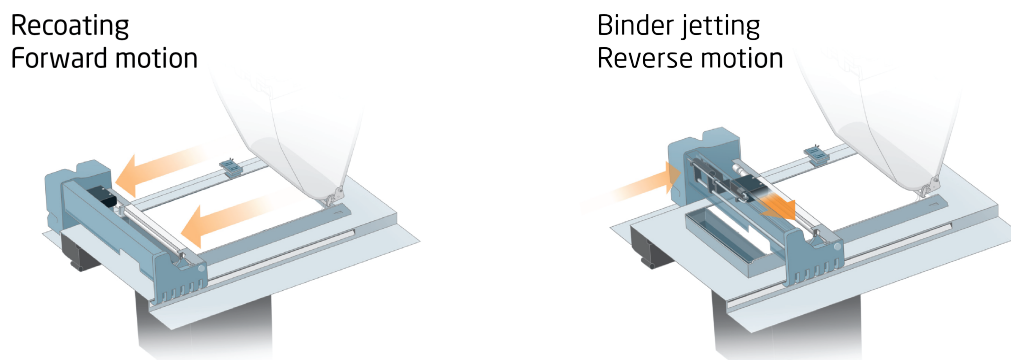


Figure 5.8: The two process steps for recoating and CMY colour binder jetting as advertised by 3D Systems. Adapted from: [211]

The recoater system was fully redesigned to improve the processing capabilities according to the list of critical system elements and features described below in subsection 5.4.4. The new build plane is produced by lowering the vertical-stage allowing for the selected layer height to be filled by the new powder distributed by the recoating system.

### 5.3.4 Original vertical-stage System

Linear motion of the vertical-stage that moves the build plate up and down in the build piston is designed on one lead screw linear motor and three load-carrying and stabilising rods. The stepper is a NEMA23-type rotating a core around the stationary lead screw producing linear motion. The lead screw has a pitch of 2.54 mm (10 threads per inch), resulting in a minimum vertical motion of 0.0127 mm per step. A plate housing the three load-carrying rods and the motor moves the build plate mounted opposite vertically to the motor as seen in Figure 5.9.

Inside the build piston, a gasket centres the build plate and minimises the powder loss on all four sides. The gasket material is a ceramic paper made for sealing moveable components in a sliding motion. Precise control of the build plate is achieved by the pitch of the screw and the stepping of the motor. By using full stepping of the motion stage, a coarse resolution is achieved, as described above. Stepper motors are most commonly designed with a step angle of  $1.8^\circ$ , resulting in 200 steps per revolution (Equation 5.2). To optimise the vertical-stage resolution, micro-stepping is enabled, which increases the resolution by dividing each full step into multiple smaller steps. Micro-steps are handled by maintaining a current in the motor circuits, only moving the motor a fraction of the step. Micro-stepping of a stepper motor results in a lower torque for the drive of the motor but

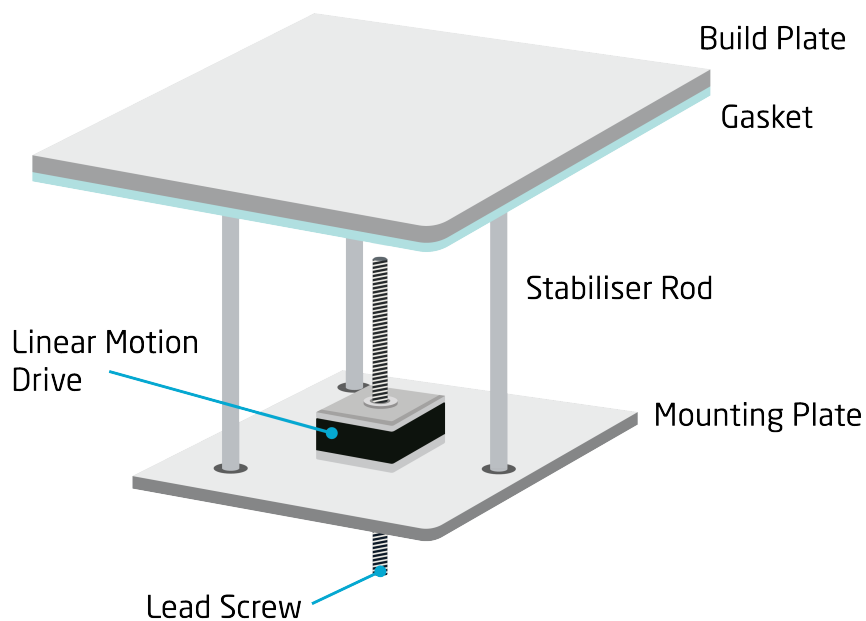


Figure 5.9: vertical-stage main components

a smoother motion due to the smaller increments during acceleration and deceleration. Micro-stepping can be achieved by utilising a stepper driver for pulsing and holding the motor signal.

$$\text{Step angle} = 1.8^\circ \quad (5.1)$$

$$\frac{\text{Step}}{\text{Revolution}} = \frac{360^\circ}{\text{Step angle}} = 200 \quad (5.2)$$

$$\frac{1}{8} \text{ Micro stepping} = \frac{360^\circ}{\text{Step angle} \cdot \frac{1}{8}} = 1600 \frac{\text{Step}}{\text{Revolution}} \quad (5.3)$$

$$\begin{aligned} \text{Linear resolution} &= \text{Full step resolution} \cdot \text{micro step factor} \\ &= 0.0127 \frac{\text{mm}}{\text{step}} \cdot \frac{1}{8} = 0.0016 \frac{\text{mm}}{\text{step}} \end{aligned} \quad (5.4)$$

$$\frac{\text{Step}}{\text{layer}} = \frac{\text{mm}}{\text{step}} \cdot \text{Layer height} = 25.2 \frac{\text{Step}}{\text{layer}} \quad (5.5)$$

Setting the micro-stepping is done in an exponential doubling of the step resolution per revolution. For the purpose of achieving an adequate linear vertical-stage resolution, a factor of 1/8 is selected (Equation 5.3). By utilising micro-stepping, the linear motion of one step is reduced by a factor of 1/8 providing a linear motion of 0.0016 mm/step (Equation 5.4). Micro-stepping for the system results in 25.2 steps per layer when selecting a layer height of 0.04 mm as seen from Equation 5.5.

The desired position of one layer height is missed theoretically by 0.2 steps resulting in an error of  $\pm 0.5$  step mismatch for each layer. By positional bookkeeping in the mechanical motion controller, referencing the zero reference plane, this error is negligible since the mismatch evens over time due to random over and under-shooting by one step per layer. Further analysing of the error for every layer highlights the minimal difference one-step mismatch per layer infers. This considers the elastic response of the powder cake during recoating and that the typical grain size of the powder is  $D_{50}$  0.045 mm, concluding how this minute error is irrelevant. Build job initialisation for the PBF-LB/P process functions by producing a powder cake in which the component can be manufactured. This powder bed is typically 5 mm tall, ensuring heat retention and stable processing. Considering this pre-build powder bed and the elasticity of this further ensures the insignificance of one full-step mismatch per layer.



Utilising a smaller micro-stepping factor could minimise the error presented above. However, to prevent further loss of torque in the motion stage, a lower micro-stepping factor is undesirable. If a finer powder is to be investigated in the system, a smaller micro-stepping factor can be implemented, with a loss of power of the vertical-stage, causing the Z-height to be minimised. The implementation of a different micro-stepping setting is an easy task based on the open framework of the entire infrastructure.

### 5.3.5 Original System Framework & Ideology

A general approach to minimising the complexity of the system was followed during the system breakdown, analysis, and for redesign and development. The complexity of the sub-systems, whether based on the original machine or newly implemented, has been reduced, aiming for a low-maintenance system. Several parts of the original machine were removed to introduce a redesigned version. To allow for easy integration, the servo-controlled motors located on the recoater system (Y motion) were replaced with a stepper motor, which aligns with the rest of the machine, being entirely stepper motor driven, this lowered the complexity of the individual as well as the holistic motion control. The heating system was changed to allow for an elevated level of heater control and heaters capable of reaching higher temperatures based on the process requirements. The entire binder jetting system located on the X-gantry was removed from the system since it was not desired and took up a large amount of space. This principle also applies to the powder feedback system, as mentioned above.

The internal wall dividing the Projet machine was removed to allow for the installation of an optical breadboard as seen in Figure 5.10. The optical breadboard mounting sys-

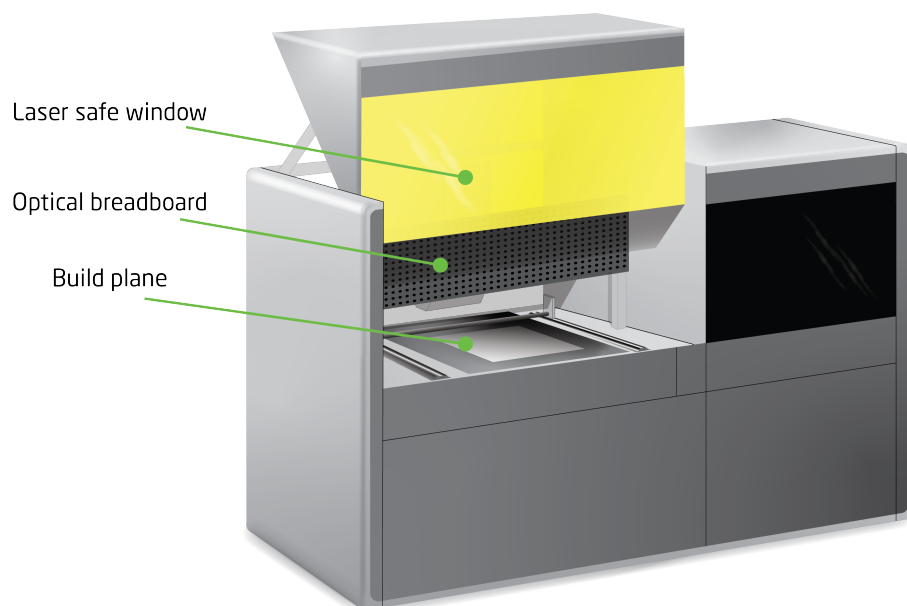


Figure 5.10: Low complexity overview of the developed system

tem was selected for its versatility in mounting and fine-tuning the critical aspects of the laser delivery system, such as the galvanometer scanner system, mirrors, and monitoring devices. The controller computer was replaced, only maintaining the power supply, delivering 12, 24, and 36-volt DC. A substantial part of the original machine has been changed to allow for the new processing capabilities.

Repurposing an older machine has proved viable from the analysis presented. Sub-systems from the original machine were reutilised for powder handling and the vertical-stage. Nevertheless, several new sub-systems required either a redesign based on the structure of the original machine or a full new development cycle to provide the desired capabilities. This effort for redesign or new development is explained in-depth below.

## 5.4 System Upgrades for the Polymer LPBF Process

Developing a system to comprehend the complex process cycle of a PBF-LB/P requires several iterations. As explained above, these iterations are not displayed in this section, as only the final solutions are presented. The development of each sub-system required an intimate process understanding to define the requirements and process results. Therefore, the new sub-systems introduced in the machine are developed based on the knowledge obtained during the literature survey presented in Chapters 3 and 4. Each sub-system relates to several influential process parameters and signatures, as shown in Figures 4.4, 4.10, and 4.24. Analysing the influential process parameters and signatures for each sub-system has ensured that development was focussed on delivering the critical elements required for the specific process.

### 5.4.1 Control Systems

Control of the system relies on three different parts; a computer, the Unified Systems Controller, and the motion controller. The computer functions as the central controlling unit, hosting the job file preparation and controller communication software. Build job commands are communicated from the computer to the Unified Systems Controller and the Arduino, each controlling the laser and the mechanical motions, respectively.

The software for job file generation and controller communication was developed by Andrea Luongo as part of the work achieved during the Open Additive Manufacturing Initiative (section 1.3). It is released to the public along with the results from the initiative in the GitHub repository. The job preparation function of the software allows the input and setting of all parameters relevant to the PBF-LB/P process. It further provides a function for setting up a desired manufacturing configuration. The job generation window is shown in Figure 5.11 Left. Controller board communication is shown in the right window of the same Figure.

A unique level of system control is achieved using the control board communication and



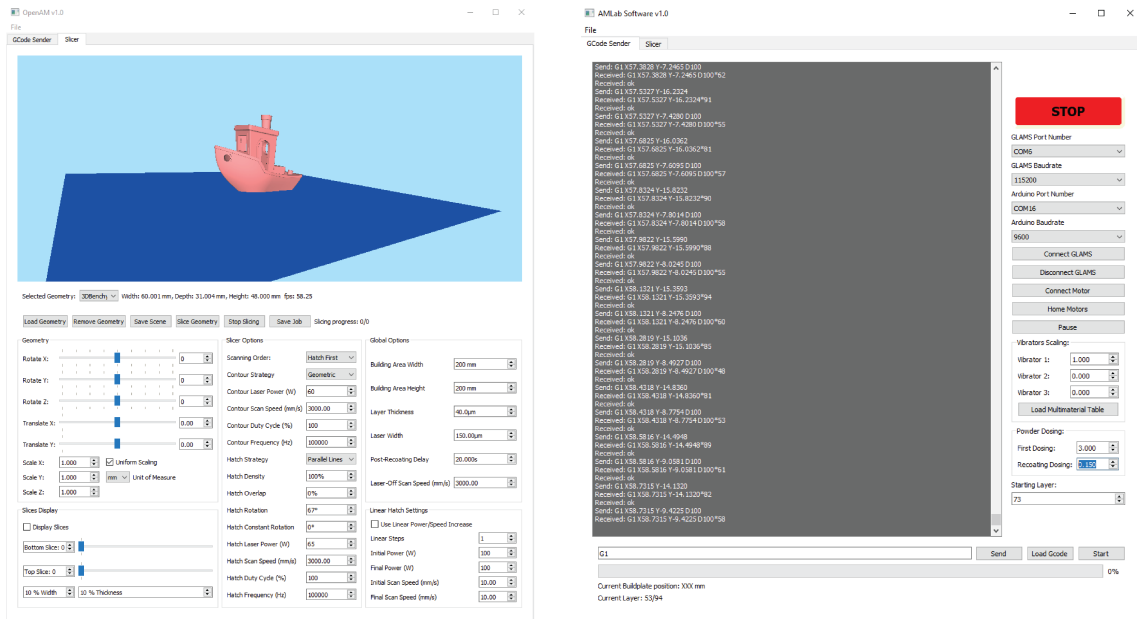


Figure 5.11: The two interfaces of the controller software

job preparation software developed for the Open Additive Manufacturing Initiative. The software allows access to the entire range of process parameters, enabling direct input in the job file generator or communication software. The job file generator further allows the loading of multiple individual parts, each possessing unique process parameters and settings. This multi-component capability is seen in Figure 5.12. This level of process control allows the research to extend further than what is commonly possible on commercial machines.

Individual sub-systems can be controlled through the communication software. This permits the configuration and calibration on a sub-system level rather than for the entire sys-

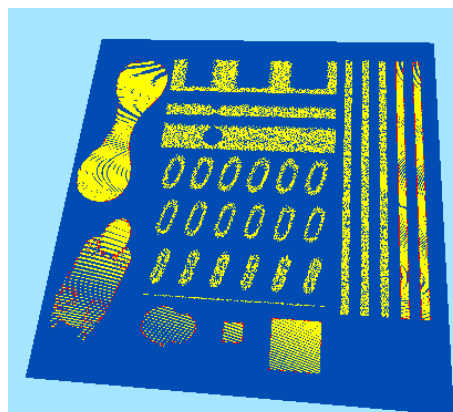


Figure 5.12: Slice of a job file with multiple components in the same job

tem at once. The software communicates to two separate Arduino-based controllers. Each controller runs a distinct part of the entire process, utilising one controller for the mechanical motion of physical sub-systems. While the other controls the laser, concerning the setting of power, the On-Off, and the positioning of the spot on the build plane. Both controllers and the details of these are explained below concerning the various influential process parameters and signatures.

## Mechanical Motion & Control

The PBF-LB/P process involves a series of mechanical motion stages focussed on producing a new layer of powder during the manufacturing cycle. The main components in this involve the powder feed system, the recoating system, and the vertical-stage or build piston. The system must function in a choreographed manner, ensuring that the mechanical motions follow a step-by-step process, which permits stable processing during new layer deposition. The process parameter and signature analysis relevant to the mechanical motion is constructed in Figure 5.13.

From the analysis, it is evident that the final build quality is significantly influenced by the build plane. Besides the build plane quality, a secondary measure is needed. This considers the vertical-stage motion, where precise control is required to produce an accurate motion of 0.04 mm. On-Off of the heaters to terminate the build cycle allowing the powder cake to cool, is built into the mechanical controller. Terminating the heating when the job is finished reduces the risk of excessive material degradation and energy use. Based on the analysis, a list of critical system elements (Table 5.4) was produced concerning the mechanical motion and control system. Descriptions of the critical elements reflect a desire to build a low-maintenance and easily integratable system by considering the physical and logistical boundaries set by the system frame of the repurposed machine.

An Arduino Mega 2560 was selected for the control based on the interface and programmable capabilities. By incorporating this hardware solution, an added ability to switch the heaters On-Off was installed. The knowledge base of the Arduino program language is extensive, with several online communities available for inspiration and help on various




<b>Mechanical Motion System</b>	Defined by	
Build Plane Topography Powder Cake Density	<i>Feed and Recoater</i>	
Defects in the build plane	<i>Final Part Quality in PBF-LB/P</i>	

Figure 5.13: Process parameters and signatures relevant for the development of the mechanical motion system

issues. By utilising this framework, it is possible to achieve a shorter development time while maintaining a narrow control proficiency, ensuring repeatability for the controlled hardware.

The mechanical motion controller is explicitly developed for managing the stepper motors and heaters in the system. The control complexity is minimised by selecting stepper motors for all motion stages in the system. Stepper motors have no feedback control without an encoder to know the actual position. Due to the added complexity of encoders, a different approach was selected. A homing procedure was built for all stepper motors that require spatial control, preventing issues during operation. The homing process is carried out by moving the specific stage to a known position, making this location the home of the motion from start to finish. Two sub-systems require homing for their operation. These are the valve of the powder dosing unit (shown in Figure 5.6) and the recoater traverse motion (shown in Figure 5.5). The homing procedure of the stages was performed by Hall effect sensors which detect a magnetic field. Mechanical switches are commonly used for homing stepper motor motion systems but were undesirable due to powder ingress. The Hall effect sensor relies on a magnet that interacts with the sensor. The sensor can be fully encapsulated in a resin, minimising powder ingress. The solution is viable since the polymer powder does not interact with the sensor or the magnet.

The stepper motors are all driven by the same DM320T stepper from the company OMC STEPPERONLINE, producing the required signals to the two coils for moving a step in a selected direction, as seen in Figure 5.14. The stepper drivers accept a threefold signal from the controller. Therefore, the control board output is a signal of enable, step, and direction. The enable command allows the rotation of the motor while locking it in place

Table 5.4: Mechanical motion elements and features derived from the analysis in Figure 5.16 and the physical constraints of system

<b>Critical Mechanical Integration Elements</b>	
Critical element	Elaboration
Can communicate with the control computer and software	To utilise the software presented above, the controller must communicate with the software
The controller must be programmed to the specific operation of the system	Programming the controller in a "language" accepted largely in the open source community allows for the widespread adoption of the control system
Motion control must produce repeatable motion	Ensuring repeatability of the motion system, and the control sequence allows for larger build jobs
Accurate positionability	Moving motors to a known position ensures repeatability during operation

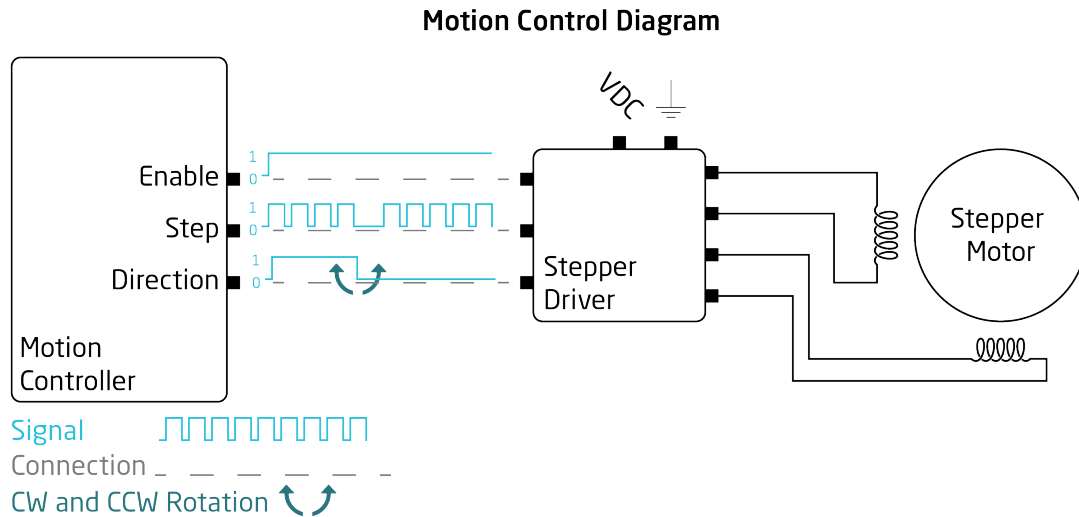


Figure 5.14: Exemplification of the motion control from the controller unit to the stepper motor

during periods of no-motion requirement. When this command is engaged, the motor is locked by a passivating current from the driver. This ensures that the motion stage is locked in position even if other components interact with it. The system's repeatability is increased by locking each stage to the desired position. The step signal from the controller is a pulse with a minimum pulse width, as instructed by the driver specification. Finally, the direction is a command of setting the rotation of the motor to a clockwise or counterclockwise rotation.

## Laser Control

A Unified Systems Controller, built to interface with LPBF systems, has been utilised for laser control in the developed system. This controller has previously been developed by the AM group at DTU and is a drop-in system used as a substitute for standard industrial laser controllers. The controller has been developed as part of the Open Additive Manufacturing Initiative by Sebastian Aa. Andersen as part of his PhD and is described in [212, 213]. The Unified Systems Controller incorporates a Teensy 3.6 for fast processing speed of the laser motion and control signals. The program for the laser control is embedded in the Unified Systems Controller and has been developed by Sebastian with input from the author to optimise the program for PBF-LB/P.

The Unified Systems Controller is designed to manage the XY100-2 protocol. This protocol communicates the desired position of the laser spot to the galvanometer. By accepting this protocol, the galvanometer-controlled mirrors are set, redirecting the laser to the position. Besides the XY100-2 protocol, a series of options for communication is allowed by the Unified Systems Controller. One parameter sets the laser power value determined by a 0-10v signal accepted by the laser source. Secondly, either a TTL or 24v signal instructs

the laser when to fire. Utilising all these features allows the control of the laser position and the laser parameters of power and On-Off in a synchronised manner. The original intent of the Unified Systems Controller was the laser and system control of a PBF-LB/M system. The optimisations required for polymer powder processing have therefore been limited.

A significant difference between the two processes is the desired scanning speed. Metal processing systems rarely process faster than 2m/s [214]. For polymer powder processing, the scanning speed is typically up to an order of magnitude greater. As presented in Table 3.1, commercial systems utilise rapid scanning motions to optimise the processing time. It was a desire to mimic these scanning speeds in the developed system. A limit was found based on the current controller platform, not allowing scanning speeds greater than 3 m/s. Scanning fast has a considerable influence on the system because the high-power fibre laser delivers enough energy to set the build plane on fire if left at a 'too' low-speed setting. By tuning the scanning speed and power input, a correlation and stable region was found for the powder processing as explained in chapter 7.

Optimisation of the embedded programming for achieving faster scan speeds and general tweaking for the PBF-LB/P process has been the main contribution to the development of the Unified Systems Controller, with the controller manufacturer producing the actual changes. Besides this, the Unified Systems Controller has acted as a black box piece of electronic equipment utilised for laser control. Below is the system diagram for the control system feeding into the separate sub-systems of the Mechanical and Laser systems.

Control of the process mandates several layered sequences of controller systems, as seen in Figure 5.15. Initially, the process control resides in the host computer that handles the controller board communication of the processed job file. This job file is a result of

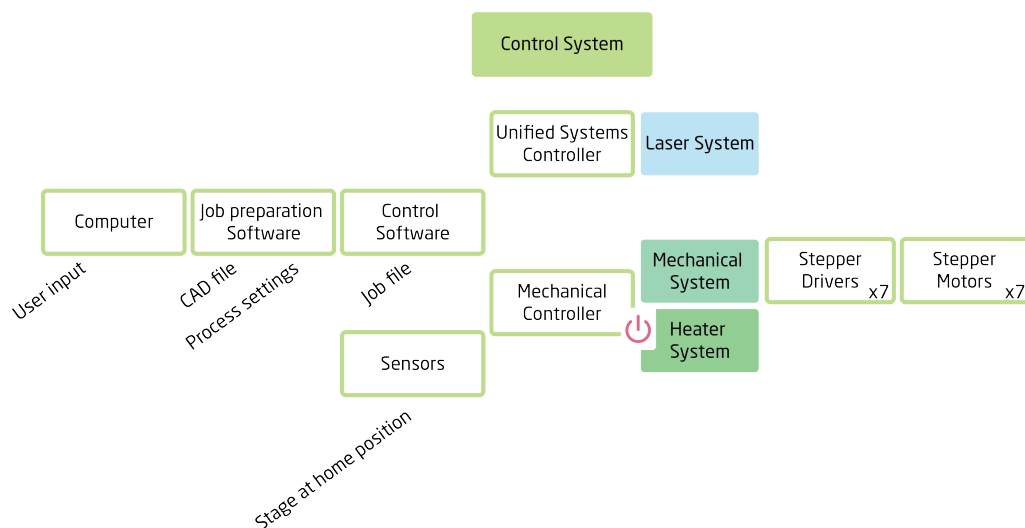


Figure 5.15: Controller system diagram

the job file generation sequence on the computer and is based on the CAD file and user input. Communication between the computer and controllers acts in both directions. The computer relays instructions from the job file while receiving processing status' from the controller boards. The process status message confirms an action has been executed, and the following job file command can be sent for processing in the controllers. Depending on the type of command, the computer either sends the command to the Unified Systems Controller or the mechanical controller. These then handle the translation of the command into the desired output of the system, being either a laser control command or a physical action.

## 5.4.2 Laser and Laser Delivery System

For consolidation of the polymer powder, a laser system is implemented, delivering heat energy for fusing the powder into a component. The laser selectively fuses the powder, producing the part one layer at a time. The selection process for the laser is described below, including the choice of the fibre laser type and the laser delivery sub-system, focussing and translating the laser spot on the build plane.

### Laser Selection

Utilising the correct laser source is imperative to successfully repurposing the system for PBF-LB/P. The Projet system sets up a unique set of boundaries and conditions for delivering the laser to the build plane, both considering the physical limitations of the Projet








Laser Source	Defined by	
Laser Power $P$ (W)	User	
Spot Size $L_s$ (mm)	System	
Laser Wavelength $\lambda$		
Beam Shape		
Powder Absorptivity $A_p$ (%)	Powder Material	
Laser Penetration Depth $L_{pd}$ (mm)	True Energy Delivered	
Laser Reflection & Transmission $L_L$ (%)		
Laser Stabilisation Time	Laser	
Laser fluctuation		
Powder Absorptivity $A_p$ (%)		
Laser Penetration Depth $L_{pd}$ (mm)	Final Part Quality in LB-PBF/P	
Laser Absorptivity (%)	Material Processability in LB-PBF/P	

Figure 5.16: Defining parameters and derived process signatures for selection of an appropriate laser source for processing polymer powders

system and the interfaces. Secondly, the operational constraints, such as the laser mode and beam quality, have been determined by the main hypothesis of the investigation. The physical boundaries and selection constraints can be derived into a list of critical system elements for the laser source based on the knowledge obtained in the literature study as presented in Figure 5.16.

The definitions of process parameters and signatures from the literature survey for laser source selection indicate a laser that permits good absorption in the polymer powder, such as a CO<sub>2</sub> laser. As stated in section 1.1, a desire to investigate the fibre laser utility in the process is a main driver of the laser type. Hence no further investigation of the CO<sub>2</sub> has been conducted.

Based on the list of critical system elements, several types of lasers can be an appropriate

Table 5.5: Elements for consideration of laser source selection derived from the analysis in Figure 5.16 and the physical constraints of the repurposed Project system

<b>Critical Laser Source System Elements</b>	
Critical element	Elaboration
High laser power	High-power lasers allow for faster processing, making the experimental setup more relevant for industry
Capable of producing a small spot size	The spot size has a direct influence on the minimum possible feature size and is influenced by the laser wavelength
Produce wavelength that matches the absorption spectra of polymers	Matching the wavelength and the absorption in the polymer system allows for effective energy transfer from the laser
Long-term stability of laser power	A stable laser source will ensure minimum process deviation during production and between production runs
Produce adequate penetration depth	The penetration depth of a focussed laser permits the fusion of several layers, stabilising the final part and geometry
Gaussian beam shape	A Gaussian beam shape allow for fine definition and control of the laser focus, penetration depth, and power density
Easy beam delivery	Delivering the laser beam in the correct area facilitates larger stability of the processing and system utilisation
Laser source location	Only one area of the system is not utilised for the powder processing capabilities. Therefore the laser source must fit into this area



choice. Fibre lasers producing an appropriate wavelength for polymer processing do exist. One technology, the Thulium doped fibre laser, produces a  $\approx 2 \mu\text{m}$  wavelength correlating well with the absorption spectrum for polymers often used for PBF-LB/P. However, this laser source is not as established as the Yb fibre laser. This causes elevated prices, and limited options regarding the beam delivery equipment, between the fibre and the build plane. The effect of this is a price range elevated by an order of magnitude compared to employing Yb fibre lasers. Yb fibre lasers produce outstanding beam qualities with an  $M^2$  typically below 1.3. Secondly, the theoretical spot size is much smaller, with the Rayleigh length significantly greater than the  $\text{CO}_2$  laser and is expected to be improved compared to the Thulium laser. The fibre laser provides easy beam delivery directly in the beam guidance equipment. It is a well-known technology, making the beam delivery equipment selection range wider, reducing time and effort in sourcing adequate equipment. A downside of utilising a Yb fibre laser for polymer powder processing is the limited absorption in the material. Investigation of the laser absorption and how to optimise this have been explored throughout this work and are presented in chapter 7.

From the analysis, a MaxPhotonics Co Ltd, 300 W, CW, 1080 nm, fibre laser was selected for the experimental setup [215]. The fibre laser is a cost-efficient solution for the polymer processing investigation. Several other fibre laser options were found during the selection phase of the laser source. All the different suppliers and systems provide similar laser specifications and qualities, with premium brands delivering the highest-grade lasers, at a premium cost. The choice of laser was heavily influenced by cost efficiency while maintaining the quality of the laser. The Max photonics laser delivers a laser with an  $M^2$  value of  $< 1.2$  and power stability of  $\pm 1\%$ . It is an air-cooled laser source easing the integration in the developed system and hosts a powerful red dot alignment laser. The laser can be tuned from 10 to 100% in power and provides a narrow wavelength distribution at  $1080 \text{ nm} \pm 10 \text{ nm}$ . The fibre laser main unit is housed below the electronics cabinet of the system in an area previously containing the powder recycling capability, as seen in Figure 5.17. The fibre delivery terminates at the interface to the beam guidance system positioned on the optical breadboard located inside the build chamber, directly above



Figure 5.17: Laser from Maxphotonics installed in the system



the build plane. The fibre laser is terminated in a QBH connector, which determines the connection constraint of the beam delivery between the fibre and build plane, which is discussed in the following section.

## Laser Delivery to the Build Plane

Delivery of the laser to the build plane required several features to be either removed or redesigned in the original Projet system to allow for installation and adjustment of the laser setup. The main influential parameters and process signatures are reported in Figure 5.18. Based on the analysis of the parameters and process signatures, a list of system-critical elements is produced as seen in Table 5.6.

Three main components accomplish the beam delivery from the fibre termination to the build plane. These are the beam collimator, which produces a collimated laser beam from the fibre output. Secondly, the galvanometer scanner directs the collimated laser light in the build plane. Lastly, the f-theta lens ensures a flat focal plane of the collimated laser, ensuring the focus of the spot is at a constant size for the entire build plane motion of the galvanometer scanner. Several parameters and process signatures determine the critical aspects of these components, which are listed below.

The laser delivery system must produce a collimated and focussed laser spot to the build plane, ensuring spot size stability and repeatability. For this, three components have been selected, pursuing a small spot size with fast and repeatable motion. All the components of the laser delivery system can be seen in Figure 5.19.








<b>Laser Delivery</b>	Defined by	
Scanning Speed $S_s$ (mm/s)	User	
Spot Size $L_s$ (mm)	System	
Laser incident Angle $A_i$ (°)	True Energy Delivered	
Laser Stabilisation Time Laser fluctuation	Laser	
Scanning Speed $S_s$ (mm/s) Focal Plane Scanner repeatability	Scanner and Optics	
Laser Penetration Depth $L_{pd}$ (mm)	Final Part Quality in LB-PBF/P	

Figure 5.18: Defining parameters and derived process signatures for designing the laser and optical setup

Table 5.6: Critical elements and aspects of laser delivery to the build plane derived from the analysis in Figure 5.16 and the physical constraints of system

<b>Critical Laser Delivery System Elements</b>	
Critical element	Elaboration
Adequate scanning speed	Fast laser scanning allows the use of the high-power capabilities of the selected laser
Capable of producing a small spot size	The spot size has a direct influence on the minimum possible feature size
Adequate power capability	The selected components must withstand high-power laser going up to 300W
Minimise the laser incident angle in the powder bed	Ensuring that the laser is scanning as close to normal to the build plane as possible, ensure minimum part deviation caused by laser transmission in the powder material
Repeatable movement	Repeatability ensures laser movement accurately scanning the desired geometry
500 mm back working distance in the system	The beam delivery equipment cannot protrude outside the physical system boundary
Versatile mounting surface	By implementing a versatile mounting surface for the laser, a large degree of freedom for adjustment of the laser is possible
Must mate to the QBH connector	Fibre delivery terminates in a QBH connector, it is necessary for the first component here to interface this standard connector
Required secondary equipment	Does any equipment need processing gas, cooling, or other secondary equipment, to stabilise the process

Translation of the laser spot on the build plane is done by a galvanometer scanner. Rapid motions and translation speeds can be produced for the laser spot since the motion is produced by a mirror placed on the galvanometer control motor. Increasing the distance from the galvanometer to the build plane increases the potential laser marking speed while lowering the resolution. The scanner was selected based on the critical aspects of laser delivery presented above. A Sunny Technologies 9320D galvanometer scanner [216] capable of producing marking speeds of 3 m/s and with a repeatability of 8  $\mu$ Rad was selected for the system. The scanner is cost-efficient. The XY2-100 communication protocol is accepted directly at the scanner interface, which is output from the Unified Systems Controller, making the system easy to integrate. Easy integration and support for the scanner are achieved by selecting the same as utilised by other systems during the Open Additive Manufacturing project, making it a known solution in the research group. Selecting the scanner system infers several choices and constraints for the other components in the laser

delivery system. These constraints are described below.

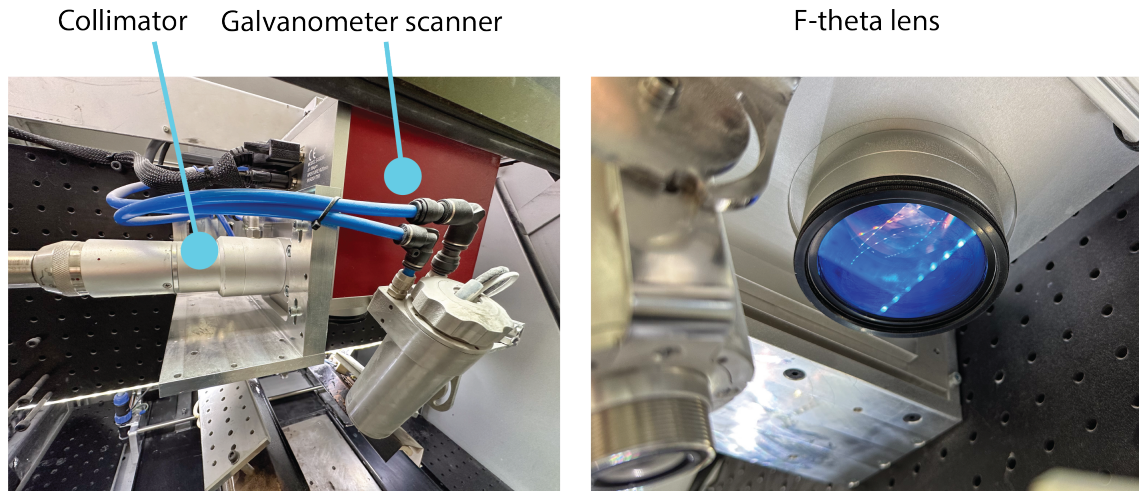


Figure 5.19: Laser delivery system

The selected galvanometer scanner has an input aperture of  $\text{Ø}20$  mm based on the size of the mirrors. The X and Y axis mirrors accept up to a  $\text{Ø}20$  mm beam, making these suited for high-power lasers due to the relatively low energy density in a  $\text{Ø}20$  mm spot. This constraint of input aperture determines the maximum size of the input collimated beam. When the input beam diameter is known, a collimator can be selected from the requirements. The collimator was selected with an output beam of  $\text{Ø}20$  mm to allow for the smallest possible spot size produced by the laser delivery system. The collimator was also selected based on the mounting flanges and the QBH connector, which were both set as requirements for the component. The mounting flange is important for mounting and alignment of the laser into the galvanometer scanner. If the laser is misaligned towards the mirrors, a certain amount of laser energy will pass by the mirrors, causing uncontrolled reflections, heat generation and possible damage to the galvanometer housing. A collimator was selected based on these requirements derived from the galvanometer scanner and the functionality analysis of the system's critical elements. The collimator selected was a Wavelength Opto-Electronics (D30F100-WC). The selection was based on a cost-efficient solution which delivers the desired characteristics as described above.

By selecting the collimator, and galvanometer scanner, the laser spot is determined prior to being focussed by the f-theta lens at the build plane. For focussing the beam in a flat plane, an f-theta lens is used. A relation between the input and output beam size is considered when defining the focussed spot size. Here the laser input size is related inversely to the spot size as seen by Equation 5.6. Here  $C$  is a constant, which for a Gaussian beam is 1.83,  $\lambda$  is the wavelength of the laser,  $f$  is the effective focal length of the f-theta lens, and  $A$  is the beam diameter when entering the f-theta lens. By this, a smaller spot can be obtained with a larger entrance beam. The larger entrance beam minimises the requirements

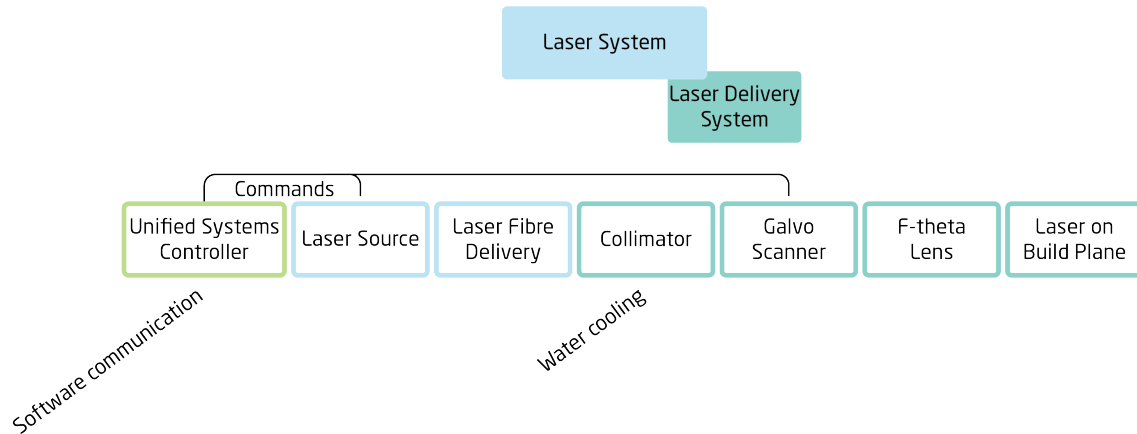


Figure 5.20: Laser system diagram

for the remaining setup by lowering the energy density in the collimator lens array, the galvanometer scanner mirrors and f-theta. By minimising the power density, the effect of thermal lensing can be minimised. Thermal lensing occurs due to the heating of the collimator, mirrors, and f-theta lens changing their properties and shifting the focus point, which is typically reverted when no more energy is applied.

$$Spotsize = C \cdot \lambda \cdot \frac{f}{A} \quad (5.6)$$

The final beam delivery and scanning system component is the f-theta lens. The f-theta lens is constrained by the selected beam diameter, the galvanometer mirror distance, and the connector between the f-theta and the galvanometer scanner. The f-theta lens was selected based on a cost-efficient solution that would withstand the desired processing conditions and not endure thermal lensing during operation. The lens should furthermore not be damaged during operation caused by the high-power laser. A Cloudray Laser f-theta (HY-SL-1064-200-290 [217]) was chosen for the system. This lens produces a scan field comparable to the build plane size and a focal length that suits the physical limitations of the system. The scan area of the lens is 200 by 200 mm, which covers the majority of the build plane in the system. It further provides a short focal distance of 290 mm and a working distance of 324 mm, making it ideal in the laser setup.

The laser delivery system required an auxiliary component, a water cooling system for the collimator, ensuring that the power delivered through the collimator does not build up heat and ruin the lens array inside. An overview of the laser system can be seen in Figure 5.20.

### 5.4.3 Heater Design

Designing a new heating system for PBF-LB/P was engaged by developing the knowledge about the critical process influential parameters and signatures as seen in Figure 5.21. A list of critical system elements can be constructed based on these parameters and signatures. The list provides crucial information for the heater design concerning the delivery of sufficient energy for maintaining the process temperature in the powder cake for extended periods while minimising any thermal gradients in the powder cake. The list is shown in Table 5.7, relating the critical aspect and elements to the primary reason for these.








<b>Chamber Heating system</b>		Defined by	
Material Properties $T_m$ & $T_c$ (°C)		<i>Powder material</i>	
Heater Wavelength $\lambda_H$		<i>System</i>	
Powder bed surface Temperature $T_s$ (°C)		<i>True Energy Delivered</i>	
Powder Cake Temperature (°C)		<i>Heater</i>	
Build Plane Temperature (°C)			
Build Chamber Temperature (°C)			
Powder Cake Density		<i>Feed and Recoater</i>	
Powder Temperature (°C)			
Process Chamber Stability		<i>Final Part Quality in PBF-LB/P</i>	
Material Degradation			
Powder bed surface Temperature $T_s$ (°C)			

Figure 5.21: Process parameters and signatures - heating system

Table 5.7: Critical elements and aspects for heater design derived from the analysis in Figure 5.21

<b>Critical Heater System Elements</b>	
Critical element	Elaboration
Maintain process temperature	Processing PA11 and other mid-range temperature polymers
Easily adjustable during operation	Fine-tuning the process during operation is critical to the build stability
Temperature stability	Stable heating allows for easier processing
Build piston vs powder cake temperature	The heaters must maintain heat in the centre of the powder cake and not just powder / build piston interface
Cover the build piston sides	Reducing cold areas in the powder cake to ensure more stable processing

## Contact Heaters

Design of the contact heaters that, by conduction, heat the powder cake was based on aspects of the critical elements presented in Table 5.7. The heaters were designed with inspiration from the original setup but designed to match the layout of the build piston closer. A unique design of the heater layout was created for each side of the build piston, covering the entire build piston wall. This included cutout regions where elements from the build piston walls protrude. These protrusions are utilised for anchoring the retaining plate holding the insulation and heater in place on the build piston outer wall. The heating elements were designed and developed in collaboration with the company HeatXperts Aps from Denmark. A heating element was also designed and installed for the build plate. In total, three heater designs were developed since the heaters located on the build piston wall are symmetric on the opposite side. Making the heaters conform to the build piston implies a possibility of achieving a consistent heat distribution.

Technical drawings in Figure 5.22 (Appendix A) show the overall dimension, including the cutouts and details for the retaining plate anchoring. The wire location and direction are also shown, where the most significant difference is seen for the build plate heater. Because the heater takes up the entire build plate, the wires needed to run on top of the heater instead of away. However, these wires are directed through insulation material and away from the intense heat.

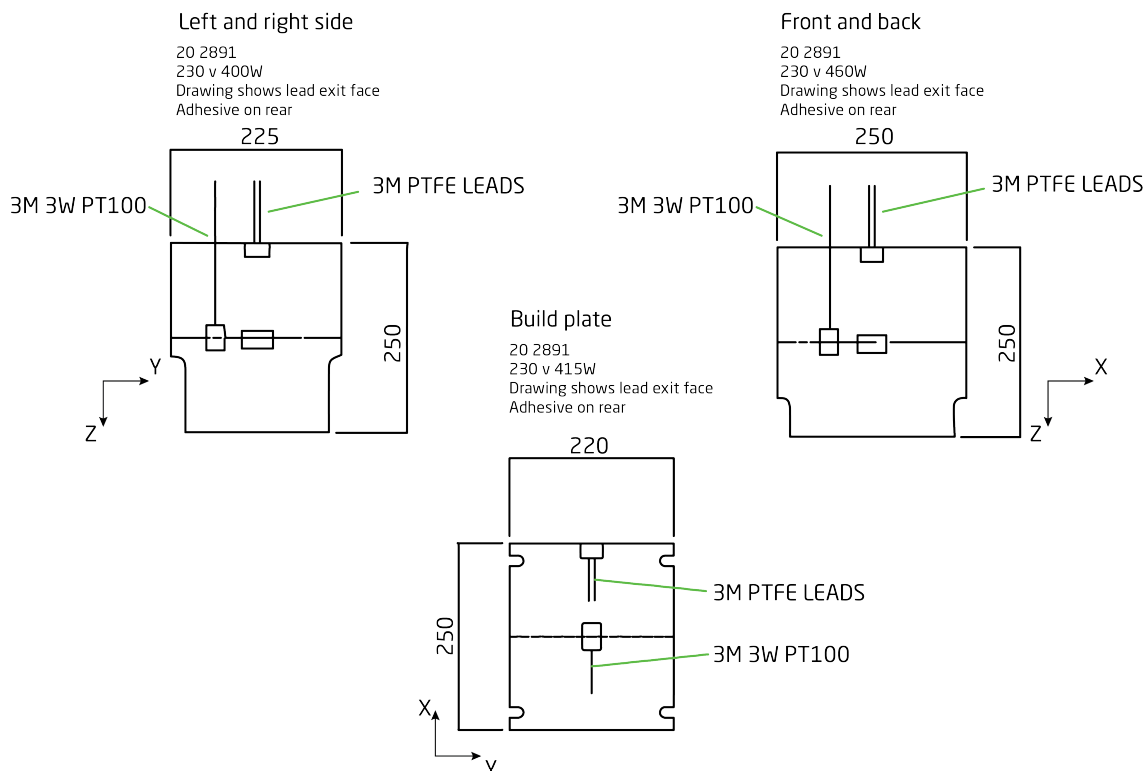
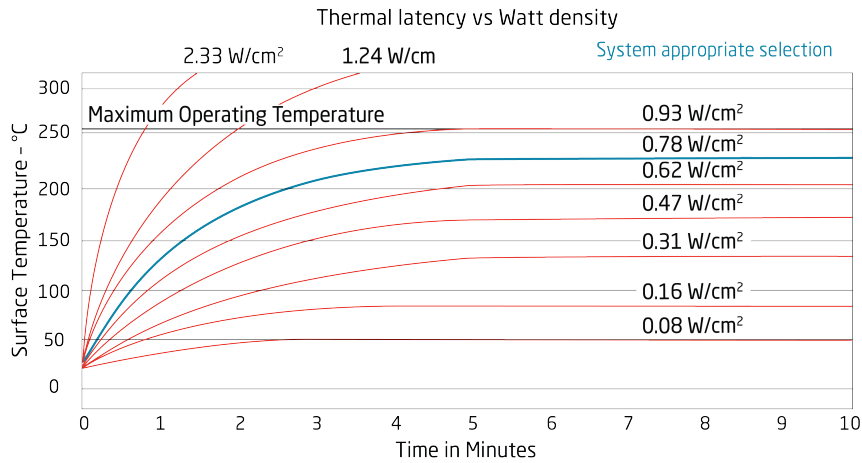
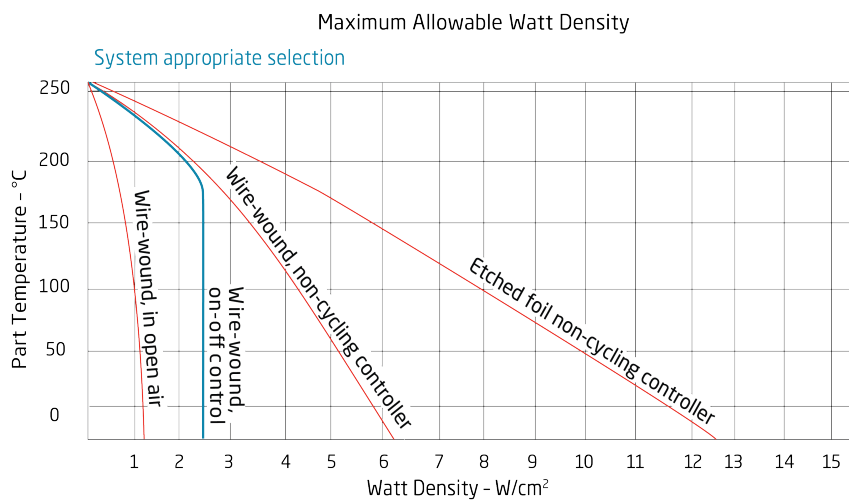


Figure 5.22: Heater specification. Full technical drawing found in Appendix A



(a) Typical selection of Watt densities for silicon heaters



(b) Maximum allowable Watt densities for silicon heaters

Figure 5.23: Heater selection guide. Adapted from: [218]

To determine the power density of the heaters, two key aspects play a role. One is the maximum allowable Watt density (Figure 5.23b), defined by the type of heater installed. Secondly, the desired thermal latency of the system determines the surface temperature vs time constant (Figure 5.23a). High-power-density heaters produce low thermal latency in a system, rapidly minimising the deviation between the set point and measured temperature. This type of heater is, however, not suited for elevated temperatures over extended durations. A trade-off between the two is therefore evident. The thermal latency of the system is expected to be low since a large heating area is produced for the build piston. Heating is carried out from the start of a build job, meaning that a large powder volume is never heated instantaneously but rather layer-by-layer throughout a build. Finally, the maximum allowable Watt density is determined by considering power control and whether or not the heating element is insulated. Since the entire build piston is insulated from the



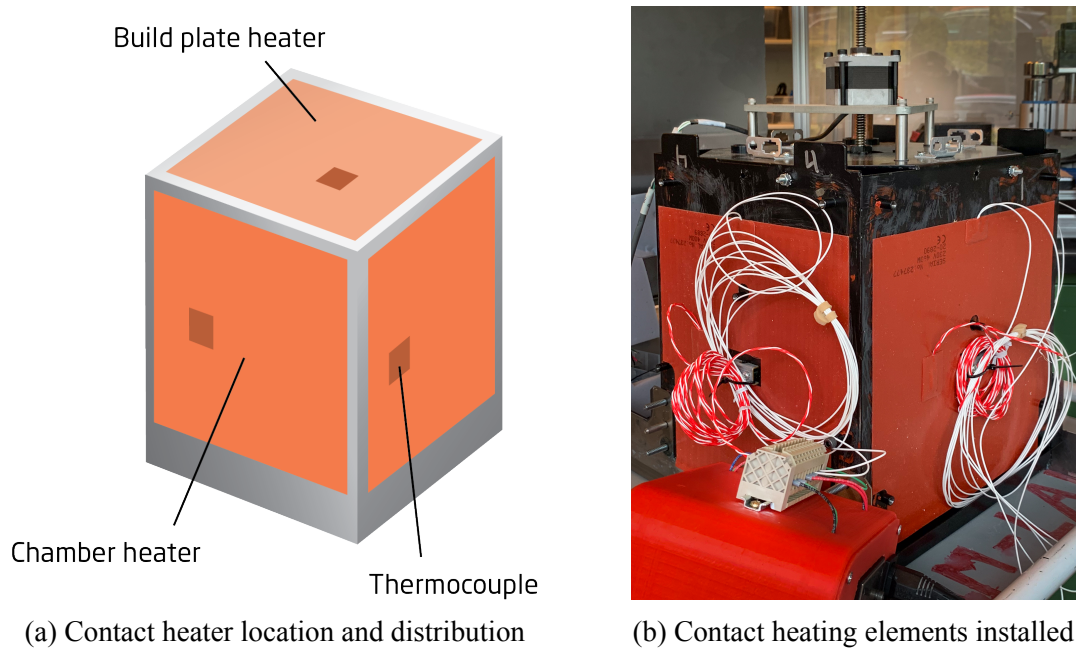


Figure 5.24: Contact heating system layout with the heater and thermocouple location exemplified

outside, keeping the heating elements pressed against the build piston. A design limitation is already met. A rule of thumb stated by Watlow [218], producer of silicone heaters, is that if insulation is used, the Watt density must be downrated by one-third ( $1/3$ ). The control for the heating elements is On-Off control, by PID regulators and solid-state relays, which then defines another limitation in defining the allowable Watt density.

The design of the heaters was based on the above-presented limitations. By following the design and selection guide presented by Watlow [218] and seen in Figure 5.23, a choice of power density and maximum wattage was defined. The heater was designed around wire wound contact heating, On-Off control and a power density of  $0.78 \text{ W/cm}^2$  as stated in Figure 5.23. A lower power density can be selected by covering the entire build piston since the power is distributed evenly to the piston over a larger area.

A crucial parameter for the installed heaters was a process temperature up to  $200 \text{ }^\circ\text{C}$  for the duration of a production run, which can be 24 hours or more. The heaters were designed to cover the entire face of the build piston, as seen from Figure 5.24, utilising the whole surface to heat the powder cake. For the contact surfaces of the build piston, three different heater layouts were designed since the build piston is symmetrical across the Z-axis. Five heaters were installed, delivering  $2135 \text{ W}$  to the build piston.

Individual PID controllers have been fitted in the system to allow for temperature adjustment during operation. These allow for  $0.1 \text{ }^\circ\text{C}$  adjustment during processing. The temperature of each heater is fed back to the PID controller by the PT100 thermocouples



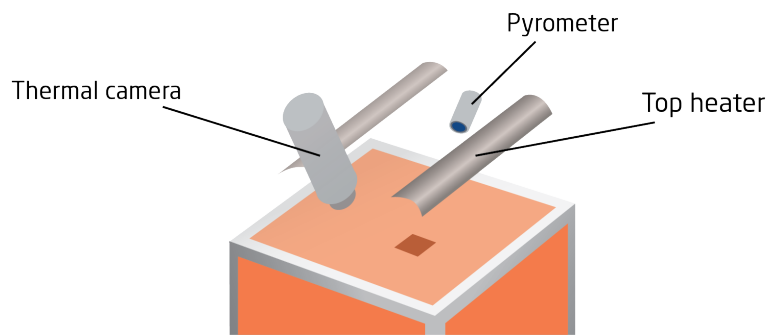
located on the heater, as shown in Figures 5.22 & 5.24. The installed PID controllers are adjusted by the automatic tuning sequence following the manufacturer's guidelines. The PID controllers are of the type PXU21A20 from Red Lion. The current switching for the heaters is performed by three double-sided solid-state relays (Crydom CD2425W1U), ensuring robust switching over the long duration of a build cycle.

## Top Heaters

Two heaters are placed above the build plane, aiding the temperature stabilisation of the powder cake, alongside the contact heaters located on the build piston. The intention is to maintain a stable process temperature in the build plane and the powder cake. Where the main focus of the top heaters is the build plane temperature. Several approaches are utilised in industry, mainly considering heat lamps in some variation. The top heating can not draw on the same benefits as the contact heaters having an even distribution over a surface area. Instead, these heat lamps must be selected to allow for the even distribution of energy. Secondly, the heaters should respond rapidly to changes in the temperature of the build plane. The short response time of the top heaters provides a stable processing environment for the laser, mitigating the risk of warping or curling. To fully comprehend the utilisation of top heaters, an analysis of the heating regime has been conducted as shown above in Figure 5.21.

The design of the top heaters follows the same methodology as the contact heaters, utilising the same list of critical system elements as described in Table 5.7. The top heaters must supply a large amount of energy to the build plane since conduction and radiation occur in the surrounding process chamber. The conduction heats up anything in contact with the build plane, especially the recoater. Radiation is the general loss of energy to the surroundings, either to the process chamber or the sub-systems around the build plane.

Two types of heaters are adequate for heating the polymer powder to the process temperatures often utilised in AM. One type is quartz lamps, which produce heat radiation in the visible light spectrum. The lamps, therefore, supply a mix of heat and light to the build plane and are commonly seen in industrial machines. The other type often used is the ceramic heater, which supply infrared radiation. Both types are highly efficient in delivering energy to the build plane and incur a directionality to some extent. Ceramic heaters have a longer heat-up and cool-down latency, supplying smoother energy when controlled in an On-Off mode, whereas quartz lamps tend to heat and cool faster, producing a more rapid response during operation. Both types of On-Off cycling can be beneficial, with the added opportunity of controlling the amount of energy emitted by quartz lamps from a scale of 0 to 100% by "dimming" the energy emission. To lower the complexity of the heater system, a set of two 1kW ceramic heaters (RS Pro - 196-6462) was selected, supplying an adequate amount of energy for retaining the process temperature in the build plane. The two



(a) New top heater location and distribution



(b) Ceramic heaters installed in the machine

Figure 5.25: Top heater system, and the pyrometer for control

ceramic heaters can be seen in Figure 5.25 with the location of the heaters and pyrometer presented in Figure 5.25a, and the installed configuration shown in Figure 5.25b.

To control the heaters, a pyrometer is installed facing the build plane. The pyrometer (Calex - PC21MT-0) supplies the PID controller with a temperature signal, which determines the On-Off control action for the heaters. As mentioned above, the PID controller regulates the solid state relay, ensuring the stability and rapid cycle ratio needed for this power control.

Implementing the contact and top heaters ensured a stable processing regime of the entire powder cake, with a high degree of adjustability. Adjustability and control of the heaters fulfil the critical element analysis, which aids the processing of polymer powders. The heaters are an integral part of PBF-LB/P processing, with the vast majority of research carried out for heated environments. Moreover, to the best of the author's knowledge, no industrial systems currently run the process under cold conditions. '

Niino T et al. [219] presented a solution for processing polymer powder in the PBF-LB/P with no heat added besides by the laser. The results point towards a solution similar to the

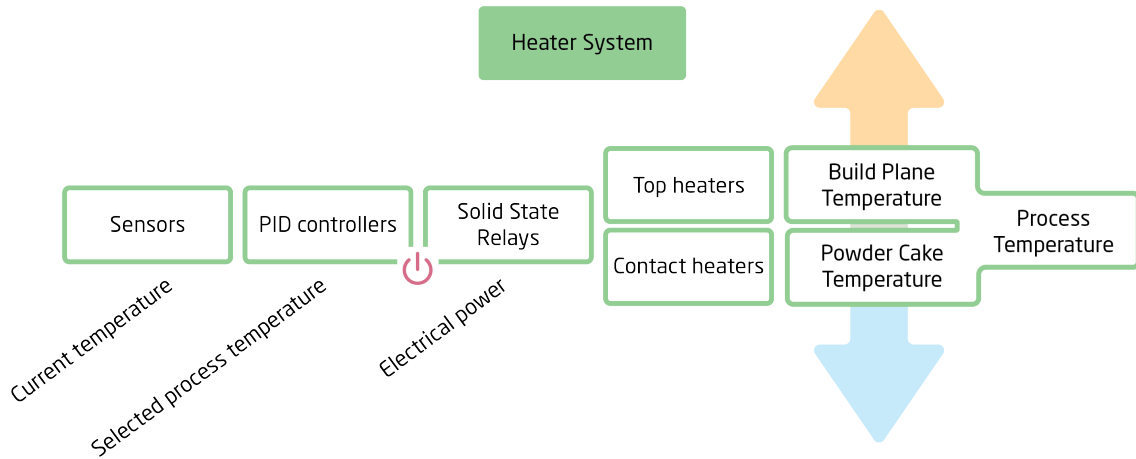


Figure 5.26: The heater system diagram

PBF-LB/M process where the parts are constructed with anchors or support structures to the build plate, alleviating the curling effect of residual stresses in the material. Polymer powder processing is successful, with significant issues found in the inter-layer adhesion and consolidation, proving a further need for process optimisation and research in this field. Unheated laser processing of polymer powder causes large internal stresses in the material due to the chain ordering and crystallisation during cooling from the molten state as explained in subsection 2.2.1. Utilising amorphous polymers for an unheated process can yield more stable results due to the smaller shrinkage factor of these materials. An investigation of this is interesting for future work exploration once the stable processing by fibre laser has been defined.

A system diagram for the heating system is shown in Figure 5.26. An On-Off cycle was selected for the heater control to minimise complexity. A discrepancy between the internal temperature of the powder cake and the measured value by the sensors at the build piston walls is evident. It is not possible to measure the temperature in the powder cake during the operation of the system, as to why the sensors are located in the depicted areas. This discrepancy and the calibration hereof is the focus of the work presented in section 6.1.

#### 5.4.4 Recoating System

The recoating system of the original machine was a versatile system capable of both the recoating and binder jetting action, as described in section 5.3. The binder jetting functionality depended on a gantry for controlling the X-direction motion of the binder jetting print head. The height of the gantry interfered with the optimisation of the top heaters, and a redesign was crucial for the functionality of the system. The influence of the recoater system on the successful manufacturing cycle was analysed by defining the process parameters and signatures related to this. The analysis is shown in Figure 5.27.

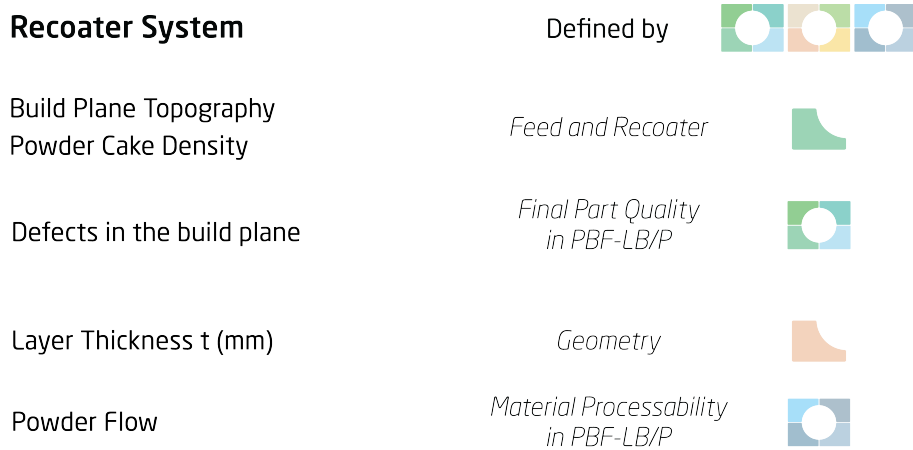


Figure 5.27: Defining process parameters and signatures considering the desired capabilities of the recoating system

Table 5.8: Critical aspects and elements for the recoater system

Critical Recoating System Elements	
Critical element	Elaboration
Produce a flat new build plane	The flatness of the build has a large influence on the final part properties
Roller recoater action	By utilising the correct geometry and recoating action, a more diverse material portfolio is possible to process. This is due to the design of the recoater determining the type of powder that the machine is capable of distributing in an even flat layer
The recoating speed must be adjustable	Adjusting the recoating speed further increases the processing capabilities of the machine by allowing fine-tuning for different powders
Roller speed and direction must be adjustable	The adjustability of the roller allows for complex process and recoating action development
Recoater must be as short as possible	When the recoating system protrudes from the build plane further than necessary, issues can arise with the interaction of the top heaters or other sensor equipment
Must encompass sensor mounting capabilities	By providing power and redundant connectivity, other sensors relevant to the recoating process can be mounted directly to the sub-system
It must fit on the original rail system	The original recoating system in the machine provides two rails, one guided and one for sliding on top.

A versatile recoating system that allows different speed settings and controls over the recoating action was desired to improve the performance of the sub-system. One crucial parameter when discussing the recoater system is the fluidisation behaviour of the powder in the system during recoating. To guarantee the recoater sub-system delivers the capabilities desired, a list of critical system elements is developed, as shown in Table 5.8. By adhering to this list during the development of the recoater, a sub-system allowing research beyond what can be achieved traditionally is produced.

## Recoating Gantry

From the original machine, size and location limitations are constructed for the new recoating system. As seen from Table 5.8, the system must adhere to the original motion system and mount onto the rails of the original machine. Inspiration of the old system facilitated the designing of the new recoating system. By adhering to the design constraints of the original system, easy integration of the new recoater sub-system was ensured. The roller design is limited by the clearance gap in the original machine since the powder feed mechanism is kept in its unaltered state. Furthermore, the location of the roller is limited by the linear motion range designated by the original machine. A roller of 20 mm in height, spanning the width of the recoater assembly and placed at the back of the assembly, as seen from the viewing window, has been developed following the limitations set by the original machine. The design of the recoater system was constructed on two rails. One rail is a linear guide with two ball-bearing guides on it. The second is a sliding rail, where the recoating system slides on top of two low friction pads. Utilising the same guides for the new recoater assembly ensure that the original recoater can be replaced if added functionality of the X gantry is required.

The linear guide rail houses the stepper motor and belt drive for the recoating motion. The stepper motor is a NEMA 17 motor, delivering up to 180 N-cm by a 5:1 gearing, ensuring stability and no step skipping during operation. Selecting a geared motor minimises the risk of the motor stalling and losing position. High fidelity of this linear motion is critical to ensure a complete recoating action for every process cycle of a build. The number of layers determines the number of recoating cycles during a build job, which can reach several thousand.

Utilising a geared stepper motor infer backlash in the gearing. The backlash for the motor is specified by the manufacturer to  $< 0.8^\circ$ , which is acceptable for the use case since only two shifts of direction are needed for every cycle. The backlash is seen to be less than one step of an ungeared motor ( $1.8^\circ$  per step) and is the same as missing close to 2 steps in the geared setup.

A hall effect sensor for homing the recoater is located on a red bracket at the back of the machine, as shown in Figure 5.28. The recoater features a redundant electrical connection,



which can be utilised for sensor integration as needed. It provides the added functionality of swapping between the old and the new recoating device. The old recoater, including the X-gantry, can be utilised for testing material layout or combinations of laser and binder fusion. The old recoating system was kept in the eventuality that research in any of these or other fields could be of interest in the future.

## Roller

A stepper motor was selected for the belt drive of the roller in the assembly. The choice of a stepper motor allowed for precise control of the roller's speed and direction. The build complexity could be minimised by having one motor and driver type. The roller on the recoater is a 20 mm polished stainless steel rod. It is mounted on the recoater and rests in two ball bearings on either end. A belt drive connects the motor and roller, producing the motion. The two pulleys located on the motor and the roller are the same size to ensure no further gearing. This ensures the roller and motor drive are synced in revolutions, producing one revolution per 200 steps, limiting the complexity when selecting other rotational speeds.

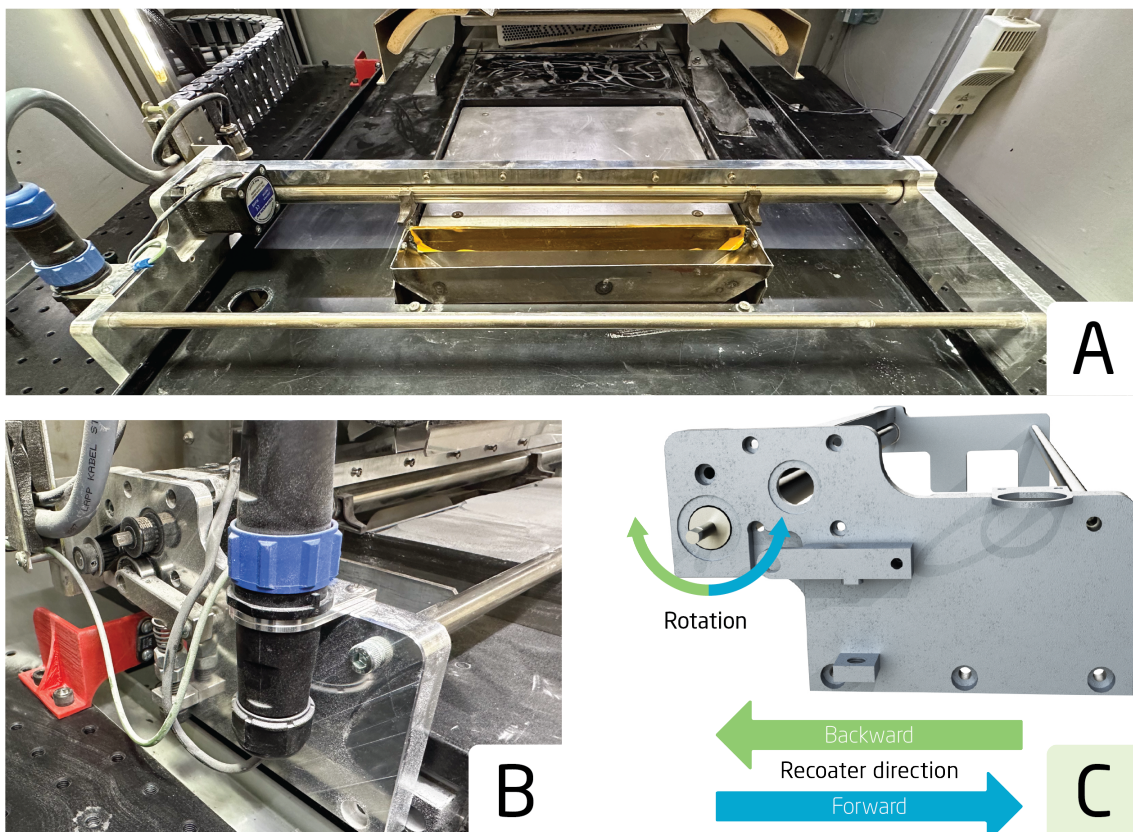


Figure 5.28: A: Recoater assembly installed in the machine  
 B: Recoater at the home position (red bracket hosts the homing sensor)  
 C: Render of recoater plate for mounting motor, drive belt, electrical wire harness, and belt tightener for the roller recoating action

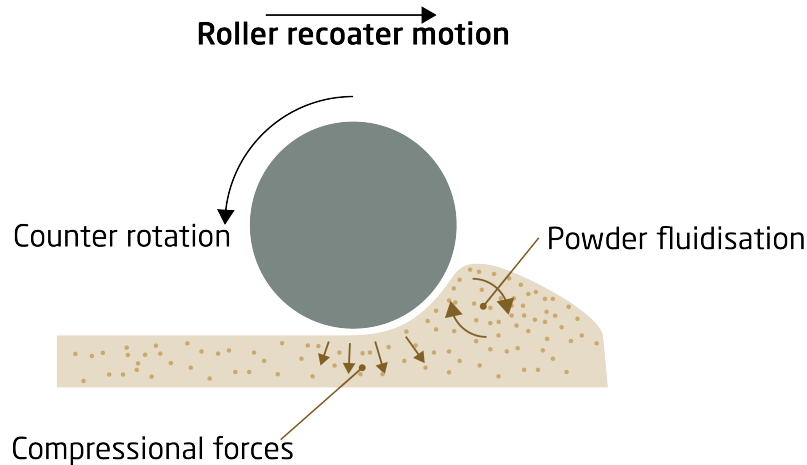


Figure 5.29: Powder fluidisation behaviour caused by the counter-rotation of the roller

The Stepper motor is a NEMA 14, which is adequate, considering the limited amount of torque needed for the roller operation. The system can be used in a wiper mode where the motor locks the roller in position. For this, the stepper motor provides 40 N-cm holding torque. The wiper effect has been tried successfully but produced an uneven and degraded build plane, hence this was not investigated further. The design of the roller is not ideal for a wiper action and will need a redesign for this option to function. A wiper is often shaped like a blade, as described in subsection 4.2.1, while the roller produces a significantly larger area of downward contact with the bed, causing the issues found for the wiper action testing.

The recoating routine involves a forward and backward motion, in which the direction of the rotation of the roller is reversed. The roller always functions in a counter-rotating

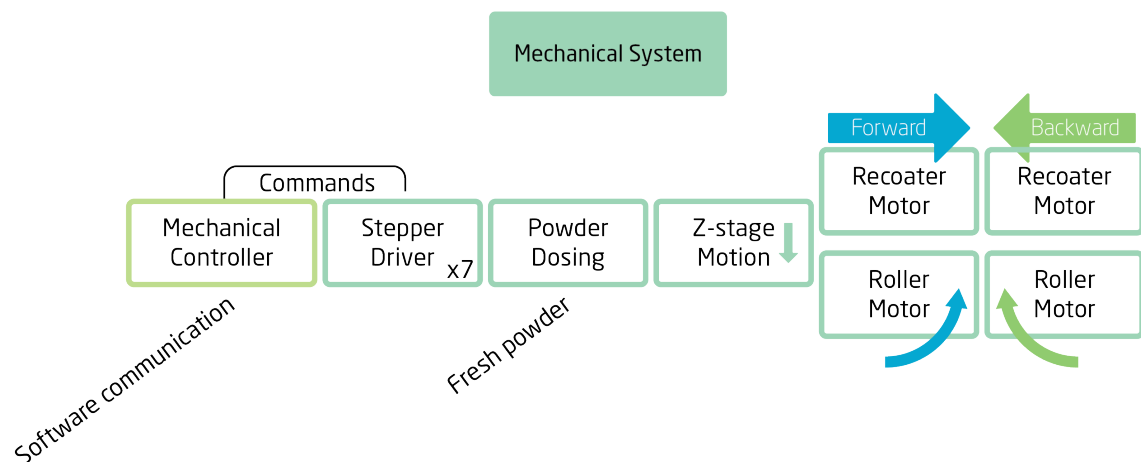


Figure 5.30: Recoating and mechanical motion system diagram for the production of a fresh build plane

action meaning that the rotation is counterclockwise going forward and clockwise going back when viewed as seen in Figure 5.28 C. By switching the direction between the forward and backward motion, a fluidisation behaviour of the powder is retained as seen in Figure 5.29. The fluidisation behaviour of the powder is critical for even distribution and good powder packing. By constantly agitating the powder in the flow front, non-spherical powders can be utilised in the process since the flow behaviour of powder relies on the shape and the agitation.

The counter-rotation motion during the forward and backward motion aid powder packing. The backward motion increases the packing density in areas of the bed less compacted by the forward motion. During recoating, the vertical-stage only moves once to provide space for the new layer. Most industrial printers utilise double-sided recoating and only move the vertical-stage once per layer. Single-sided powder feeds are often seen to have a secondary motion of the vertical-stage, to omit the interaction of the recoater during the return motion. During testing, the secondary packing step during the reverse move increased the build pane quality. Figure 5.30 shows the process cycle and sub-systems involved in producing a new build plane. Most of the mechanical system is engaged to create the new build plane. All of the mechanical motion sub-systems in the developed system is controlled by the Arduino, managing the powder dosing, recoating and vertical-stage motions. The control feeds into 7 individual stepper drivers, exemplified by Figure 5.14. A number of these systems are not changed from the original machine, and no further explanation of these are therefore provided.

### 5.4.5 Thermal Imaging System

A thermal imaging device is installed in the system to comprehend the laser and powder interaction during manufacturing. The thermal imaging device, or thermal camera, is mounted above the build plane, producing an almost perpendicular viewing angle. A perfect top-down view of the build plane is the ideal location for the thermal imaging system. The camera, however, cannot be located directly above the build plane since the laser delivery system is located there. The angle slightly obscures the collected data. By experimental investigation of the viewing angle and setup, data processing parameters have been developed for producing reliable and valuable process insights, as described in section 6.1. The thermal camera was selected based on a list of critical system elements as seen in Table 5.9, based on the desired capabilities of the camera. The process parameter and signature analysis has been omitted since the thermal camera does not directly inflict the process quality of the PBF-LB/P system.

The camera selection process provided several possible candidates, which were narrowed down to the Optris XI400 seen installed in Figure 5.31. The selected camera model offers an adequate level of calibration options, fast recording speed (up to 80 Hz), and the



Table 5.9: Critical aspects for designing the thermal imaging system

<b>Critical Thermal Imaging System Elements</b>	
Critical element	Elaboration
Large view area	Ensures thermal imaging of the entire build plane
Adequate framerate	The beam delivery moves the laser irradiation spot at up to 3 m/s. The capability of motion capturing permits high fidelity in the process analysis
Tolerate elevated temperatures	The build chamber is heated by the heater system, causing chamber temperatures above 60 °C
Robust and easy access to data	Data acquisition and analysis is the main purpose of the thermal imaging device
Provide calibration options	Due to the less ideal location of the camera, it must be tuned to accurately provide the actual temperature of the build plane.

option of a water-cooled sleeve to enable high-temperature operation. The camera entails good accuracy of  $\pm 2\%$  and the ability through software to record and do snapshot measurements of the process (Figure 5.33). The thermal camera implementation is seen in Figures 5.31 & 5.32, showing the deployment and angle of the camera in the system. The water-cooled sleeve with the input and output lines in blue at the top of the camera is fed by coolant from the same supply as the collimator.

Besides the software output of the camera Figure 5.33, an Industrial process interface (PIF) can be connected to the thermal camera. The PIF box delivers a programmable interface to obtain data collection by three individually programmable 4-20 mA output signals. The box also allows inputs for an external trigger. This trigger can produce either video or

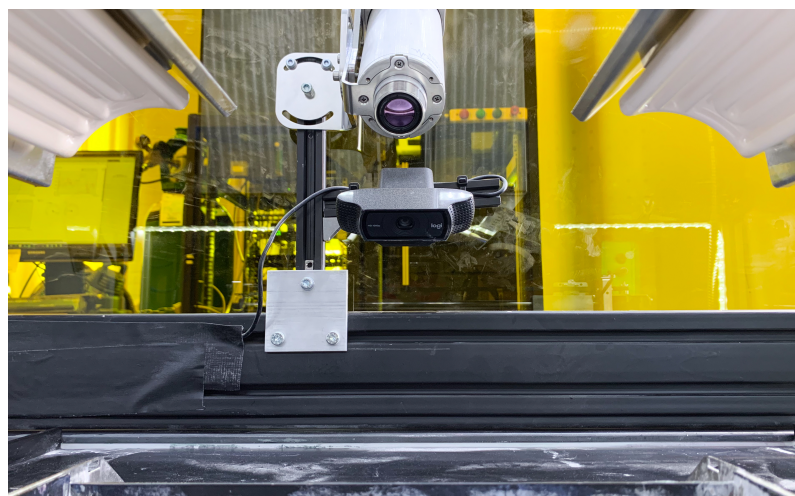


Figure 5.31: Thermal camera pointed towards the build plane

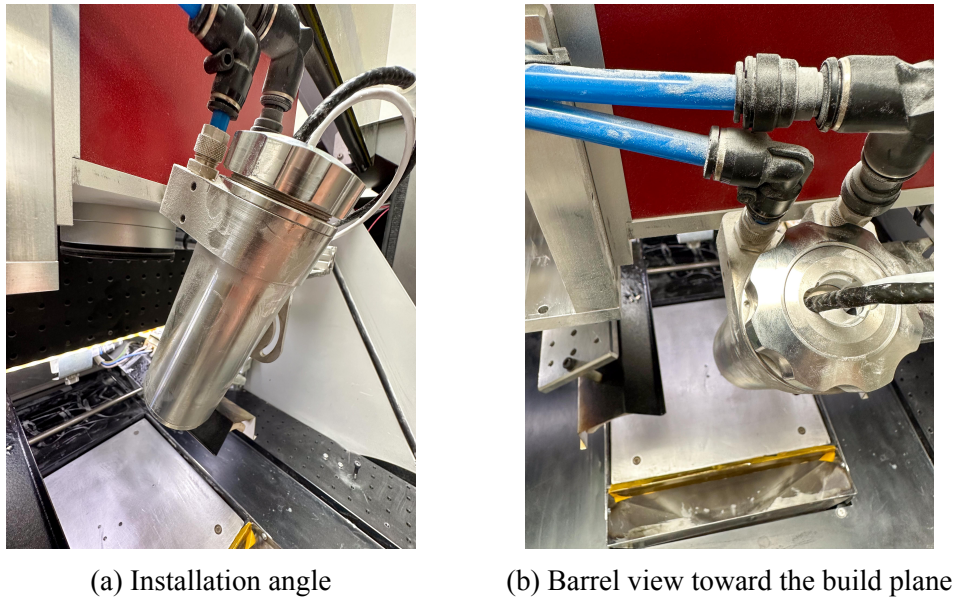


Figure 5.32: Thermal camera installation in the developed system

image capture at specific points during the process. Additionally, the box has an external emissivity setting. This setting is crucial when dealing with different materials within the same process. Overall, the thermal camera provides a diagnostic tool for determining the process stability not seen often for industrial systems. Other camera solutions could have been made, but the selected system produced the best capable solution concerning cost efficiency and versatility. The utilisation of the thermal imaging system is shown in

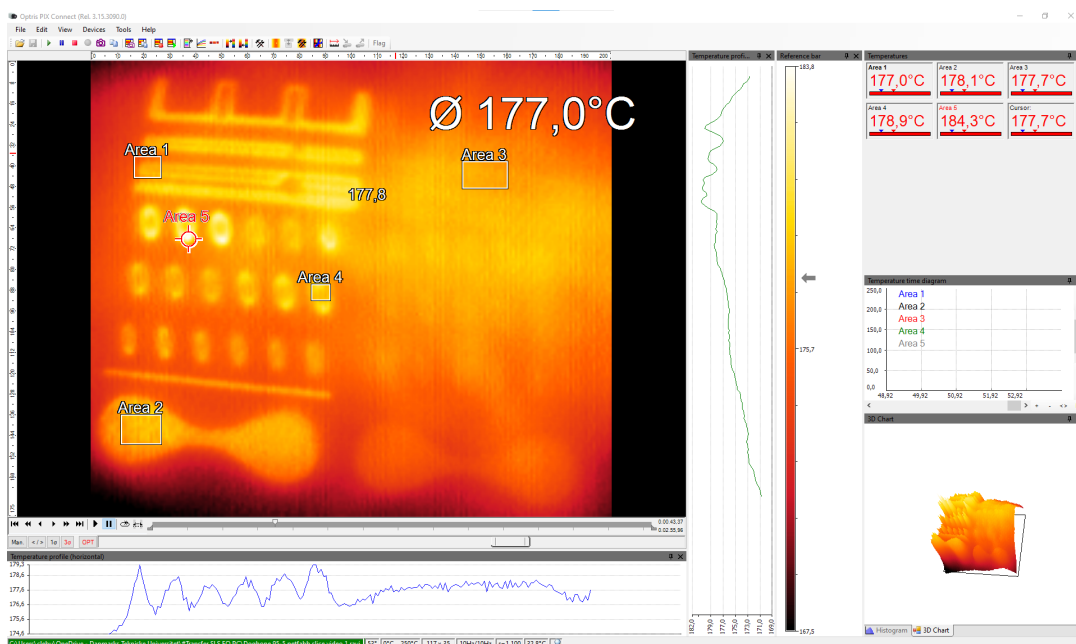


Figure 5.33: Software for the thermal camera

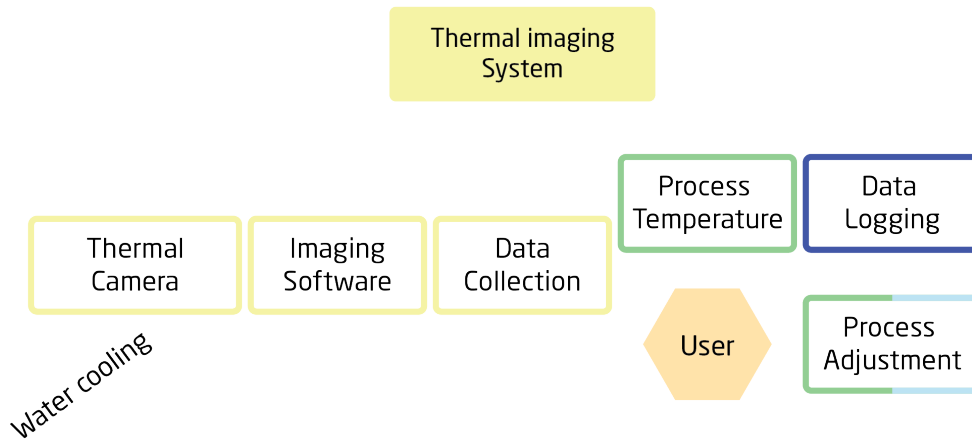


Figure 5.34: Thermal imaging system diagram including the process of process interference by user input based on the thermal imaging data

Figure 5.34.

The thermal imaging data is used routinely during the process optimisation of materials. The effect of warping during initial layers is pronounced in the thermal camera view. The system can thereby be used for tuning the process parameters during the process optimisation routine used for introducing new materials in the system. Besides this, data logging of the process temperature can be carried out for a single layer or the duration of an entire build job.

### 5.4.6 Data Capture System

A data capture system was implemented to monitor the process remotely (including the heat-up, cool-down, and power consumption) and provide process insights throughout the manufacturing cycle. A colleague from the University of Pisa designed the system. The system is described in his contribution to the *"Joint Special Interest Group Meeting on Additive Manufacturing held in Leuven September 2023"* [220]. The system is developed on an Industrial Internet of Things (IIoT) platform, delivering a process overview consisting of the temperatures read at each heater location as well as the chamber temperature and humidity. The system reads the temperature from the PID controllers that provide an RS485 output. The chamber temperature and humidity are read from a dedicated sensor.

Besides temperature monitoring, the IIoT system also reads the power consumption for each heater. This utilises six current transformers (CT sensors) where each heater power consumption is measured. The power consumption can be used for finding errors in the heater system prior to total failure. Utilising the IIoT device as a measure for predictive maintenance can ensure consistent performance of the build quality over the use of the system. For the present work, the temperature readout is the most relevant output of this system. It is used for measuring the heating and cooling time and temperatures. These

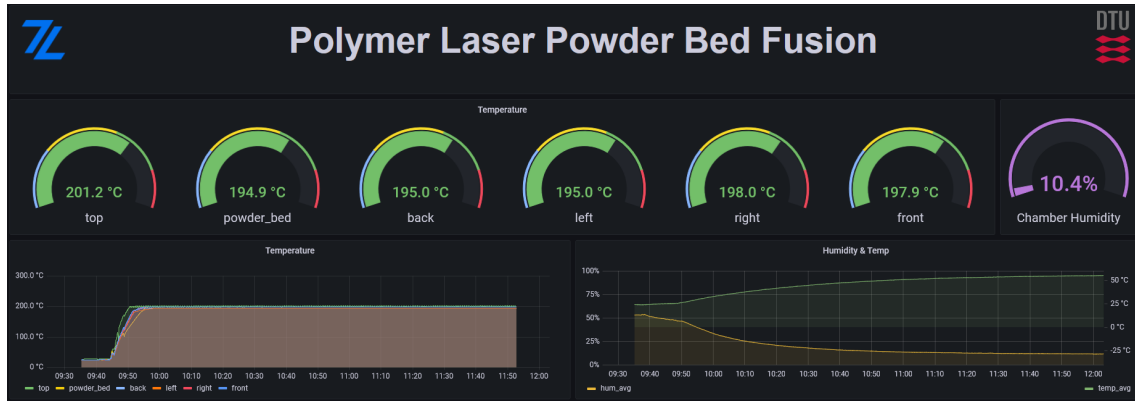


Figure 5.35: IIoT dashboard from "Zeryth"

measurements are utilised in comparing the powder cake cool-down temperature and time, as presented in subsection 6.1.3.

The IIoT system collects the data through a 4ZeroBox from the company Zerynth. The company also provides the data visualisation tool utilised as seen in Figure 5.35. The data shown are the individual heater temperatures and the humidity on a curve over time, as well as the current average reading for the past five seconds. The dashboard visualises the data collected with a data reading frequency of 1 Hz. The data is published to the cloud every five seconds. A fine resolution of data is obtained by this method, which clearly shows the heating and cooling and any deviation in the temperature or power usage during manufacturing.

The data collection and visualisation system is illustrated in Figure 5.36. The sub-system only takes inputs from the machine and does not have control capability. An effect of the system is the knowledge of a build job's start and end times. From the insight into job duration, a metric for determining material degradation over time is possible. This enables an investigation of whether the material can be used more than once and what time limit exists for the material before detrimental degradation.

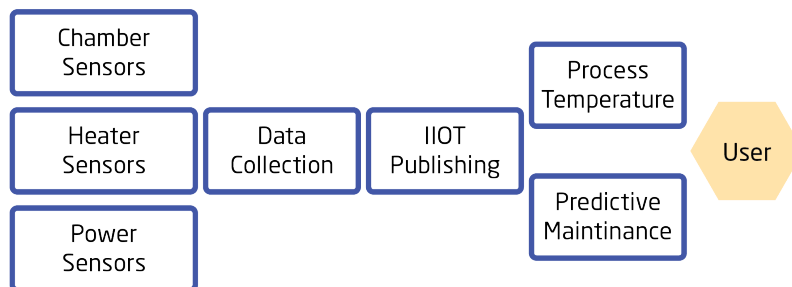


Figure 5.36: System diagram for the IIoT system for predictive maintenance and process monitoring

## 5.5 Finalised System for Fibre Laser Polymer Processing

The system developed for testing the main hypothesis required several redesigns of the original machine and new introductions of several sub-systems. To fathom the holistic approach of developing the system, a complete diagram is constructed in Figures 5.39 & 5.40 (last pages in this chapter).

The development entailed a complete reconfiguration of the build chamber in the original machine, where several pieces of the original infrastructure were removed to make room for installing the laser delivery sub-system as seen from Figure 5.37.

Manufacturing components on the system require two external inputs, which are not mentioned in the system diagram. These are an external 16 amp power supply and water for the water cooler. Besides this, the system is a standalone unit that can process polymer powders into fully formed 3D components. One significant difference between the system view of the traditional functionality and the developed system is the lack of shielding gas within the build chamber of the developed system. The shielding gas is usually utilised for minimising the degradation of the polymer during processing at elevated temperatures. This shielding effect removes oxygen and moisture by having a flow of inert nitrogen gas at a constant flow rate into the build chamber. The polymer degradation mechanisms of oxidation and hydrolysis are minimised by having a continuous flow of inert gas, fa-

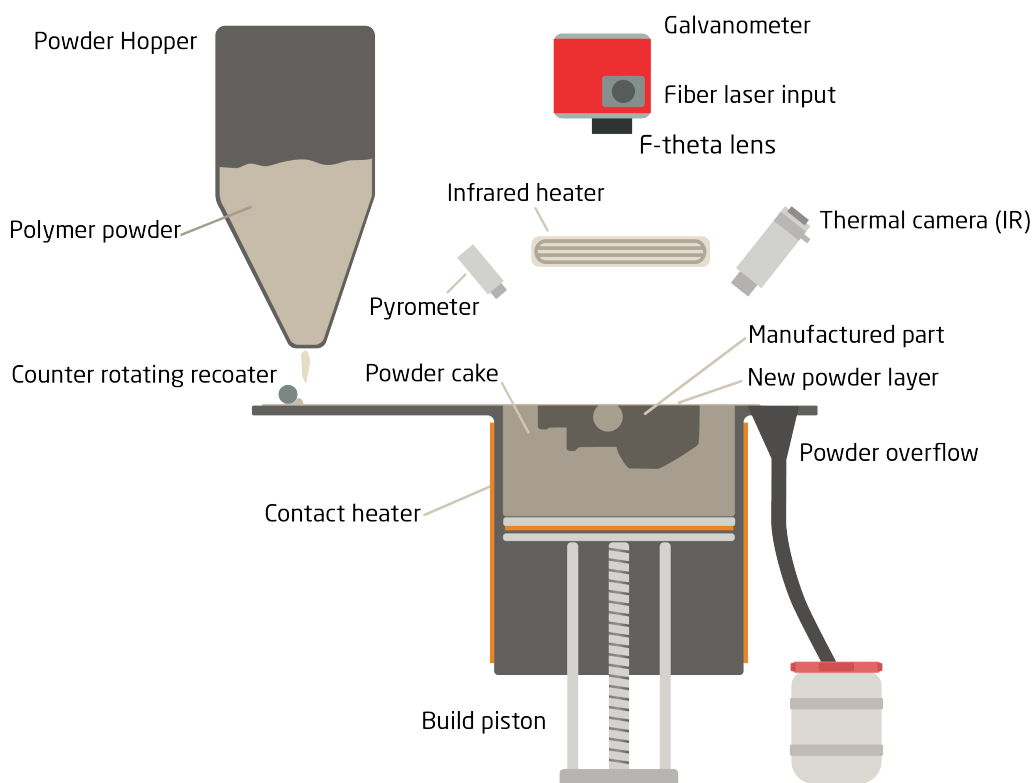


Figure 5.37: Final system developed

ilitating a larger amount of powder reuse. The degradation of the polymer is a limiting factor of the system, where until a full degradation study is completed, only virgin powder can be processed. Utilising virgin material ensures the material properties with minimal degradation but is a point of interest in further research.

Besides the sub-systems developed allowing the processing by a fibre laser, a safety circuit and a laser-safe window is installed in the system. The safety circuit is developed on the ABB Pluto PLC hardware, employing one door sensor and two emergency stops. Any interaction with the door during active manufacturing disables the laser output to ensure operator safety. Secondly, the emergency stops disable the laser and the mechanical motion of the system. This safety equipment is necessary to provide a safe working environment, even for an experimental infrastructure. The sensors are designed to have redundancy and only allow operation when the system is in a safe state.

The laser-safe window is the original viewing port of the machine. The window is made to order, considering the laser source and power. As well as the possible reflection and minimal distance of the laser reflection to the window. Considering these factors, a laser-safe window that does not transmit harmful light can be designed. The window is dimensioned after the original machine to ensure complete coverage of the viewing port.



## 5.6 Chapter Summary

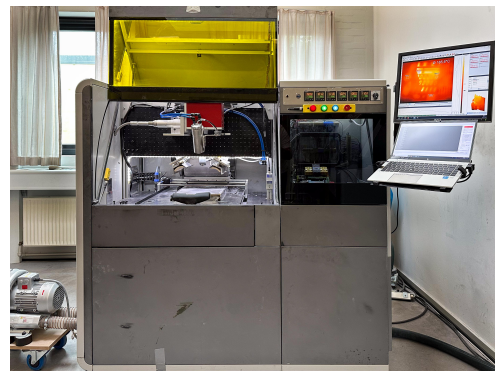
The original binder jetting machine was deconstructed and analysed. The individual sub-system was classified as; useful for laser processing, needing redesign or removal. Each useful sub-system was examined to ensure stability and integration in the developed system.

The new sub-systems introduced allow the processing of polymer powders by laser irradiation. The system is focussed on a fibre laser and would require several reconfigurations to encompass other laser sources. The fibre delivery system is the main driver for selecting a fibre laser, making this a versatile and easily implementable choice.

A comparison between the old machine and the new system is seen in Figure 5.38. Besides the frame of the original machine, only a few critical components and sub-systems have been retained, as explained above. All changes made have been focussed on the capability of processing polymer powders by fibre laser. The comparison between the original machine and the developed system does not reveal the significant changes made to the control system, the recoater, or the heating system. These are explained above in-depth and are installed in the machine to provide the desired functionality. Test and validation of the functionality of each sub-system is the focus of the next chapter.



(a) Original machine



(b) Developed system for PBF-LB/P

Figure 5.38: The comparison between the old machine and the developed system

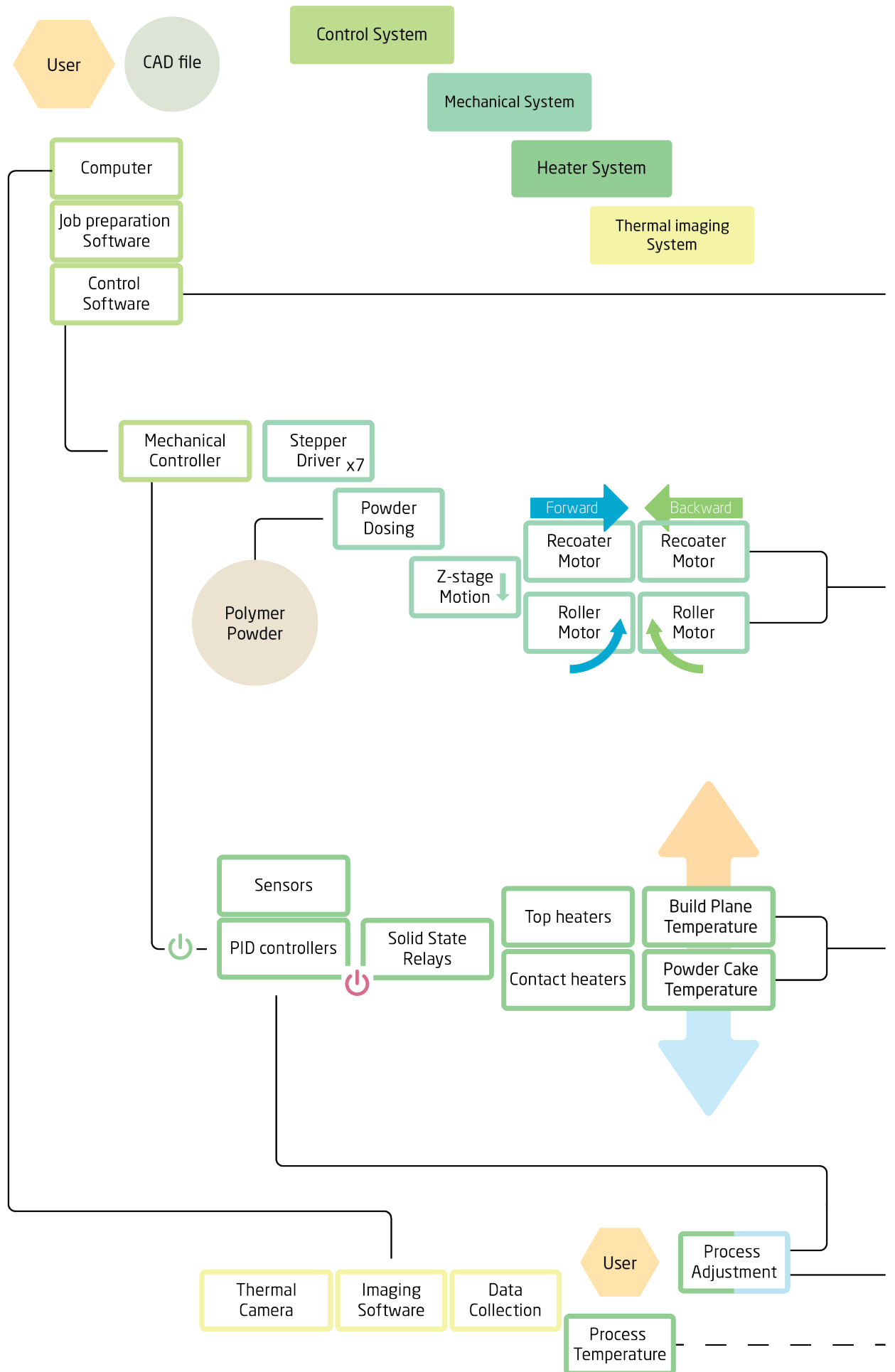


Figure 5.39: System diagram for the entire machine/system (part: one)



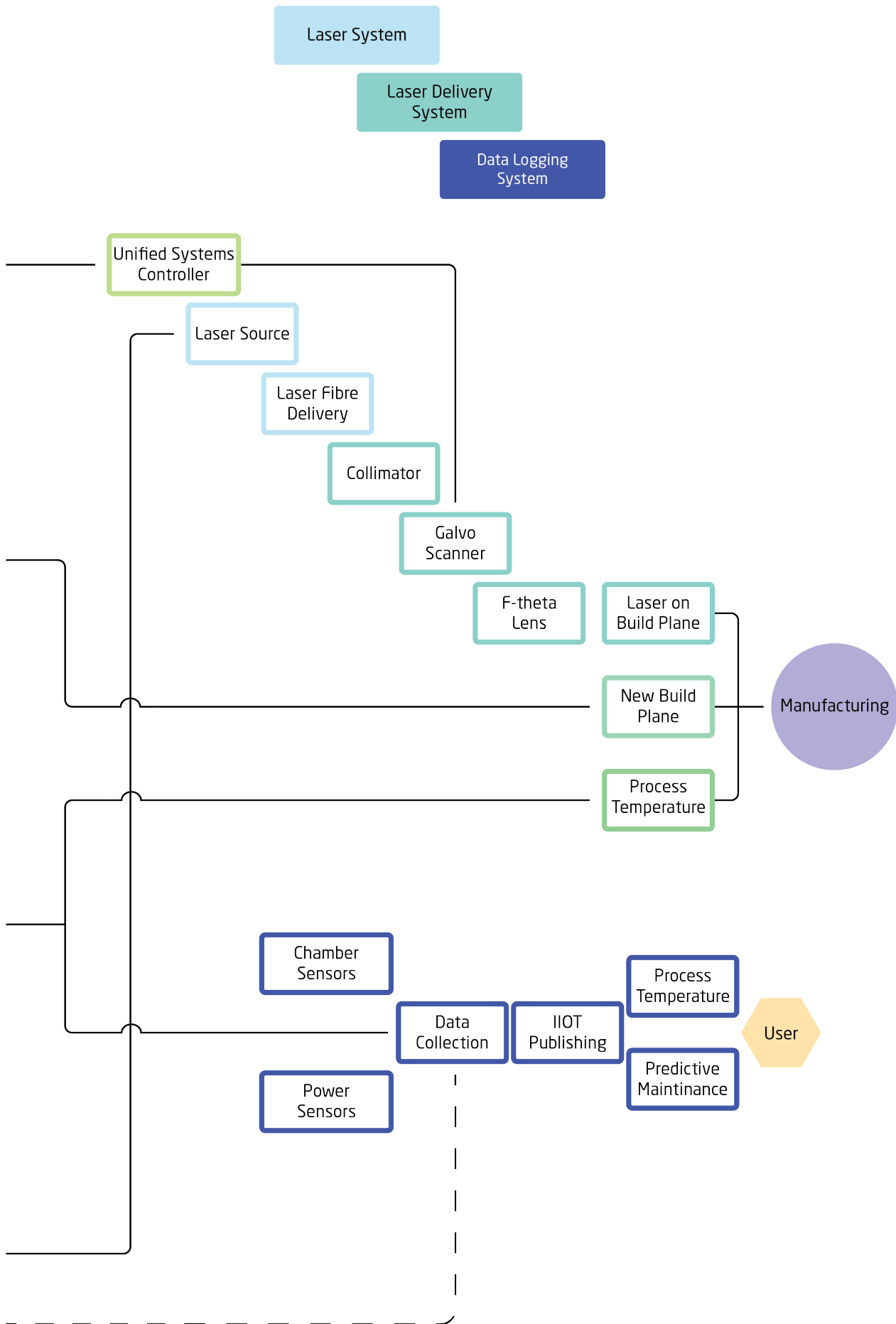


Figure 5.40: System diagram for the entire machine/system (part: two)



# Validation of the Experimental Infrastructure

This chapter aims to validate the developed system designed for verifying the main hypothesis of fibre laser utilisation in the Laser Based Powder Bed Fusion of Polymers process. The experimental infrastructure presented above utilises components of the original machine mixed with new additions and heavily modified components. The design relies on the knowledge of the process and desired system capabilities developed throughout the investigation. Originating within the sub-system design, this investigation concerns the validation of these sub-systems, defining the utility of each, and ensuring the research capabilities concerning the PBF-LB/P process.

Studying the system's functionality necessitates individual experiments for each developed sub-system. Additionally, a comprehensive process study is essential to evaluate the success of the entire system development. Hence each sub-system is examined through specific experiments and procedures designed to validate its relevance to the fibre laser processing of polymer powders.

The validation study presents an investigation of the three tiers of the system developed for the process. The first study focusses on the heaters validating the capabilities ensuring adequate heating for the desired process regime. The second study defines the capabilities of the laser system, including an examination of the laser spot size and translational speed. Finally, the third study delves into the motion stages, validating the accuracy of the build piston and recoating action.

## 6.1 Heater Validation

Validation of the heating system necessitated a study of the heating and cooling regime during manufacturing. An approach to studying the heater's influence on the powder cake is undertaken. The study mimics a large build and finds the actual temperature in the powder cake, including the temperature distribution through it. The validation was approached by heating the powder cake from a "cold" state at room temperature to the process temperature. The method revealed several interesting details of the heating system and defined the limiting factors for the process capabilities.

Supplying the energy to the powder cake is performed by six heater units as described in subsection 5.4.3. The heat system study is done by first studying the entire heating system, defining the internal powder cake temperature produced by all six heaters. Secondly, an analysis of the directionality and energy distribution on the build plane, considering the top heater's location and direction, is conducted.

The study shows how the heaters do not produce an entirely uniform energy distribution on the build plane nor in the powder cake. A definition of a volume with adequate heating for the process is found and utilised during further investigations of manufacturability in the system.

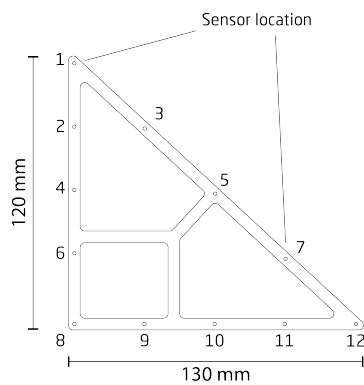
### 6.1.1 Build Piston Heating

To define the utility and successful integration of the heaters surrounding the build piston, a study of the stabilised temperature was carried out. The study was presented at the "2022 Summer Topical Meeting Advancing Precision in Additive Manufacturing" - by ASPE - University of Tennessee, Knoxville. The published conference contribution can be found in its entirety in Appendix B, from [221]. To describe the work done, outtakes from the article are presented here, with additional information and a further dive into the heating and stabilisation of the powder cake.

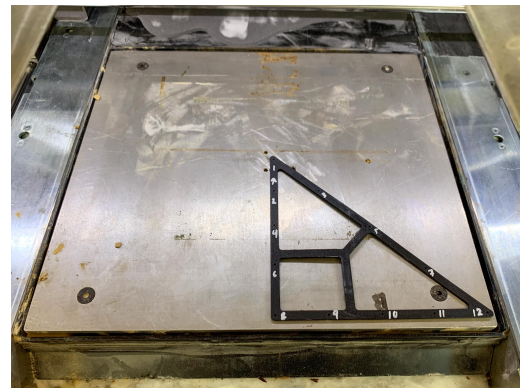
Measuring the internal temperature of the powder cake is not an easy task. Josupeit S. et al. [163] presents a method for permanent implementation of thermal data acquisition in the powder cake. Here rods fitted through the build plate allow sensor integration in the powder cake as the build piston moves down during the manufacturing cycle. These rods host thermal sensors equally distributed along the Z-axis. They are placed in a triangular array originating at the centre of the build plane, as well as a sensor location for each corner. The sensor rods are stationary to the machine frame, meaning that the powder cake will travel along them, revealing new sensors to the powder cake as the build progresses. The sensor location is maintained during the cooling part of the study. Studying the powder cake behaviour in the developed system required a similar approach to the one described. However, in the work presented by Josupeit S. et al. [163], the build plate is perforated by the rods, making these permanent installations in the system.

A permanent installation of the thermal sensors was not desired since the largest build volume possible was of interest in future research. An approach of a stationary study, where a sensor array is integrated into the powder bed, which then could be heated to process temperatures, was deemed sufficient while maintaining the largest possible build volume for future experiments. The interest of the current study is the definition of the heat stability and thermal gradient in the powder cake, determining if any regions are unsuited for laser powder processing, according to the knowledge for the process developed in section 4.1.

Twelve sensors were integrated into the temperature sensor array producing a triangular shape that was inlaid at the centre location of the powder cake. The array configuration resulted in data points from the centre to the build piston wall along the machine's Y-axis. As well as data points from the centre to the corner of the build piston and along the build piston wall. The sensor array and configurations are seen in Figure 6.1a. All the physical sensors in the array are K-type thermocouples to ensure consistency in the measurements.



(a) Sensor array



(b) Sensor array on the build plate



(c) K-type thermocouples integrated into the plastic sensor array

Figure 6.1: The sensor array for the K-type thermocouples placed in the powder cake during the heating and cooling experiment

The sensors were produced specifically for the experiment, minimising the deviation in length of each sensor and between all the thermocouples, making the measurement more robust. The sensor array was produced from plastic to alleviate heat transport from the sides to the centre by the sensor array, as seen in Figure 6.1b. Minimising the thermal conductivity of the array was crucial since the experiment aimed to determine the heater stability and energy input. Determining whether the installed heaters were sufficient for maintaining the desired process temperature.

A cycle of heating and cooling the powder cake was carried out to analyse the heat stability. In the machine, 100mm of powder was deposited in the build piston producing the powder cake. The sensor array was placed in the centre of the powder with the K-type thermocouples (seen in Figure 6.1c) pointed downwards, resulting in a distance of 50 mm of powder above and below the sensor points. At the very bottom, a sensor was mounted to the build plate. The sensor locations are shown in the cross-section view presented in Figure 6.2.

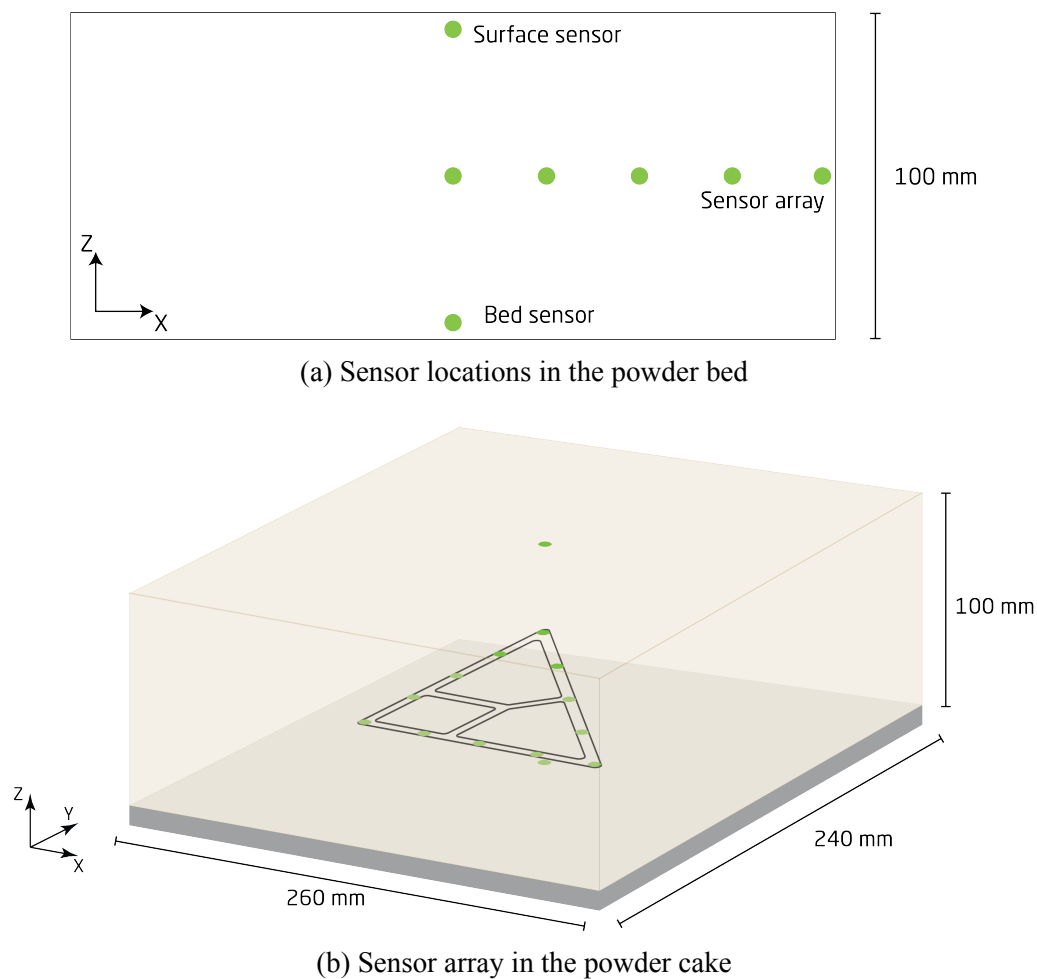


Figure 6.2: Sensors integrated into the powder cake, showing the location during the experiment

All the heaters were set to 180 °C and left to heat for 24 hours. A subsequent 24 hours of cooling were allowed in the same condition. The cooling regime is described below in subsection 6.1.3, defining the cooling rate in the powder cake and the appropriate component retrieval temperature and wait time before opening the machine.

At the end of the 24-hour heating period, a temperature-steady state of the powder cake was found. The steady-state temperature was defined by the decrease in heating rate after the 22-hour heating period. As expected, the heating rate dropped significantly as the temperature in the powder cake reached closer to the set point. In Figure 6.3, it is seen how the temperature increase for the centrally located thermocouple only deviates by 0.8 °C over the final two hours of heating. Based on these results, a slight discrepancy between the reported and actual fully heated temperature can be expected. The overall stability is, however, found by utilising the final reached temperatures as reported below.

Three regions in the powder cake were determined based on the analysis of the results presented in Appendix B. These three regions are represented in Figure 6.4. It was found that only the centre part of the cake was heated sufficiently for stable polymer processing.

After 24 hours of continuous heating, a steady temperature range is found for the three zones. The deviation of temperature for the last two hours of heating reported above shows an increase in temperature still occurring at the end of the heating period. This can cause the deviation reported to be over-exaggerated since this increase will further minimise the variation between the setpoint and measured temperature. A minimum expected process

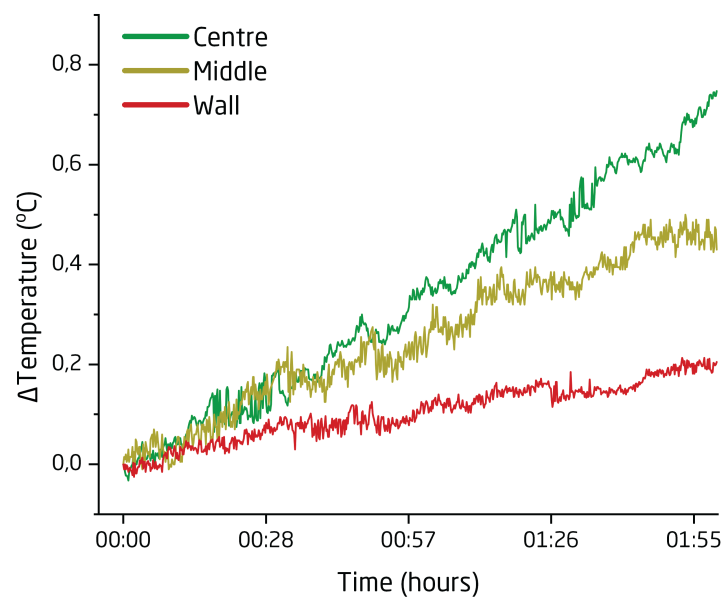


Figure 6.3: Temperature deviation during the final two hours of heating

temperature can be determined from the heating curves as seen in Figure 6.4. Here the temperature stable area is shown, qualified for processing as a maximum deviation from the set temperature of 5 °C.

From the heating graphs, it is clear that the build plate reaches the desired temperature rapidly, with a much slower heating response of the central part of the powder cake. It can be seen how the heat seeps in over an extended period of time. This heat input calculated for the initial six hours is  $0.36\text{ °C} / \text{min}$  ( $\approx 22\text{ °C} / \text{hour}$ ). This prolonged heating is a testament to the low thermal conductivity of the polymer powder. The powder cake contains air in the interparticulate spaces, providing low thermal conductivity, further hindering reaching the set point temperature during the experiment. The powder cake reacts slowly to heat input, which is essential to consider when tuning the process parameters during manufacturing. The actual powder cake temperature will lack behind the setpoint by a significant amount, depending on the desired change. From Figure 6.4, it can be seen how the heating rate decrease when moving towards the setpoint. During the final two hours of heating, as seen in Figure 6.3, a heating rate of less than  $0.5\text{ °C} / \text{hour}$  is realised.

When starting a new build job, it is crucial to introduce the heat in the initial powder cake, ensuring an even heat distribution. Often a base layer of 5 mm powder is put in before turning the heaters on. This base layer absorbs the initial energy input and is prepared for the start of a job. To ensure a homogenised powder cake, minimising the temperature gradient is necessary. This is done by adding several layers of powder while heating the powder cake prior to starting the build job. This pre-heating routine is first done for the base powder where this base is stationary, and then for up to 100 layers of powder, maintaining the same process temperature. After the initial 100 layers of buffer layering a heat retention powder bed is produced, preparing the system for part manufacturing. The

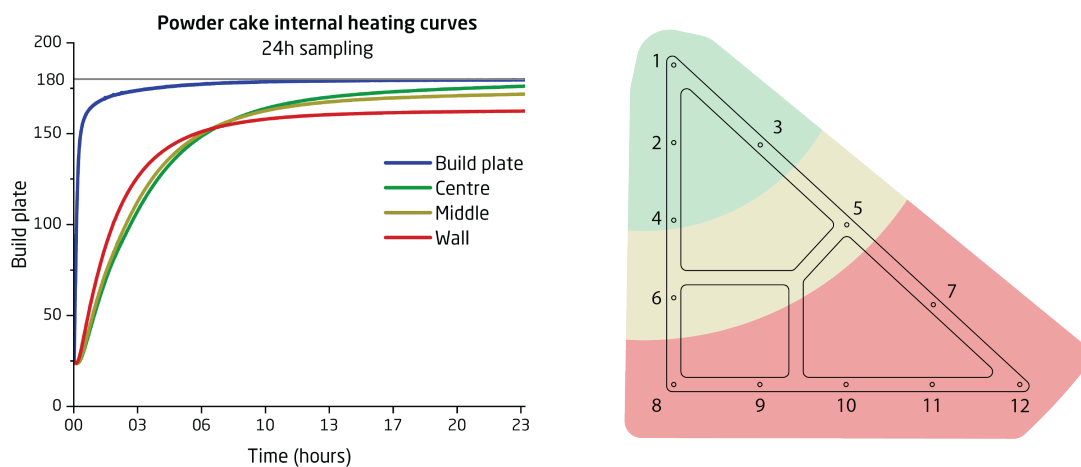


Figure 6.4: Heating curves for the process temperature definition



pre-build routine is called the buffer layers or buffer routine. It is utilised for all the manufacturing cycles done on the developed system, ensuring uniformity in the build process. This routine has been developed empirically and is inspired by the production cycle of an industrial machine.

Figure 6.5 shows the maximum temperatures recorded for each sensor during the experiment. Here it is clear how the corners are much colder than the side walls or central temperature.

From the analysis, an apparent lack of heating is evident towards the corners of the build piston. The corners lack heating and insulation due to the design of the heaters and the way the insulation is installed. The heater design focussed on covering the face of each build piston wall, enabling a large and evenly spread energy input area that was assumed to heat the powder cake uniformly. This uniformity is not achieved by the current design. The lack of uniformity causes a large temperature gradient in the powder cake, making a large part of the build volume unsuited for active powder processing and research. In the centre of the build piston, a stable region is observed. Only this region (build envelope) is considered when preparing the location of parts in the job file during job file generation for further experimentation. The stable region is seen in Figure 6.6. The octagon shape of the build envelope is caused by the excessive heat loss occurring at the corners of the build piston. It can be expected that the stable region extends further towards the middle of the side walls. However, from the temperature gradient shown in Figure 6.5, this extension would increase the stable area minimally, as shown by the highlighted area at the top of the image (Figure 6.6), limiting the actual utility.

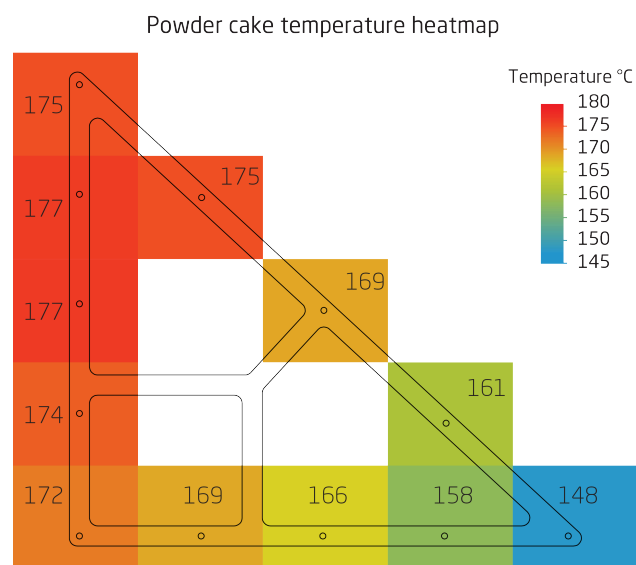


Figure 6.5: Average temperature recorded for each sensor during the final 15 minutes of heating. From Appendix B & [221]

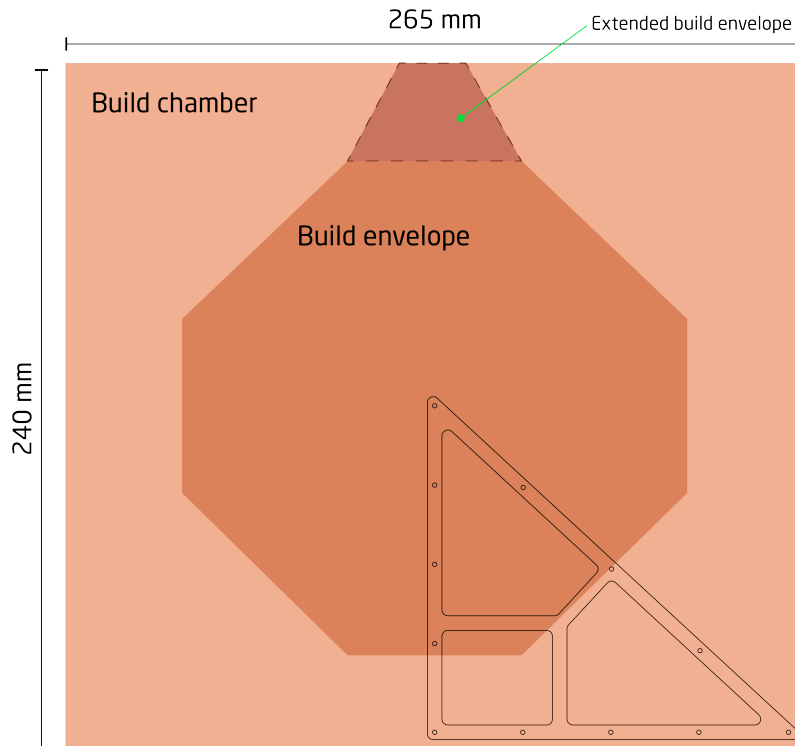


Figure 6.6: Temperature stable processing region (The build envelope)

The investigation presented above highlights a discrepancy between the temperature setting and the actual powder cake temperature. This discrepancy is adjusted for in the experimental section by offsetting the process temperature input by +5 °C. This increase adjusts for the heat loss in the machine, ensuring the correct process temperature. This adjustment is used in all dissemination, communicating the actual powder cake internal temperature and not the setting of the individual system. Powder cake heating is done from all six sides, with the discrepancy between the internal temperature and the setpoint described mainly considering the heaters on the build piston. Verifying the utility and adjustment of the top heating lamps are therefore described in the following.

### 6.1.2 Top Heater Directionality

Top heating of the powder cake ensures that the build plane and newly produced layers adhere to the process temperature as closely as possible. When selecting a material for use in the PBF-LB/P process, a DSC analysis must be carried out to define the process temperature. This process temperature must ensure minimal crystallisation of the polymer to alleviate any internal stresses which ruin the build job as described in section 4.1. Even energy distribution is essential when supplying heat from above the build plane. If the build plane temperature varies, internal stress build-up or material degradation can occur in areas that are either too cold or too hot, respectively. A narrow build plane temperature distribution is imperative for process stability, considering the processing regime of

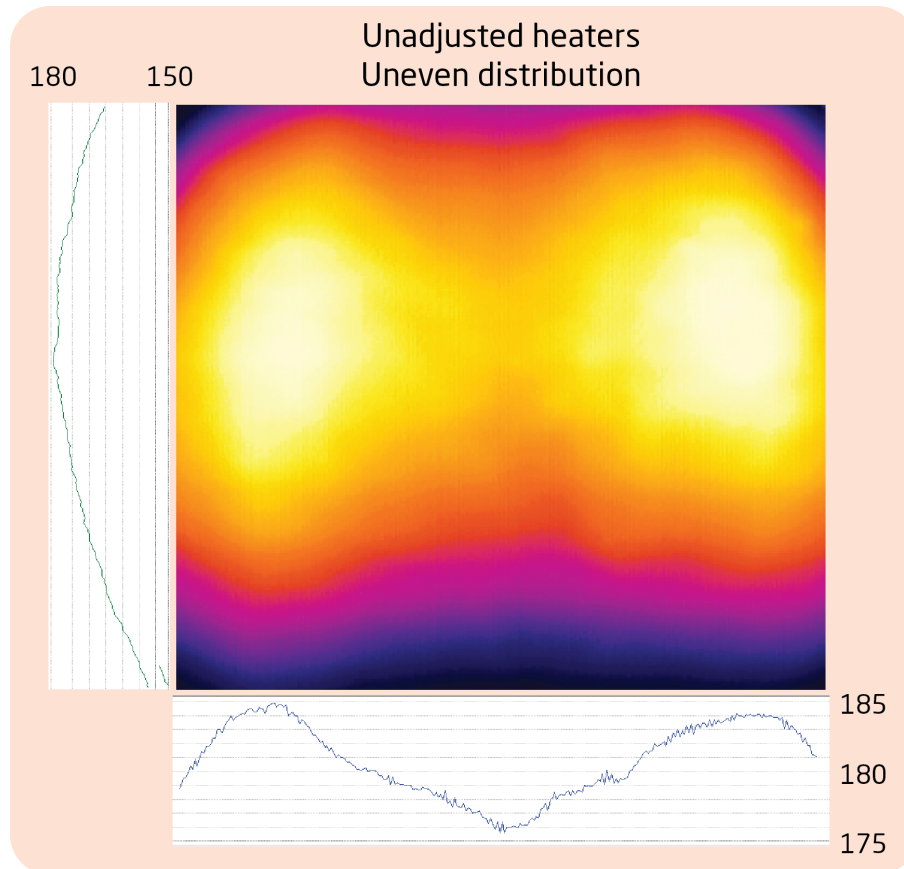


Figure 6.7: Unadjusted heaters producing an uneven energy distribution

the laser and that only just enough energy to push the polymer past the melting point is delivered to the build plane.

Validation of the top heaters concerns the directionality and adjustment, realising an even heat distribution. The adjustment must consider the directionality of the heater, trimming it so the energy output covers an adequate area of the build plane, minimising cold or hot zones as seen in Figure 6.7. Coverage of each heater must be considered by determining the number of heaters, the desired processing region, and the energy distribution.

In the developed system, two ceramic heaters are located above the build plane. On top of the heaters, a reflector shield is placed, directing the energy downward. The mounting of the heaters allows for angular adjustment, trimming the heaters from side to side on the build plane, as well as an up-and-down adjustment (vertical direction) option for setting the focus of the heaters.

Trimming the heaters is a simple task utilising the thermal imaging system for verifying the position of each lamp. One lamp is switched on and adjusted by monitoring the energy distribution on the build plane in the software. After one side is calibrated, the opposite side follows, by the same method of calibration. As seen in Figure 6.8, the heating can

be directed into a more uniform heating of the entire build plane. The aim is to have an even energy distribution in the middle of the build plane due to the issue mentioned above concerning the build envelope.

Since the heating is non-uniform in the powder cake, the distribution of the energy from the heat lamps is crucial. During cleaning and system maintenance, the top heaters can be knocked out of alignment, causing a need for recalibration. The heater alignment is checked prior to every build, ensuring an even heat distribution. The procedure is to produce a powder cake with an even build plane from the powder to be utilised. The powder cake is irradiated by the heaters and checked in the thermal image for uneven distribution. Based on the results, the system is calibrated by physically adjusting each lamp one side of the time. After adjusting each lamp, both heaters are turned on, allowing the chamber to heat once more. The second stage of heating is to verify the energy distribution and coverage for both heaters simultaneously, ensuring an even distribution as seen from Figure 6.9. By following this procedure, any thermal gradient in the build plane can be minimised, producing a stable processing region. The powder used for heater alignment must be discarded due to excessive degradation.

In the two figures 6.7 and 6.9, an increase in the heated area is evident by directing both

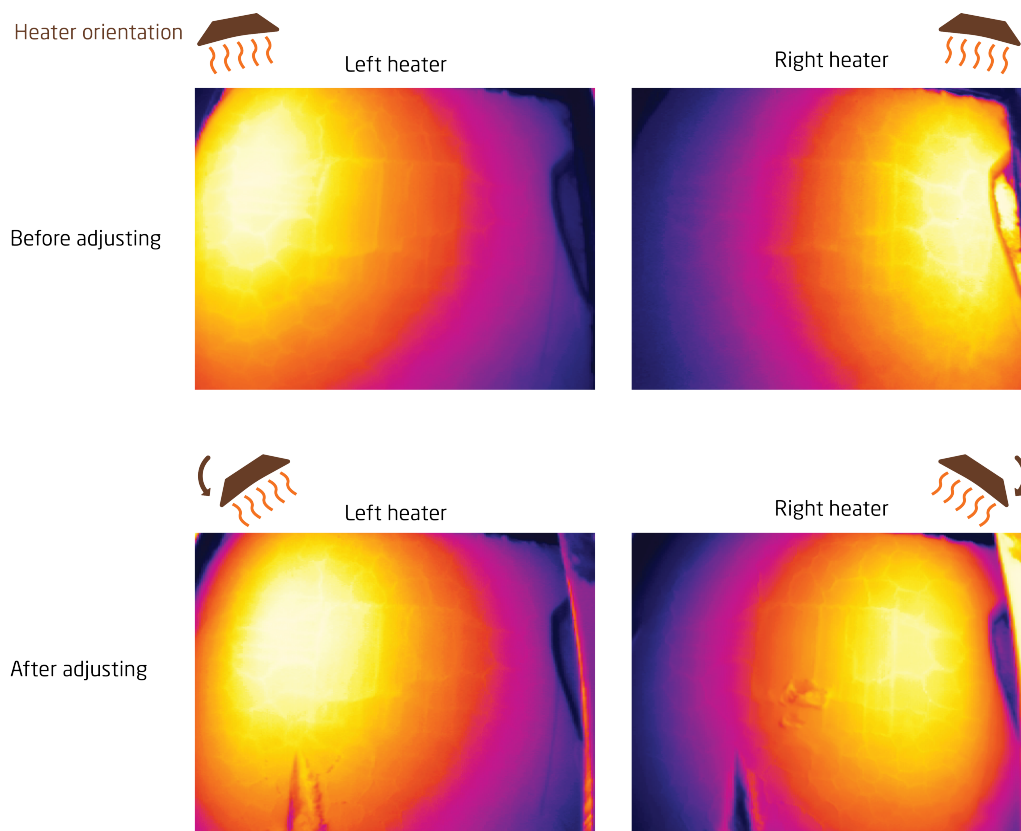


Figure 6.8: Top heater trimming resulting in an even heat distribution on the build plane. The hot zone (bright yellow) are minimised

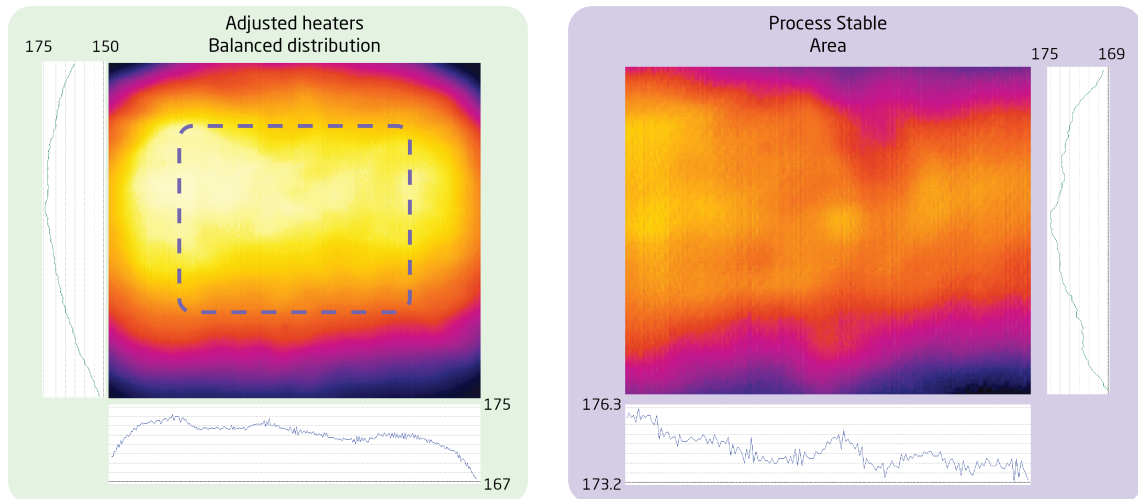


Figure 6.9: Left: Energy from both heaters producing a stable processing region. Right: Focused on the stable processing region of the build plane

heaters towards the centre of the build plane. A smaller thermal gradient in the processing region can be realised by utilisation of this bleed of energy across the build plane. Two cases can be seen in Figure 6.9. The Left image shows the heaters trimmed to a narrow energy distribution producing an ideal processing region in the centre of the build plane. Here the sides of the build plane, close to the build piston walls, are colder. This can cause processing issues. The right is a zoomed-in image of the processing region, where the thermal stability is excellent. For all experiments described in chapter 7, only the central region has been utilised for powder processing, as shown in the figure.

The max temperature gradient of the images in figures 6.7 and 6.9 are shown in Table 6.1. Even in the adjusted scenario, a significant temperature gradient is evident. This gradient is minimised when focussing on the processing region of the build plane, determined above by the temperature stable region internally of the powder cake Figure 6.6. If the entire build plane is to be utilised, an upgrade of the top heating array is necessary. This was, however, not possible within the limitations of this project.

Table 6.1: Temperature deviation for each gradient map

Temperature gradient deviations from figures 6.7 and 6.9		
Figure reference	Side to side Deviation range °C	Front to back Deviation range °C
Unadjusted heaters	10	30
Adjusted heaters	7	25
Processing region	3	6

### 6.1.3 Powder Cake Cool Down Study

After a build job cycle, the powder cake is left to cool. A desired metric for this cooling is threefold, concerning the temperature gradients arising in the powder cake, the cooling rate of the cake, and the safe removal temperature. The temperature gradients in the powder cake are influenced by the insulation of the machine and the build piston. Just as the temperature gradient of the heated powder cake, the cooling rate is influenced by the insulation properties of the build piston and chamber. A variation in cooling rates is evident for the three regions in the powder cake, leading to a difference in the point of crystallisation of the parts.

The safe removal temperature, in contrast, depends on the crystallisation ( $T_C$ ) and glass transition temperatures ( $T_g$ ) of the polymer used in the process. For speeding up production cycle times, it is critical to know when the powder cake is cooled sufficiently below the  $T_C$  and  $T_g$  to be able to remove the parts with minimal risk of warping or other distortions caused by internal stresses arising from uneven cooling.

#### Safe removal temperature

The crystallisation temperature of a polymer into ordered regions, mimicking crystal structures, is determined by the organisation of the polymer chains. The DSC curve in Figure 6.10 show a distinct peak during the cooling part of the curve. Two critical temperatures for the crystallisation behaviour of the tested polymer are the onset and end crystallisation temperature  $T_{oC}$  and  $T_{eC}$  as mentioned in Table 4.1. Each critical temperature location is highlighted on the DSC curve in Figure 6.10.

The onset crystallisation temperature is critical during processing since the process temperature in the powder cake should be maintained above this to minimise the degree of crystallisation. Secondly, the crystallisation end temperature is critical when considering the safe removal temperature for parts from the powder cake. Removing parts at temperatures above the crystallisation temperature cause excessive internal stresses and part warpage due to uneven cooling and crystallisation. Finally, the  $T_g$  is essential to consider when removing parts. When polymers are above the  $T_g$ , they are malleable and soft. An elastic behaviour becomes available, making these polymers able to bend and stretch further. When cooling the polymer below the  $T_g$ , this behaviour is reversed, and the polymer is now prone to brittle fracture, showing only a minute elastic region. Depending on the polymer, a cooling state below  $T_g$  is possible, as in the case of nylons.

The glass transition temperature of polymers can be above and below room temperature. A classic example is Polyethylene having a  $T_g$  around  $-100\text{ }^\circ\text{C}$  with the opposite case of Nylon 6,6 showing a  $T_g$  close to  $50\text{ }^\circ\text{C}$  [222]. The removal temperature should be as low as possible, ensuring the greatest geometrical stability of the removed parts. In mass manufacturing setups, this wait time can prolong the time a build job occupies the

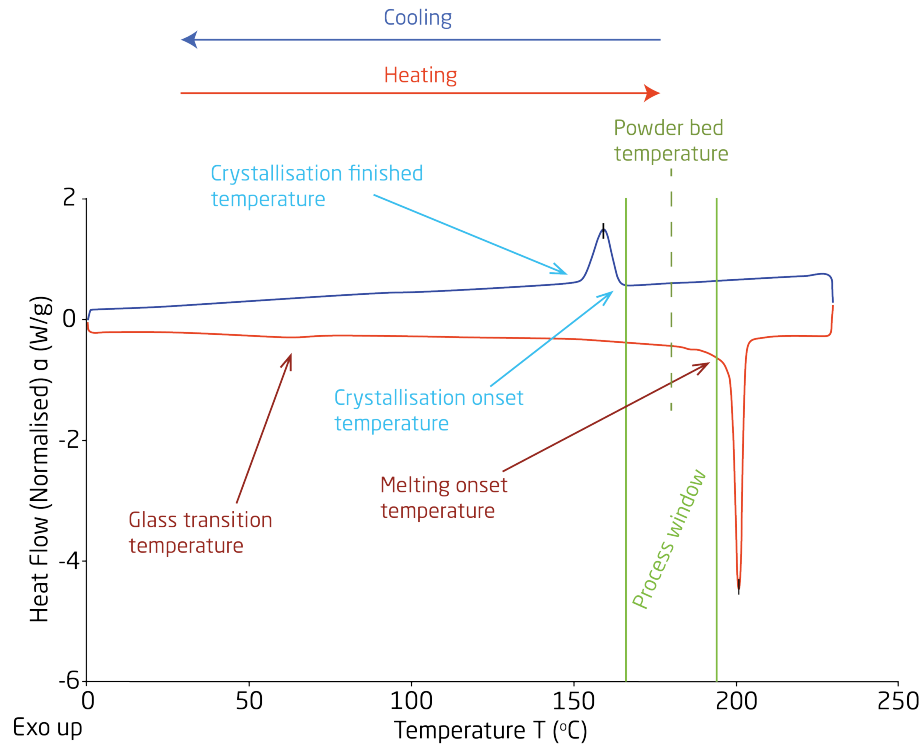


Figure 6.10: DSC curve for safe removal temperature identification

machine. Why a desire to reduce this is evident, enabling larger production throughput. Therefore, knowledge of the individual polymer is critical. The DSC curve in Figure 6.10 is the analysis of a PA11 powder used in PBF-LB/P, showing the  $T_C$  and  $T_g$ . In no case is it viable to have operators or other personnel clean out parts close to  $T_C$  due to the increased risk of burns and other injuries. However, waiting until the powder cake is below the  $T_g$  (if possible) can still be beneficial.

Allowing the entire powder cake to cool below  $T_g$  substantially reduces the risk of warping and part distortion since parts are locked in the molecular structure below this temperature. This is possible when utilising nylons in the process since most nylon types show  $T_g$  above room temperature. The safe removal temperature can be determined based on the heating and cooling experiment described above. By knowing the core temperature of the powder cake, the temperature on the top of the build plate, and the build plate heater sensor, a time frame and cooling regime can be constructed, describing how long the cooling of a build job takes prior to safe removal.

Powder cake cooling curves are seen in Figure 6.11. In the graph, the entire cooling time is presented, showing the extensive time for cooling the central location of the powder cake. A cooling rate of 0.33 °C/min (20°C/hour) is observed in the centre of the powder cake, with the cooling appearing much more rapid for the other locations. The sensor points in the graphs are the same as presented for the heating study, seen in Figure 6.2, with an added sensor point on the heater side of the build plate. Recording the temperature signal, which



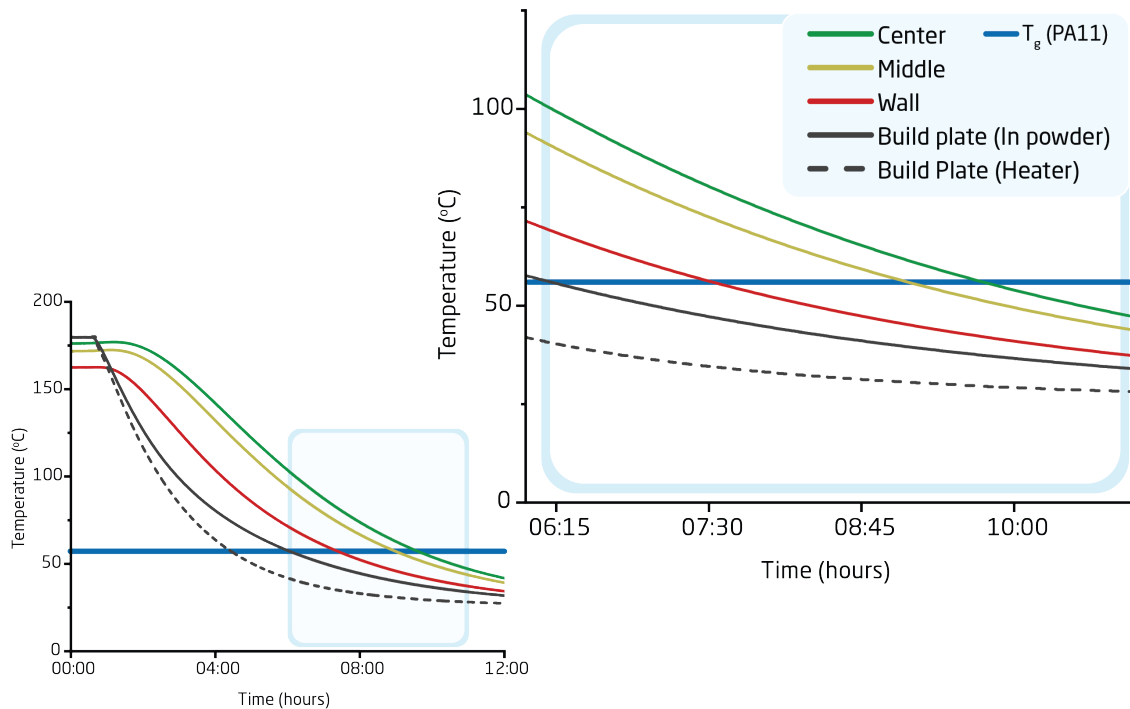


Figure 6.11: Cooling curves with sensors in the same location as for heating. One extra sensor for under the build plate in the heater

can be read from the IIoT dashboard, shows that the cooling rate is rapid, leading to a false indication of a safe temperature in the powder cake for part removal. The build plate sensor is utilised in the system's regular use since the sensors incorporated in the powder cake (as seen in this investigation) cannot be fitted during production. In the graph, a dip within the first hours of data collection is seen for the sensors located at the build plate. This dip indicates when the heaters were switched off, not supplying heat any further. At the beginning of cooling, the rate is observed to be very slow, only picking up after an hour of no energy supply. This latency further skews the safe removal temperature. The outer positions in the 100mm powder cake are seen to pass  $T_g$  within eight hours. However, the central position only passes below  $T_g$  after ten hours of cooling the powder cake. In the zoomed-in graph, these cross-over points clearly show the extended wait times needed for safe part removal, not forcing any sudden quenching of the polymer. The readout temperature of the IIoT dashboard must show 25 °C for the internal temperature to reach below the  $T_g$  of the investigated PA11.

If the parts are to be removed after passing  $T_C$  for the investigated PA11, a significantly shorter cooling period is needed. Here parts can be removed after four hours of cooling. Here operator safety must be considered seeing that the parts and powder at this point are above 100 °C. For this the readout temperature in the dashboard corresponds to 60 °C.

The data presented above is valid for a powder cake of 100 mm height filling the entire build piston. If a production run does not require this powder cake height, the cooling



rate and time will change. Shorter and smaller powder cakes will cool faster, while bigger builds will require longer cooling time to ensure complete crystallisation of the polymer before removal. During unpacking, the powder cake rapidly loses temperature due to the low density and large surface area-to-air ratio. For the production runs on the system, the IIoT dashboard build plate sensor readout is utilised to determine the powder cake's current temperature. Here a temperature below 30 °C is considered the safe removal temperature since the powder cake will have cooled sufficiently for stable parts to be recovered.

## Temperature Gradients During Cooling

Considering the steep temperature gradient in the powder cake at process temperature, a gradient is unavoidable during cooling. This gradient causes parts closer to the sides of the build piston to cool faster than centrally located parts. A difference in cooling is evident for large parts taking up the central part of the build volume. From the graphs, the temperature variance between the centre and the middle sensors is significantly different ( $\approx 10$  °C). Hence the crystallisation of the parts is expected to initialise crystallisation from the corners and towards the middle. The influence on the final part geometry caused by the gradient can be mitigated by mindfully placing the parts during build job generation, minimising inhomogeneous cooling and crystallisation. Secondly, the powder cake surrounding the parts produced will lock the parts in the manufactured location during cooling. This further aids the geometrical stability, minimising warping and curling caused by uneven crystallisation. An investigation of the geometrical stability of parts produced in the system by fibre laser is presented in section 7.3.

### 6.1.4 Validated heating setup

All the critical elements for heating, including the stable temperature processing range, the build envelope, the top heater positions, and the cooling of the powder cake, are presented above. Several valuable metrics can be extracted from this. One crucial aspect to consider is the lack of heating at the build piston corner edges. This causes a temperature gradient and a discrepancy between the setpoint of the PID controllers and the actual powder cake temperature. Another critical element is the top heater alignment verification before every build, which ensures an even energy distribution in the build plane, minimising part defects and build failures. Finally, the safe removal temperature is critical for achieving parts with the geometrical stability desired. Table 6.2 presents a list of the critical aspects for tuning the heaters during system operation. The list functions as a guide for the safe and easy operation of the system. Powder cake cooling is presented in Table 6.3, highlighting the critical aspects for the safe removal of parts.

Table 6.2: Powder cake heating guide for processing powder in the system

Critical element	Utilisation	Elaboration
Powder cake temperature	5 °C below setpoint	During operation, the setpoint must be adjusted +5 °C than the desired powder cake temperature
Top heater adjustment	Thermal image validation	Top heaters must be aligned prior to starting each build to minimise temperature gradients in the build plane
Build plane temperature gradient	< 6 °C across the build plane	The gradient across the build plane is minimised by the top heater adjustment

Table 6.3: Powder cake cooling guide for processing powder in the system

Critical element	Utilisation	Elaboration
Powder cake cooling rate	20 °C/hour	Tall powder cakes cool slowly. Shorter can cool faster (see removal temperature)
Safe removal temperature	Build plate sensor < 30 °C	Only remove produced parts from the powder cake after passing the safe removal temperature

## 6.2 Laser validation

Validation of the laser takes three approaches. The initial approach is the determination of laser power output, defining the loss of power in the optical delivery system. Second, is a validation of the laser spot size determining the relevant factor for processing polymer powder into dense parts. The third approach considers a method of defining the scanning speed of the laser setup, determining the relation between the setpoint in software and actual translation speed. Below all three validation strategies are unfolded.

### 6.2.1 Laser Output Power

Determining the laser power output is critical for validating the process parameters utilised during laser powder processing in the system. Two metrics are essential for determining power stability. One metric is the power setting vs measured power. The power setting is done by a 1-10 volt signal from the Unified Systems Controller. The signal is determined by the setpoint value, with 10v corresponding to the maximum power of the laser. When selecting a percentage power setting, this is converted into the voltage signal in the controller, which is then converted to laser power in the laser source. This conversion can infer an error between the desired and the actual power level. Secondly, the laser trav-

els through several optical components that absorb an amount of the laser energy. This energy absorption is minimised by utilising equipment appropriate for the laser and wavelength. The loss, however, must be measured to define the actual power delivered at the build plane. A second metric is power uniformity across the build plane. An even power distribution ensures less laser correction across the build plane. The correction can be implemented in laser planning and programming but is preferred to be homogenous from the laser system itself.

## True Laser Power Delivered

Measuring the power delivery at the build plane is done by utilising a Gentec-EO pronto-500 (Gentec-EO USA Inc.) laser power meter. Finding the laser power along the power setting range is done by incrementing the laser power 10% and measuring each power setting five times. The order of the measurements was randomised in power setting (%), measuring a total of 50 times from power setting 10% to 100%. The power meter was physically moved between each measurement to allow for energy dissipation in the measuring device. The results presented are the average values of the five individual measurements at each level, including the 95% confidence interval for each average.

Results from the power measurements indicate a discrepancy between the power setting and energy delivered, as seen in Figure 6.12. An unstable region of the laser power can be identified when utilising low power levels, where the most considerable deviation is identified at the 10% power setting. The power level stabilises when moving towards a 60% power setting, after which it delivers slightly more power than anticipated. The

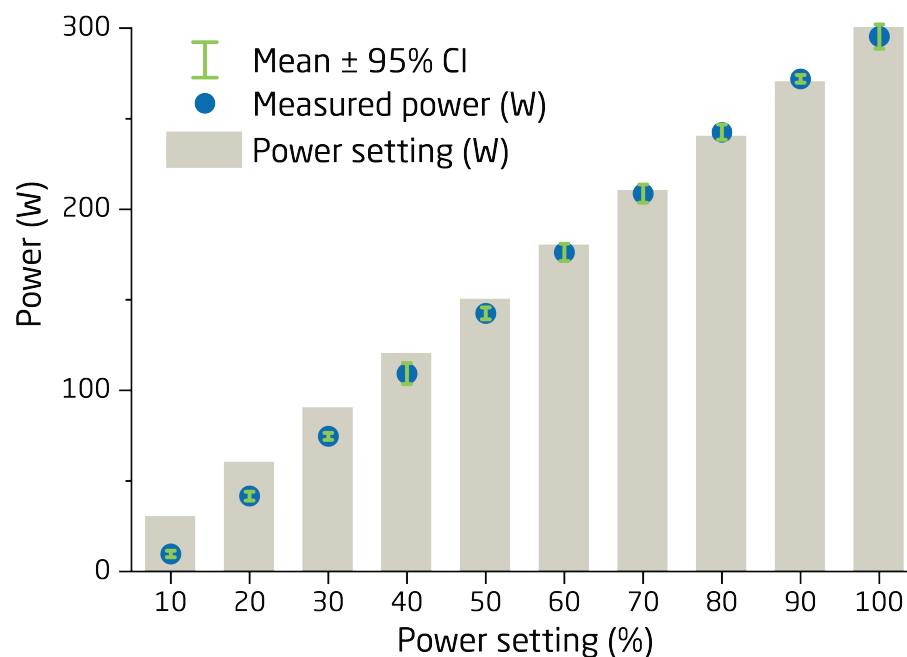


Figure 6.12: Laser power measurement results

large discrepancy at the low power setting shows an unstable laser source behaviour. It is not recommended to use a power setting lower than 20% due to the significant deviation between expected output and measured power.

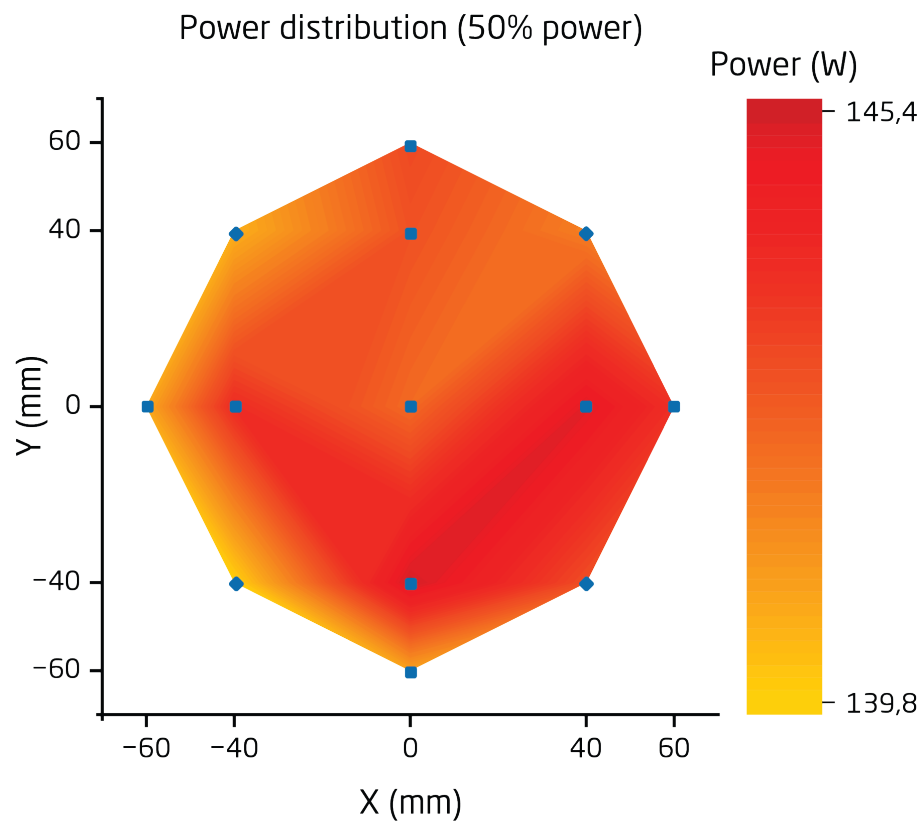
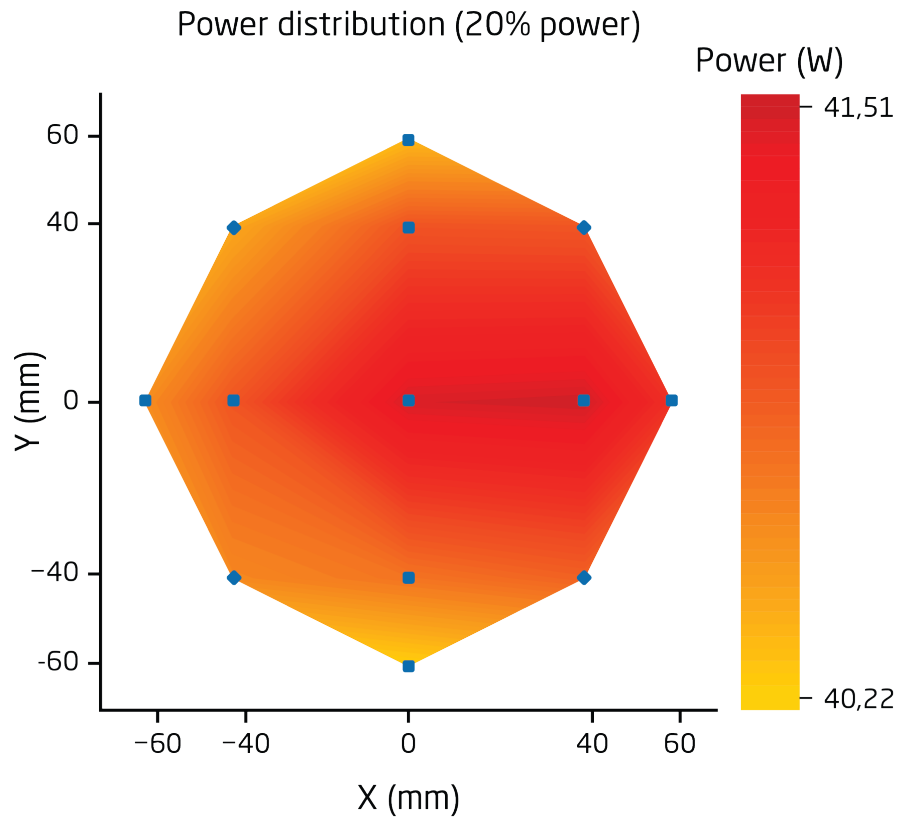
From the power level reading, an offset factor is introduced during job file generation, where the power level is input. The graph is utilised to determine the setpoint to input in the job file to achieve the correct power level. The offset factor is determined by fitting a line to the data defined by linear regression, as seen in Equation 6.1. Here  $x$  is the desired power setting as a percentage of the total power. In published works concerning processing polymer powder by the fibre laser in the developed system, the true power is reported to ensure correct dissemination of the power level utilised.

$$\text{True Power (W)} = 3.245 \cdot x - 21.27 \quad (6.1)$$

## Laser power Stability Across the Build Plane

When laser processing powder, the stability of the laser across the build plane is critical. If the laser is less powerful in one area than the others, issues such as delamination or insufficient sintering can occur. Contrary to too little power is too high power delivery in an area. These areas will be prone to polymer degradation or powder-burning issues. Hence minimising any gradient in the laser power is crucial for stable processing.

Two separate measurements were carried out to determine if any power gradient interfered with the laser processing. Both follow the same methodology as presented above for the power measurements, ensuring comparability measurements. In the contour plots shown in Figure 6.13, a deviation can be seen for the power at different locations on the build plane. The most significant deviation for the measurement at 20% power is a deviation of 3.1%, while for the 50% power measurements, this was 3.9%. The most intense laser radiation areas are located in the same place for the two measured power levels. This can be caused by deviations in the laser delivery system, allowing higher power in this region. The deviation in the measured values is seen to be small and on a similar level for the datasets of both power levels measured. They are, therefore, not expected to interfere with the quality of the process. Deviation across the build plane is a crucial aspect to consider for laser processing. Taking into account that the optical components are sourced based on a requirement of cost efficiency and can become less repeatable over extensive use. Hence this calibration will need to be part of the regular system maintenance, ensuring the stability of the laser processing equipment. From the measurements, it is found that the deviation of laser power across the build plane will not influence the process at the current levels.



- ◆ Data collection point

Figure 6.13: Power distribution at 20% and 50% power of the laser

## Laser power summary

Summarising the laser power delivered at the build plane considers the laser power stability over (the possible) power range and power delivered across the build plane. Results from the analysis presented above are shown in Table 6.4.

Table 6.4: Laser power delivery metrics

Metric	Unit	Laser power	Measurement standard deviation
Average deviation over power range	W	-7.7	-
Power at 20% setpoint	W	41.7	2
Power at 50% setpoint	W	142.5	2.6
Build plane stability (20%)	W	40.8	0.4
Build plane stability (50%)	W	142.6	1.8

### 6.2.2 Laser Spot Size

Defining the laser spot can be approached in two different directions. One is the theoretical approach determining the spot size based on the f-theta lens and spot size calculation. This method often underestimates the actual spot size measurable in the build plane. From the theoretical approach, a spot size according to Equation 5.6 is for the current setup 0.029 mm, as seen below. However, this is a gross underestimation of the spot size compared to the value measured by Light Optical Microscopy (LOM).

$$Spot\ size = 1.83 \cdot 1080\ nm \cdot \frac{290\ mm}{20\ mm} = 0.029\ mm$$

For the processing of polymer powder by the developed system, a different approach is needed. Since the relevant spot size parameter is defined by the Heat Affected Zone (HAZ), a method of defining this is required. A strategy utilising focus variation, shifting the target away from the laser source in defined increments, is utilised. Here a plate is engraved by the laser shifting the distance from the laser delivery system between each engraving. From this, the line width of each line can be identified, correlating to the laser focal plane and subsequent spot size measurement.

The focus verification of the system involved studying the actual spot size delivered to the build plane. To determine the true focussed distance between the laser delivery system and the build plane, a series of lines were scanned side by side on a black anodized aluminium plate. By adjusting the target by physically moving the aluminium plate from above to below the focal plane of the laser, a series of lines of varying sizes are produced, as seen in Figure 6.14.

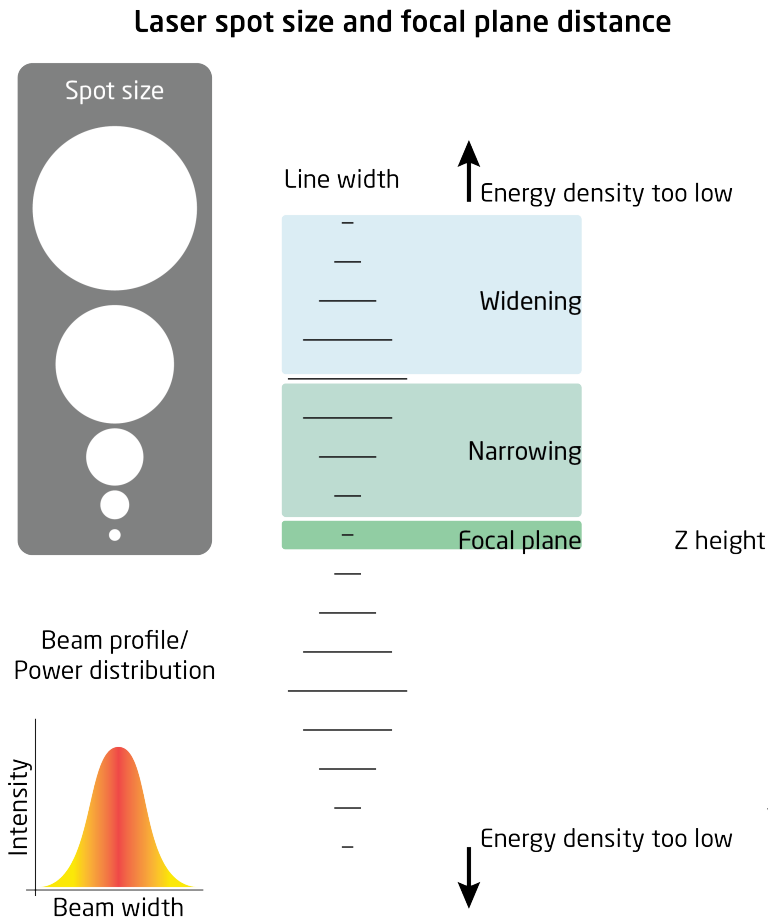


Figure 6.14: Laser focus identification method by focus variation

During this process, the line width is initially thin due to only the central part of the Gaussian power distribution delivering sufficient energy to mark the plate. The width of the scan line grows with each incremental motion, representing the changing processing distance and increasing energy density due to the smaller spot size (Figure 6.14 widening). When moving towards the focal plane, the line's width gets narrower (Figure 6.14 narrowing), revealing the true focus point as the thinnest line produced (Figure 6.14 focal plane). As the target is moved further from the focal plane, the line width again grows larger until the energy density becomes too small, causing the line to initially diminish in size and finally vanish. The process and physics incurring the waveform distribution of line width along the Z direction distance from the focussing optics are shown in Figure 6.14. This method measured the focal distance of the optics in the developed system, which was applied for defining the focussed width of the HAZ, as presented below.

A black plastic plate was used to determine the laser width of the HAZ delivered in the build plane. The black colourant promotes energy absorption for producing the imprint of the scan line on the plate. The laser scanned this plate at settings similar to the processing settings for build jobs in the system (50W & 3000 mm/s). This produced scan lines in



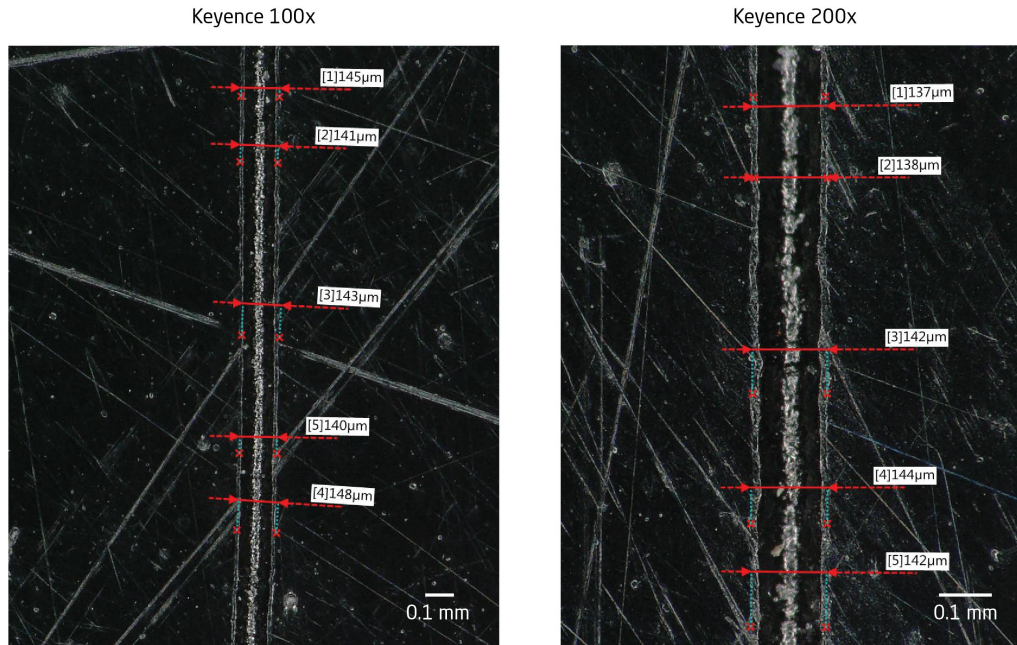


Figure 6.15: Keyence measurements  
Left: Scan line 1 - Right: Scan line 2

the black plastic plate, measured by Light Optical Microscopy. The measuring equipment is a Keyence VHX 6000, with a magnification of up to 200x. The measurement strategy focussed on two individual scan lines, which were measured five times each at two different magnifications minimising measuring error. The HAZ width is defined as the average of these ten measurements.

The metric of interest when dealing with the laser delivery system and spot size is not the theoretical method, but rather the HAZ. The width of the HAZ is determined as the verification of the delivered spot size since the setup for producing the HAZ mimics the conditions of the polymer powder containing a black optical absorber. The spot size is used for determining the hatch spacing during laser processing, ensuring an even heat input adequate for melting two tracks situated next to each other.

The results of the measurements of the HAZ are presented in Table 6.5. The scan line width depends on the system and the scan settings, meaning that this test is only valid for

Table 6.5: Spot size measurements

Metric	unit	Spot size
Theoretical	$\mu m$	29
Measured (HAZ)	$\mu m$	142
Measurement standard deviation	$\mu m$	2



these specific settings. Moreover, the HAZ in the black plastic plate is an indication of the spot size in this material and not a true definition of the HAZ in the powder and build plane. It is, however, expected to be in close comparison of the true experienced spot size, why the method has been utilised. For all experiments described in the following chapter 7, a spot size of  $150\ \mu\text{m}$  has been utilised for defining the hatch spacing between each scan line (unless otherwise noted).

### 6.2.3 Scanning Speed

Validating the translational speed of the laser spot between two points is essential for system qualification. Just as the laser power, the laser speed significantly influences the final part properties. As mentioned above in subsection 4.1.1, the translation speed of the laser is used when determining the energy density or any other form of conveying the energy input at the build plane - atmosphere interface. Industrial systems are available for measuring the beam profile and scan speed. These are often significant investments, which was not possible within the frame of this project.

To determine the speed, a measuring device was constructed. The speed-measuring device was designed to measure the speed of the laser between two holes in a plate (Figure 6.16). Both holes are designed with a specific size that is later measured and calibrated. The distance between the two holes is also measured and correlated to the data processing. These two critical dimensions are defined for improving the robustness of the scan speed measurement by accounting for any deviation in the data processing. Beneath the holes, a photodiode is located. This diode delivers a signal to a high-frequency oscilloscope

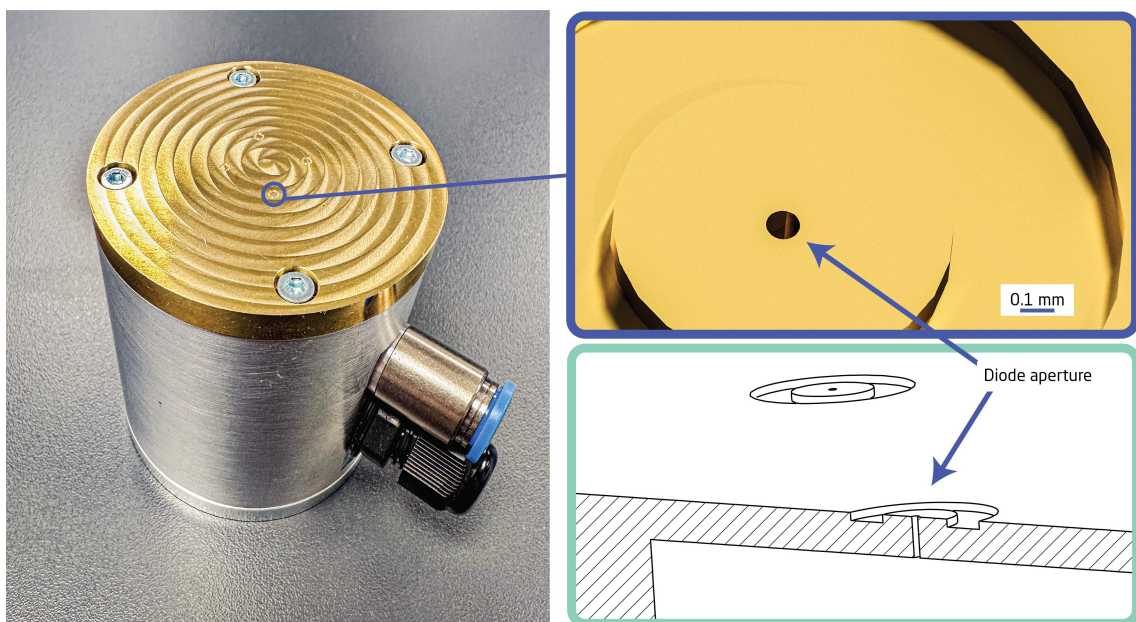


Figure 6.16: Scan speed measuring device and the hole for laser radiation of the photodiode

(Tektronix Inc. - TDS210) setup for recording the data from the diode.

The device consists of a top plate, a base plate, and a housing. The housing and base plate are made from aluminium to conduct the energy away from the top plate during laser scanning. The housing hosts two connections, one for the electronic connections and one for flowing inert gas (nitrogen) through. The inert gas flow minimises the material oxidation during laser scanning. By flowing inert gas, the holes are actively cooled by convection, ensuring minimal change in size or position caused by thermal expansion. The top plate of the device is made from brass, containing a large concentration of copper. Copper is reflective of the laser wavelength and does not react with the laser, since the majority of the laser energy is reflected off the surface. The four holes are located in the top plate. The scan speed verification test utilises two holes placed next to each other. The remaining holes are spares for when the laser processing eventually compromises the hole's roundness or diameter. Each hole is  $\text{\O}0.1$  mm and is placed in a square pattern measuring 10 by 10 mm. Around each hole is a brim designed for aligning the laser during data capture setup.

The photodiode signal data is digitally recorded to individual data points containing a time stamp and signal value. When passing the laser over one hole, a spike in the energy from the photodiode is recorded on the oscilloscope. The laser then passes the distance over the plate and traverses the second hole producing the second signal. This motion is carried out for five cycles back and forward, producing ten measurements of the time between the two recorded signals. The time between the two signals, the size of each hole, and the distance between the holes are then used to define the scanning speed.

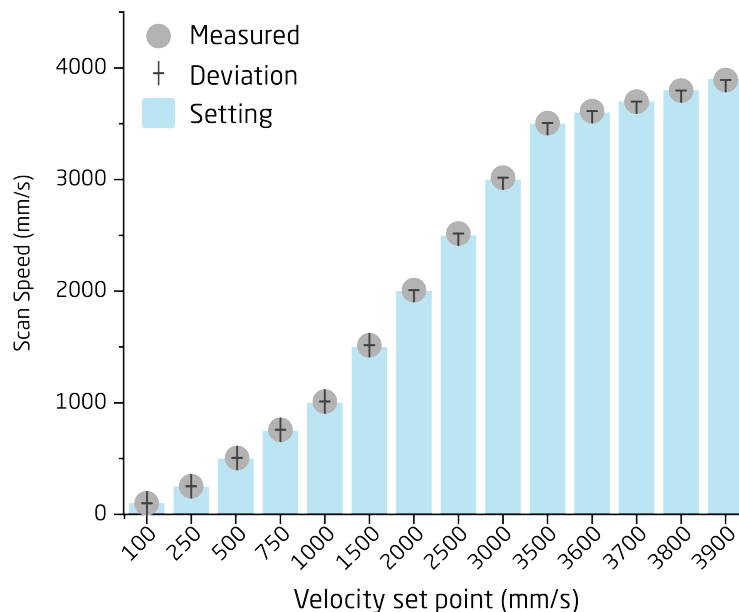


Figure 6.17: Scan speed measurements and comparison to setpoint

The scan speed is calculated from the data processing of the two-peak signal obtained during the experiment. The data analysis was carried out by a colleague (*Magnus Bolt Kjer*), presenting the results here. Setting the scan speed in the controller software, and communicating this to the Unified Systems Controller, produced laser movements close to the setpoint velocity. The most significant deviation is seen for the slowest scan speed, where a deviation of 1.7% is recorded. The largest discrepancies are recorded at slow scan speeds (<1000 mm/s). Here all speed settings produce an error of > 1%. Looking into scan speeds close to the desired processing range ( $\approx 3000$  mm/s), it is found that the system provides accurate speeds, only deviating by 0.6%. This further decreases when analysing velocities greater than the process desired scan speeds.

The measuring system shows a stable correlation between the set velocity and the recorded scan speed, as seen in Figure 6.17 and Table 6.6. From the data presented above, it is expected that setting a scan speed in the system controller delivers the specific speed, with no adjustment necessary.

Table 6.6: Scanning speed metrics

Metric	unit	Scan speed
Average delta over scan speed range	mm/s	8.6
Average deviation over scan speed range	%	0.8

#### 6.2.4 Laser Accuracy in the Horizontal Plane

The laser motion in the horizontal plane plays a pivotal role in the final part quality, determining the geometrical accuracy of the part produced. Reducing the error in the scanning system is critical, as several aspect influence the final position and repeatability of this. The Unified Systems Controller handles the setting of the laser point and interpolates the X and Y position provided by the g-code format (in mm) into the correct command according to the XY2-100 protocol. A detailed description of the controller unit and command translation is found in [212].

An initial investigation considered measuring a scan line and tuning the embedded programming of the controller to correlate with the desired motion. This method delivers a result close to the true motion required for accurate processing but does not produce the entire result for the final part geometrical accuracy.

Defining the geometrical accuracy of the final part in the PBF-LB/P fibre laser system requires physical objects produced in the system. Several aspects influence the size and fidelity of the objects produced, which are condensed in Table 6.7.

Different handles can control a selection of the factors influencing the geometrical ac-

curacy of the system. The triangulation and mesh production can be tuned in the CAD software, ensuring the level of detail and resolution required for the individual component. The build plane position can be controlled by accurate conversion in the Unified Systems Controller and by providing an adequate resolution of the scanning system, as described below. The process temperature can be verified and controlled as described in section 6.1.

Ensuring an adequate resolution of the scanning system is verified by determining the minimum step size of the system, correlating the scanner, f-theta and focal distance to the build plane. The resolution expected of the system is determined by the scan angle of the galvanometer scanner and the digital resolution embedded in the 16bit XY2-100 protocol [223]. The Sunny galvanometer installed in the system provides a scan angle of  $\pm 12.5$  degrees. Considering the 16bit protocol of the scanner communication, the angular resolution is estimated to:

$$\text{angular resolution} = 25/2^{16} = 0.00038^\circ = 6.7\mu\text{Rad}$$

Utilising an f-theta lens for producing the flat focus scan field, a direct proportionality of the positional resolution between the focal length and angular resolution [224] can be constructed as:

Table 6.7: Factors influencing the size of a manufactured part

Factor	Elaboration
Triangulated mesh	Depending on the resolution of the triangulation, the part can resemble the desired geometry closely
Build plane position conversion	The conversion of set points from the job file to the position in the galvanometer scanner protocol
Laser absorption	Laser absorption in the build plane is critical since transmitted laser energy can cause part growth into the bed
Process temperature and stability	Depending on the build piston temperature and gradient parts can either shrink or grow
Polymer swelling due to atmosphere	Depending on the polymer and atmosphere, moisture uptake can distort or increase the part size (e.g. nylons)
Polymer shrinkage during cooling	During cooling, the polymer partly settles into crystal structures which take up less space than the amorphous region causing shrinkage

$$\textit{positional resolution} = \textit{angular resolution} \cdot 290\textit{mm} = 2\mu\textit{m}$$

Sunny galvanometer defines the repeatability of the galvanometer scanner at  $\leq 8\mu\text{Rad}$ , equating to  $\approx 2\mu\text{m}$ .

The polymer powder has a significant influence on the smallest possible geometry. Seeing that the resolution of the laser positioning is less than 1/5 of the smallest polymer powder grain from an industrial PBF-LB/P powder. It is expected that the powder grain will influence the minimal feature size to a larger extent than the positional resolution. A minimum feature size, as stated by HUBS, concerning PBF-LB/P is 0.8 mm [18], seeing the clear influence of the powder sizing. The positional resolution is, by this, deemed adequate for fine detail manufacturing by the developed system.

Lastly, the swelling of the polymer influences the final part's geometrical stability and can be minimised by introducing a dry, oxygen-depleted atmosphere when processing nylon-type materials. By adhering to these guides, stable scanning and part production can be achieved. However, the polymer shrinkage, which has a significant influence in an otherwise calibrated system, must be accounted for by an empirical investigation as described in section 7.3. The laser motion introduces an error in the geometric dimension of the components produced. However, so does the physical motion systems. To investigate this, a verification of the physical motions is presented.

## 6.3 Motion Control

Two main motion systems influence the process stability of PBF-LB/P. These are the vertical-stage and the recoater. The vertical-stage and the accurate motion of this ensure the correct layer height according to the profile selected during job file generation. The recoater motion produces the new build plane for every layer during a build. It is critical that both of these systems produce the required motion to ensure the highest possible build plane fidelity. Below is an in-depth analysis of both systems, developing the metric required for understanding and setting up the desired processing routines of these.

### 6.3.1 Build Piston Accuracy

In subsection 5.3.4, the theoretical capabilities of vertical-stage motion were defined. Here an error in the positional accuracy was deemed irrelevant due to the positional bookkeeping in the software control of the stepper motors. An experiment has been undertaken to validate the accuracy of the vertical-stage considering the narrow (0.04 mm) layer height. To define the vertical-stage accuracy, a measure of the layer height motion over 100 layers was performed. The measurement utilised a digital dial gauge (sylvac - S\_Dial WORK BASIC 25/0.001), measuring the distance travelled between each layer motion over a



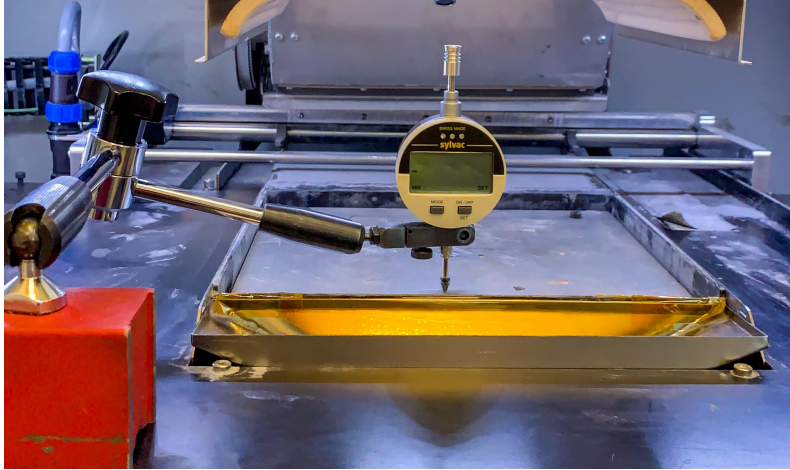


Figure 6.18: vertical-stage measurement setup

range of 100 layer height represented by a total motion of four mm. The dial gauge was placed in a measuring stand with the tip located on the bed. The measuring setup is seen in Figure 6.18, showing the dial gauge location and setup.

A uni-directional motion moving the vertical-stage away from the build plane was utilised for the measurement since the vertical-stage motion in the PBF-LB/P system only moves in one direction during the process. Due to this motion, measuring the vertical-stage repeatability and error could be done in a continuous procedure of moving one layer height, settling for 10 seconds, recording the data, and repeating the process. Two sets of measurements were conducted to verify the quality of the lead screw. One data set concerned the motion of the vertical-stage close to the top part of the lead screw, resembling the initial 100 layers in a build. The second measurement considered the motion during a build larger than 50 mm by moving the vertical-stage 50 mm further down, away from the build plane. Both measurements followed the same method to minimise the uncertainty between the two data sets.

From the measurement sets recorded over a four mm simulated build motion, a trend of variation between each layer is evident. This error between each layer is measured to be  $\approx 2\mu\text{m}$ , which does not amount to a significant error when considering other factors of the process, i.e. the elastic reaction of the powder cake during recoating and the powder grain size. The analysis results are presented in Figure 6.19.

From the build plane position measurements, a larger error of  $\leq 5\mu\text{m}$  is seen. During the recorded 100-layer cycles, a cyclic trend is observed. The cycle is seen as the large variations in measured motion in Figure 6.19 occurring twice during the 100 layers. This considerably large error in the motion is observed around Z-distance one and three mm. The distance on the linear stage motion between the two cycles is close to 60 layers, observed in the measurement data. This results in a spacing between the two areas of large

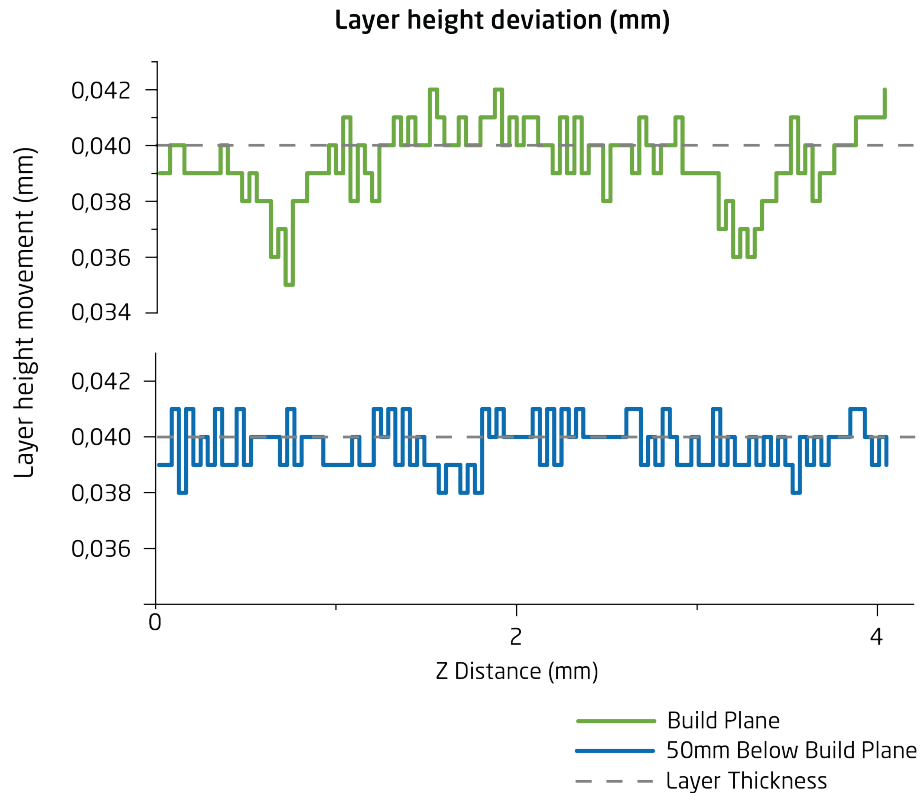


Figure 6.19: vertical-stage deviation from intended layer height

variation of  $\approx 2.5$  mm, similar to the pitch of the lead screw in the system (described in subsection 5.3.4). This cyclic error is presumed to be caused by wear in the system. Before receiving the system for repurposing, it was utilised for several years in active proto-type manufacturing. The cyclic behaviour is not observed when moving the build plate further away from the build plane, hence backing the hypothesis of wear in the top section of the lead screw.

When analysing the vertical-stage error from the data sets recorded 50 mm away from the build plane, a more stable response is obtained. Here an error of  $\approx 2$   $\mu m$  is found, similar to the behaviour at the build plane if disregarding the cycling behaviour.

The positional accuracy of the vertical-stage determines the actual layer height of the parts produced by the system. From the analysis, it is clear that an error occurs for every layer,

Table 6.8: Factors influencing the geometric size of a part

Metric	unit	Build Plane	Build Plane + 50 mm
Average layer height	$\mu m$	39.4	39.7
Average error per layer	$\mu m$	-0.6	-0.3
Accumulated error over 100 layers	$\mu m$	-60	-31

accumulating over the build's extent as seen in Table 6.8. The error in the top part of the vertical-stage motion is more pronounced than further along the lead screw. From the results, it is observed that for every intended new layer, the vertical-stage will travel less than one layer height. Caused by the tendency of the vertical-stage to perform a motion that is slightly smaller than what is required. This is especially evident at the beginning of each build job, with the error decreasing as the build progresses. The measurement procedure and method identified a cyclic error in the top part of the lead screw, which is deemed to be the wear of the components in the system. Causing a significant deviation between the intended and recorded movement near the build plane. The accumulated error at 50 mm from the build plane is still significant and does need further calibration to ensure an accurate layer thickness. To further improve the system's reliability, a new stepper motor and lead screw should be installed. This has, however, not been possible within this project's scope. The error causing a decrease in layer height will influence the final part's geometrical fidelity. For verifying the main hypothesis of the utility of a fibre laser in the PBF-LB/P process, the error is negligible. The error is, however, be further investigated in section 7.3, where compensation for the Z-height error and shrinkage is concluded upon.

### 6.3.2 Recoating Motion

Recoating motion is the predominant influence on the build plane quality as described in subsection 4.2.1. Ensuring a constant motion and roller rotation is critical for the topography of the plane produced during recoating. By utilising the counter-rotating recoater, an array of particle morphologies and sizes can be used and processed due to the versatility of the system. Counter-rotation ensures an even flow during recoating by constantly tumbling the excess powder in front of the recoater in an avalanche motion, as seen in Figures 5.29 & 6.20. Verifying the motion of the recoater has three critical components. First is the recoater translation velocity ( $V_t$ ), which is the speed at which the recoater traverses the build plane. Second is the roller rotational velocity ( $V_r$ ), and more importantly, the rotational velocity at the boundary between roller and powder. Finally, these two components interact, producing the resultant velocity of the recoater assembly ( $V_{res}$ ) as seen in Figure 6.20, producing the avalanche motion of the excess powder in front of the recoater.

Two trials investigating the avalanche behaviour of uncommon use modes of the roller recoater have been conducted. One trial of switching the rotational direction was performed. The resulting build plane showed large crevices and areas of high and low peak topography, causing no further investigation into this mode. The recoater has also been tested in an action of no rotation, acting as a wiper, as presented in subsection 5.4.4. Here the angle of attack between the roller and the build plane caused powder packing in front of the roller, leading to a rise in the recoater system, producing a plane skewed from one side to the other. From this investigation, the recoater is always run in counter-rotation



mode.

The roller recoater system can be tuned in the motion controller programming setting the speed of the traverse motion and the rotation. For simplicity, this study has focussed on one setting of both actions, presented below. If new materials or powder morphologies are to be investigated in the system, a further study of the settings required for producing the flat build is recommended For the individual materials.

The recoating system's resultant velocity was assessed by measuring the time of travel for the recoater to pass over the build plane. The measurement focussed only on the build plane traverse motion since the start and end motion of the stage has built-in acceleration parameters in the controller programming, which skew the actual speed over the build plane. At both ends of the recoating movement, a zone of no build plane and no powder contact enables the recoater to accelerate to the desired speed, as reported in this validation study. The acceleration aid the stepper motor in reaching the desired velocity while minimising the potential error from missing steps due to elevated torque requirements at the beginning and end of a motion.

The rotational velocity of the roller was assessed by filming the recoating motion with a high-speed camera, counting the number of revolutions occurring over the build plane. A physical marking on the roller allowed for the visual inspection and counting of rotations over the build plane, which is afterwards correlated with the time for the build plane traverse motion described above. By knowing the size of the roller and the revolutions per second, the rotational velocity can be defined.

Determination of the traverse and rotational speed considered five measurements of each parameter defining an average time for traversing the build plane, as well as an average number of rotations recorded by the high-speed camera. The number of rotations showed no deviation over the five samples. The recoater and roller analysis result is presented in Table 6.9, presenting the relevant data for the resultant velocity of the two components in

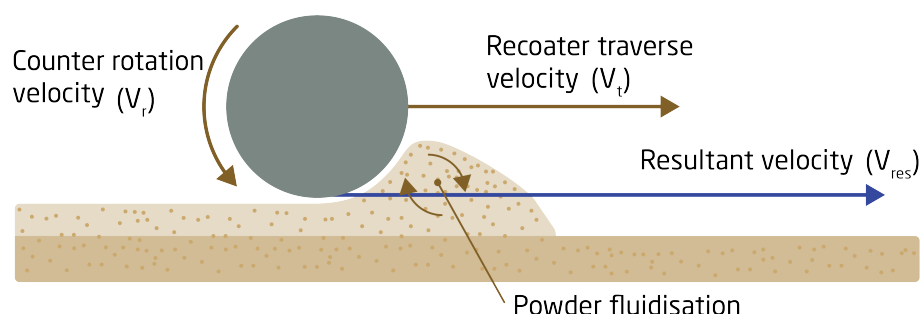


Figure 6.20: Recoater resultant velocity (blue arrow) consisting of the translational and rotational speeds (brown arrows) of the recoater assembly. Inspired from [155]

Table 6.9: Recoater traverse and roller rotational velocity metrics

Metric	unit	At the build plane
Roller diameter	mm	Ø20
Roller circumference	mm	62.83
Roller Revolutions		14
Roller distance covered	mm	879.65
Roller revolution per second	RPS	2.23
<b>Roller rotational velocity (<math>V_r</math>)</b>	mm/s	<b>140.3</b>
Recoater motion	mm	251
Recoater traverse time	s	6.27
Recoater traverse time deviation	s	0.1
<b>Recoater traverse velocity (<math>V_t</math>)</b>	mm/s	<b>40.7</b>
<b>System resultant velocity (<math>V_{res}</math>)</b>	mm/s	<b>181.2</b>
Recoater travel per revolution	mm	17.9
Roller distance per mm traverse motion	mm	3.5
Roller to recoater velocity ratio		3.43

the system.

Based on the results of the recoating motion, a resultant velocity similar to the one reported in the counter-rotation recoater study [155] is found. In the study, a resultant velocity of

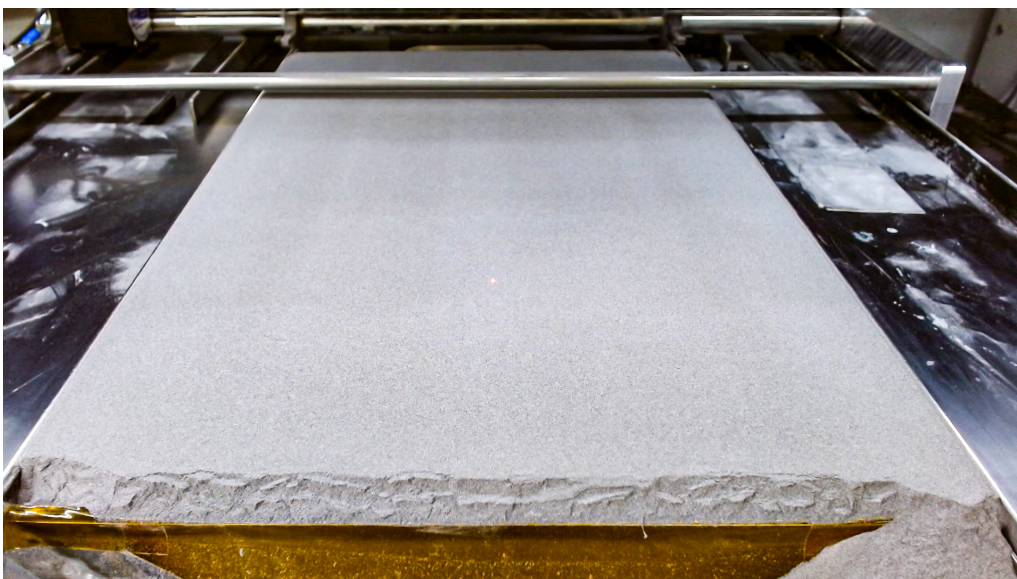


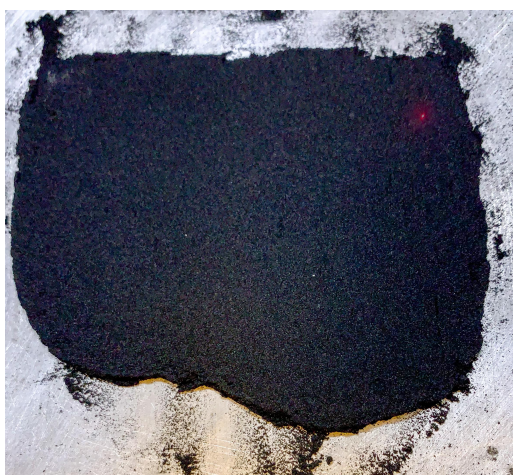
Figure 6.21: Build plane quality

140 mm/s is found to produce the highest packing density in the bed. The study concludes that this velocity also produces the flattest surface topography for PA12. This work has not explicitly measured the surface topography and packing density. The system, however, is seen to produce flat and even build planes, as shown in Figure 6.21. The quality of the build is representative of both heated and cold powder beds, with a flat surface and full coverage.

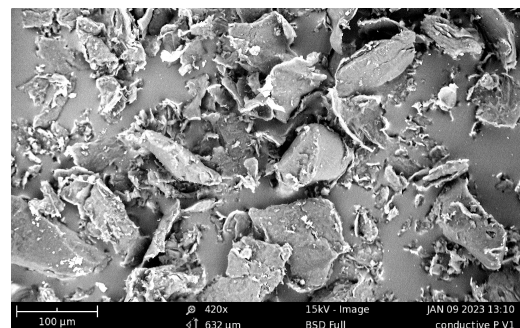
The system utilises a roller significantly smaller than what is typically found in industrial systems. This causes a need for a much faster roller rotation than what is utilised elsewhere. Fast rotation of the roller allows the powder avalanche to form and unify rapidly. In doing so it is observed not to cause the powder to become airborne, producing a hazardous atmosphere.

A cryogenic milled powder was tested to verify the integrity of the selected parameters. A source of error in the experiment is that the powder did not fill the entire build volume, which causes only the plane to be visually inspected. The coarse and uneven powder is seen from the Scanning Electron Microscope (SEM) image in Figure 6.22b. As stated in subsection 4.1, powders for PBF-LB/P processing is preferably spherical and with a narrow size distribution. Coarse powders can, however, function if the flowability is ensured by i.e. flow aids. Nevertheless, the system was capable of producing a flat plane for laser processing from the powder, as seen in Figure 6.22, using the settings presented above.

A stable behaviour of the avalanche effect from the roller recoater is seen in Figure 6.23. Here the recoating cycle is presented, (1) showing the layer prior to new powder distri-



(a) Powder bed produced from powder below



(b) Coarse powder grain

Figure 6.22: Build Plane quality of coarse and uneven-sized powder

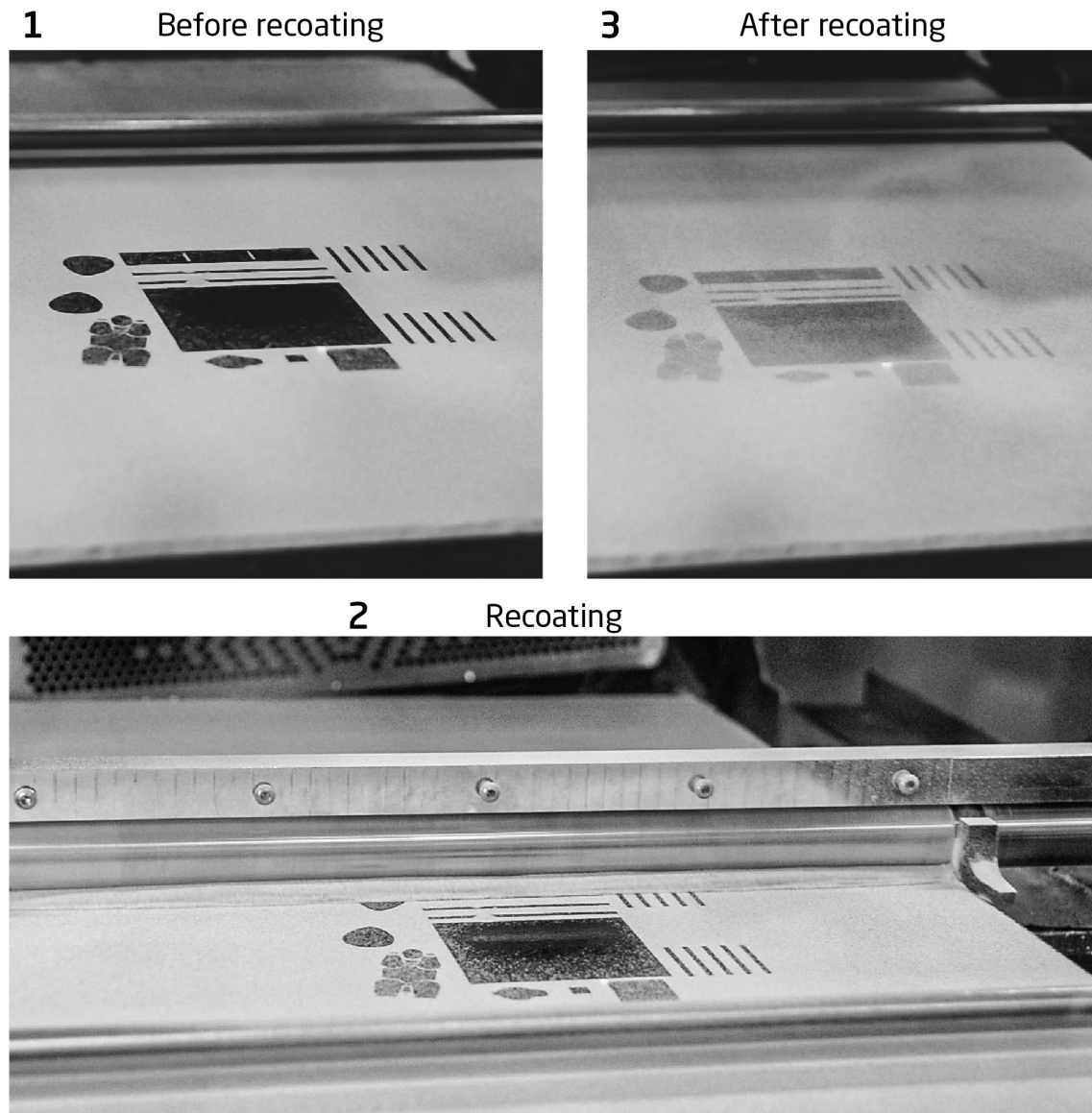


Figure 6.23: Recoating routine in three steps

bution, (2) the recoating action and powder avalanche in front of the roller, (3) and the thin layer of  $\approx 40 \mu m$ . In image 3, the previously processed layer is seen beneath the freshly recoated powder, bearing testimony to the layer height of  $\approx 0.04$  mm being reproduced during powder distribution. The black powder constituent causes the sheen of black from the previously build geometry, making it visible through the newly distributed powder layer. New build plane deposition has been observed to produce consistent and even layers for the entire plane, ensuring the stability of the process cycle.

## 6.4 Build sequence execution

From the analysis of the critical system elements and the validation of these, a build sequence must be verified. This test confirms the process steps acting as one system produc-



ing the powder cake and build plane, heating this, laser scanning it, and repeating these steps to produce an entire geometry, following the process cycle described by Figure 6.24. To verify the build sequence as presented in section 2.1, a geometry designed to challenge the system features and components, proving the capabilities of the developed system, is utilised. This geometry was selected due to its simplicity while still delivering information on the process capability and sequence as described below.

Verification of all the sub-systems working in unison focusses on producing a simple geometry that, to an extent, challenges the system's capabilities. During this complete system verification procedure, any misalignments in the system can be found by analysing the sequence during the build, actively monitoring the process, and by the parts produced by this build job. The geometry was explicitly designed to define errors in the process while maintaining a small footprint in the build plane, hence allowing multiple parts to be produced in one build job. The geometry is a double sphere connected in the centre, as seen in Figure 6.25. By having two spheres connected by an organic shape, the system's capabilities are challenged. The simple geometry challenges the process cycle by evaluating the fabricated component on layer shifting, stair stepping, and mechanical stability. Laser Based Powder Bed Fusion of Polymers is known for not requiring any support structures in the build since the powder cake acts as the support in itself. During the production of the geometry, one half will show downward-facing surfaces, while the other will show upward-facing surfaces. Flat sections could have been introduced to opti-

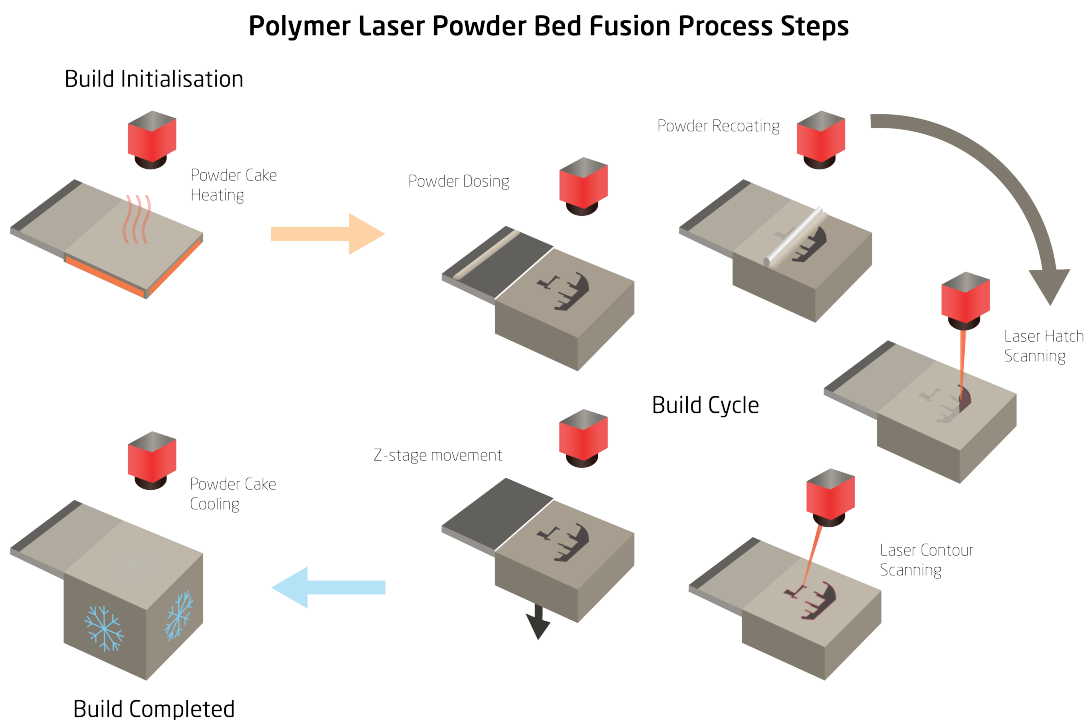


Figure 6.24: Build cycle steps for Laser Based Powder Bed Fusion of Polymers processing

mise the geometry, showing the system capabilities for flat sides of the part or as a down- or upward-facing flat surface. This was, however, not targeted for this verification build.

For the build sequence verification, a white PA11 from BASF (Appendix C) was used for laser processing. The point of the initial build job was not to produce mechanically stable and geometrically accurate parts. But rather a holistic process verification and build sequence definition. The job file for the initial build was prepared in the job file generator and controller software (subsection 5.4.1). During the verification build, an initial process study was conducted, determining the adequate energy density and heater setting for the process. The selected settings are presented in Table 6.10.

Nine parts were made for the build sequence investigation. Here the build sequence execution as well as the laser power, scanning speed, and heater's utility, were defined. The nine parts were produced at three different energy density settings. Since this build was carried out in the early stages of the project, a full definition of the scanning speed capabilities was not understood yet. Hence the selected scanning speeds are much lower than what is later found feasible for laser sintering of polymers by fibre laser presented in chapter 7. The settings selected for the build verification study were in part developed during a Student project, which focussed on fibre laser scanning of polymer powders. The author supervised the project, which was conducted by "*Student - DTU-s206719, Sofronija Sharlamanov*". During the project, more than 200 variations of scanning speed and power settings were trialled, laying the basis of the settings presented in Table 6.10.

The selected process temperature was defined by a Differential Scanning Calorimetry (DSC) analysis, shown in Figure 6.26. The analysis only focusses on the initial melting and crystallisation of the powder since these are most relevant for the process study. This approach is not typical for a DSC analysis but is deemed fit considering the analysis objective. The DSC analysis shows two distinct and narrow peaks. The melting temperature is defined as  $T_M$  201 °C at the melting peak (red curve) with the onset point of melting  $T_{oM}$  occurring close to 197 °C. Moving to the crystallisation temperature  $T_C$ , a peak value

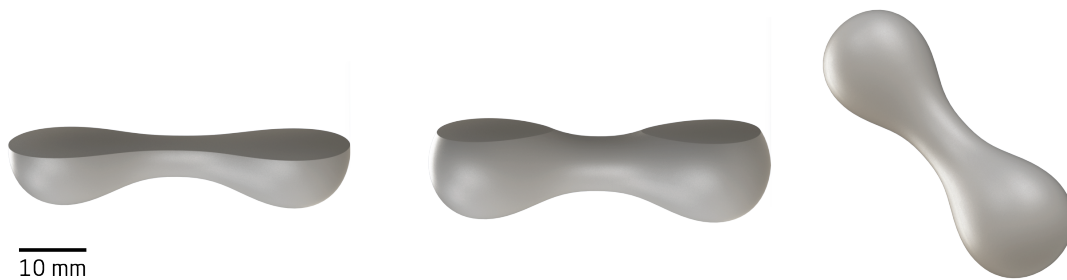


Figure 6.25: Barbell geometry for verifying build sequence and process strategy

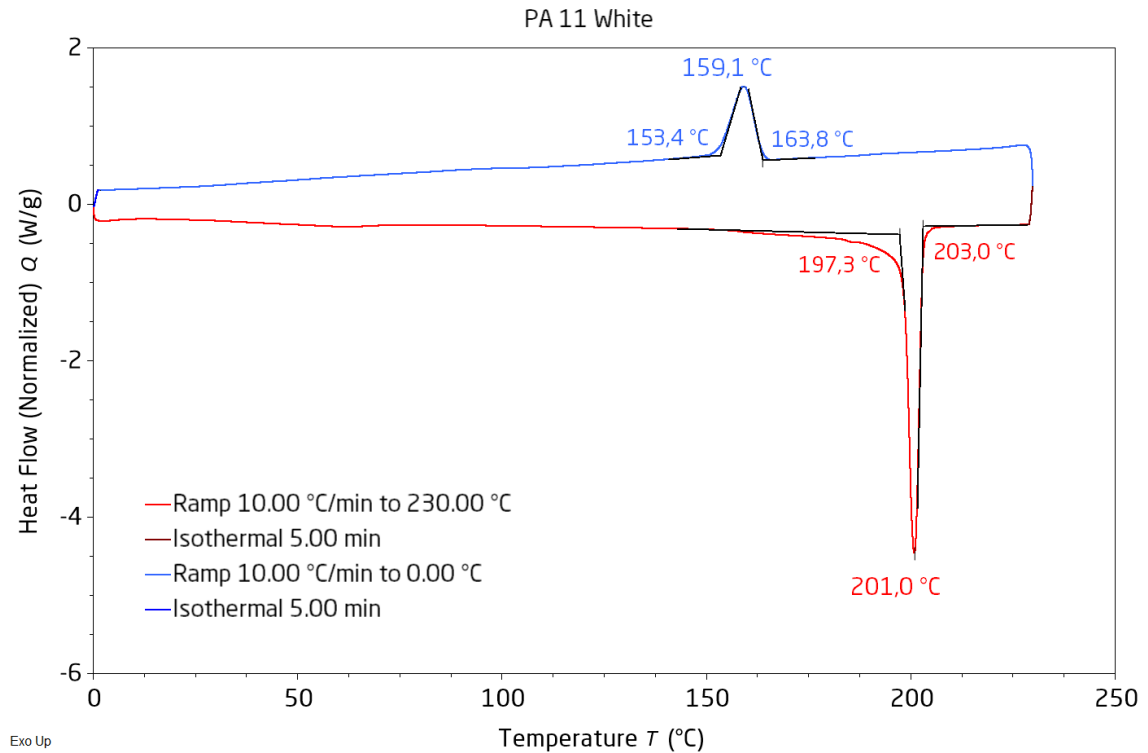


Figure 6.26: PA11 White DSC curve showing the initial heating and cooling curve only

of 160 °C is found with the onset of crystallisation  $T_{oC}$  occurring at 164 °C.

Between the two onset temperatures  $T_{oM}$  and  $T_{oC}$ , is the process window defined as explained in section 4.1. The process temperature was selected based on this process window. By aiming for a temperature located centrally between the two onset temperatures, as seen in Table 6.10.

The build sequence verification job ran successfully, as seen in Figure 6.27, achieving all

Table 6.10: Job file settings for the build sequence verification

Metric	unit	At the build plane
Hatch distance	mm	0.15
Heater	°C	175
Layer thickness	mm	0.1
Scan speed	mm/s	100 - 150 - 200
Laser power (in software)	W	70 - 75 - 80
Laser power	%	23.3 - 25 - 26.7
Laser power (delivered)	W	54.5 - 59.9 - 65.3

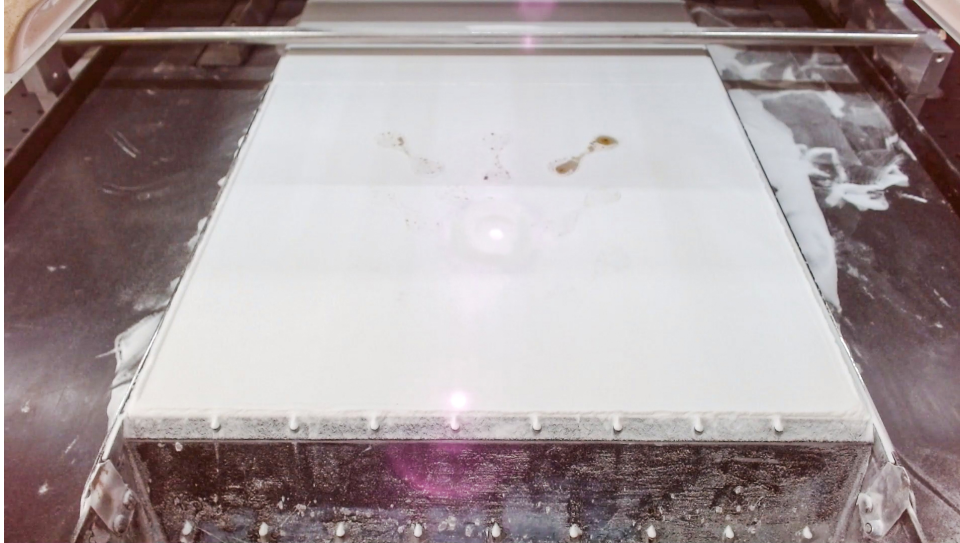


Figure 6.27: Build Sequence verification with the laser processing the white PA11 powder. Image from web camera monitoring build process

the metrics required for the laser processing of the powder. The build sequence followed the cycle of initial heating, layer-by-layer laser irradiation, and a final cool-down stage.

The build sequence verification is summarised in Table 6.11, showing only two areas of the tested sequence-producing problems. One is the white powder selected in the trial. The absorptivity in the white powder is controlled by the absorption of the laser light wavelength in the polymer, additives, and colourants. PA11 does not show sufficient absorption at the laser wavelength as shown in Figure 4.8 with the white colouring often being a ceramic powder consisting of  $\text{TiO}_2$  [225], which also does not show good absorp-



Figure 6.28: White parts manufactured during the initial build sequence verification



Table 6.11: List of build sequences verified in the test

Sequence	Go	No Go	Elaboration
Powder dosing (cold)	X		
Recoat motion (cold)	X		The build plane is produced prior to heating
Even layer production (cold)	X		
vertical-stage motion (cold)	X		
Heating powder cake	X		Heating prior to laser processing
Powder dosing (heated)	X		Powder flows at heated temperature
Recoat motion (heated)	X		Stable motion at heated temperature
Even layer production (heated)	X		Powder distribution for highly planar build plane
vertical-stage motion (heated)	X		Seen from parts to be accurate
Safety circuit functional	X		Safety circuit shuts Off laser if triggered
Laser On-Off	X		Laser turn On during active pass
Laser position	X		Laser moves to the desired location
Scanning speed	(X)	(X)	Faster scan speed required for full power range processing
Laser processing white powder		X	Laser absorption too little in white material
Thermal camera monitoring	X		Thermal camera can locate heated zone close to processing area
PID controller temperature monitoring	X		PID regulator shows build plane temperature, defining safe removal

tion [226]. Any other additive is likely to be in such small amounts that any absorption by these is negligible. Nevertheless, the system was capable of producing parts from the white powder. This part production owes its success to the meticulous investigation of the required parameters. The rigorous study developed a process regime allowing powder consolidation to the extent of three-dimensional components being produced in the system.

The parts produced during the initial build sequence investigation are presented in Figure 6.28. The image shows two parts, from the same build, with the left part showing the downward-facing surface with significant defects caused by the low laser absorption. The right part shows the upward-facing surface with minimal imperfections and significantly better surface topography.

From the build sequence verification, several conclusions are drawn. The first is the successful processing capabilities of the system. It is shown how the system can produce a flat build plane, sufficiently heat the powder cake, laser process the cross-sectional area of a geometry, and repeat this cycle for the entire build. The second conclusion is that white powder is not a viable solution for manufacturing geometrical and mechanically stable parts. An optical absorber is required for this, capturing the laser energy and delivering this in the form of heat (for powder consolidation) rather than laser reflection and transmittance to the surrounding powder. The optical absorber and an investigation of new materials is the focus of chapter 7, thus defining the use of fibre lasers in the PBF-LB/P process.

## 6.5 Chapter Summary

To determine the efficacy of the installed sub-system, rigorous testing and validation have been conducted. A discrepancy between the set point temperature for the heaters and the actual powder cake temperature is found. The same is true for the laser power, where the power is less than the setpoint. An offset factor is implemented for the heaters and laser power to correct these discrepancies. The heating study further found the actual powder cake temperatures and a region of minimal temperature gradient resulting in the creation of a build envelope where any thermal gradient is negligible within its boundaries. Besides a study of the heating, a cool-down period is investigated, developing the metric for the safe part removal temperature as read from the build plate PID regulator or data collection IIoT dashboard.

Besides the laser output over the power range, an investigation into the power stability in different positions across the build plane is presented. The results proved excellent power stability across the build plane. Fluctuation in power across the build plane is comparable to the measured power at each setpoint, demonstrating the consistency of the measurements with minimal deviation. Investigation of the laser spot size is, from theory, expected to be much smaller than what is achieved in the setup. Here the measured spot size is close to five times larger than the theoretical value. This is not problematic due to the excess power provided by the laser source, allowing for a stable processing range at this spot size. The theoretical value of the spot size is deemed too small to be effective in the process due to the laser delivering power in an area smaller than the average powder grain size. If this were the case, localised overheating would occur, leading to polymer degradation in the individual powder grain or the selection of a power setpoint lower than the stable region, which is undesirable.

An investigation of the achieved scanning speed is also presented, showing the capabilities of the Unified Systems Controller and galvanometer scanner. Here close agreement between the setpoint scan velocity and the measured scanning speed is found. Ensuring

this close agreement allows for easy process qualification during part manufacturing, with less added complexity. Lastly, a discussion of the laser positional accuracy considers the fact of polymer laser processing and the added uncertainties, which can be minimised by process and laser control. However, a final calibration of the system is needed to define the shrinkage factor of the selected material. This shrinkage factor is dependent not only on the laser scanning parameters but also on the general processing signatures of the system. Hence a calibration for each material used in the system is needed for the fabrication of high fidelity components.

A significant influence on the geometrical fidelity and final dimension of the parts produced in the systems is the accurate motion of the vertical-stage. This showed, during the investigation, an error throughout a build. This error accumulates, causing the part produced to be smaller in height. This error was only identified in the later stages of the project and will receive attention in future work. The error is defined as more significant in the initial phase of the build, caused by (what is assumed to be) wear on the vertical-stage mechanism. The error in the mechanism is expected to be due to not replacing the original lead screw and motor assembly in the machine during the repurposing efforts. The error may have been minimised if this had been completed.

The specification of the lead screw is designated for use in an imperial framework and unit system, shown by utilising 2.54 mm per revolution, equalling 10 threads per inch (a common pitch in imperial units). Considering the likelihood that the embedded programming of the original machine also observed this approach, an error in the setup could have been smaller. This, coupled with the fact that the embedded programming on the motor controller is done in a metric unit system, causes a misalignment in the number of steps per mm (theoretical = 629.9 / empirically found for embedded program = 633). If the lead screw had been in a metric standard, an even number of steps per mm would have been utilised in the programming minimising the error in the positional bookkeeping of the controller. When using micro-stepping, as is done for the vertical-stage, an error can occur where steps are skipped or missed by the mechanical system. If feedback monitoring of this potential error is not fitted, the system will not "know" that this error is occurring and will only move the designated number of steps. This can also be an influential factor in the error of the vertical-stage. Skipping steps leads to the movement of the vertical-stage being less than designated by the controller, even though the controller is set up with a larger step count based on empirical calibration of the stage. The wear can have increased throughout the project, which can be a root cause for the motion discrepancy between the reported error and the initial calibration. Based on these conclusions, a change of the vertical-stage linear motion assembly is needed for greater accuracy of the sub-system for future experiments.

The investigation of the recoater stage found a total velocity of the recoating motion and

rotational speed comparable to that presented as the optimal value in subsection 4.2.1. A flat build plane with minimal topographical errors is produced during the recoating motion, permitting better layer-to-layer adhesion based on the flat layer produced. The resultant velocity has not been investigated further in this study due to the surface characteristics produced initially. The system's open architecture allows for changing and tweaking close to any parameter and setting. Due to this, future exploration of the recoating system is planned. Hence an investigation concerning the change of rotational and traverse velocity and the installation of a blade recoating system.

An effort to prove the entire systems capabilities focussed on the build sequence verification. Here a build job was fully processed, utilising the systems described above for producing the job file, making the powder cake and build plane, heating this, and laser scanning layer-by-layer producing the final parts. This proved that the entire system is capable of producing parts from polymer powder, utilising a fibre laser for consolidation. The build sequence ran as planned, creating new powder layers and scanning these with the laser. Several parts were produced as shown in Figure 6.28, with the predominant issue being the low energy absorption in the white material. To develop the system's capabilities and prove the fibre laser's utility for polymer processing, an investigation of optical absorbers is required. This investigation, including a conclusion on the versatility of a fibre laser for processing polymers, is presented next in chapter 7.

# Fibre Laser Utility in Polymer Powder Processing

Fibre laser processing of polymers has been regarded as challenging due to the low absorption properties of the material, leading to doubts about the feasibility of producing functional parts. The results obtained from the previous tests demonstrate that fibre lasers can indeed process polymer powders that, to some extent, resemble the original design in the CAD file. Nonetheless, one significant issue identified in the previous tests is the uncontrolled absorption in the polymer, resulting in the irregular surface finish of the fabricated parts.

During laser processing of white powder, an observation of fully melted nodule formation is seen in the powder. These are influenced by altered absorption properties in the melted nodule. The white barbell parts showed these nodules on the downward-facing surfaces, causing an irregular surface finish. The variation between absorption in the powder and melted regions of the nodules results in these growing larger with each new layer, producing the nodules into the powder cake as shown in Figure 6.28.

This chapter investigates the application of fibre lasers in polymer powder processing, with a major focus on the introduction of an optical absorber to enable the stable production of polymer powder parts. The initial study delves into the utilisation and optimal amount of the optical absorber required for achieving stable fibre laser processing. The second part concentrates on evaluating the geometrical accuracy of a benchmark geometry produced by the system. Lastly, a new material suitable for the Laser Based Powder Bed Fusion of Polymers process is introduced, demonstrating the feasibility of producing conductive polymer parts through fibre laser processing.

## 7.1 Fibre laser absorption in polymers - A recap

In subsection 4.2.4, an explanation of the difficult processing regime between fibre lasers and polymers, specifically PA11, was described. The wavelength interaction between fibre lasers at 1080 nm and the polymer molecule is exceptionally low. Due to this, the energy from the laser is not absorbed in the polymer but rather transmitted and reflected. This process causes the laser to diffuse into the powder bed producing the results shown in section 6.4.

An optical absorber can be employed to enhance the interaction between the laser and the powder, effectively transferring heat into the powder bed from the laser. By absorbing the laser energy and transforming this to heat, an optical absorber allows otherwise un-processable materials to be processed by the laser wavelength. Utilising these absorbers means that the excellent fibre laser beam properties can be converted into a useful tool for processing polymers. A selection of optical absorbers is available as various additive compounds or colourants, described in the following.

### 7.1.1 Optical absorbers available

A range of materials is suitable as an optical absorber for fibre laser (1060-1080 nm) processing. Often the composition varies widely, with the most low-tech solution being carbon black, which absorbs the majority of the energy delivered by the laser light, converting this into heat [227, 228]. Other solutions for optical absorption include graphene, carbon nanotubes, and the commercial products Clearweld LWA 983A from the American company Clearweld and PeroLab from the German company Sindlehauser Materials.

Clearweld and PeroLab are both green chemical formulations which allow laser energy absorption specifically at wavelengths relevant for Ytterbium Fibre lasers (1060 - 1080 nm). The chemicals can be compounded into the desired resin allowing for effective laser processing. Depending on the concentration required for laser processing, a green hue of the final part can be expected if either the Clearweld or PeroLab compounds are utilised. Both providers of optical absorbers recommend that the concentration be found empirically since the utilisation is not yet widely disseminated. Based on the success of utilising the system with known material compositions, these additives are desired for further investigation in the developed system but have not been possible to incorporate in the presented work.

Using graphene and carbon nanotubes as the optical absorber encompasses the characteristics of utilising carbon black, based on the constituent element and chemical bonds prevalent in the compounds. The main focus of this study has been on PA11, which was preferred due to the bio-sourced feedstock material for the production of the polymer. Both compounds are compelling and worth investigating, considering fibre laser processing into final thermoplastic parts. However, for this work, it has not been possible to find

or produce relevant material containing either.

All the above-mentioned materials or compounds are interesting solutions for obtaining fibre laser absorption in the PA11 material utilised in this study. The study has, however, concentrated on the use of two kinds of PA11. One white and one black, investigating the material properties of both materials separately and in conjunction. The study strives to characterise the useful case of mixing two similar polymer grades, with one main difference being the colour. By using the same kind of polymer, lower complexity in the material preparation, study, and classification is achieved. This has allowed an in-depth analysis of the two materials, which is the focus of the following.

## 7.2 Optical Absorbers in Polymer Fibre Laser Processing

Optical absorbers are used widely for laser welding of clear polymers, allowing energy absorption for wavelengths which otherwise do not interact with the polymer. Incorporation of an optical absorber in a polymer can be carried out in several ways. A low complexity method for introducing the optical absorber is by physical mixing of two distinctive batches of a polymer, with one containing the absorber and one pure. The utility of a black optical absorber-filled material mixed with a white base material is investigated. The investigation seeks to describe the functionality of fibre laser processing in a mix of two alike materials. The study further examines the level of black constituents required for successful part production by mixing the two materials. Evaluating the efficacy of mixing includes a study of the rheological behaviour of the constituent powders defining the process of laser absorption in the black constituent and subsequent consolidation behaviour of the powder mix.

### 7.2.1 Mixing PA11 White and Black for Optical Absorption

The initial study of employing PA11 black (Appendix D) as an optical absorber mixed with PA11 white investigating the manufacturability was presented at the "2022 Annual International Solid Freeform Fabrication Symposium" - University of Texas, Austin. The peer-reviewed publication is found in Appendix E, from [229]. To clarify the applicability of a fibre laser in the PBF-LB/P process, a method of consolidating a white and black PA11 mix is used. The PA11 constituents in the mix are henceforth denominated as white and black. The approach follows a framework of material and powder characterisation, process development for the different compositions of white and black, and process and part characterisation, analysing the mechanical properties, and surface characteristics of the parts produced.

Five mixed compositions have been tested within the framework as seen in Table 7.1. Batches 1 through 3 have been tested within this section, with batches 4 and 5 described and tested in the following subsection 7.2.2. Working from an initial hypothesis that pure

Table 7.1: Powder mixing ratios for the optical absorber study

Batch No.	White content (wt%)	Black content (wt%)	Designation
1	50	50	50-50
2	80	20	80-20
3	95	5	95-5
4	98	2	98-2
5	99	1	99-1

white cannot be processed by fibre laser alone and that pure black absorbs too much energy for the available process range described in subsection 6.2.3. Processing pure white results in an uncontrolled process of a mix of the different powder binding mechanisms presented in subsection 4.1.2. Causing the parts to show limited mechanical stability with highly degraded surface characteristics. Processing pure black PA11 leads to polymer degradation and a potential fire hazard due to the energy absorption of the powder being much higher than required leading to an exceedingly high energy melt ratio as presented in Equation 4.8.

## Material charecterisation

Characterisation of the materials provides a basic understanding for determining the initial processing conditions in the system. Several aspects are relevant for processing mixed

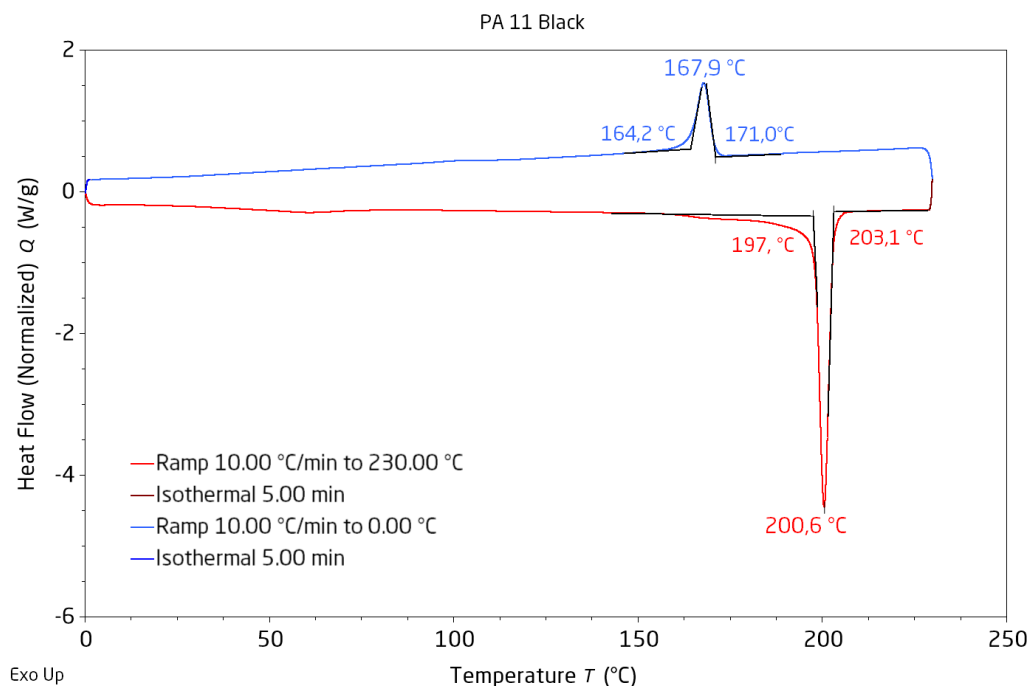


Figure 7.1: DSC analysis of the black PA11 powder



Table 7.2: DSC analysis results. Critical temperatures concerning the process settings, including the process window for both materials

Characteristic	Abbr.	Unit	PA11 White	PA11 Black
Melting onset	$T_{oM}$	°C	197.3	197.0
Melting	$T_M$	°C	201.0	200.6
Melting end	$T_{eM}$	°C	203.0	203.1
Crystallisation onset	$T_{oC}$	°C	163.8	171.0
Crystallisation	$T_C$	°C	159.1	167.9
Crystallisation end	$T_{eC}$	°C	153.5	164.2
Process window	$T_{window}$	°C	33.5	26

powder batches. The melting and crystallisation behaviour and temperatures, the powder morphology and size, and the amount of black constituent in the material. To develop the process parameters, a DSC analysis for both materials was conducted. The results of the analysis are shown in Figures 6.26, 7.1, and are summarised in Table 7.2. Data concerning the analysis methods are presented in Appendix E.

From the DSC analysis, it is evident that the two colours of PA11 are in close resemblance. By analysing the critical temperatures, it is seen that the process window is significantly narrower for the black type PA11, which will be used as the determining factor for setting up the build job in the system. The density and powder size is critical to ensure that the mixing of the powder will produce a homogeneous blend. In table Table 7.3 and in Figure 7.2, the critical sizes as well as the powder morphology are displayed.

When analysing the mixing properties of two materials, three main components are critical [230]. One is the powder morphology. Homogeneous powder morphology reduces the risk of powder sticking and clumping, causing higher gradients of one material compared to the other. Second is the sizing which influences the homogeneity by producing segregated mixes if the grains are of different sizes. Third is the density of the two components. If these are far from each other, another segregation mechanism occurs, causing

Table 7.3: Powder specification and sizing

Polymer	Unit	PA11 White	PA11 Black
Dv (10)	$\mu\text{m}$	20,3	23,8
Dv (50)	$\mu\text{m}$	44,1	46,7
Dv (90)	$\mu\text{m}$	78,5	79,9
Density (TDS)	$\text{kg/m}^3$	520	540

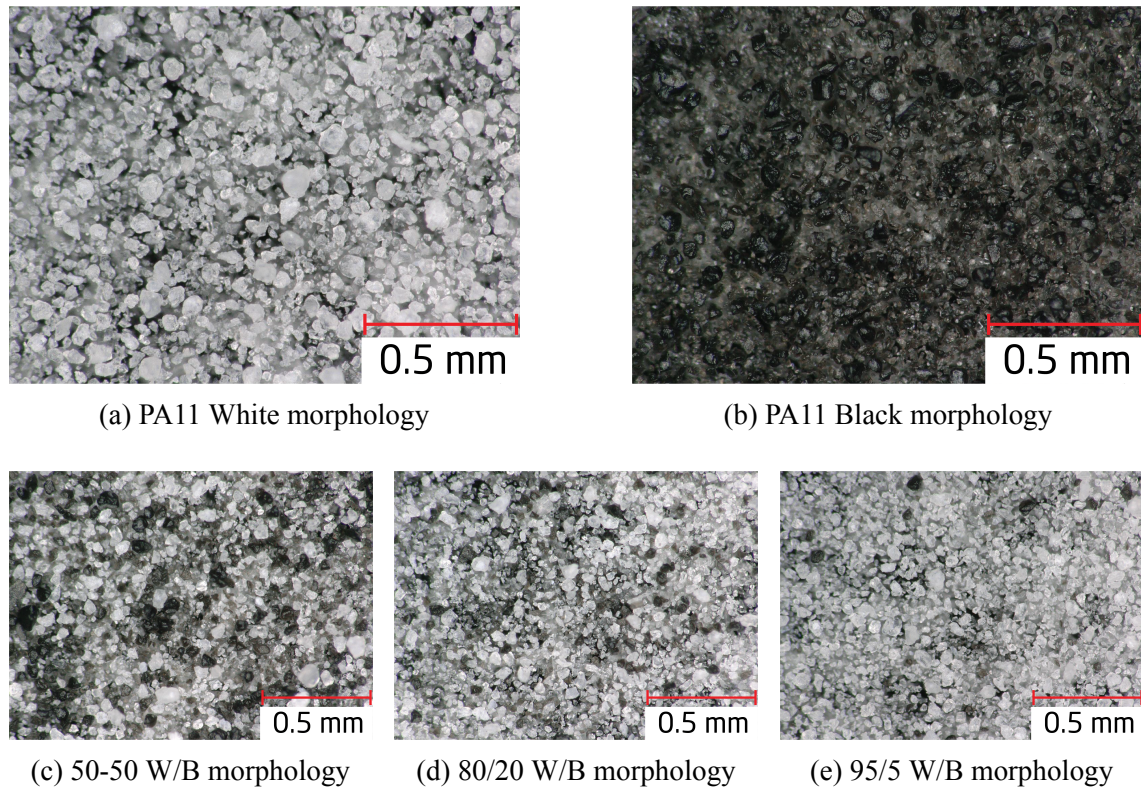


Figure 7.2: Morphology comparison between the different batches of powder (Keyence optical microscope 200x)

an uneven mix. From the analysis of the two separate powders and the mixed batches, no uneven mixes have been produced. From the mixing analysis, it is expected that the material will produce uniform parts resembling the mixing ratio of the powder blend.

Defining the process temperatures and ensuring a homogeneous mixture of the blends permit further investigation of the processing by fibre laser. Both materials are produced by the same company, as shown in section 4.1 and Table 4.2, and are also from the same material vendor (BASF), causing them to be nearly identical. The processing of the material, therefore, considers the mix as one material instead of an investigation concerning the individual constituents. By this, the results are presented for the mixed batches, showing the results of process optimisation, production, and mechanical properties.

### Process development of mixed powder

Process development of the different batches was rooted in the material study presented above. The volume energy density (Equation 4.4) was decided to be used for dissemination of the process settings (ensuring an understandable metric) commonly used for dissemination of laser power, scanning speed, and other relevant parameters for the process. Only two of the possible parameters to vary during the investigation were selected, minimising the process complexity. The hatch spacing and laser power were varied over

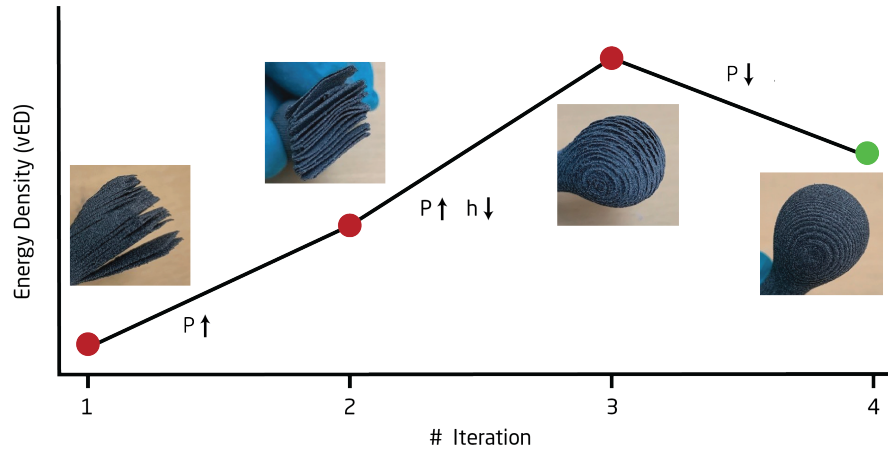


Figure 7.3: Exemplification of the iterative approach for the process optimisation, here shown with parts from the 50-50 batch

the course of the process optimisation, producing a number of trial-and-error attempts for powder consolidation before reaching a point of satisfactory process settings.

The study utilised a process optimisation routine inspired by the design of the experiment approach varying the two parameters, tracking the result obtained by the variation. An exemplification can be seen in Figure 7.3. Here the arrows indicate how the parameter was changed for each iteration. Between iterations two and three, a change of higher power and less hatch spacing was needed, achieving better parts compared to the previous iteration. An excessive power setting was selected, causing over-sintering of the parts. This led to the fourth iteration of marginally lower power. Resulting in the fabrication of parts closely resembling the desired test geometry.

The process development resulted in three different processing routines as seen in Table 7.4, one designed for each batch. Based on these process settings, a build job containing eight tensile specimens of the size ISO 527-2 5A [231] were produced for each powder mix batch. The powder cake and build plane temperature settings were main-

Table 7.4: Process parameters for the batches of the material tested

Parameter	Unit	50-50	80/20	95/5
Scan speed	mm/s	3000	3000	3000
Layer thickness	$\mu\text{m}$	60	60	60
Hatch spacing	$\mu\text{m}$	300	234	200
Laser power	W	35	35	60
Top temperature	$^{\circ}\text{C}$	180	185	185
Build temperature	$^{\circ}\text{C}$	175	175	175

tained at a similar level, with a minor adjustment to the top heaters, when introducing lower amounts of black powder. The effect of a whiter powder mix is twofold. One is the fact that the white powder absorbs less energy from the heaters than the black, due to the higher reflectance of the white powder. Secondly, the greater emissivity of the black powder causes a different temperature to be read from the pyrometer, causing an error for the PID regulator controlling the temperature. An increase of the build plane heaters of 5 °C, was observed for enabling the stable production of the batches containing larger amounts of white than 50-50.

Parts which could be tested for mechanical properties and surface characteristics were produced using the process parameters found in the study. The parts were built in the YZX orientation, which minimises the cross-sectional area in the build plane. This orientation further ensures that the recoating motion traverses the parts in the longest direction making these less prone to shift in the build plane caused by the dragging motion of the recoater [232]. Figure 7.4a shows an exemplification curve of a tensile test for an 80-20 (W-B) composition specimen. Figure 7.4b presents the build direction and the areas where the surface characterisation is conducted. The exemplification tensile test curve show engineering stress and strain, since no equipment for testing true stress-strain behaviour was available at the time of testing. The powder cake temperature was maintained at the same level for all experiments, just above the crystallisation temperature for the black powder. This ensures lower polymer degradation during processing by using the lowest possible setting, while maintaining the processed part in the uncrystallised state.

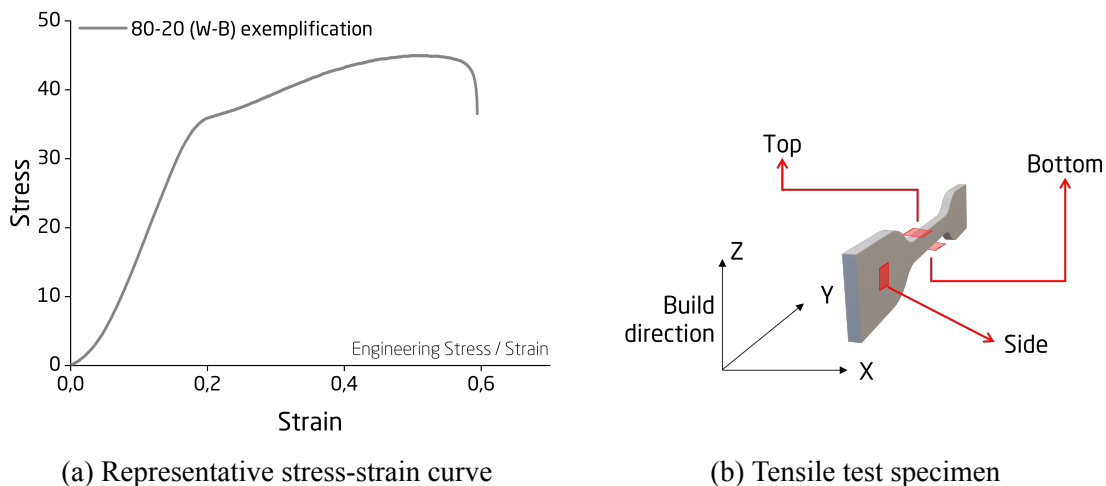


Figure 7.4: Tensile curve and the part build orientation, showing the surface roughness measurement locations

## Charaterisation of the produced parts

Analysing the results of the parts produced from the three batches described above follows two routes. One route characterises the mechanical properties of the parts, defining the

success of the part stability. The second route investigates the surface topography of the parts determining whether the parts are influenced by defects arising from the powder or the laser processing. From the white part production, large nodules were found on the surface caused by the laser processing. The investigation concludes on the root cause of the surface topography in parts containing black PA11.

Mechanical properties of materials are defined, among others, by the tensile properties. The tensile properties of manufactured parts varying in white-black composition are presented in Figure 7.5. A significant deviation is seen between the fabricated components and the datasheet values of the as-printed results from the supplier. The data shows how components processed by fibre laser in the system display mechanical properties resembling those of the conditioned samples in the datasheet values. Here a close correlation between the ultimate tensile stress of the manufactured samples and the datasheet is found. Considering the strain at break values, a similar relation between the manufactured parts and the datasheet values is determined. Here a larger strain at break is found for the manufactured samples. This discrepancy is expected to be caused by the uncontrolled atmosphere in the machine, resulting in material degradation, into shorter polymer chains. These shorter chains rearrange easier during the tensile test allowing the crystal regions to deform and stretch, allowing larger deformations prior to breaking.

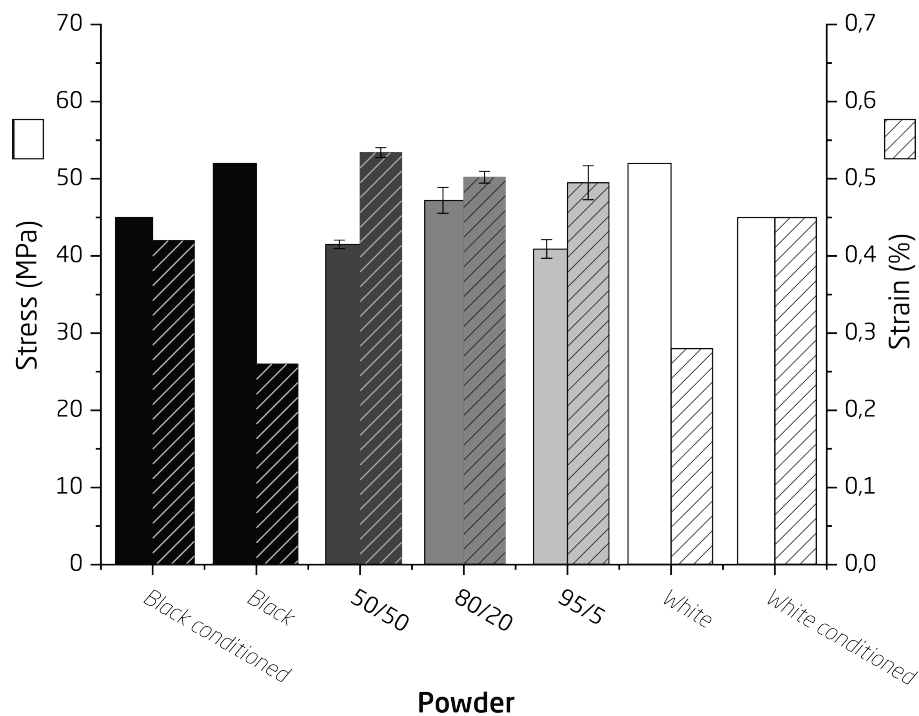


Figure 7.5: Engineering Stress and strain results for varying Black to White powder ratio. Far left and right columns concern supplier datasheet values (White & Black)



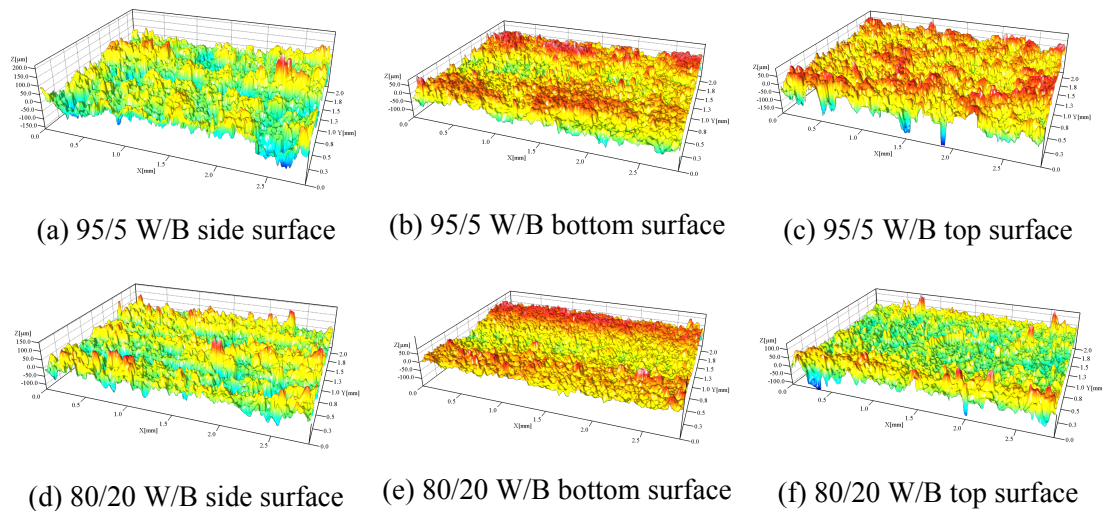


Figure 7.6: Surface topography comparison of parts with lower content optical absorber

Analysis of the mechanical properties supports the fibre laser's capability to process polymer powder into fully consolidated parts, resulting in robust components that closely resemble those produced by industrial machines. However, in the case of PA11, material degradation caused by hydrolysis or oxidation occurs during processing facilitated by the atmospheric conditions within the system. The study presented in subsection 7.5.2 reports on the influence of the atmosphere on material behaviour, with a focus on the rheological differences between virgin and degraded powder. Having confirmed that the mechanical properties align with the supplier's datasheet values, a test of laser processing stability based on surface morphology is conducted.

Three regions of interest were identified for studying the surface topography of the parts manufactured as seen in Figure 7.4b. The regions correspond to the sidewall, the top of the part where the powder is added during the final stages of the production, as well as a downward-facing surface, which are the initial layers produced onto powder in the build plane. The topographies are obtained by using a focus variation microscope and are shown in Figure 7.6. Results from the three sides are represented for the two visually lightest compositions (80-20 and 95-5, W-B). The surface topography stems from powder-sized defects, which are caused by the solid state sintering of powder to the surface. The numerical result of the surface topography mapping for the three different material blends can be seen in Figure 7.7. From the mixing ratios, it is observed that the surrounding powder and the effect of solid state sintering is the main cause of the rough surfaces detected on parts. From these findings, the appropriate level of black absorber required for stable processing is determined, resulting in an adequate surface topography determined by the surrounding powder.

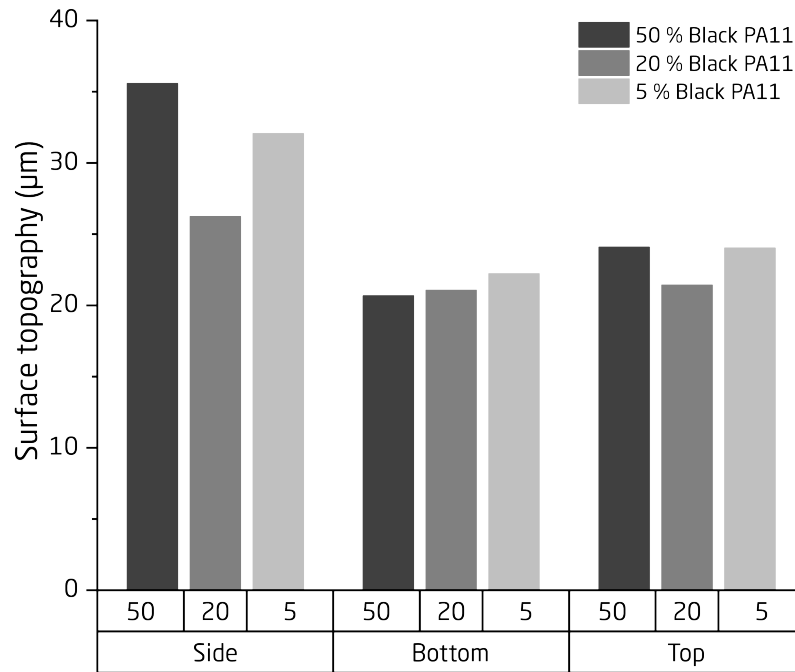


Figure 7.7: Surface topography, for varying mixing ratios

Only the top surface shows a random distribution of the surface profile, with the side and the bottom being affected by the laser scanning. For the side wall surfaces, an effect of laser scanning can be seen as a cyclic repetition of tall ridges among lower valleys. Analysing the cyclic profile found a period between two cycles of  $300\mu\text{m}$  resembling every 6<sup>th</sup> layer. During laser scanning, the hatch scan direction is rotated by  $67^\circ$ . Every time a scan line is set to start at the edge of the component, an error in the laser and scanner control causes local overheating. This is due to a delay setting mismatch in the controller programming, leading to over-sintering occurring in this repetitive cycle. Rotating the hatch direction by  $67^\circ$  is common practice in laser sintering (Figure 7.8). The rotation ensures a constant overlapping of the previous scan tracks, minimising the risk of 'dead' areas where the powder is left unsintered for multiple layers. If 'dead areas' are produced, then these will cause lower densities and weak points in the part produced. Over-sintering occurs due to an issue in the laser control managed by the unified system controller, caus-

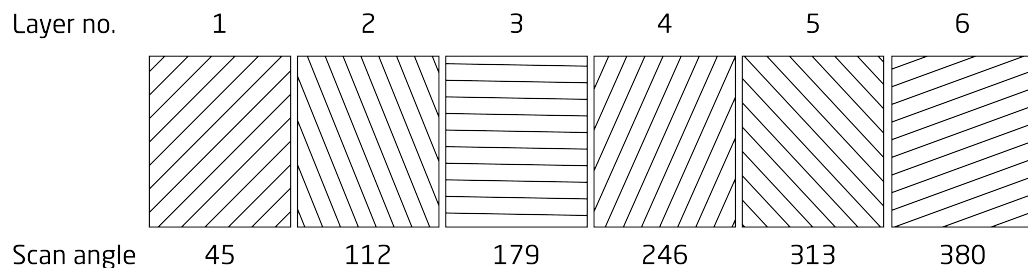


Figure 7.8: Exemplification of the hatch rotation

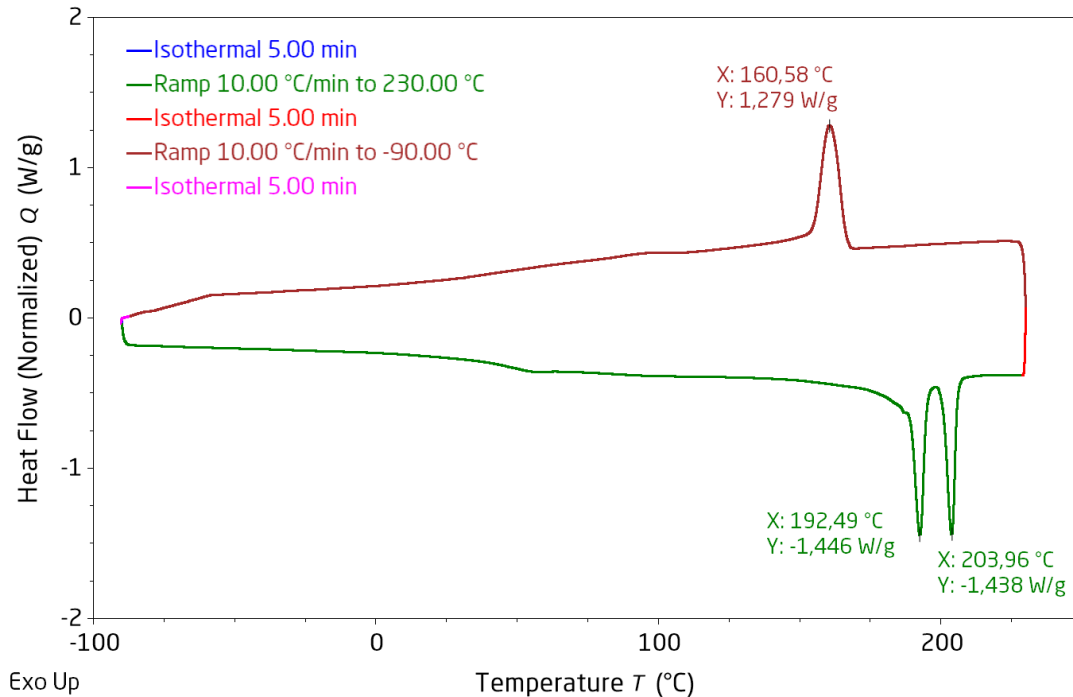


Figure 7.9: DSC analysis with two melting peaks in the first ramp, showing the sample from a side wall containing powder and melted polymer, which are fused by solid state sintering. Also in Figure 4.12

ing a peak in energy at the start of each scan line. This initial peak causes a larger area of the powder cake to rise above the melting point of the polymer causing part growth. Secondly, this heated region allows for solid state sintering of powder grains onto the part as described in subsection 4.1.2. The effect of over-sintering is also evident in the bottom surface, where the contours of the part are seen to rise taller than the central part.

Partial melting of particles, fixed in place on the side, is seen when analysing a manufactured part by DSC analysis, as seen in Figure 7.9. In the DSC analysis, two distinct peaks are present, resembling the original degree of crystallisation and melting point and the modified degree of crystallisation, where the melting point is shifted to a lower temperature.

Over-sintering causes large variations in the data of the surface topography profile between the locations measured. However, the batches are found to be in close agreement, except for the side profiles, which, as stated, are not determined by the powder but are an effect of an error in the laser control. The error is not unique to fibre laser processing and would occur for any laser controlled by the Unified Systems Controller. Since the time of this study, the error has been improved and updated in the Unified Systems Controller software, based on feedback from this and other experiments. The surface topography seen in Figure 7.7 is the average deviation from the median plane, as specified for the





Figure 7.10: Test geometry produced from the 95/5 batch and parameters found by the study

measurement of surface roughness. However, the measurement does not include a surface area large enough to qualify as a surface roughness measurement, due to the limited area at the up and downward-facing measurement points. Hence the surface characterisation is focussed on topography instead. Both the top and bottom surfaces show a surface profile resembling half the average powder grain size, with close agreement between all the different tested mixing ratios.

It can be concluded that fibre laser processing is possible for polymer powders from the analysis of part production utilising different mixing ratios of black and white PA11. The study found that the system is capable of producing parts resembling the datasheet mechanical properties and that the surfaces are dominated by powder grains stuck to the surface by solid state sintering. Utilising the fibre laser allows darker materials to function well in the system, permitting the laser energy to be absorbed by the polymer powder. Two test geometries are presented in Figure 7.10, showing the stable processing regime developed for the 95-5 material system. The parts show the ridges along the edge caused by the rotation of the hatch scanning.

From the study, it can be seen how the 80-20 (W-B) mix produces the highest mechanical properties and the lowest average surface topography. The 95-5 mix, however, also produces high-quality parts, showing that the breakdown level of optical absorption is not met, at 5% black material. An investigation of when the black content becomes too low is therefore investigated as described in the following.

## 7.2.2 Breakdown Level of Black Optical Absorber

The breakdown level of black powder in the white powder matrix has been investigated during a student project conducted under the supervision of the author, by "*Student - DTU-s212567, Inigo Trueba Merino*". The work followed the methodology described above for the initial study of utilising black and white powder mixed for fibre laser processing. The project elaborated on the processability of the materials, investigating the use of 5, 2, and 1 % black powder in the mix. The 5 % mixture resembles the data found previously but was incorporated due to upgrades of the laser system, as compared to the previous section. The results of the 5 % black content are comparable to the ones shown above and are therefore not included herein.

Investigation of the breakdown level of black material has focussed only on the mechanical properties of the parts produced, characterised by tensile testing. For this study, only the power level was changed, maintaining the remaining process parameters the same as seen in Table 7.5. The process parameters presented below show the effect of the laser delivery system upgrade, where a hatch spacing of 0.15 mm was utilised as described in the systems development chapter, subsection 5.4.2. A sweep of different laser power settings found the most suitable power setting for each composition, as shown in Table 7.5. By stepping 10 W between each level in software resulting in the steps shown below. The resulting power settings are converted as described above in subsection 6.2.1 and are converted by the power conversion calculation Equation 6.1. An increase in temperature was incorporated in the process parameters based on the finding of the required change in temperature as presented above. This increase in temperature ensures stable processing, minimising internal stresses and curling, which was required for processing the batches containing low amounts of black PA11 powder.

Processing polymer powders containing minute amounts of black optical absorber using fibre laser proved to be problematic. The laser energy absorption did not lead to stable parts, and a clear tendency of breakage or other defects were observed during the experi-

Table 7.5: Process parameters for the breakdown level of black powder for fibre laser processing

Parameter	Unit	98/2	99/1
Scan speed	mm/s	3000	3000
Layer thickness	$\mu\text{m}$	40	40
Hatch spacing	$\mu\text{m}$	150	150
Laser power (setting)	W	50 - 100	70 - 120
Build plane temperature	$^{\circ}\text{C}$	185	185
Build temperature	$^{\circ}\text{C}$	185	185

Table 7.6: True power settings tested

Parameter	setting	Unit	True laser power
Laser power	50	W	32.9
	60		43.7
	70		54.5
	80		65.3
	90		76.1
	100		86.9
	110		97.8
	120		108.6

mental phase. Only a few samples produced in the 99-1 batch proved successful, resulting in large deviations as seen from the resultant data of Figure 7.11. The figure illustrates significantly deteriorated process capabilities in both batches. A trend of improving part performance is identified when moving towards higher powers. However, excessively high-power causes material degradation and uncontrolled part growth into the powder

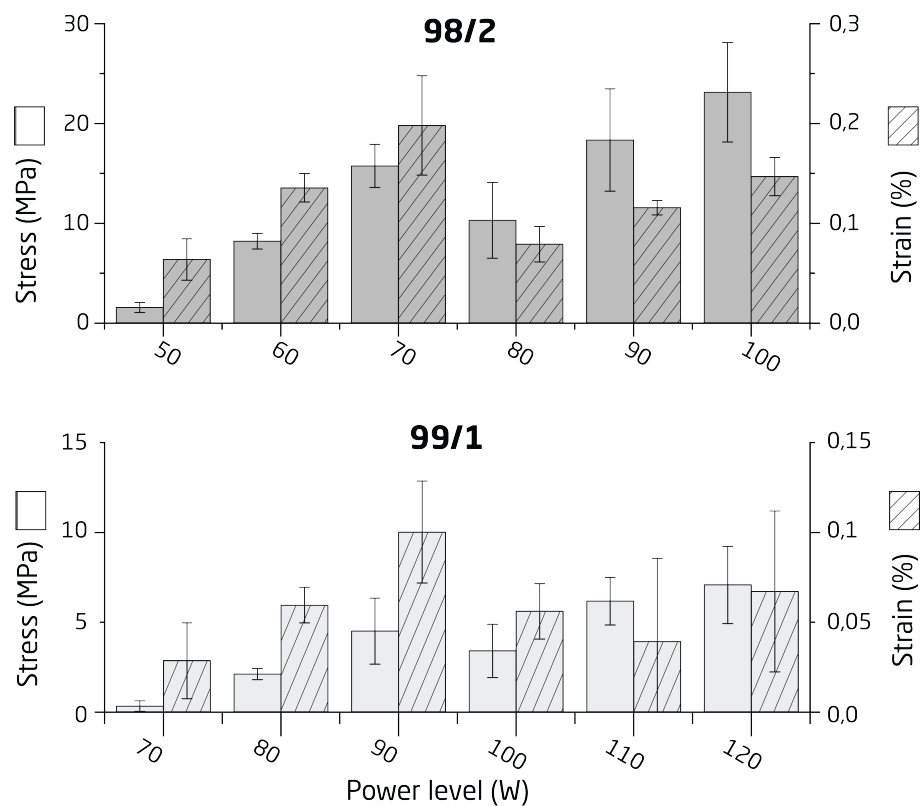


Figure 7.11: Mechanical properties of the tested power levels for 98/2 and 99/1 parts

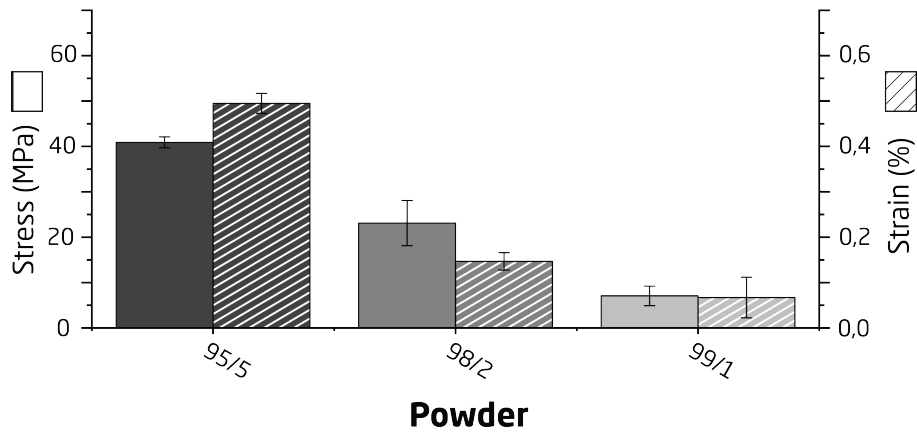


Figure 7.12: Mechanical properties of the batches containing varying levels of black powder

cake, as observed during the processing of pure white.

The study demonstrated that reducing the black content to lower than 5 % is not feasible. The material degradation resulting from elevated laser power during processing, along with issues like warpage and uncontrolled part growth, makes these batches undesirable for fabrication purposes. Figure 7.12 presents the significant deterioration of the mechanical properties when utilising lower black contents. A steep decrease is seen between the 5 and the 2 % batch. The difference is close to a 40% decrease in the ultimate tensile strength.

Based on the study, a black content of 5 % is employed throughout the project. Utilising this percentage enables the production of mechanically sound components within a stable process regime. Using this percentage produces fully black components with a slightly



Figure 7.13: Cross-section view of a part produced from the 95-5 batch

grey hue, as seen from Figure 7.12. The white hue is expected to be caused by particles fused to the part by solid state sintering and does not inflict mechanical stability. When investigating the cross-sectional area of parts produced by the 95-5 composition, a full black component is visible, as seen in Figure 7.13. The black powder in the mix is expected to show very low viscosity when heated, further aided by the main energy absorption of this powder constituent. To understand the process of using black powder mixed with white, a study of the low shear viscosity has been undertaken, as described in the following.

### 7.2.3 Polymer Rheology of White and Black PA11

Dominantly black components were produced even when low amounts of black absorber was used. From initial visual inspection, it seemed that the black would seep into the white powder and distribute, causing the colouration. An investigation into this behaviour of the black has therefore been conducted with a focus on testing the viscosity of the two materials, defining the difference in flow behaviour at low shear rates, which mimics the process conditions.

The rheological test was conducted on an Anton Paar MCR502 utilising the CTD600 thermal cell for heating the polymer above the melting temperature, as described by the DSC analysis presented above. All the settings of the three experiments conducted concerning the polymer rheology are described in Table 7.7. To conduct the test, disks were moulded by hot pressing in an oven heated to 240 °C. All visually identifiable degraded polymer was removed prior to rheology testing. The disk moulded was necessary to remove any air present in the powder sample. The same method and process was utilised for all samples, minimising any difference in polymer degradation caused by the moulding step.

An initial test of defining the Linear Viscoelastic Region (LVER) of the two powders observed that a one per cent oscillation strain to be adequate. Based on this, a frequency sweep defining the viscoelastic behaviour at different shear rates was conducted, as shown in Figure 7.14. The frequency sweep was performed at 230 °C, ensuring a molten state

Table 7.7: Process parameters for the breakdown level of black powder for fibre laser processing

Parameter	Unit	Amplitude sweep	Frequency sweep	Temperature sweep
Angular amplitude ( $\gamma$ )	%	0.1 to 100	1	1
Frequency	Hz	1	-	-
Angular frequency ( $\omega$ )	rad/s	-	0.01 - 628	0.1
Temperature	°C	230	230	240 to 180

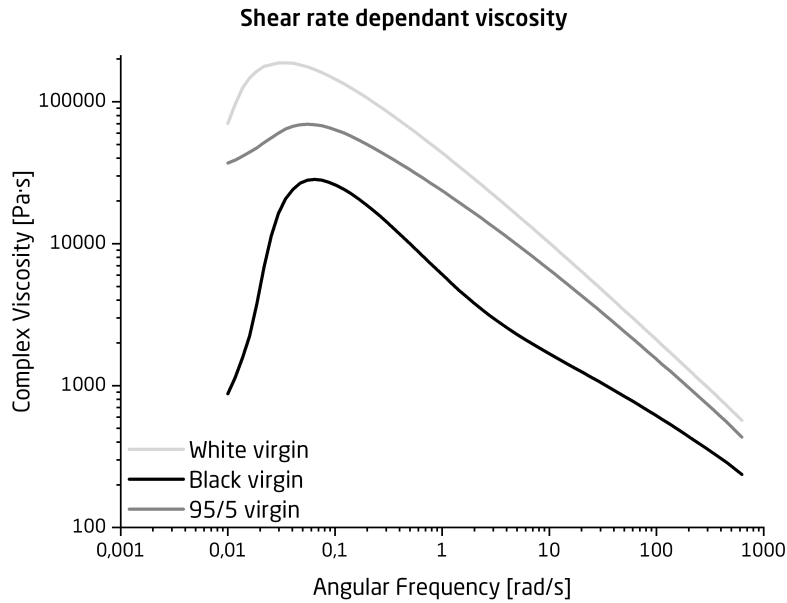


Figure 7.14: Viscoelastic behaviour of the two PA11 powders of different colours and the mixed batch

relevant to the laser processing. From the trials of minimising black content, a laser processing temperature was identified close to the region irradiated by the laser. The temperature was measured by the thermal imaging system resulting in a rise in temperature between 220 and 240 °C. Peak temperatures in the laser spot can reach higher temperatures, reaching towards 250 °C. However, to maintain a stable polymer, this temperature was selected for the study. The temperature spike captured by the thermal imaging camera also shows how the energy is retained in the area after laser processing. The experiment is designed to mimic this heat retained after laser exposure, where the polymer powder coalesces into the final part.

To study the rheological behaviour of the viscoelastic polymer, a frequency sweep was employed. From the analysis of the frequency sweep, a lower complex viscosity can be expected from the black sample compared to the white. This is especially evident at low shear rates, which is the region of interest considering the laser processing induces minimal shear of the molten polymer. It is clear from the analysis that the mixed batch powder reacts as expected by showing a viscosity response located between the two pure samples. Seeing that the complex viscosity appears different in the two powders, an investigation of the temperature dependant viscosity was introduced. A sweep across the relevant build temperatures was conducted, heating the polymer sample to above the expected process temperature previously defined as 230 °C. To investigate the viscosity response 230 °C, the start temperature was set to 240 °C, and the sweep was carried out down to 180 °C. Ensuring a steady state of the measurement when collecting the data in the range of interest between 230 and 180 °C.



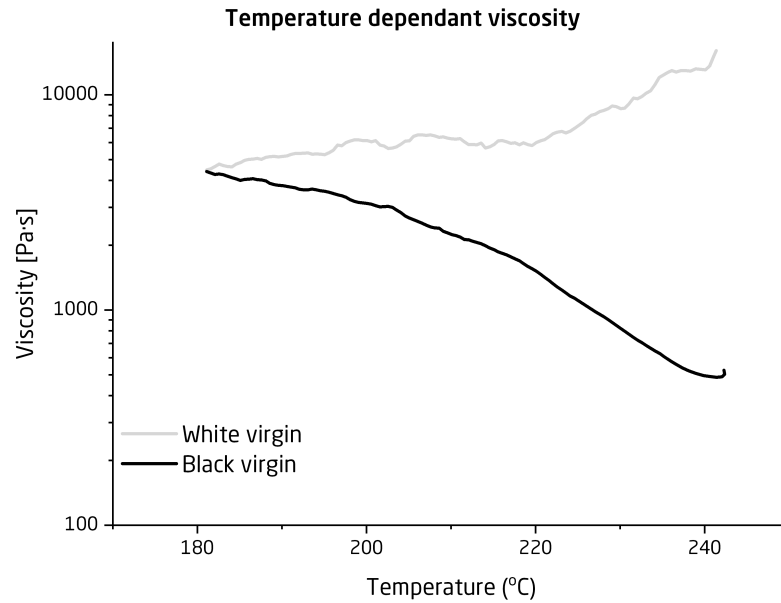


Figure 7.15: Viscoelastic response of the two PA11 powders, at low shear rates over a range of temperatures

Figure 7.15 shows how the two similar polymer systems behave differently based on colour. The black material is seen to produce very low viscosity compared to the white when considering the temperatures relevant for laser processing. This behaviour is believed to cause the polymer to flow easier, filling the area around the white powder and thereby distributing the heat uniformly in the laser-processed area. The black, when seeped into the powder cake, produces a boundary layer which will absorb the energy faster during the next layer scanning. The effect of enhanced flow in the black polymer when molten is expected to cause the parts to become fully black, as shown in Figure 7.13. By surrounding the white particle in the black matrix, these can be melted in the next layer cycle, considering the thin layer height utilised in the system. As seen in the recoating routine presented in Figure 6.23, the thin layer is translucent to the black-coloured layer beneath the build plane. This means the processing stabilises further with the new layer deposition, where a large black surface is present for laser absorption. This is not an ideal case considering part production in the powder cake directly, which can lead to a diminished surface quality of downward-facing surfaces. This has not yet been encountered as an issue but should be investigated further.

An investigation into the black powder and a determination of why this behaviour arises has not been conducted within this study. The behaviour merits an investigation. However, for defining the fibre laser processing capabilities within PBF-LB/P processing, it has been deemed unnecessary at this point. Utilising an evenly dispersed black powder of the same powder size and morphology causes the powder mix to be homogeneous. However, other solutions are possible candidates for incorporating the optical absorber with the powder,

such as a film coating on the particles, as a filler in the individual powder grain, or as a two-component system as explained in subsection 2.2.4 and subsection 4.1.

As mentioned above, both of the optical absorber systems require further investigation in the PBF-LB/P process and are not included in this work. Instead, further focus on the processability of the 95-5 powder mix has been investigated. Developing a stable processing routine and defining the laser scanning requirements for producing components resembling the geometrical data and size defined in the CAD model. The processing routine and geometrical accuracy of produced parts are described in the following.

### 7.3 Benchmark Testing at the Optimal Level of Black

From the study above, a stable processing regime was observed for the 95-5 white-black powder composition. This composition was found to produce mechanically sound components, which show adequate geometrical fidelity, considering no true size investigation has been conducted. The following study, therefore, characterises the geometrical accuracy of a benchmark component produced by the 95-5 mixed material processed by fibre laser in the developed system. The study is based on the contribution for the conference *"euspen - Special Interest Group: Advancing Precision in Additive Manufacturing 2023"* - KU Leuven, Belgium. The paper is presented in Appendix F from [233], where refer-

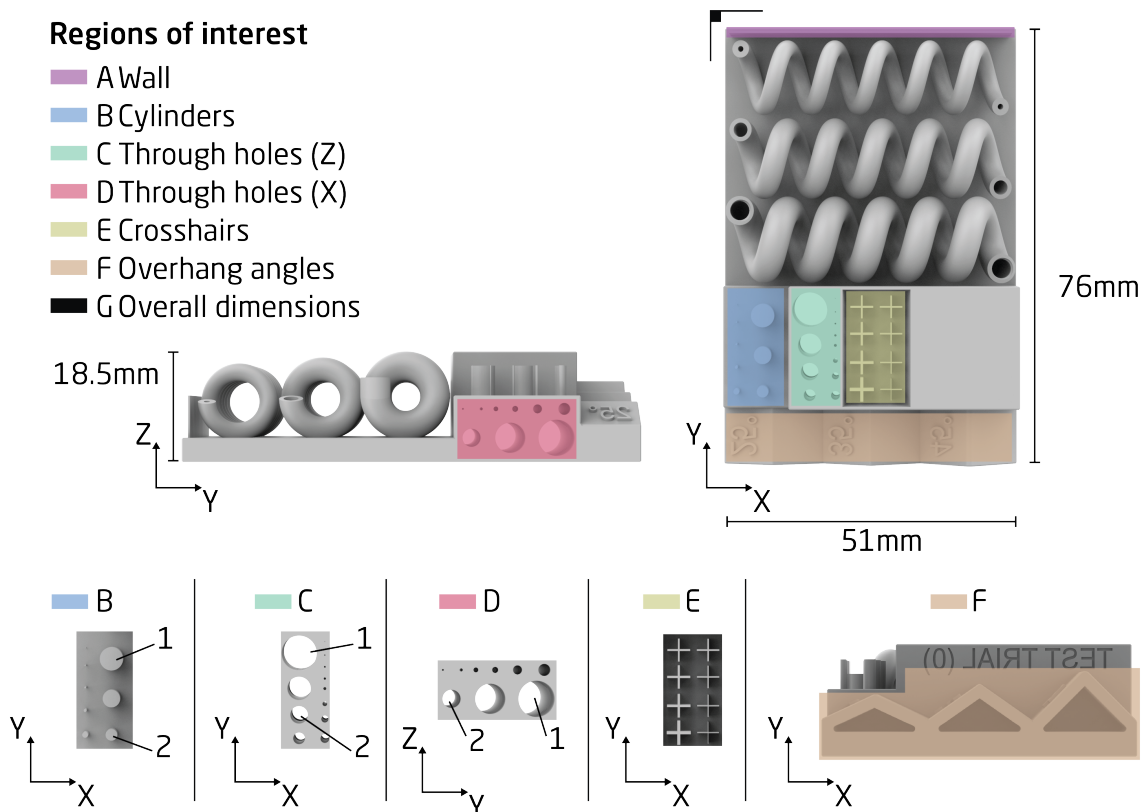


Figure 7.16: The benchmark geometry including the areas of interest



Table 7.8: Shrinkage measurement of the initially produced benchmark geometry

Dimension	Unit	Nominal	Average	Std dev.	Delta	Deviation (%)
Length	mm	76	73.94	0.04	-2.06	2.8
Width	mm	51	49.96	0.09	-1.04	2.0

ences for the production of the benchmark part, measurement equipment and procedure are found. The study focussed on defining the required job generation and process settings for producing parts resembling the CAD file data. The part produced is a benchmark component originally intended for use with PBF-LB/M processing [234–236]. Utilising the benchmark geometry for polymer powder laser processing, inferred changes to the layout of the geometry. By hollowing the part to a shell thickness of 1 mm, a part capable of laser processing in polymer powder is achieved.

An initial study produced the part with no changes in dimensions, not accounting for any shrinkage or other defects originating from fibre laser processing of polymer powder. By measuring this geometry, a size difference between the nominal and produced part can be achieved, as shown in Table 7.8, defining the shrinkage of the part manufactured, caused by the reorganisation of the polymer chains during crystallisation as shown in Figure 2.4. Due to a failure during manufacturing, the part was not produced in full, and the Z-shrinkage factor could not be determined. A decision was made to use the same shrinkage for the vertical axis as for the minor build plane dimension in the job file generation.

Using the shrinkage corrections factors found in Table 7.8, the job file was generated for

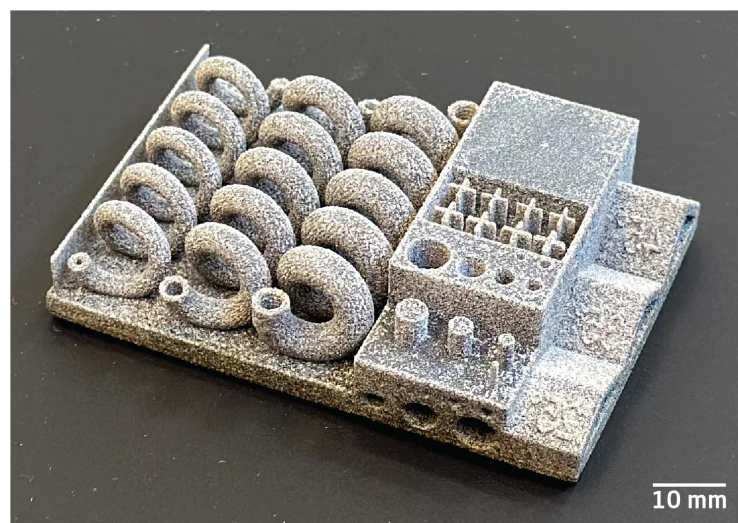


Figure 7.17: Manufactured benchmark geometry produced by the developed system in 95-5 material composition

	A	A1	A2	B	C	C1	C2	D	D1	D2	E	F	G1	G2	Z
Insp.															
Feat.				1,0	1,5			2,0							
$\mu$ [mm]	0,66	6,32				5,61	2,68	5,50	2,47				76,44	50,55	18,44
$\sigma$ [mm]	0,0093	0,0085				0,0009	0,0028	0,0022	0,0063				0,0003	0,0003	0,1458
Nom. [mm]	0,3	7,0				6,0	3,0	6,0	3,0				76,0	51,0	18,3
$\Delta$ [mm]	0,36	-0,68				-0,39	-0,32	-0,50	-0,53				0,44	-0,45	0,14
$\Delta$ [%]	121,19	-9,76				-6,57	-10,52	-8,39	-17,51				0,58	-0,89	0,77
R [mm]	-	-				0,23	0,20	0,41	0,33				-	-	-
$\sigma$ R [mm]	-	-				0,0015	0,0011	0,0015	0,0266				-	-	-

Figure 7.18: The validation table of the measurements for the benchmark geometry measured by CMM and callipers (Z)

the final production run of the benchmark geometry. An improved method of utilising the Autodesk software Netfabb Premium for job generation ensured a more robust processing profile in the job file. The job file generation was realised by *Magnus Bolt Kjer*, who also utilises the software and Unified Systems Controller for the metal LPBF system. The benchmark geometry was produced by parameters determined by the process and powder composition study, achieving a satisfactory result for the number of features reproduced as seen in Figure 7.17.

Qualification of the produced benchmark geometry was conducted by an optical coordinate measuring machine. The critical parts and areas of interest are possible to measure by either using the top or the bottom light approach. The Z dimension was measured by callipers, which have a higher intrinsic uncertainty than the Coordinate-Measuring Machine (CMM). The CMM was not suitable for measuring the Z dimension, which is why the callipers were selected. The results of the part inspection considering the dimension measured and the visually inspected geometries are presented in Figure 7.18. Here each category refers to an area of interest as shown above in Figure 7.16. A green mark means a full representation of the features as described by the CAD file, with red marks showing missing features. Beneath a red mark, a number represents the minimum feature size completely produced and verified by visual inspection. For a feature to pass, the entire component must be present. For through holes, this means a hole through the entire geometry. For pins, a verification of the presence and full height is considered. Aiming for consistent reporting of the results has led to the presentation of two decimal resolution (.01). The majority of results are presented by this, with the exemption of the standard deviation, which was observed to be so low that a four decimal resolution (.0001) was required. This resolution is not indicative of the actual measurement since this equipment does not allow this resolution and is, therefore, only presented for the standard deviation.

The results from the manufactured benchmark geometry show how large-scale features

Table 7.9: Stable geometrical feature sizes and tolerances when processing polymer powder by fibre laser radiation

Geometrical feature	Denominator	System stable size
Major dimension	%	< 1
Through holes build plane direction (XY) ( $\emptyset$ )	%	< 20
Through holes build plane direction (XY) ( $\emptyset$ )	mm	< 2
Through holes vertical direction (XZ) ( $\emptyset$ )	%	< 12
Through holes vertical direction (XZ) ( $\emptyset$ )	mm	1.5
Pin vertical direction (XZ)	$\emptyset$ mm	1.0
Unsupported wall	mm	> 0.7

and geometries are in close agreement with the inscribed size of the CAD file. However, when investigating smaller geometries and features, these are significantly different from the intended geometrical size. The largest deviation is seen for the wall section (A), which has grown to more than twice the intended size in width (A1 measurement). This growth is related to the scanning of the laser, where during the hatch scanning of the area, the laser will traverse the wall at an angle close to the normal, with reference to the length, resulting in minute scan lines resembling laser dots rather than actual line scanning. This, coupled with the contour scan surrounding the wall, causes excessive part growth into the surrounding powder. To optimise this, a study of thin walls is required to define the optimal laser strategy concerning scanning and power. An investigation utilising no contour scanning during the production produced a wall (A) which measured 0.51 mm in width. This is still much larger than the nominal geometrical size, proving that a thin wall of less than 0.5 mm is not feasible in the system when utilising a fibre laser consolidation source. By improving the scanning parameters, it is possible that thinner geometries can be realised in the system. These are, however, not investigated further in this study.

HUBS, a global print service provider in the AM industry, has produced a guide for minimal features and general tolerancing expected by the majority of AM processes. Figure 7.19 highlights the feature sizes of conventional PBF-LB/P processed features based on the knowledge base of HUBS presented in the book "The 3D Printing Handbook" [18]. Through the analysis of the benchmark, the stable feature size has been found for several different geometries. Table 7.9 describe each type of feature and the minimal geometrical size considering the results of Figure 7.18. The table presents the measured and visually inspected results from the benchmark part. Presenting the average tolerance achieved as well as the minimum feature realised in the system.

Comparing the minimum feature sizes achieved in the system with the recommendations

### Design and Manufacturing Rules for Polymer Laser Powder Bed Fusion

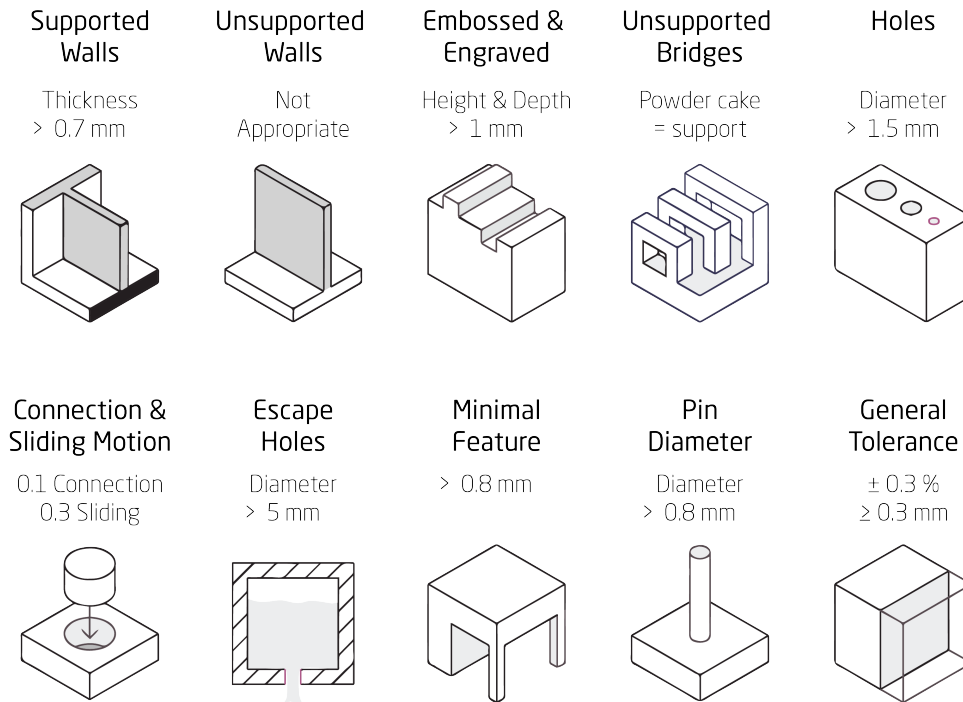


Figure 7.19: The design rules and production guide fro PBF-LB/P from HUBS. Adapted from [18]

and general rules from HUBS, some features are found to be close to the expected dimensions. The overall dimensional stability is also close to what is expected from industrial systems, with a possibility of further improvement through iteration-based optimisation of the benchmark study. This involves defining even tighter shrinkage factors for all axes and optimising the scanning of small features.

During the investigation, an error in the scanning routine was discovered, causing a skipping pattern in the laser power when producing curved sections in the contour. This finding indicates that the laser is only stable for straight lines. This error needs further investigation to ensure even more stable processing. However, it is evident that adequate dimensional fidelity can be achieved by processing polymer powder using fibre laser radiation. Nonetheless, conducting additional, comprehensive studies may have the potential to further enhance the process.

A desire to compare the results of the developed system with an industrial system led to a comparison using the benchmark geometry. To investigate the state-of-the-art production capabilities within PBF-LB/P, an inspection was conducted on the part produced by the industry-leading EOS Formiga P110 FDR system. The EOS system utilises a 55W CO laser source, along with the EOS software and hardware solution. The material used is

<i>Industrial</i>	A	B	C	C1	C2	D	E	F	G1	G2	Z
<b>Insp.</b>											
<b>Feat.</b>	3,0			3,0							
<b><math>\mu</math> [mm]</b>				5,83	1,74				76,06	51,03	18,37
<b><math>\sigma</math> [mm]</b>				0,0006	0,0015				0,0000	0,0002	0,0167
<b>Nom. [mm]</b>				6,0	3,0				76,0	51,0	18,3
<b><math>\Delta</math> [mm]</b>				-0,17	-1,26				0,06	0,08	0,07
<b><math>\Delta</math> [%]</b>				-2,79	-41,87				0,03	0,05	0,36
<b>R [mm]</b>				1,16	1,12				-	-	-
<b><math>\sigma</math>R [mm]</b>				0,0109	0,0109				-	-	-

Figure 7.20: The validation table of the measurements for the benchmark geometry produced by an industrial machine measured by CMM and callipers (Z)

a PA11 grade from EOS (PA 1101) in white. The part was produced at nominal settings provided by EOS for the selected material, incorporating the years of research and development of the company, aimed at the highest part quality in the polymer powder AM industry. The same geometry with the enhancements for PBF-LB/P was utilised for the industrial system capability study.

The benchmark part production was executed by an industrial partner, who subsequently delivered the parts encased in powder from the build. Receiving the parts encased in powder enabled us to perform post-processing in a manner consistent with the initial benchmark study, thus eliminating potential sources of uncertainty from this process. Figure 7.20 shows the geometrical fidelity achieved by the state-of-the-art system from EOS. The major dimensions are kept well below what is expected, according to HUBS. Only the Z-axis is seen to be slightly larger than what is expected. However, this tolerance still falls below what can be expected in terms of production capabilities concerning the absolute tolerance of 0.3 mm.

Note that the small through holes in the XZ direction of the industrial benchmark exhibit limited production capabilities. During the cleaning process, it was observed that the powder in these small holes was compacted to a hard solid, making these areas difficult to remove and clean, resulting in measurements that resembled the powder rather than the intended manufactured size. This issue arises due to the consistent cleaning method and rigidity employed, which avoids removing powder stuck to the part with excessive force. The same challenge applies to achieving the minimum feature size in any through hole, as the powder can become too densely packed within these holes to be effectively removed. It is worth considering that the original geometry was intended for powder metal processing, and the tight packing of polymer in these holes differs from the flowability of metal.



The benchmark part produced by the industrial system was seen to incorporate finer details than what was achieved by the system processing using a fibre laser. Figure 7.21 shows the two benchmark parts produced for the study. The right image shows how the two samples are very alike, with only minor differences. The industrially produced part contained all the small features, whereas the fibre laser processed component was missing several of the fine pins visible on the surface facing the camera.

In Figure 7.21, the left image reveals that both systems caused warpage of the component, primarily attributed to the challenging production of the large flat surface area. To mitigate this warpage, a method can be implemented: producing the parts on a slight incline of  $5^\circ$ , resulting in a smaller cross-section of the part during production. This approach leads to lower levels of internal stress as the laser scans smaller areas per layer. This effort was not carried through during this investigation. In the part manufactured by the developed system, the through holes are observed to have collapsed during the fabrication, resulting in oval-shaped holes that do not meet the required specifications. This collapse is noticeable in the layers towards the top of the part, occurring in the middle of the build job. The oval shape is anticipated to be a consequence of the vertical-stage error, as detailed in subsection 6.3.1. The lack of appropriate layer height motion is expected to be a contributing factor, resulting in the oval shape due to insufficient Z-motion per layer. An additional contributing factor could be insufficient powder packing during recoating, leading to the part's collapse. It is less likely that the laser processing significantly influenced the oval shape of the holes; rather, inadequate motion control is considered the primary cause.

A higher level of geometrical fidelity can be achieved by incorporating a shrinkage compensation factor during the job file generation, as demonstrated in the above study. The findings of the study also indicate that the major dimensions closely align with the accuracy presented by a prominent actor in the AM industry.

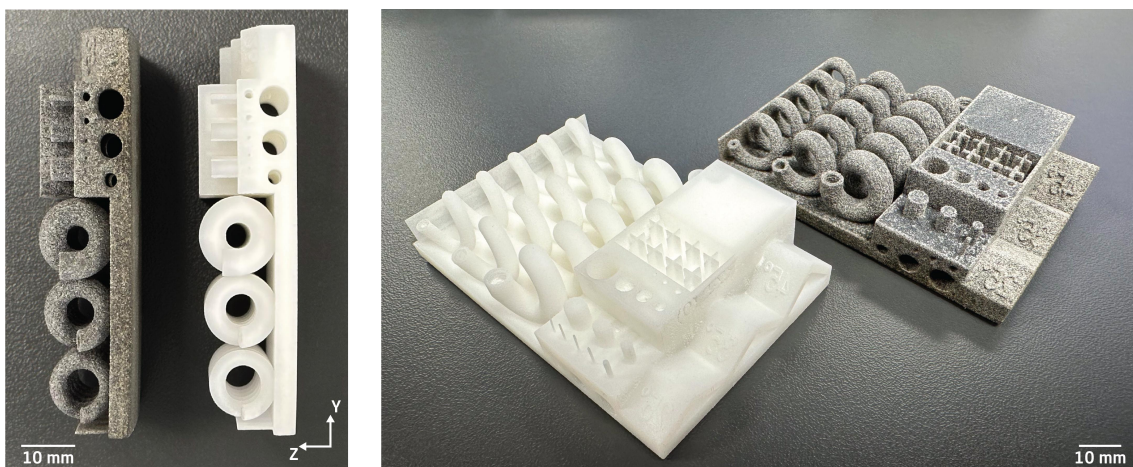


Figure 7.21: A comparison between the benchmark parts produced by the industrial (CO laser) and the developed system (fibre laser)

Although even higher geometrical accuracy could potentially be attained through process re-iteration and a comprehensive shrinkage factor study, such endeavours were not feasible within the constraints of this study. An alternative approach could have involved producing various objects of different sizes and defining the span and shrinkage factor on a more generic level rather than being specific to a particular geometry. However, this approach might not have included the small features that received significant focus during this study, leaving other geometrical aspects unaddressed.

Given these considerations, the study adopted the presented approach while considering the potential for further investigation in the future.

The studies presented above focus on PA11 as the material characterised, both in the optical absorber and the geometrical fidelity investigation. To broaden the prospect of utilising fibre lasers for polymer powder processing, the characterisation and understanding of more materials are required. To broaden the horizon of fibre laser processing, a material with the potential for realising electrically sensor components produced by a conductive polymer blend is presented in the following.

## 7.4 Conductive Polymer Part Production by Fibre Laser

A study of conductive polymer blends has been undertaken to study the efficacy of utilising other polymers than the previously investigated PA11. The work presented is based on the contribution to *"euspen - 23rd International Conference & Exhibition, DTU, Copenhagen, Denmark"*. The contribution is shown in Appendix G from [237]. The relevant information on the methods of powder production as well as powder and part quantification, is available here, including descriptions of the equipment utilised throughout the study.

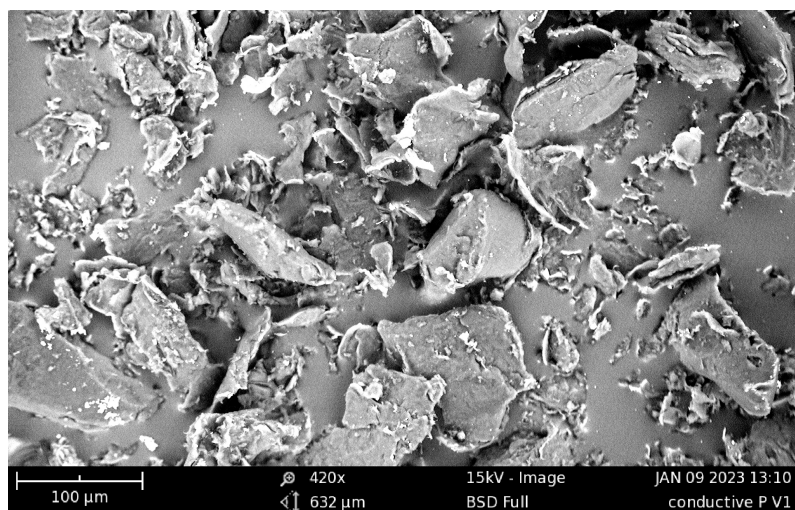


Figure 7.22: Coarse powder grain (also in Figure 6.22b)



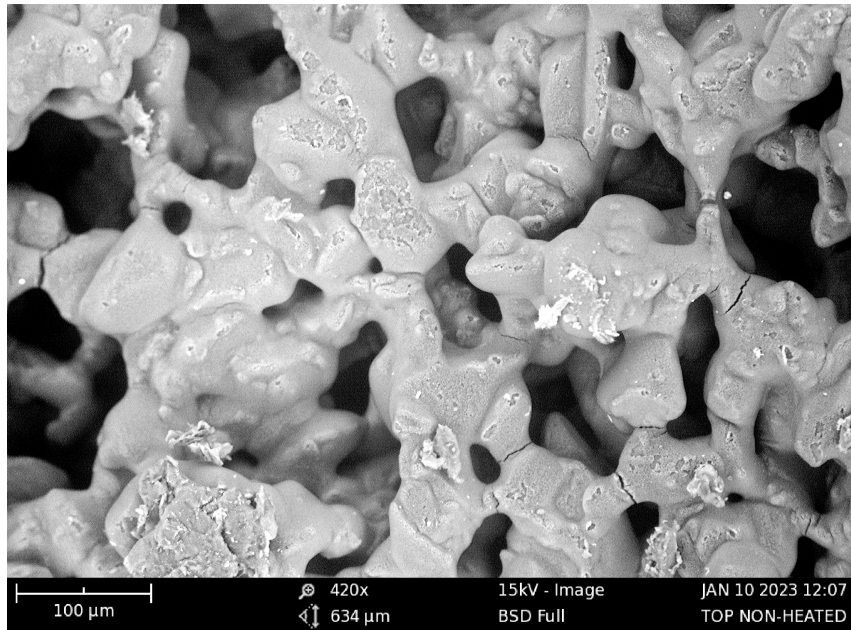


Figure 7.23: The conductive network manufactured by fibre laser processing of coarse powder

Manufacturing conductive polymer parts can prove to be useful in sensor components, where a perfect fit significantly influences the measurement and sensor output. By utilising the PBF-LB/P process, complex geometries with no additional support structures can be realised. The aim of this study has been to identify whether the fibre laser processing of a conductive polymer powder can be a useful tool. To verify this, an approach of material compounding and micronising was utilised for producing the powder used in the process. The powder was cryogenically milled, causing issues with the coalescence behaviour, as explained below. The verification utilised the developed system for consolidating the powder into a Two-and-a-Half Dimensional (2.5D) component, which could be tested for conductivity. By analysing the part produced, a conductive polymer was realised, showing the capabilities of the system and fibre laser processing. The study focussed on a two-pronged approach, one processing the powder in an unheated environment to verify the consolidation behaviour when no additional heat is supplied. The second considered a heated environment, heating the polymer blend to a stable region inside the process window, found by DSC analysis.

The polymer blend designed for the experiment consisted of conductive carbon black filled polypropylene (PP) and a propylene elastomer, producing a flexible conductive polymer, as described by Grønborg F. et al. [238]. The two components were mixed in a ratio of 60/40, respectively, ensuring the high content of carbon black filler providing the conductivity of the blend. The cryogenically milled powder had a coarse yield powder, which was separated into a size distribution similar to the PA11 utilised above. The coarse powder shown in Figure 6.22b proved to cause large issues with the final parts produced.

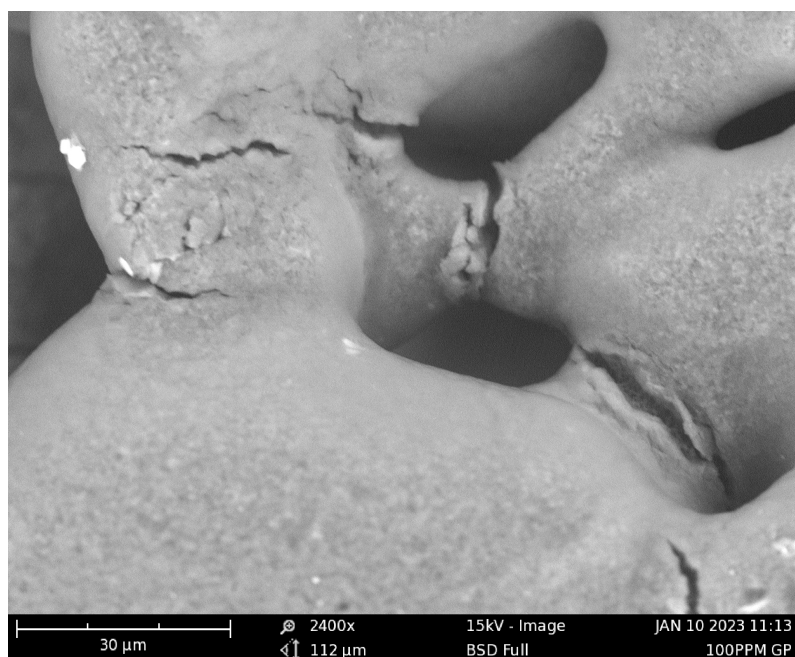


Figure 7.24: Cracks and areas of less conductivity in the conductive network manufactured by fibre laser processing of coarse powder

The production of the parts utilised a similar method for process development, as explained above, shifting the energy density and verifying the consolidation of the powder. The parts produced showed an inherent conductivity and were able to be measured as shown in the publication Appendix G, but were found to break up when handled. By stretching the parts, areas of nonuniformity were found. This behaviour was investigated by SEM to characterise the structure of the produced components. The SEM analysis was possible since the conductivity minimised the charging effect, often seen when imaging polymers. The result of the analysis is the high-resolution images seen in Figure 7.23. The network structure was unexpected, as the processing resembled normal laser processing of a black powder but with two major differences compared to the previous experiments

One significant difference was the colour of the powder, which was entirely black due to the amount of conductive carbon black filler. This allowed for excessive laser absorption, requiring low power settings and rapid scan speeds. Secondly, the powder did not fill the entire bed due to the difficulties of producing large amounts during the cryogenic milling process. The two differences, combined with the coarse powder, resulted in a lack of packing density in the powder cake and build plane and a high energy absorption. This led to the network-like structure in the sample, resulting from the laser processing.

The conductivity of the samples produced was found to be highly inconsistent, showing a large standard deviation during the measurements. It was concluded that the network-like structure deteriorated the conductivity in the samples, further aided by the fact that the network showed cracks in the structure, as highlighted in Figure 7.24. Secondly, it was

found that the two materials in the blend behaved differently, unveiled by the two different processing regimes of the unheated and heated build environment. Part analysis by SEM imaging showed how the network formed in both experiments. It was, however, clear that the unheated part was not maintained in the molten state for long enough to allow the polymer to flow evenly, causing only one of the polymers to produce the network bridges between two powder particles. The network was, therefore, mainly consisting of the black conductive constituent, which had separated from the blend and produced a shell-like structure around the other polymer component. This behaviour resulted in higher conductivity, with a larger chance of the network structure fracturing due to the less elastic behaviour of the black polymer, compared to the elastic component mixed in.

Fibre laser processing of a conductive polymer blend yielded positive results, resulting in a conductive part. However, the network structure is less than ideal for achieving the desired final part quality and can be attributed to material properties and packing density. By ensuring a spherical particle shape, it is expected that the issues encountered during part production could be alleviated by achieving an increased powder cake density.

Challenges arise when processing the black material due to its high energy absorption, necessitating the use of low power. To improve stability and enhance part properties, higher scan speeds or lower power settings could be employed. Additionally, utilising a larger spot size may also help lower the energy density to a more suitable level. Overall the fibre laser processing was successful, with several steps presented for improving the outcome of the parts, not relating to issues in fibre laser processing. The black content holds the responsibility of laser absorption, as presented for the optical absorber study. The blend contains two kinds of propylene, which, as reported by Nguyen N. et al. [239], does show a slight absorption of close to 5 % at wavelengths of the Yb fibre laser. Nevertheless is, the black constituent of the material the main reason for the successful manufacturing of components, showing conductivity.

## 7.5 System Material Processing Capabilities

The system exhibits promise in producing high-fidelity components and facilitating materials investigation, especially considering the open platform's ability to accommodate any material. Nevertheless, a significant limitation is the lack of control over the atmosphere within the system, leading to uncontrolled polymer degradation. Hence, the following investigation focusses on the laser processing and system capabilities comprehensively, determining the overall efficacy of the PBF-LB/P processing system.

### 7.5.1 Fibre Laser Processing of Polymer Powders

Based on the studies conducted above, it is evident that fibre lasers can be effectively utilised for polymer powder processing. By incorporating an optical absorber, the process

can be stabilised, leading to the production of high-fidelity components. However, major challenges are encountered in the powder handling and heating system rather than in the laser processing itself.

It has been shown how the open platform allows for material integration of any kind. The basis for new material introduction relies on rigorous testing of the material prior to introduction in the system. That is developing the required knowledge of the material's thermal behaviour, as well as the specific powder constitution. A list of the critical material understanding prior to processing is described in Table 7.10. Here the three components are outlined and explained, including the relevant test for each metric.

Table 7.10: Knowledge of the material parameters critical prior to laser processing in the open system

Knowledge metric	Common metric	Elaboration
Thermal behaviour	$T_M$ and $T_C$	DSC analysis of the powder elaborates on the process window and critical temperature ranges
Laser absorptivity	Absorption and reflection	By knowing the absorptivity of the material, a decision on the use of absorber agents can be carried out defining the absorber system, and concentration
Powder character	Size, distribution, and shape	Ensuring a spherical powder increase the packing density of the bed, increasing the final part density

## Thermal properties

Conducting a common DSC analysis sweeping the temperature range at a heating and cooling rate of  $10\text{ }^\circ\text{C}/\text{min}$  allows for critical knowledge of the thermal behaviour of the material. By further extending this to an isothermal DSC analysis, particular knowledge of the temperature changes relevant to the process can be obtained, as described in section 4.1. Of particular interest is the shift in crystallisation temperature, as described by Drummer D. et al. [97]. Secondly, a sweep of much higher temperature rates is of interest, considering the steep temperature gradients experienced during the laser scanning cycle. During laser scanning, sharp peaks in temperature are induced locally, pushing the polymer past the melting point, making it less viscous, and allowing the powder to coalesce into the desired geometry. An elaboration of the process cycle as described by Drummed

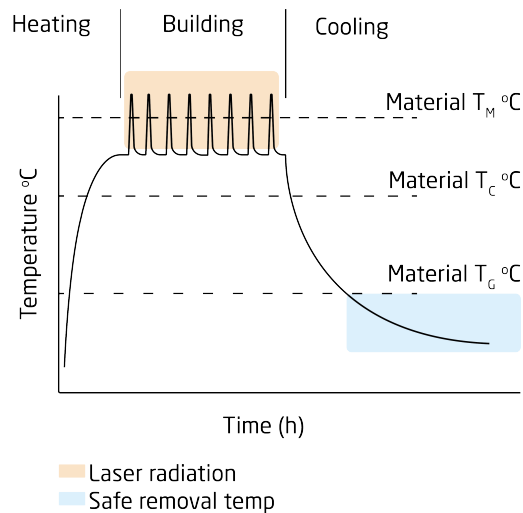


Figure 7.25: Temperature cycle during processing, Adapted from [97]

D. et al. [162] shown in Figure 4.20, are developed in Figure 7.25. Mimicking these sharp peaks of material melting and subsequent cooling to above the crystallisation temperature can be conducted by utilising high sweep rates. However, to truly conform to the process cycle and time scale of events, a method of laser-induced heating rates in a DSC analysis setup can be used. Such an approach has been demonstrated [240, 241], finding a change in the crystallisation temperature caused by the rapid heating of the polymer. By this, a change is induced due to maintaining the elevated temperature and the scanning routine, inducing an extremely high-temperature gradient.

This heating regime is similar to fibre laser processing, with one minor change, in the process, being the optical absorber. Incorporating the optical absorber in the otherwise optically translucent polymer (at 1080nm wavelength), a different heating approach is obtained. Here the black constituent in the powder mix will experience extremely rapid heating rates and will, by this, deliver the energy to the surrounding powder, as described above. These rapid heating rates can result in thermal degradation of the optical absorber component.

## Laser Absorption Properties

Depending on the absorber system utilised, fibre laser processing can be regarded as a laser processing sequence resembling that of a conventional system. The added benefit from the optimised beam profile aids the stable processing and allows for low absorber contents to be used. As shown here for a two-component system using only 5 % to produce stable parts with adequate surface roughness.

Defining the absorptivity of the selected polymer is commonly carried out by a Double-Integrating-Sphere System, as presented by Schuffenhauer T. et al. [242]. The analysis method is used for detecting the amount of a laser reflected and transmitted by a material.



This is done by irradiating a sample located between two internally reflective spheres with a laser beam. By measuring the amount of reflected light in the same sphere as the laser input, and transmitted light in the sphere located after the laser has passed through the sample, a measure of the amount of laser light absorbed can be determined. The method is laser or light-type agnostic, making it ideal for the investigation of laser sources and the inherent absorptivity in materials. The clear definition of laser absorption in the pure polymer, as well as for any absorber component, aids the processing capabilities.

## Powder Morphology and Size

The powder size and morphology have a significant impact on the final part properties. This was highlighted by the study of cryogenically milled conductive powder. The powder was unstable in size and with rough edges, causing a lack of packing and a low density of the powder cake. The ideal shape for polymer powders is fully spherical since this allows the powder to pack closely. An SEM image of a commercial PA11 black powder from BASF is shown in Figure 7.26a. Here it is evident that the powder is not fully spherical but slightly rough. This is caused by the manufacturing method of grinding the polymer to the final size as mentioned in subsection 4.1. By introducing powder grains in varying sizes, besides the major narrow distribution, the packing can be enhanced.

A narrow size distribution promotes flowability and packing during recoating. The com-

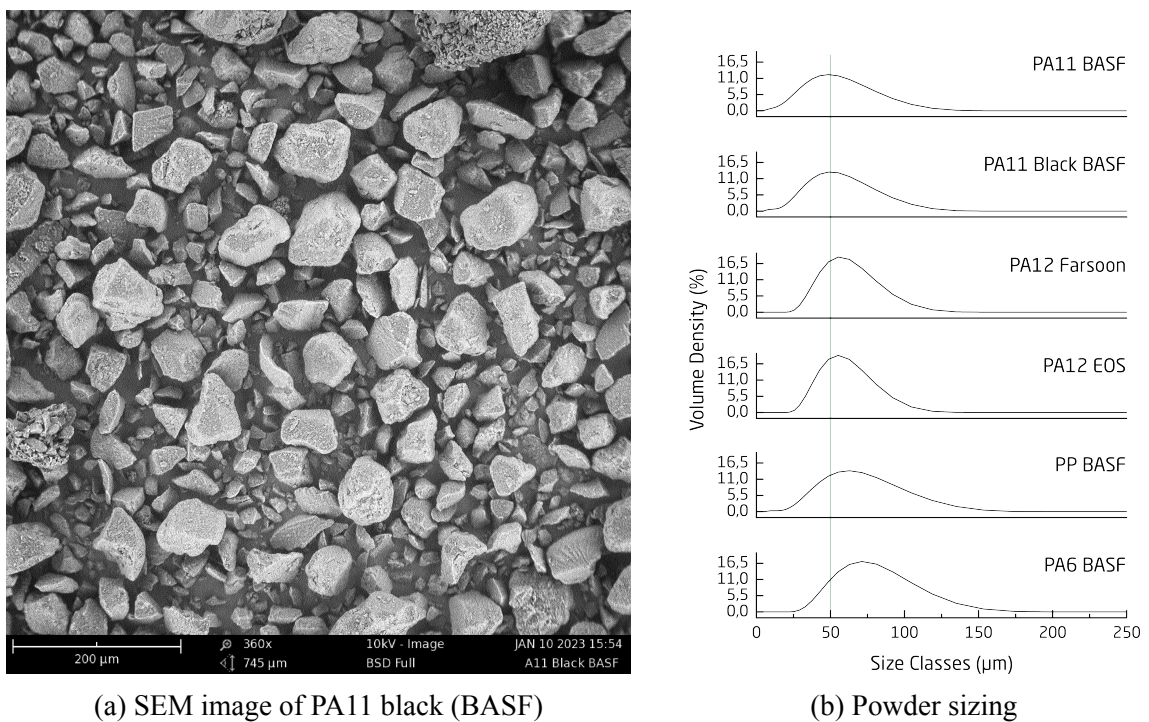


Figure 7.26: Commercial powder morphology and size distributions of an array of powders relevant for the PBF-LB/P industry

mercial powders tested during this project have shown a narrow size distribution for the majority of the powder blends, as seen in Figure 7.26b. None of the powders show a distinct bi-modal distribution. It can be noticed how the two PA11 grades incorporate an amount of small powder seen to the left side of the curves. This can either be by design to increase the packing density or, by default, from the size separation method, not fully removing any small powder constituents. The particle size analysis was done on the Mastersizer 3000 from Malvern Panalytical following the method described in Appendix E.

All the tested powders have been seen to flow well and produce a flat build plane during recoating. Even the irregularly-shaped conductive powder produced a flat build plane, with lower packing density, due to the powder morphology and insufficient powder to fill the build plane. By utilising the counter-rotating recoater, a wide selection of powders can be processed by the recoating system. However, by analysing the powder before using it in the system, an educated decision of how to recoat can be made. Moreover, an option is to round irregularly-shaped powders prior to processing a possibility, ensuring higher packing density and flatter build plane surface topography.

Enhanced part quality can be achieved by pre-defining each of the three metrics before processing the material using a fibre laser system. This knowledge is obtained through a comprehensive analysis of the material in four main aspects. The first involves LOM analysis to characterise the powder morphology. The second analysis focusses on powder sizing, ensuring a narrow size distribution of the powder. The third analysis focusses on understanding the thermal behaviour of the material to determine appropriate process temperatures. Lastly, the fourth analysis examines the absorptivity of the powder at the laser-specific wavelength. By diligently following these four general steps, process optimisation and effective part production can be achieved. When introducing a multi-modal or two-component mixed powder system, adherence to general rules for powder mixing is essential to minimise segregation. During counter roller recoating, the avalanche behaviour enforces similar physical interactions to tumble mixing. Adhering to the analysis suggested successful production of parts from polymer powder by fibre laser radiation is possible, as presented above. However, issues in the system cause excessive powder degradation, as seen from the mechanical properties and the discrepancy between the datasheet and obtained values. The root cause of this discrepancy and the powder degradation is presented next.



## 7.5.2 Polymer Degradation During Processing

Several methods can be employed when investigating polymer degradation behaviour. Commonly used is the Melt Flow Index (MFI) or Melt Flow Ratio (MFR), determining the amount of polymer flowing through a specified crevice at a certain temperature for a set amount of time. By analysing the change in the amount which has flowed, a determination of the polymer degradation type can be determined. Another method is the previously mentioned DSC, which determines the change in melting and crystallisation temperatures and defines the change in the structure of the polymer. Finally, a method of rheological testing can be employed, investigating the change of average molecular weight and the distribution of this [243].

The molecular weight and distribution are closely related to the zero shear viscosity, as seen at very low shear rates in the test of complex viscosity. Given the susceptibility of Polyamides of hydrolytic degradation and chain scission, a measurement of complex viscosity can be employed to determine if such degradation occurs during the processing of the PA11 powder in the system.

It is essential to note that the system lacks an inert or dried atmosphere, resulting in a significant presence of water vapour during processing. The relative humidity, measured in the system, decreases as the process chamber temperature increases, as seen in Figure 7.27. However, the overall amount of water vapour remains constant during processing, providing sufficient water for the hydrolysis of polyamide bonds.

Hydrolysis in polyamides results in a decrease in average molecular weight, which leads to a lower no-shear viscosity [244]. The change in the low shear viscosity of the tested

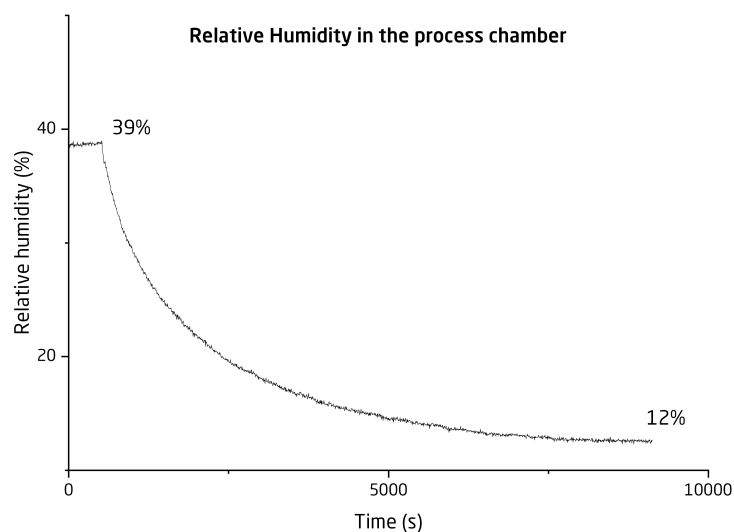


Figure 7.27: The relative humidity in the build chamber. Relative humidity decrease as the chamber heats up

mixed batches of virgin and used, as well as the pure virgin polymers, are presented in Figure 7.28. The method of testing, including the relevant settings, are found in Table 7.7. Here it is clear how the used 95/5 mix has been altered by being held at an elevated temperature for an extended period of time. The dark blue curve shows the smallest low-shear viscosity of the presented samples indicating a significant change in the molecular weight and distribution.

To investigate the change further, the storage and loss modulus plot is presented in Figure 7.29. Here a shift in the initial cross-over point between the storage and loss modulus indicates the average molecular weight and the molecular weight distribution. A shift towards the upper left corner indicates a higher average molecular weight in a narrower distribution, with the inverse result when moving towards the lower right corner.

Analysing the cross-over points of the curves revealed a significantly lower molecular weight with a slightly wider distribution, as expected from the used mix batch. This correlation aligns well with the degradation behaviour of hydrolysis, leading to chain scission and the production of shorter molecules with a more random distribution. Such degradation behaviour is particularly prominent in polyamide polymer systems. To assess the impact of this degradation behaviour caused by the lack of an inert atmosphere, further investigation of other polymer types is necessary. This will help determine whether the absence of an inert atmosphere poses a critical error, rendering the entire system ineffective.

In the event that the lack of an inert atmosphere is deemed crucial, appropriate actions

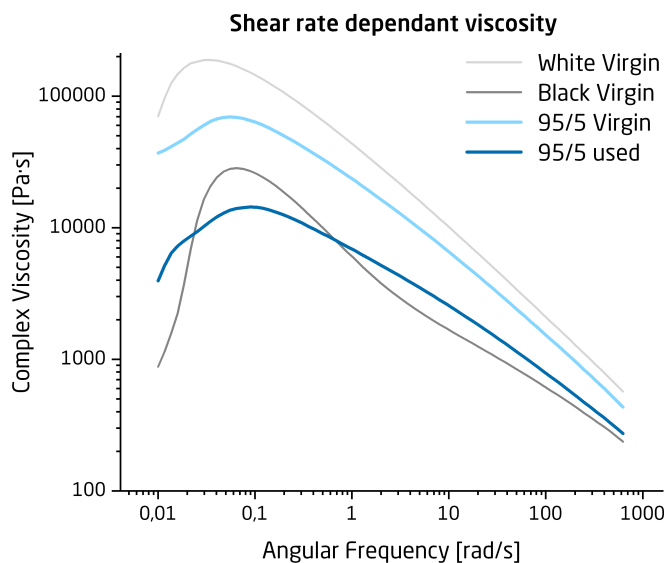


Figure 7.28: The shear dependant viscosity curves of the pure materials and the mixed batches, showing virgin and used powder mix

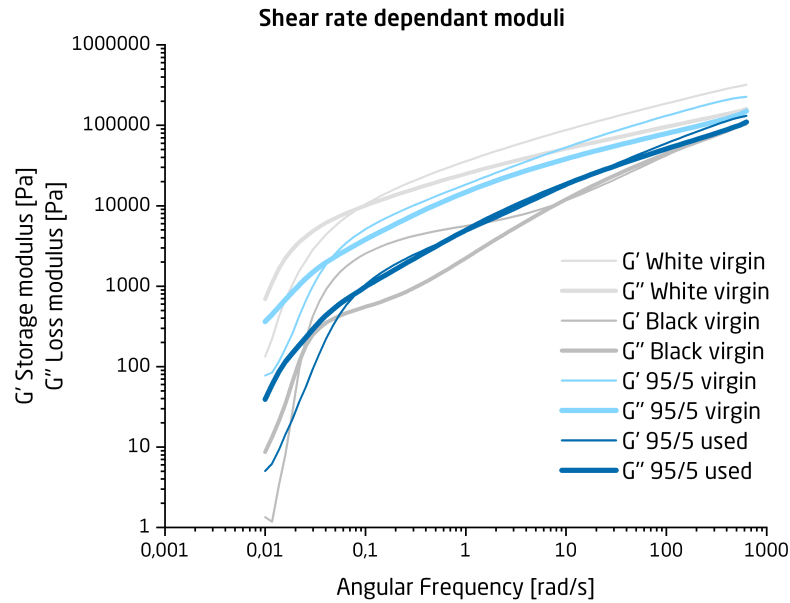


Figure 7.29: The shear dependant modulus curves of the pure materials and the mixed batches, showing virgin and used powder mix

must be taken to mitigate this issue and preserve the system's functionality.

## Minimising Polymer Degradation

The state of research (subsubsection 4.1) presented the main degradation mechanism experienced by polymers utilised for PBF-LB/P processing. Three mechanisms predominantly influence the polymer. For the developed system, a lack of inert atmosphere leads to hydrolysis and chain scission. This is aided by the elevated process temperatures, causing greater mobility of the polymer molecules, as well as the water molecules penetrating the polymer and degrading these.

During processing, the system has been noted to run at very high process temperatures compared to industrial machines. Besides the introduction of an inert atmosphere, a higher degree of thermal tuning can be implemented to improve the processing and powder stability of the system. The entire system would benefit from lower heating implemented for the build piston while maintaining excellent powder processing capabilities. This must be investigated further, developing a metric for adequate heating and possibly a heating routine of lowering or shutting down the build piston heaters after a set build height is achieved.

## 7.6 Chapter Summary

The chapter presents several studies focussing on materials processing in the system using a fibre laser.

The initial study demonstrates the utilisation of optical absorbers to enhance laser absorption in the polymer powder. Incorporating a black PA11 into a white PA11 enables stable processing of the powder. The stability in the production is investigated by analysing the mechanical properties of parts produced in the system. The functional breakdown level of the black optical absorber is found by utilising very low amounts of the absorber. Low levels of the optical absorber led to inadequate laser energy absorption, resulting in part failure and deteriorated mechanical properties. This led to the conclusion that 5 % black material is an adequate solution for the fabrication of stable components.

The study finds that the rheological properties of the black material aid the processing capabilities by showing significantly lower viscosity when heated, resulting in a black matrix flowing around the white particles, causing the production of fully black components. These components are found to inherit the stability and processability of the constituent powder, explaining the need for a dimensional fidelity study.

The geometrical sizing and fidelity study showcase how complex geometries can be produced in the system by fibre laser radiation. Intricate features and fine details are replicated as per the CAD file, proving the efficacy of fibre laser processing of polymer powders. The component produced is compared to the same CAD geometry produced on a flagship system by EOS, showing the resemblance and lack of fidelity. This comparison highlights the potential of the system and identifies areas for further development.

To develop the knowledge of fibre laser processing of polymer powders, an investigation of a conductive polymer blend is performed. Here parts are realised, showing a conductive network. The analysis focusses on the difficulties of processing coarse and irregular powders and showcases how the black constituent of the powder acts as the optical absorber, allowing fibre laser processing. The results of the processing show promise and further investigation of the material in the process is planned for the future.

Finally, the chapter concludes by evaluating the processing capabilities of the fibre laser and system. The analysis and identification of the change in the molecular weight reveals the impact of the lack of an inert atmosphere on the processed nylon, leading to the presented explanation. A potential solution for future research involves focussing on hydrophobic materials to minimise the risk of hydrolysis and thermal degradation.

The capabilities of the fibre laser have been shown not to cause any of the issues observed in the aforementioned studies. The main distinction between conventional and fibre laser processing of polymers lies in the requirement of an optical absorber to facilitate energy delivery from the laser to the polymer. Through the incorporation of this absorber, a stable process has been established, as evidenced by the studies on mechanical properties and geometrical fidelity.

The chapter has identified several areas of interest for the extension of the study. The

extension or desire to study a process further is often necessary for large complex projects that analyse a process holistically. The experiments and material challenges projected for this extension are outlined in the following chapter, along with the rationale for their relevance and the proposed methodology.



## Conclusion & Perspectives

During the project, a holistic approach to PBF-LB/P has been utilised for developing the experimental infrastructure and conducting experiments for verification of the main hypothesis. The main hypothesis concern the definition of the utility of fibre lasers for processing polymer powders into mechanically sound and geometrically accurate components. Over the past three years, the project has approached this hypothesis from various perspectives, striving to ensure a holistic approach in the project definition and execution.

Three phases of the project are identified throughout the thesis.

- The initial phase broadened the understanding of the process, developing the knowledge and metrics of how the industry and research approach PBF-LB/P. During this phase, a study of the process and intimate workings of the PBF-LB/P process and systems were developed, defining the critical elements and aspects relevant to the next project phase.
- The project's second phase considered the development of the experimental infrastructure. The infrastructure development was rooted in the findings of the previous project phase, ensuring the developed system delivered the desired processing capabilities. The systems development phase concludes by proving the system's capabilities through a thorough sub-system validation practice and a holistic build sequence analysis.
- The final project phase sought to develop an understanding of fibre laser processing of polymer powders through a practical approach. Here two different polymer powders were investigated. An initial investigation concerning a PA11 PBF-LB/P polymer was conducted, focussing on the activation of fibre laser absorption in a powder mix of white and black powder. A second polymer powder explored the possibility of processing a non-commercial material in the system. This polymer



powder was developed to demonstrate the efficacy of producing conductive parts by laser processing, further expanding the metrics for powder coalescence in fibre laser processing.

The intended purpose of this work has been to establish the processing capabilities of a fibre laser in Laser Based Powder Bed Fusion of Polymers. Therefore, a processing system that addresses the main hypothesis must be capable of translating information from a digital model into a physical object through conversion in a job file generator and processing system. A prerequisite for this process is the accurate translation of geometrical characteristics from the digital file to the physical realm. The three main phases described above have been employed to bring forth these capabilities. This has ensured the capable fibre laser processing system presented herein, based on the knowledge of the critical elements and the process characteristics incorporated in the developed system.

The introductory part described the recently published research and the common use of PBF-LB/P. The study identified an evident gap in the research between the two processes of metal and polymer powder laser processing, showcasing the discrepancy and lack of research within the field of polymers. A further dive into the industrial PBF-LB/P processing systems highlighted the lack of fibre laser utilisation. This lack of information on the utility and proof of validity was the primary motivation for developing the experimental infrastructure designed to examine the main hypothesis.

Process understanding and knowledge of the critical elements and aspects of PBF-LB/P processing laid the foundation for developing an experimental infrastructure. From the analysis, several aspects of an PBF-LB/P system were defined and implemented in a repurposed binder jetting machine. Repurposing allowed the rapid development cycle for the initial experimental infrastructure, which was further developed through several iterations defining the developed system. This system encompassed the critical elements of heating the powder cake sufficiently above the crystallisation temperature, the capability of dosing powder and distributing this to an even build plane, with the narrow Z-layer height adjustment required for the process. Furthermore, a laser processing system was installed, introducing the fibre laser capability of the system.

The developed system utilised a Ytterbium fibre laser to process polymer powders. Several other types of lasers have been identified for their increased capability of polymer processing. One such laser is the thulium laser which produces a laser beam with a wavelength of  $\approx 2 \mu m$ , which interacts with the molecular agitation frequency often present in polymers, enabling the laser energy transformation from light to heat. By this, the thulium fibre laser could have been a superior choice for polymer powder processing. However, a desire to introduce the Yb laser in the process was a driver for this selection. This desire is closely tied to the cost-efficient nature of the laser type. The Yb laser has seen extensive use in other material processing applications, contributing to this technology's significant

---

advancement and cost reduction. Due to the stabilisation of this technology, the laser and beam delivery equipment can be acquired at a fraction of the cost of a thulium laser and beam delivery equipment for this wavelength.

The concluding part of the work focussed on utilising the developed system, describing the achieved processing conditions of fibre laser polymer powder processing. An optical absorber requirement was identified early in the project during the process understanding phase. Several methods can realise optical absorption in the powder. An approach of physical mixing of two colours of one type of polymer was selected, utilising a black material for obtaining optical absorption. Following this methodology, a PA11 powder with a grey hue was produced from a mix of white and black PA11. A study of the required mixing ratio defining the lowest possible amount of black is presented. The investigation tested several different compositions of white and black mix to determine the adequate amount for stable production of components. The defined mixing ratio is found to be 5% black material content in an otherwise white powder. Utilising this level of black, an investigation into the surface characteristics and geometrical fidelity was undertaken. This investigation proved the feasibility of using 5% black powder in the production of parts adhering to the geometrical size as inscribed by the CAD model and realised by the developed system. When processing the mixed material by a fibre laser, entirely black components are fabricated. This led to an investigation into the cause of the black powder colouring the entire part, even when a low mixing ratio of 5% was used.

A study of the flow and viscoelastic behaviour of the two materials showed a low viscosity of the black material compared to the white. This behaviour is observed to cause the black powder to start flowing and distributing among the white particles instantly after being heated by the laser, leading to fully black parts. During the flow of the black material, the energy is transferred from the black to the surrounding particles allowing these to melt. If any particles are not molten in the initial layer processing, these will be molten in the next, where a dense matrix of black material surrounds and lock in the white particles. If the laser is allowed to transmit through the build plane layer and onto the previous one, an instant laser absorption is produced by the fully black colour of the previous layer.

The low viscosity flow behaviour of the black material can cause detrimental effects on the part's geometric fidelity. If the black material seeps into the powder surrounding the component, uncontrolled part growth can occur. This effect is likely part of the cause for the ripples seen along the side walls of the components, where the laser causes an overheating impact resulting in very low viscosity of the black polymer. From this, a solid state sintering effect in the powder can occur, locking un-molten particles to the surface of a part. The geometrical fidelity is highlighted as an area of interest for the perspective work of the project.

Fibre laser processing of polymer powders delivers interesting new perspectives to the

PBF-LB/P process. The laser can enhance the process by allowing a narrower spot size and a larger Rayleigh length, enabling the production of high-fidelity components. As seen from the industrial study, a company have recently brought a fibre laser-based polymer processing system to the market. Allowing high scanning speeds and large production throughput. Another company have based their Fine Detail Resolution capabilities around a different laser source, utilising the enhanced processing capabilities. The laser improves the processing by utilising a shorter wavelength, permitting a smaller spot size and larger Rayleigh length. Both of which are further enhanced in the fibre laser wavelength.

When deciding on pursuing a holistic approach for tackling the problem of fibre laser utilisation in LPBF polymer systems, some areas of this utility cannot be fully covered. This is the case for the complete identification of the fibre laser capabilities. As presented, the fibre laser beam properties are unmatched compared to those of the traditional CO<sub>2</sub> laser. This study has not fully demonstrated the utilisation of this beam profile or the extended Rayleigh length. The study has proven how the laser can be utilised in the developed system. The study, however, lacks a clear definition of how and if the enhanced beam quality can increase the quality achieved by PBF-LB/P. This is a significant deficit of the study, also highlighted in the extensions and perspectives below.

A clear tendency for fibre laser utilisation is the requirement of an optical absorber. This absorber is a requisite for stable processing, evidenced by the atrocious downward-facing surfaces produced by the white components in the build sequence study (section 6.4). Optical absorption does not necessitate black colourant, with technical optical absorbers presented for the extension of the work presented by this study.

## Extensions & Perspectives

Any extension of the project can include several prospect investigations described here for presenting the recommended direction and steps of the project. Each potential investigation delves deeper into the development and utilisation of the experimental infrastructure, thereby enhancing the comprehension of the capabilities of fibre laser processing and the materials involved.

By iterating the developed sub-system, a fully developed system perform to a higher standard. However, the iterative process of an experimental infrastructure is never final since a new iteration is always possible. By this, the developed system is a dynamic entity that evolves further as research is conducted utilising the experimental infrastructure. Five areas of particular interest have been identified during the project, requiring extended focus. These areas of interest could not be integrated during the project. Still, they will receive priority for further uncovering the efficacy of the fibre laser to enhance the research infrastructure integrity and processing capabilities. Each of these is described below, including a methodology for the execution.

---

## Fibre Laser Utility

The clear-cut definition of the enhanced beam quality of the fibre laser over the CO<sub>2</sub> was not possible to achieve during the limitations of the three years of work. During the project, substantial attention has been granted towards the systems development and validation. If a different approach, only focussing on the fibre laser processing, had been selected, it is expected that the outcome of this study would have been different.

An approach for studying the fibre laser in a closed system where the true utility of the fibre laser was defined is possible. The study could have utilised a simpler setup where the laser penetration, absorption, reflectance and transmittance were identifiable. This setup would most likely not be capable of producing complex geometries as those presented in the work. It would, however, be capable of answering a different array of questions relevant to defining the fibre laser utility.

The decision to develop a system capable of complex geometry production was selected based on the project's relation to the Open Additive Manufacturing Initiative. The system, therefore, caters to a different set of research questions and capabilities, focussing on the dissemination of industrially relevant AM processes.

## Heaters

The heating system integrated into the developed system produces an even heat distribution only for a central part of the build plane and powder cake. The investigation of the heating system presented in section 6.1 suggests two areas of critical improvement. One is the implementation of heating elements wrapping the entire build piston and the further insulation, minimising the thermal gradients towards the corner edges. This results in a larger build envelope capable of processing powder to components.

The second critical improvement is the top heating system. The two ceramic heaters are identified as sufficient for testing the main hypothesis. However, these must be improved to develop a system with greater capabilities. A study performed by two students and supervised by the author presented a possible solution for enhancing the top heater stability and uniformity.

For the further improvement of the developed system, an iteration concerning the design and implementation of the heater array developed by the student is recommended. By executing these improvements of fully wrapping contact heaters, extended insulation, and better adjustability of the top heaters, the potential for achieving a more substantial and stable build area becomes a viable prospect.

## Recoater further investigation

The investigation of the recoater system only extended to finding one set of parameters which produced an even build plane. A study of the build plane's quality is required to define the recoater function's efficacy fully. Such a study can utilise several approaches, with two relevant measurement procedures presented here.

One approach for determining the build plane quality is either fringe projection or laser line profilometry, as done for metal systems by Berez J. et al. [245]. This approach can produce a numeric value in terms of a height map, presenting the actual surface topography of the build plane.

Secondly, Meyer L. et al. [155] presents a method of determining the powder cake density. Here canisters produced by laser processing containing unsintered powder from different resultant recoating velocities can be extracted from the process and analysed by weighing the filled and emptied canisters. Utilising this method in the developed system allows for detailed knowledge of the recoating routine and possible optimisations. A study concerning the packing density will not yield a unified speed and recoating rotational setting, but rather a material-specific metric, which must be defined for each new material in the process.

The studies will either allow for the production of a flatter build plane or a greater powder cake density by studying the recoater motion, rotation and resultant velocity. By incorporating a material-specific study, even greater fidelity of fabricated components is expected.

## Other optical absorbers

In section 7.2, a thorough investigation described the utilisation of mixing two PA11 materials of different colours achieving processing by fibre laser irradiation. Two other absorber types were mentioned as possible absorbing agents.

The first is an absorber often used for laser welding of polymer sheets by fibre laser named Clearweld. This absorber is either delivered in a nano-powder or in a solution. The nano-powder is possible to compound into a polymer matrix for laser processing. While the solution potentially could be used for coating the powder, as mentioned in subsection 2.2.4. Studying the capabilities obtained for fibre laser processing by incorporating the optical absorber is a top priority for extended research utilising the system. The study is expected to show the system's capabilities further, possibly presenting new ways of achieving lighter-coloured components from the system.

The second absorber type is already found in materials developed for the process. A material developed and compounded by Sindelhauser with the PeroLab optical absorber incorporated exists and is planned for further testing.

---

The work going into this thesis has not included these optical absorbers since a method of mixing a powder with a black absorber was utilised. It can be presumed that the inclusion of either optical absorber would have steered the project in a different direction, resulting in the discovery of alternative processing regimes compared to those identified for the white and black mixture. Considering the main hypothesis of whether the fibre laser can be utilised for polymer powder processing, an observation of successful processing can be made. Seeing this, the next step is to focus on incorporating these optical absorbers allowing for the processing of commercial, experimental, and exotic materials.

## Polymer Shrinkage Factor, a Generic Investigation

As stated in the benchmark study presented in section 7.3, one iteration of fabricating the benchmark and defining the shrinkage factor was performed. The results yielded a benchmark component significantly closer to the nominal dimensions. If a second iteration of this process had been conducted, a component even closer to nominal dimensions is expected.

The polymer material and the overall dimension of the part determine component shrinkage. A unified factor describing shrinkage is, therefore, not adequate for ensuring the geometrical fidelity of any component. If a generic shrinkage factor is implemented, the geometrical accuracy of manufactured components increases towards nominal. However, this general factor will only be valid for the specific material and geometry combination by which this factor was developed. And will not guarantee true accuracy for any other geometry or material combination. By iterative production and calibration, better geometrical accuracy can be achieved for the components manufactured by the developed system. By these iterations, influences from the geometry as well as the material can be defined and countered, ensuring the geometrical accuracy required. Polymers are known for significant shrinkage in all conventional fabrication processes. The shrinkage of polymers is, among others, defined by the chain organisation into crystallites, as presented in subsection 2.2.1. Polymers will crystallise differently depending on the molecular structure, significantly influenced by chain branching [246]. A high degree of chain branching or other molecular abnormalities causes lower degrees of crystallisation, resulting in less shrinkage.

All of the above-mentioned project extensions would have further enhanced the proof of utilisation of the fibre laser in polymer powder processing. The study successfully determined the efficacy of processing PA11 in a white and black mixture to a high-fidelity component showing adequate mechanical properties. Several studies of the process, systems, and materials have been incorporated for this examination, showcasing the wide spectrum of research and holistic approach utilised during this project.

While this study has extensively sought to define the utility of fibre lasers in the process,

it is important to acknowledge that opportunities for further refinement and enhancement remain.

A critical aspect of the utility of fibre lasers in polymer processing is that polymer processing is a relatively new field. Technical polymers such as nylon have only been around since the 1930's [247]. A lack of knowledge of processing polymers is evident, especially when compared to similar process regimes for metals, as seen in the number of research publications concerning each process (section 1.4). Metal processing has been established for centuries, enabling a vast knowledge of the aspects and results when processed. An example is the normalised enthalpy described in subsection 4.1.1, a widely understood metric for the laser processing of metal powder derived originally from the knowledge of welding. A metric at the same level is not widely available for polymer processing.

Polymer processing is still being developed, despite being one of the original materials utilised for additive manufacturing. The development will see new metrics for power delivery and other critical elements of the process being developed, enabling more groundbreaking research within the field. The developed system harbours the capability of aiding this development, further enhancing the field of Laser Based Powder Bed Fusion of Polymers processing. The open architecture and the grander Open Additive Manufacturing Initiative will further aid this development. The developed system resides within the Additive Manufacturing group at DTU, enabling the further study of fibre laser-based polymer powder processing.



# Bibliography

1. Hull, C. *Apparatus for production of three-dimensional objects by stereolithography* Mar. 1986.
2. Deckard, C. *Method and apparatus for producing parts by selective sintering* Oct. 1987.
3. Gomes, L. A., Xiang, N., Jouhti, T., Okhotnikov, O. G. & Grudinin, A. Mode-locked ytterbium fiber laser tunable in the 980–1070-nm spectral range. *Optics Letters*, Vol. 28, Issue 17, pp. 1522–1524 **28**, 1522–1524. ISSN: 1539-4794. <https://opg.optica.org/viewmedia.cfm?uri=ol-28-17-1522&seq=0&html=true%20https://opg.optica.org/abstract.cfm?uri=ol-28-17-1522%20https://opg.optica.org/ol/abstract.cfm?uri=ol-28-17-1522> (Sept. 2003).
4. Yarava, V. S. *AutoCAD to G-code Converter* in *IEEE Pune Section International Conference, PuneCon 2021* (Institute of Electrical and Electronics Engineers Inc., 2021). ISBN: 9781665444798.
5. Kruth, J. P., Leu, M. C. & Nakagawa, T. Progress in additive manufacturing and rapid prototyping. *CIRP Annals - Manufacturing Technology* **47**, 525–540. ISSN: 00078506 (1998).
6. Li, Z. *et al.* High deposition rate powder- and wire-based laser directed energy deposition of metallic materials: A review. *International Journal of Machine Tools and Manufacture* **181**, 103942. ISSN: 0890-6955 (Oct. 2022).
7. Obikawa, T., Yoshino, M. & Shinozuka, J. Sheet steel lamination for rapid manufacturing. *Journal of Materials Processing Technology* **89-90**, 171–176. ISSN: 0924-0136 (May 1999).
8. Ligon, S. C., Liska, R., Stampfl, J., Gurr, M. & Mülhaupt, R. Polymers for 3D Printing and Customized Additive Manufacturing. *Chemical Reviews* **117**, 10212–10290. ISSN: 15206890. <https://pubs-acsc-org.proxy.findit.cvt.dk/doi/full/10.1021/acs.chemrev.7b00074> (Aug. 2017).
9. Stansbury, J. W. & Idacavage, M. J. 3D printing with polymers: Challenges among expanding options and opportunities. *Dental Materials* **32**, 54–64. ISSN: 0109-5641 (Jan. 2016).
10. Pugalendhi, A., Ranganathan, R. & Ganesan, S. Impact of process parameters on mechanical behaviour in multi-material jetting. *Materials Today: Proceedings* **46**, 9139–9144. ISSN: 2214-7853 (Jan. 2021).

11. Upadhyay, M., Sivarupan, T. & El Mansori, M. 3D printing for rapid sand casting— A review. *Journal of Manufacturing Processes* **29**, 211–220. ISSN: 1526-6125 (Oct. 2017).
12. Chartrain, N. A., Williams, C. B. & Whittington, A. R. A review on fabricating tissue scaffolds using vat photopolymerization. *Acta Biomaterialia* **74**, 90–111. ISSN: 1742-7061 (July 2018).
13. Lu, Y., Huang, Y. & Wu, J. Laser additive manufacturing of structural-graded bulk metallic glass. *Journal of Alloys and Compounds* **766**, 506–510. ISSN: 0925-8388 (Oct. 2018).
14. Lupone, F., Padovano, E., Casamento, F. & Badini, C. Process Phenomena and Material Properties in Selective Laser Sintering of Polymers: A Review. *Materials* **15**. ISSN: 19961944. /pmc / articles / PMC8746045 / %20 / pmc / articles / PMC8746045 / ?report = abstract % 20https : / / www . ncbi . nlm . nih . gov / pmc / articles / PMC8746045 / (Jan. 2022).
15. Gibson, I., Rosen, D., Stucker, B. & Khorasani, M. *Additive Manufacturing Technologies* 1–675 (2021).
16. ISO. *Additive manufacturing – General principles – Fundamentals and vocabulary (ISO/ASTM 52900:2021)* tech. rep. (International Organization for Standardization, Dec. 2021).
17. ISO. *Additive manufacturing – Design – Part 2: Laser-based powder bed fusion of polymers (ISO/ASTM 52911-2:2019)* eng. Tech. rep. (2019).
18. Redwood, B., Schffer, F. & Garret, B. *The 3D printing handbook: technologies, design and applications* (3D Hubs, 2017).
19. Wohlers, T., Campbell, I., Diegel, O., Huff, R., Kowen, J. & (Firm), W. A. *Wohlers report 2023: 3D printing and additive manufacturing global state of the industry* eng (Wohler Associates Inc., Fort Collins, CO, 2023).
20. Mendez Ribo, M. *Vat Photopolymerization Process Chain* eng. PhD thesis (2020).
21. Danielak, A. H. *Design, Optimization and Production of Smart Surfaces by Additive Manufacturing for Medical Applications* PhD thesis (2021).
22. Artemeva, M., Danielak, A. H., Basso, A., L. Navas, J., M. Ribo, M., Pedersen, D. B. & Nadimpalli, V. K. Additive Manufacturing of High-Resolution PZT Components: Slurry development, Characterization, Design, and Fabrication. eng. *2022 Aspe and Euspen Summer Topical Meeting on Advancing Precision in Additive Manufacturing*, 18–23 (2022).
23. Pham, D. T., Dotchev, K. D. & Yusoff, W. A. Y. Deterioration of polyamide powder properties in the laser sintering process. *Journal of Mechanical Engineering Science* **222**, 2163–2176 (2008).

24. DePalma, K., Walluk, M. R., Murtaugh, A., Hilton, J., McConky, S. & Hilton, B. Assessment of 3D printing using fused deposition modeling and selective laser sintering for a circular economy. *Journal of Cleaner Production* **264**. ISSN: 09596526 (Aug. 2020).
25. Thomas, D. Costs, benefits, and adoption of additive manufacturing: a supply chain perspective. *The International Journal of Advanced Manufacturing Technolog* (2016).
26. Leary, M. in *Design for Additive Manufacturing* 295–319 (2020).
27. Ziaee, M. & Crane, N. B. Binder jetting: A review of process, materials, and methods. *Additive Manufacturing* **28**, 781–801. ISSN: 2214-8604 (Aug. 2019).
28. Mostafaei, A., Elliott, A. M., Barnes, J. E., Li, F., Tan, W., Cramer, C. L., Nandwana, P. & Chmielus, M. Binder jet 3D printing—Process parameters, materials, properties, modeling, and challenges. *Progress in Materials Science* **119**, 100707. ISSN: 0079-6425 (June 2021).
29. Narra, S. P. in *Encyclopedia of Materials: Metals and Alloys* 85–94 (Elsevier, Jan. 2022). ISBN: 9780128197264.
30. Wong, H., Neary, D., Jones, E., Fox, P. & Sutcliffe, C. Benchmarking spatial resolution in electronic imaging for potential in-situ Electron Beam Melting monitoring. *Additive Manufacturing* **29**, 100829. ISSN: 2214-8604 (Oct. 2019).
31. Kumar, S. Modeling and Characterization Selective Laser Sintering: A Qualitative and Objective Approach. *JOM* **55**, 43–47 (2003).
32. Chernyshikhin, S. V., Pelevin, I. A., Karimi, F. & Shishkovsky, I. V. The Study on Resolution Factors of LPBF Technology for Manufacturing Superelastic NiTi Endodontic Files. *Materials* **15**, 6556. ISSN: 1996-1944. <https://doaj.org/article/a2fd10f94f944904b60858a2e6f1c850> (Sept. 2022).
33. Kruth, J. P., Wang, X., Laoui, T. & Froyen, L. Lasers and materials in selective laser sintering. *Assembly Automation* **23**, 357–371. <http://www.emeraldinsight.com/researchregisterhttp://www.emeraldinsight.com/0144-5154.htm> (2002).
34. Wietzke, S. *et al.* Thermomorphological study of the terahertz lattice modes in polyvinylidene fluoride and high-density polyethylene. *Applied Physics Letters* **97**. ISSN: 00036951 (July 2010).
35. Yan, C., Shi, Y. & Hao, L. Investigation into the differences in the selective laser sintering between amorphous and semi-crystalline polymers. *International Polymer Processing* **26**, 416–423. ISSN: 0930777X. <https://www.degruyter.com/document/doi/10.3139/217.2452/html> (Sept. 2011).
36. Crawford, C. B. & Quinn, B. in *Microplastic Pollutants* 57–100 (Elsevier, Jan. 2017). ISBN: 978-0-12-809406-8.

37. Schmid, M. *Laser sintering with plastics: technology, processes, and materials* 125–159. ISBN: 9781569906835. <http://p5070-www.sciencedirect.com.proxy.findit.cvt.dk/book/9781569906835/laser-sintering-with-plastics> (Carl Hanser Verlag GmbH Co KG, 2018).
38. Rulkens, R. & Koning, C. in *Polymer Science: a Comprehensive Reference: Volume 1-10* 431–467 (Elsevier, Jan. 2012). ISBN: 9780080878621.
39. EOS. *EOS Material Datacenter* <https://eos.materialdatacenter.com/eo/standard/main/ds> (Date accessed 01/05/2023).
40. Schmid, M. & Wegener, K. Polymers applicable for Laser Sintering (LS). *Procedia Engineering* **149**, 457–464. [www.sciencedirect.com](http://www.sciencedirect.com) (2016).
41. Seepersad, C. C., Govett, T., Kim, K., Lundin, M. & Pinero, D. *A DESIGNER'S GUIDE FOR DIMENSIONING AND TOLERANCING SLS PARTS* in *23rd Annual International Solid Freeform Fabrication Symposium* (2012), 921–931.
42. MONOQOOL. *MONOQOOL glasses* <https://monoqool.com/> (Date accessed 29/06/2023).
43. Beaman, J. J., Barlow, J. W., Bourell, D. L., Crawford, R. H., Marcus, H. L. & McAlea, K. P. *Solid Freeform Fabrication: A New Direction in Manufacturing* eng (Springer New York, NY, 1997).
44. Abd-Elaziem, W. *et al.* On the current research progress of metallic materials fabricated by laser powder bed fusion process: a review. *Journal of Materials Research and Technology* **20**, 681–707. ISSN: 22387854 (Sept. 2022).
45. Chowdhury, S., Yadaiah, N., Prakash, C., Ramakrishna, S., Dixit, S., Gupta, L. R. & Buddhi, D. Laser powder bed fusion: a state-of-the-art review of the technology, materials, properties & defects, and numerical modelling. *Journal of Materials Research and Technology* **20**, 2109–2172. ISSN: 2238-7854 (Sept. 2022).
46. Hoeges, S., Zwiren, A. & Schade, C. Additive manufacturing using water atomized steel powders. *Metal Powder Report* **72**. <http://dx.doi.org/10.1016/j.mprp.2017.01.004> (2017).
47. Sing, S. L. & Yeong, W. Y. Laser powder bed fusion for metal additive manufacturing: perspectives on recent developments. *Virtual and Physical Prototyping* **15**, 359–370. <https://www.tandfonline.com/action/journalInformation?journalCode=nvpp20> (2020).
48. Sendino, S., Silvia Martinez, ., Lartategui, F., Gardon, . M., Aitzol Lamikiz, ., Javier, . & Gonzalez, J. Effect of powder particle size distribution on the surface finish of components manufactured by laser powder bed fusion. *The International Journal of Advanced Manufacturing Technology*, 789–799. <https://doi.org/10.1007/s00170-022-10423-9> (2023).

49. Magnus Bolt Kjer. *Systems Engineering in the Pursuit of Open Architecture Additive Manufacturing a study of Laser Powder-bed Fusion* PhD thesis (Technical University of Denmark, Kongens Lyngby, July 2023). ISBN: 978-87-7475-763-4.
50. Valente, E. H., Nadimpalli, V. K., Christiansen, T. L., Pedersen, D. B. & Somers, M. A. In-situ interstitial alloying during laser powder bed fusion of AISI 316 for superior corrosion resistance. *Additive Manufacturing Letters* **1**, 100006. ISSN: 27723690 (Dec. 2021).
51. Wits, W. W. & Amsterdam, E. Graded structures by multi-material mixing in laser powder bed fusion. *CIRP Annals* **70**, 159–162. ISSN: 17260604 (Jan. 2021).
52. Gökhan Demir, A. & Previtali, B. Letters Multi-material selective laser melting of Fe/Al-12Si components. *Manufacturing Letters* **11**, 8–11. <http://dx.doi.org/10.1016/j.mfglet.2017.01.002> (2017).
53. Jia, Q. *et al.* Precipitation kinetics, microstructure evolution and mechanical behavior of a developed Al–Mn–Sc alloy fabricated by selective laser melting. *Acta Materialia* **193**, 239–251. ISSN: 13596454 (July 2020).
54. Blakey-Milner, B. *et al.* Metal additive manufacturing in aerospace: A review. *Materials and Design* **209**. ISSN: 18734197 (Nov. 2021).
55. Tan, C., Wang, D., Ma, W., Chen, Y., Chen, S., Yang, Y. & Zhou, K. Design and additive manufacturing of novel conformal cooling molds. *Materials and Design* **196**. ISSN: 18734197 (Nov. 2020).
56. Depboylu, F. N., Yasa, E., Poyraz, Ö., Minguella-Canela, J., Korkusuz, F. & De los Santos López, M. A. Titanium based bone implants production using laser powder bed fusion technology. *Journal of Materials Research and Technology* **17**, 1408–1426. ISSN: 22387854 (Mar. 2022).
57. Chen, A.-N., Wu, J.-M., Liu, K., Chen, J.-Y., Xiao, H., Chen, P., Li, C.-H. & Shi, Y.-S. Advances in Applied Ceramics Structural, Functional and Bioceramics High-performance ceramic parts with complex shape prepared by selective laser sintering: a review. *Advances in Applied Ceramics* **117**, 100–117. ISSN: 1743-6761. <https://www.tandfonline.com/action/journalInformation?journalCode=yaac20> (2017).
58. Zhang, X., Li, N., Chen, X., Stroup, M., Lu, Y. & Cui, B. Direct selective laser sintering of high-entropy carbide ceramics. *Journal of Material Research* **38**. [www.mrs.org/jmr](http://www.mrs.org/jmr) (Oct. 2022).
59. Grossin, D. *et al.* A review of additive manufacturing of ceramics by powder bed selective laser processing (sintering / melting): Calcium phosphate, silicon carbide, zirconia, alumina, and their composites. *Open Ceramics* **5**. ISSN: 26665395 (Mar. 2021).

60. Juste, E., Petit, F., Lardot, V. & Cambier, F. Shaping of ceramic parts by selective laser melting of powder bed. *Materials Research Society* **29**, 2086–2094 (2014).
61. Christian Nelson, J., Vail, N. K., Barlow, J. W., Beaman, J. J., Bourell, D. L. & Marcus, H. L. *Selective Laser Sintering of Polymer-Coated Silicon Carbide Powders* tech. rep. (1995), 1641–1651. <https://pubs.acs.org/sharingguidelines>.
62. Chuang, K. C., Gornet, T. J., Schneidau, K. & Koerner, H. *Laser Sintering of Thermoset Polyimide Composites* in *Camx 2019 - Composites and Advanced Materials Expo* (2019).
63. EOS. *Polyamide (PA12) for Industrial 3D printing* <https://www.eos.info/en/3d-printing-materials/plastic/polyamide-pa-12-alumide> (Date accessed 01/05/2023).
64. BASF. *Ultrasint® PA11 Black CF* <https://forward-am.com/material-portfolio/ultrasint-powders-for-powder-bed-fusion-pbf/pa-11-line/ultrasint-pa11-black-cf/> (Date accessed 09/05/2023).
65. Lupone, F., Padovano, E., Ostrovskaya, O., Russo, A. & Badini, C. Innovative approach to the development of conductive hybrid composites for Selective Laser Sintering. *Composites Part A: Applied Science and Manufacturing* **147**. ISSN: 1359835X (Aug. 2021).
66. Chunze, Y., Yusheng, S., Jinsong, Y. & Jinhui, L. A Nanosilica/Nylon-12 Composite Powder for Selective Laser Sintering. *Journal of REINFORCED PLASTICS AND COMPOSITES* **28**, 2889–2902. <http://jrp.sagepub.com> (2009).
67. Marschall, M., Heintges, C. & Schmidt, M. Influence of flow aid additives on optical properties of polyamide for Laser-Based Powder Bed Fusion. *Procedia CIRP* **111**, 51–54. ISSN: 22128271 (2022).
68. Satya Hanush, S. & Manjaiah, M. Topology optimization of aerospace part to enhance the performance by additive manufacturing process. *Materials Today: Proceedings* **62**, 7373–7378. ISSN: 2214-7853 (Jan. 2022).
69. Török, D. *et al.* Laser powder bed fusion and casting for an advanced hybrid prototype mold. *Journal of Manufacturing Processes* **81**, 748–758. ISSN: 1526-6125 (Sept. 2022).
70. Minguella-Canela, J., Morales Planas, S., de Medina Iglesias, V. C. & de los Santos López, M. A. Quantitative analysis of the effects of incorporating laser powder bed fusion manufactured conformal cooling inserts in steel moulds over four types of defects of a commercially produced injected part. *Journal of Materials Research and Technology* **23**, 5423–5439. ISSN: 2238-7854 (Mar. 2023).
71. Dahmen, T. *Additive Manufacturing for Fuel Injectors: Design, Processes and Materials* eng. PhD thesis (2021).



72. 3D SYSTEMS. *Selective Laser Sintering* <https://www.3dsystems.com/selective-laser-sintering> (Date accessed 17/06/2023).
73. DediBot. *Nylon 3D Printing Equipment* <https://www.dedibot.com/en/product/detail/23> (Date accessed 17/06/2023).
74. E-Plus-3D. *EP-P420 SLS 3D Printer* <https://www.eplus3d.com/products/ep-p420-sls-3d-printer/> (Date accessed 17/06/2023).
75. EOS. *Polymer 3D Printing: The EOS SLS Process* <https://www.eos.info/en/industrial-3d-printer/plastic> (Date accessed 17/06/2023).
76. FARSOON. *Plastic 3D Printing Solutions* <https://www.farsoon-gl.com/plastic-3d-printing-solutions/> (Date accessed 17/06/2023).
77. LASERADD. *LASERADD-SLS-400* <https://www.laseradd.com/en/laseradd-sls-400/> (Date accessed 17/06/2023).
78. nexa3D. *SLS 3D Printers* <https://nexa3d.com/> (Date accessed 17/06/2023).
79. PRODWAYS. *Plastic laser sintering SLS® 3D printing* <https://www.prodways.com/en/technologie/laser-sintering-en/> (Date accessed 17/06/2023).
80. ProtoFab. *SLS 3D Printer* <https://www.3dprotofab.com/sls-3d-printer/> (Date accessed 17/06/2023).
81. Sindoh. *Sindoh S100* <https://3dprinter.sindoh.com/en/product/s100> (Date accessed 17/06/2023).
82. SINTERIT. *Compact and Industrial SLS 3D printers* <https://sinterit.com/3dprinters/> (Date accessed 17/06/2023).
83. SINRATEC. *Professional SLS 3D printers* <https://sinratec.com/> (Date accessed 17/06/2023).
84. TPM3D. *TPM3D SLS Series* <https://english.tpm3d.com/index.php?m=content&c=index&a=lists&catid=10> (Date accessed 17/06/2023).
85. Weirather. *Weirather Laser Sintering 3232* <https://www.weirather.com/en/products/weirather-laser-sintering-3232/> (Date accessed 17/06/2023).
86. XYZ Printing. *Powder Based Series* <https://pro.xyzprinting.com/en-US/3d-printer#powder-base-series> (Date accessed 17/06/2023).
87. ZRapid Tech. *SLS 3D Printer* <http://www.zero-tek.com/en/sls.html> (Date accessed 17/06/2023).
88. formlabs. *Fuse Series* <https://formlabs.com/eu/3d-printers/fuse-1/> (Date accessed 17/06/2023).
89. Red Rock 3D. *Desktop SLS printer Red Rock 3D* <http://www.redrocksls.com/> (Date accessed 17/06/2023).



90. SHAREBOT. *Sharebot SnowWhite2* <https://www.sharebot.it/stampanti/snowwhite-2/> (Date accessed 17/06/2023).
91. wematter. *Wematter Gravity SLS 3D printer* <https://wematter3d.com/gravity-sls-3d-printer/> (Date accessed 17/06/2023).
92. Wang, L., Tang, D., Ji, X., Zhang, W., Jiang, H., Wang, Y., Li, Y. & Qin, W. Influence of Laser Beam Profiles on the Performance of Laser-Driven Flyers. eng. *Propellants, Explosives, Pyrotechnics* **46**, 61–66. ISSN: 15214087, 07213115 (2021).
93. Oulundsen, G., Newman, L., Shi, C. & Ermold, M. CO LASERS ENABLE UNIQUE PROCESSES. *The Laser User*, 22–23. [www.coherent.com](http://www.coherent.com) (2018).
94. Wegner, A. in *Handbooks in Advanced Manufacturing* 33–75 (2021). ISBN: 9780128184110. <https://doi.org/10.1016/B978-0-12-818411-0.00011-2>.
95. Soldner, D., Greiner, S., Burkhardt, C., Drummer, D., Steinmann, P. & Mergheim, J. Numerical and experimental investigation of the isothermal assumption in selective laser sintering of PA12. *Additive Manufacturing* **37**, 101676. ISSN: 2214-8604 (Jan. 2021).
96. Neugebauer, F., Ploshikhin, V., Ambrosy, J. & Witt, G. Isothermal and non-isothermal crystallization kinetics of polyamide 12 used in laser sintering. *Journal of Thermal Analysis and Calorimetry* **124**, 925–933. ISSN: 15882926 (May 2016).
97. Drummer, D., Rietzel, D. & Kühnlein, F. Development of a characterization approach for the sintering behavior of new thermoplastics for selective laser sintering. *Physics Procedia* **5**, 533–542. ISSN: 1875-3892 (Jan. 2010).
98. Chen, P. *et al.* Crystallization kinetics of polyetheretherketone during high temperature-selective laser sintering. *Additive Manufacturing* **36**, 101615. ISSN: 2214-8604 (Dec. 2020).
99. Brydson, J. in *Plastics Materials* 59–75 (Butterworth-Heinemann, Jan. 1999). ISBN: 978-0-7506-4132-6.
100. Brydson, J. in *Plastics Materials* 158–183 (Butterworth-Heinemann, Jan. 1999). ISBN: 978-0-7506-4132-6.
101. Hesse, N., Jaksch, A., Kaschta, J., Groh, D., Drummer, D., Peukert, W. & Schmidt, J. From trash to treasure in additive manufacturing: Recycling of polymer powders by acid catalyzed hydrolysis. *Additive Manufacturing* **71**, 103591. <https://doi.org/10.1016/j.addma.2023.103591> (2023).
102. Yang, F., Zobeiry, N., Mamidala, R. & Chen, X. *A review of aging, degradation, and reusability of PA12 powders in selective laser sintering additive manufacturing* Mar. 2023.

103. Okamba-Diogo, O., Richaud, E., Verdu, J., Fernagut, F., Guilment, J. & Fayolle, B. Investigation of polyamide 11 embrittlement during oxidative degradation. *Polymer* **82**, 49–56. ISSN: 0032-3861 (Jan. 2016).
104. Schmid, M., Vetterli, M. & Wegener, K. Polymer powders for laser-sintering: Powder production and performance qualification. *AIP Conference Proceedings* **2065**. ISSN: 15517616 (2019).
105. Schmid, M., Kleijnen, R., Vetterli, M. & Wegener, K. Influence of the origin of polyamide 12 powder on the laser sintering process and laser sintered parts. *Applied Sciences (Switzerland)* **7**. ISSN: 20763417 (2017).
106. He, Z., Ren, C., Zhang, A. & Bao, J. Preparation and properties of styrene ethylene butylene styrene / polypropylene thermoplastic elastomer powder for selective laser sintering 3D printing. *Journal of Applied Polymer Science* **138**, 50908. ISSN: 1097-4628. <https://onlinelibrary.wiley.com/doi/full/10.1002/app.50908> <https://onlinelibrary.wiley.com/doi/abs/10.1002/app.50908> <https://onlinelibrary.wiley.com/doi/10.1002/app.50908> (Sept. 2021).
107. Averardi, A., Cola, C., Zeltmann, S. E. & Gupta, N. Effect of particle size distribution on the packing of powder beds: A critical discussion relevant to additive manufacturing. *Materials Today Communications* **24**, 100964. ISSN: 2352-4928 (Sept. 2020).
108. Schmidt, J., Sachs, M., Fanselow, S., Wirth, K. E. & Peukert, W. New approaches towards production of polymer powders for selective laser beam melting of polymers. *AIP Conference Proceedings* **1914**. ISSN: 15517616. /aip / acp / article / 1914 / 1 / 190008 / 858927 / New - approaches - towards - production - of - polymer (Dec. 2017).
109. Schmidt, J., Dechet, M., Bonilla, J. G., Kloos, S., Wirth, K. E. & Peukert, W. *Novel process routes towards the production of spherical polymer powders for selective laser sintering in AIP Conference Proceedings* **2139** (American Institute of Physics Inc., Aug. 2019). ISBN: 9780735418820.
110. Dechet, M. A., Baumeister, I. & Schmidt, J. Development of Polyoxymethylene Particles via the Solution-Dissolution Process and Application to the Powder Bed Fusion of Polymers. *Materials* **2020**, Vol. 13, Page 1535 **13**, 1535. ISSN: 1996-1944. <https://www.mdpi.com/1996-1944/13/7/1535> <https://www.mdpi.com/1996-1944/13/7/1535> (Mar. 2020).
111. Dechet, M. A., Kloos, S., Peukert, W. & Schmidt, J. *Production of spherical micron-sized polymer particles for additive manufacturing by liquid phase processes in AIP Conference Proceedings* **2055** (American Institute of Physics Inc., Jan. 2019). ISBN: 9780735417830.

112. Fanselow, S., Schmidt, J., Wirth, K. E. & Peukert, W. *Production of micron-sized polymer particles for additive manufacturing by melt emulsification in AIP Conference Proceedings* **1713** (American Institute of Physics Inc., Mar. 2016). ISBN: 9780735413603.
113. Kleijnen, R. G., Schmid, M. & Wegener, K. Production and processing of a spherical polybutylene terephthalate powder for laser sintering. *Applied Sciences (Switzerland)* **9**. ISSN: 20763417 (2019).
114. Israelachvili, J. N. in *Intermolecular and Surface Forces, Third Edition* 1–674 (Elsevier, Jan. 2010). ISBN: 9780123751829. <http://p5070-www.sciencedirect.com.proxy.findit.cvt.dk/book/9780123751829/intermolecular-and-surface-forces?via=ihub=>.
115. Schmidt, J. & Peukert, W. Dry powder coating in additive manufacturing. *Frontiers in Chemical Engineering* **4**, 995221. ISSN: 2673-2718 (Sept. 2022).
116. Blümel, C. *et al.* Increasing flowability and bulk density of PE-HD powders by a dry particle coating process and impact on LBM processes. *Rapid Prototyping Journal* **21**, 697–704. ISSN: 1355-2546. [www.emeraldinsight.com/1355-2546.htm](http://www.emeraldinsight.com/1355-2546.htm) (2015).
117. Tischer, F., Düsenberg, B., Gräser, T., Kaschta, J., Schmidt, J. & Peukert, W. Abrasion-Induced Acceleration of Melt Crystallisation of Wet Comminuted Polybutylene Terephthalate (PBT). *Polymers* **14**. ISSN: 20734360 (Feb. 2022).
118. Xi, S., Zhang, P., Huang, Y., Kong, M., Yang, Q. & Li, G. Laser sintering of cryogenically ground polymer powders into high-performance parts: The role of dry particle coating with a conductive flow agent. *Polymer* **186**, 122044. ISSN: 0032-3861 (Jan. 2020).
119. Hupfeld, T., Sommereyns, A., Riahi, F., Doñate-Buendía, C., Gann, S., Schmidt, M., Gökce, B. & Barcikowski, S. Analysis of the nanoparticle dispersion and its effect on the crystalline microstructure in carbon-additivated PA12 feedstock material for laser powder bed fusion. *Materials* **13**. ISSN: 19961944 (Aug. 2020).
120. Hupfeld, T. *et al.* 3D printing of magnetic parts by laser powder bedfusion of iron oxide nanoparticle functionalized polyamide powders. *Journal of Materials Chemistry C* **8**, 12204 (2020).
121. Brandau, B., Da Silva, A., Wilsnack, C., Brueckner, F. & Kaplan, A. F. Absorbance study of powder conditions for laser additive manufacturing. *Materials & Design* **216**, 110591. ISSN: 0264-1275 (Apr. 2022).
122. Yao, X. X. & Zhang, Z. Laser-particle interaction-based heat source model of laser powder bed fusion additive manufacturing. *Optics & Laser Technology* **155**, 108402. <https://doi.org/10.1016/j.optlastec.2022.108402> (2022).

123. Ho, H. C. H., Cheung, W. L. & Gibson, I. Effects of graphite powder on the laser sintering behaviour of polycarbonate. *Rapid Prototyping* **8**, 233–242. <http://www.emeraldinsight.com/researchregistershttp://www.emeraldinsight.com/1355-2546.htm> (2002).
124. Kumar, S. in *Comprehensive Materials Processing* 93–134 (Elsevier, Jan. 2014). ISBN: 9780080965338.
125. Schmid, M. LS Materials: Polymer Properties. *Laser Sintering with Plastics*, 65–99 (2018).
126. Wen, J., Huang, D., Li, Y., Yu, X., Zhang, X., Meng, X., Cong, C. & Zhou, Q. Investigations of Thermal, Mechanical, and Gas Barrier Properties of PA11-SiO<sub>2</sub> Nanocomposites for Flexible Riser Application. *Polymers* **14**. <https://doi.org/10.3390/polym14204260> (2022).
127. Shen, F., Yuan, S., Kai Chua, C. & Zhou, K. Development of process efficiency maps for selective laser sintering of polymeric composite powders: Modeling and experimental testing. *Journal of Materials Processing Tech.* **254**, 52–59. <https://doi.org/10.1016/j.jmatprotec.2017.11.027> (2017).
128. Southon, N., Stavroulakis, P., Goodridge, R. & Leach, R. In-process measurement and monitoring of a polymer laser sintering powder bed with fringe projection. *Materials & Design* **157**, 227–234. ISSN: 0264-1275 (Nov. 2018).
129. Ho, H. C. H., Gibson, I. & Cheung, W. L. Effects of energy density on morphology and properties of selective laser sintered polycarbonate. *Journal of Materials Processing Technology* **89**, 204–210 (1999).
130. Buhairi, M. A. *et al.* Review on volumetric energy density: influence on morphology and mechanical properties of Ti6Al4V manufactured via laser powder bed fusion Apr. 2022.
131. Goodridge, R. D., Tuck, C. J. & Hague, R. J. Laser sintering of polyamides and other polymers. *Progress in Materials Science* **57**, 229–267. ISSN: 0079-6425 (Feb. 2012).
132. Gibson, I. & Shi, D. Material properties and fabrication parameters in selective laser sintering process. *Rapid Prototyping Journal* **3**, 129–136. ISSN: 13552546 (1997).
133. Hann, D. B., Iammi, J. & Folkes, J. A simple methodology for predicting laser-weld properties from material and laser parameters. *Journal of Physics D: Applied Physics* **44**, 445401–445410 (2011).

134. Ghasemi-Tabasi, H., Jhabvala, J., Boillat, E., Ivas, T., Drissi-Daoudi, R. & Logé, R. E. An effective rule for translating optimal selective laser melting processing parameters from one material to another. *Additive Manufacturing* **36**, 101496. ISSN: 2214-8604 (Dec. 2020).
135. Forien, J. B., Calta, N. P., DePond, P. J., Guss, G. M., Roehling, T. T. & Matthews, M. J. Detecting keyhole pore defects and monitoring process signatures during laser powder bed fusion: A correlation between in situ pyrometry and ex situ X-ray radiography. *Additive Manufacturing* **35**, 101336. ISSN: 2214-8604 (Oct. 2020).
136. Gullipalli, C., Thawari, N., Burad, P. & Gupta, T. V. Influence of normalized enthalpy on inconel 718 morphology in direct metal deposition. *Proceedings of the Institution of Mechanical Engineers, Part E: Journal of Process Mechanical Engineering*. ISSN: 20413009 (2022).
137. Berez, J., Jost, E., Dushaj, E. & Saldaña, C. MEASUREMENT OF LASER FOCAL PLANE ERROR IN LASER POWDER BED FUSION SYSTEMS. eng. *2022 Aspe and Euspen Summer Topical Meeting on Advancing Precision in Additive Manufacturing*, 175–179 (2022).
138. Starr, T. L., Gornet, T. J. & Usher, J. S. The effect of process conditions on mechanical properties of laser-sintered nylon. *Rapid Prototyping Journal*, 418–423. [www.emeraldinsight.com/1355-2546.htm](http://www.emeraldinsight.com/1355-2546.htm) (2011).
139. Yamauchi, Y., Kigure, T. & Niino, T. Quantification of supplied laser energy and its relationship with powder melting process in PBF-LB/P using near-infrared laser. *Journal of Manufacturing Processes* **99**, 272–282. <https://doi.org/10.1016/j.jmapro.2023.05.002> (2023).
140. Williams, J. D. & Deckard, C. R. Advances in modeling the effects of selected parameters on the SLS process. *Rapid Prototyping Journal* **4**, 90–100. ISSN: 13552546 (1998).
141. Dörmann, M. & Schmid, H. J. *Simulation of capillary bridges between particles in Procedia Engineering* **102** (Elsevier Ltd, 2015), 14–23. [www.sciencedirect.com](http://www.sciencedirect.com).
142. Kruth, J.-P., Mercelis, P., Van Vaerenbergh, J., Froyen, L. & Rombouts, M. Binding mechanisms in selective laser sintering and selective laser melting. *Rapid Prototyping Journal* **11**, 26–36 (2005).
143. Blok, L. G., Longana, M. L., Yu, H. & Woods, B. K. An investigation into 3D printing of fibre reinforced thermoplastic composites. *Additive Manufacturing* **22**, 176–186. ISSN: 22148604 (Aug. 2018).
144. Deckard, C. & Beaman, J. J. Process and control issues in selective laser sintering. eng. *American Society of Mechanical Engineers, Production Engineering Division (publication) Ped* **33**, 191–197. ISSN: 08876150 (1988).

145. Miao, G., Du, W., Pei, Z. & Ma, C. A literature review on powder spreading in additive manufacturing. *Additive Manufacturing* **58**, 103029. ISSN: 2214-8604 (Oct. 2022).
146. Haferkamp, L., Haudenschild, L., Spierings, A., Wegener, K., Riener, K., Ziegelmeier, S. & Leichtfried, G. J. The Influence of Particle Shape, Powder Flowability, and Powder Layer Density on Part Density in Laser Powder Bed Fusion. *Metals* **2021**, Vol. 11, Page 418 **11**, 418. ISSN: 2075-4701. <https://www.mdpi.com/2075-4701/11/3/418/htm%20https://www.mdpi.com/2075-4701/11/3/418> (Mar. 2021).
147. Mussatto, A., Groarke, R., O'Neill, A., Obeidi, M. A., Delaure, Y. & Brabazon, D. Influences of powder morphology and spreading parameters on the powder bed topography uniformity in powder bed fusion metal additive manufacturing. *Additive Manufacturing* **38**, 101807. ISSN: 22148604. <https://doi.org/10.1016/j.addma.2020.101807> (2021).
148. Wang, L., Yu, A., Li, E., Shen, H. & Zhou, Z. Effects of spreader geometry on powder spreading process in powder bed additive manufacturing. *Powder Technology* **384**, 211–222. ISSN: 1873328X (May 2021).
149. Han, W., Kong, L. & Xu, M. Advances in selective laser sintering of polymers. *IMMT International Journal of Extreme Manufacturing Int. J. Extrem. Manuf* **4**. <https://doi.org/10.1088/2631-7990/ac9096> (2022).
150. Haeri, S. Optimisation of blade type spreaders for powder bed preparation in Additive Manufacturing using DEM simulations. *Powder Technology* **321**, 94–104. ISSN: 0032-5910 (Nov. 2017).
151. Beitz, S., Uerlich, R., Bokelmann, T., Diener, A., Vietor, T. & Kwade, A. Influence of Powder Deposition on Powder Bed and Specimen Properties. *Materials* **12**, 1–19. [www.mdpi.com/journal/materials](http://www.mdpi.com/journal/materials) (2019).
152. Chen, H., Chen, Y., Liu, Y., Wei, Q., Shi, Y. & Yan, W. Packing quality of powder layer during counter-rolling-type powder spreading process in additive manufacturing. *International Journal of Machine Tools and Manufacture* **153**, 103553. ISSN: 0890-6955 (June 2020).
153. Zhang, J., Tan, Y., Bao, T., Xu, Y., Xiao, X. & Jiang, S. Discrete Element Simulation of the Effect of Roller-Spreading Parameters on Powder-Bed Density in Additive Manufacturing. *Materials* **13**, 1–15. [www.mdpi.com/journal/materials](http://www.mdpi.com/journal/materials) (May 2020).
154. Haeri, S., Wang, Y., Ghita, O. & Sun, J. Discrete element simulation and experimental study of powder spreading process in additive manufacturing. *Powder Technology* **306**, 45–54. ISSN: 0032-5910 (Jan. 2017).



155. Meyer, L., Wegner, A. & Witt, G. *Influence of the Ratio between the Translation and Contra-Rotating Coating Mechanism on different Laser Sintering Materials and their Packing Density in Solid Freeform Fabrication symposium* (2017), 1432–1447.
156. Fish, S., Booth, J. C., Kubiak, S. T., Wroe, W. W., Bryant, A. D., Moser, D. R. & Beaman, J. J. Design and subsystem development of a high temperature selective laser sintering machine for enhanced process monitoring and control. *Additive Manufacturing* **5**, 60–67. ISSN: 22148604. <http://dx.doi.org/10.1016/j.addma.2014.12.005> (2015).
157. Sanders, B., Cant, E., Amel, H. & Jenkins, M. The Effect of Physical Aging and Degradation on the Re-Use of Polyamide 12 in Powder Bed Fusion. *Polymers* **14**. <https://doi.org/10.3390/polym14132682> (2022).
158. Tamura, A., Fujita, T. & Takeuchi, A. Selective powder feeding system in additive manufacturing using laser-induced forward transfer technique. *Additive Manufacturing* **46**, 102226. ISSN: 2214-8604 (Oct. 2021).
159. Neirinck, B., Li, X. & Hick, M. Powder Deposition Systems Used in Powder Bed-Based Multimetal Additive Manufacturing. *Accounts of Materials Research* **2**, 387–393. <https://doi.org/10.1021/accountsmr.1c00030> (2021).
160. Tampi, T. *Columbia researchers develop multi-material SLS 3D printer without powder bed - 3dprint.com: The Voice of 3D printing / Additive Manufacturing* <https://3dprint.com/271117/columbia-researchers-develop-multi-material-sls-3d-printer-without-powder-bed/> (Date accessed: 06/06-2023, Oct. 2021).
161. Whitehead, J. & Lipson, H. Inverted multi-material laser sintering. *Additive Manufacturing* **36**. <https://doi.org/10.1016/j.addma.2020.101440> (2020).
162. Drummer, D., Greiner, S., Zhao, M. & Wudy, K. A novel approach for understanding laser sintering of polymers. *Additive Manufacturing* **27**, 379–388. <https://doi.org/10.1016/j.addma.2019.03.012> (2019).
163. Josupeit, S. & Schmid, H. J. Temperature history within laser sintered part cakes and its influence on process quality. *Rapid Prototyping Journal* **22**, 788–793. ISSN: 13552546 (2016).
164. Greiner, S., Jaksch, A. & Drummer, D. *Understanding Cylinder Temperature Effects in Laser Beam Melting of Polymers in 1st International Joint Conference on Enhanced Material and Part Optimization and Process Intensification* (2021), 123–141. [https://doi.org/10.1007/978-3-030-70332-5\\_12](https://doi.org/10.1007/978-3-030-70332-5_12).



165. Baranowski, M., Völger, L., Friedmann, M. & Fleischer, J. Experimental Analysis and Optimisation of a Novel Laser-Sintering Process for Additive Manufacturing of Continuous Carbon Fibre-Reinforced Polymer Parts. *Applied sciences* **13**. <https://doi.org/10.3390/app13095351> (2023).
166. Lanzl, L., Wudy, K., Greiner, S. & Drummer, D. Selective laser sintering of copper filled polyamide 12: Characterization of powder properties and process behavior. *Polymer Composites* **40**, 1801–1809. ISSN: 1548-0569. <https://onlinelibrary-wiley-com.proxy.findit.cvt.dk/doi/full/10.1002/pc.24940> <https://onlinelibrary-wiley-com.proxy.findit.cvt.dk/doi/abs/10.1002/pc.24940> <https://4spepublications-onlinelibrary-wiley-com.proxy.findit.cvt.dk/doi/10.1002/pc.24940> (May 2019).
167. Diller, T. T., Sreenivasan, R., Beaman, J., Bourell, D. & Larocco, J. *Thermal Model of the Build Environment for Polyamide Powder Selective Laser Sintering in SFF Symposium Preceedings* (2010), 539–548.
168. Dadbakhsh, S., Verbelen, L., Verkinderen, O., Strobbe, D., Van Puyvelde, P. & Kruth, J. P. Effect of PA12 powder reuse on coalescence behaviour and microstructure of SLS parts. *European Polymer Journal* **92**, 250–262. ISSN: 0014-3057 (July 2017).
169. Wudy, K. & Drummer, D. Aging effects of polyamide 12 in selective laser sintering: Molecular weight distribution and thermal properties. *Additive Manufacturing* **25**, 1–9. ISSN: 2214-8604 (Jan. 2019).
170. Silfvast, W. T. in *Encyclopedia of Physical Science and Technology* 267–281 (Academic Press, Jan. 2003). <https://linkinghub.elsevier.com/retrieve/pii/B012227410500363X>.
171. Goodridge, R. & Ziegelmeier, S. in *Laser Additive Manufacturing: Materials, Design, Technologies, and Applications* 181–204 (Woodhead Publishing, Jan. 2017). ISBN: 9780081004340.
172. Patel, C. K., Tien, P. K. & McFee, J. H. CW HIGH-POWER CO<sub>2</sub>-N<sub>2</sub>-He LASER. *Applied Physics Letters* **7**, 290–292. ISSN: 0003-6951. [/aip/apl/article/7/11/290/65293/CW-HIGH-POWER-CO2-N2-He-LASER](https://aip/apl/article/7/11/290/65293/CW-HIGH-POWER-CO2-N2-He-LASER) (Dec. 1965).
173. FARSOON. *FLIGHT 403P Series* <https://www.farsoon-gl.com/products/flight-403p-series/> (Date accessed 08/06/2023).
174. EOS. *Formiga P 110 FDR - high detail resolution* <https://www.eos.info/en/industrial-3d-printer/plastic/formiga-p-110-fdr> (Date accessed 08/06/2023).
175. Davies, S. *Eos introduces fine detail resolution polymer 3D Printer & Sustainable Materials* Nov. 2022. <https://www.tctmagazine.com/additive-manufacturing-3d-printing-news/polymer-additive-manufacturing-news/eos-introduces-fine-detail-resolution-polymer-3d-printer-sus/>.

176. Peels, J. *Farsoon unveils dual fiber laser 403p powder bed fusion 3D printer - 3dprint.com: The Voice of 3D printing / additive manufacturing* May 2021. <https://3dprint.com/281884/farsoon-unveils-dual-fiber-laser-403p-powder-bed-fusion-3d-printer/>.
177. Hohnholz, A., Rettschlag, K., Desens, M., Taschner, P. A. & Overmeyer, L. in *Handbook of Laser Micro- and Nano-Engineering* 1–37 (Springer International Publishing, 2020). ISBN: 9783030636470. [https://link.springer.com/referenceworkentry/10.1007/978-3-319-69537-2\\_4-1](https://link.springer.com/referenceworkentry/10.1007/978-3-319-69537-2_4-1).
178. Andrew Held. *New Co Laser Technology offers processing benefits* Sept. 2015. [https://www.photonics.com/Articles/New\\_CO\\_Laser\\_Technology\\_Offers\\_Processing\\_Benefits/a57681](https://www.photonics.com/Articles/New_CO_Laser_Technology_Offers_Processing_Benefits/a57681).
179. THORLABS. *Can the thin-lens equation be used with laser light?* (Date accessed 02/08/2023, 2021).
180. Gregory, B. A. in *Encyclopedia of Physical Science and Technology* 1–37 (Academic Press, Jan. 2003).
181. Chatham, C. A., Long, T. E. & Williams, C. B. A review of the process physics and material screening methods for polymer powder bed fusion additive manufacturing. *Progress in Polymer Science* **93**, 68–95. <https://doi.org/10.1016/j.progpolymsci.2019.03.003> (2019).
182. Lexow, M. M., Drexler, M. & Drummer, D. Fundamental investigation of part properties at accelerated beam speeds in the selective laser sintering process. *Rapid Prototyping Journal*. [www.emeraldinsight.com/1355-2546.htm](http://www.emeraldinsight.com/1355-2546.htm) (2017).
183. Shi, W., Fang, Q., Zhu, X., Norwood, R. A. & Peyghambarian, N. Fiber lasers and their applications [Invited]. *Applied Optics* **53**, 6554–6568. ISSN: 2155-3165. <https://opg.optica.org/viewmedia.cfm?uri=ao-53-28-6554&seq=0&html=true%20https://opg.optica.org/abstract.cfm?uri=ao-53-28-6554%20https://opg.optica.org/ao/abstract.cfm?uri=ao-53-28-6554> (Oct. 2014).
184. Koester, C. J. & Snitzer, E. Amplification in a Fiber Laser. *Applied Optics* **3**, 1182–1186. ISSN: 2155-3165. <https://opg.optica.org/viewmedia.cfm?uri=ao-3-10-1182&seq=0&html=true%20https://opg.optica.org/abstract.cfm?uri=ao-3-10-1182%20https://opg.optica.org/ao/abstract.cfm?uri=ao-3-10-1182> (Oct. 1964).
185. Poole, S. B., Payne, D. N. & Fermann, M. E. Fabrication of Low-Loss Optical Fibres Containing Rare-Earth Ions. *Electronics letters* **21**, 737–738 (1985).
186. Ter-Mikirtychev, V. V. in *Fundamentals of fiber lasers and fiber amplifiers* (2019). ISBN: 30338909\_11. [https://doi.org/10.1007/978-3-030-33890-9\\_11](https://doi.org/10.1007/978-3-030-33890-9_11).

187. Novikov, A., Usenov, I., Artyushenko, V., Eichler, H.-J. & Novikov, A. S. *CO and CO<sub>2</sub> laser beam guiding with silver halide polycrystalline fibers and hollow waveguides* in *XXIII International Symposium on High Power Laser Systems and Applications* **12347** (SPIE, Nov. 2022), 44–51. ISBN: 9781510657670. [https://www-spiedigitallibrary-org.proxy.findit.cvt.dk/conference-proceedings-of-spie/12347/1234706/CO-and-CO<sub>2</sub>-laser-beam-guiding-with-silver-halide-polycrystalline/10.1117/12.2656305.full%20https://www-spiedigitallibrary-org.proxy.findit.cvt.dk/conference-proceedings-of-spie/12347/1234706/CO-and-CO<sub>2</sub>-laser-beam-guiding-with-silver-halide-polycrystalline/10.1117/12.2656305.short](https://www-spiedigitallibrary-org.proxy.findit.cvt.dk/conference-proceedings-of-spie/12347/1234706/CO-and-CO2-laser-beam-guiding-with-silver-halide-polycrystalline/10.1117/12.2656305.full%20https://www-spiedigitallibrary-org.proxy.findit.cvt.dk/conference-proceedings-of-spie/12347/1234706/CO-and-CO2-laser-beam-guiding-with-silver-halide-polycrystalline/10.1117/12.2656305.short).
188. Samson, B. & Dong, L. Fiber lasers. *Handbook of Solid-State Lasers: Materials, Systems and Applications*, 403–462 (Jan. 2013).
189. Schmidt, M., Merklein, M., Bourell, D., Dimitrov, D., Hausotte, T., Wegener, K., Vollertsen, F. & Levy, G. N. Laser based additive manufacturing in industry and academia. *CIRP Annals - Manufacturing Technology* **66**, 561–583. <http://dx.doi.org/10.1016/j.cirp.2017.05.011> (2017).
190. Liang, Y. J., Liu, F., Chen, Y. F., Wang, X. J., Sun, K. N. & Pan, Z. New function of the Yb<sup>3+</sup> ion as an efficient emitter of persistent luminescence in the short-wave infrared. *Light: Science & Applications* **2016 5:7 5**, e16124–e16124. ISSN: 2047-7538. <https://www.nature.com/articles/lisa2016124> (Mar. 2016).
191. Saifi, M. Optical Amplifiers. *Encyclopedia of Materials: Science and Technology*, 6416–6423. <https://linkinghub.elsevier.com/retrieve/pii/B0080431526011359> (Jan. 2001).
192. Silva, L. C. & Segatto, M. E. Advances in multi-wavelength Brillouin fiber lasers: An outlook across different spectral regions. *Optical Fiber Technology* **76**, 103246. ISSN: 1068-5200 (Mar. 2023).
193. Larionov, I. A., Gulyashko, A. S. & Tyrtyschnyy, V. A. Tunable Near 3- $\mu$ m Difference Frequency Generation Using Ytterbium and Broadband Seed Erbium Fiber Lasers. *2019 Conference on Lasers and Electro-Optics Europe and European Quantum Electronics Conference (2019), paper cd\_p\_19*. [https://opg.optica.org/abstract.cfm?uri=CLEO\\_Europe-2019-cd\\_p\\_19](https://opg.optica.org/abstract.cfm?uri=CLEO_Europe-2019-cd_p_19) (June 2019).
194. Larionov, I. A., Gulyashko, A. S. & Tyrtyschnyy, V. A. *Mid-infrared difference frequency generation of Er and Yb fiber lasers radiation in periodically poled crystals* in *CLEO Pacific Rim 2018* © OSA (2018). <https://ieeexplore-ieee-org.proxy.findit.cvt.dk/stamp/stamp.jsp?tp=&arnumber=8700010>.

195. Pandey, A. R., Powers, P. E. & Haus, J. W. Experimental performance of a two-stage periodically poled lithium niobate parametric amplifier. *IEEE Journal of Quantum Electronics* **44**, 203–208. ISSN: 00189197 (Mar. 2008).
196. Myers, L. E., Eckardt, R. C., Fejer, M. M., Byer, R. L., Bosenberg, W. R. & Pierce, J. W. Quasi-phase-matched optical parametric oscillators in bulk periodically poled LiNbO<sub>3</sub>. *J. Opt. Soc. Am. B* **12** (1995).
197. Larionov, I. A., Gulyashko, A. S. & Tyrtyschnyy, V. A. *PP-crystals Lengths Optimization to Improve the Efficiency of Two-Cascade Nearly-Degenerate DFG of 3 $\mu$ m Radiation from Fiber NIR Lasers in Conference on Lasers and Electro-Optics Europe and European Quantum Electronics Conference (2021), paper cd\_p\_32* (Optica Publishing Group, June 2021). ISBN: 978-1-6654-1876-8. [https://opg.optica.org/abstract.cfm?uri=CLEO\\_Europe-2021-cd\\_p\\_32](https://opg.optica.org/abstract.cfm?uri=CLEO_Europe-2021-cd_p_32).
198. Gulyashko, A. S., Larionov, I. A. & Tyrtyschnyy, V. A. Optimization of the efficient single pass two-stage DFG of Er and Yb fiber lasers radiation into mid-infrared region. eng. *2019 Conference on Lasers and Electro-optics Europe and European Quantum Electronics Conference, Cleo/europe-eqec 2019*, 8873059 (2019).
199. Ostapiv, A. Y., Tsympkin, V. P., Cherpak, P. S., Gulyashko, A. S., Larionov, I. A. & Tyrtyschnyy, V. A. *Pump and idler beams parameters dependence on pump power under conditions of mid-infrared difference frequency generation in PPLN in International Conference Laser Optics, ICLO 2022 - Proceedings* (Institute of Electrical and Electronics Engineers Inc., 2022). ISBN: 9781665466646.
200. Guerra, A. & de Ciurana, J. *Fibre laser cutting of polymer tubes for stents manufacturing in Manufacturing Engineering Society International Conference 2017*, (2017), 190–196.
201. Böhm, S., Schmidt, M., Stichel, T., Kahlmeyer, M., Kryukov, I. & Sommer, N. Single-step Laser Plastic Deposition (LPD) using a near-infrared Thulium fiber-laser. *Polymer Testing* **81**, 106185. ISSN: 0142-9418 (Jan. 2020).
202. Thiele, M., Kutlu, Y., Dobbstein, H., Petermann, M., Esen, C. & Ostendorf, A. Direct generation of 3D structures by laser polymer deposition. *Journal of Laser Applications* **33**, 022002. ISSN: 1042-346X (May 2021).
203. TREFFERT. *Laser Welding and Laser Marking of plastics* <https://treffert.eu/product-expertise/laserwelding-lasermarking-plastic/> (Date accessed 20/06/2023).
204. Kutlu, Y., Wencke, Y. L., Luinstra, G. A., Esen, C. & Ostendorf, A. *Directed Energy Deposition of PA12 carbon nanotube composite powder using a fiber laser in Procedia CIRP* **94** (Elsevier, Jan. 2020), 128–133.

205. Kumar Goyal, D., Yadav, R. & Kant, R. Laser transmission welding of polycarbonate sheets using electrolytic iron powder absorber. *Optics & Laser Technology* **161**, 109165. ISSN: 0030-3992 (June 2023).
206. Aden, M., Mamuschkin, V. & Olowinsky, A. Influence of carbon black and indium tin oxide absorber particles on laser transmission welding. *Optics & Laser Technology* **69**, 87–91. ISSN: 0030-3992 (June 2015).
207. Hartley, S., Sallavanti Scott Hartley, R. & Sallavanti, R. A. *Clearweld laser transmission welding of thermoplastic polymers: light transmission and color considerations* in *Third International Symposium on Laser Precision Microfabrication* **4830** (SPIE, Feb. 2003), 63–68. <https://www-spiedigitallibrary-org.proxy.findit.cvt.dk/conference-proceedings-of-spie/4830/0000/Clearweld-laser-transmission-welding-of-thermoplastic-polymers--light-transmission/10.1117/12.486516.full>.
208. Wittmann, A., Heberle, J., Huber, F. & Schmidt, M. Consolidation of thermoplastic coatings by means of a thulium-doped fiber laser. *Journal of Laser Applications* **33**, 042032. ISSN: 1042-346X (Nov. 2021).
209. Schembri, M., Sahu, J., Aboumarzouk, O., Pietropaolo, A. & Somani, B. K. Thulium fiber laser: The new kid on the block. *Turkish Journal of Urology* **46**, S1. ISSN: 21493057. </pmc/articles/PMC7731960/?report=abstract> (2020).
210. Barua, P., Clarkson, W. A., Jefferson-Brain, T. L., Burns, M. D., Shardlow, P. C. & Sahu, J. K. 47 W continuous-wave 1726 nm thulium fiber laser core-pumped by an erbium fiber laser. *Optics Letters* **44**, 5230–5233. ISSN: 1539-4794. <https://opg.optica.org/viewmedia.cfm?uri=ol-44-21-5230&seq=0&html=true%20https://opg.optica.org/abstract.cfm?uri=ol-44-21-5230%20https://opg.optica.org/ol/abstract.cfm?uri=ol-44-21-5230> (Nov. 2019).
211. 3D Systems. *White paper - How 3D Printing works* [https://www.officeproductnews.net/sites/default/files/3dWP\\_0.pdf](https://www.officeproductnews.net/sites/default/files/3dWP_0.pdf) (Date accessed 25/06/2023, 2012).
212. Andersen, S. A. *Open Architecture Laser Power Bed Additive Manufacturing* PhD thesis (2020).
213. Andersen, S. A., Meinert, K. Æ., Kjer, M. B., Nadimpalli, V. K. & Pedersen, D. B. A Unified System Controller for Open-Source Powder Bed Fusion Systems. eng. *Proceedings of the 33rd Annual International Solid Freeform Fabrication (sff) Symposium*, 1273–1285 (2022).
214. Thomas, M., Baxter, G. J. & Todd, I. Normalised model-based processing diagrams for additive layer manufacture of engineering alloys. *Acta Materialia* **108**, 26–35. ISSN: 1359-6454 (Apr. 2016).
215. MaxPhotonics. *MAXMaxphotonics Co.,Ltd.* <http://en.maxphotonics.com/product/18.html> (Date accessed: 04/08/2023).

216. Sunny Technologies. *S-9320A/D 2D Scanning Head* [http://www.sunny-technology.com/pro\\_con.aspx?type=143&id=850](http://www.sunny-technology.com/pro_con.aspx?type=143&id=850) (Date accessed: 04/08/2023).
217. Cloudray. *Cloudray K9 M85 Fiber Laser F-theta Scan Lens* <https://www.cloudraylaser.com/products/cloudray-k9-m85-fiber-laser-f-theta-scan-lens?variant=12869282431027> (Date Accessed 04/08/2023).
218. Watlow. *Silicone Rubber Heaters* <https://www.watlow.com/Products/Heaters/Flexible-Heaters/Silicone-Rubber-Heaters> (Date accessed 27/06/2023).
219. Niino, T., Haraguchi, H. & Itagaki, Y. *Feasibility study on plastic laser sintering without powder bed preheating in 22nd Annual International Solid Freeform Fabrication Symposium* (2011), 17–29.
220. Vuković, M., Budden, C. L., Calaon, M., Mazzei, D., Pedersen, D. B. & Fantoni, G. *External temperature and power consumption monitoring in an Open Architecture Polymer Laser Powder Bed Fusion in Special Interest Group Meeting: Advancing Precision in Additive Manufacturing, September 2023* (Leuven, 2023).
221. Budden, C. L., Meinert, K. Æ., Lalwani, A. R. & Pedersen, D. B. *Chamber Heat Calibration by Emissivity Measurements in an Open Source SLS system in ASPE and euspen Summer Topical Meeting Volume 77 77* (Knoxville, 2022), 180–185.
222. Greene, J. P. in *Automotive Plastics and Composites 27–37* (William Andrew Publishing, Jan. 2021). ISBN: 978-0-12-818008-2.
223. Scanlab. *Position Resolution | Scanlab* <https://www.scanlab.de/en/service/glossary/position-resolution> (Date accessed: 20/07/2023).
224. Thorlabs. *F-Theta Lenses Tutorial* [https://www.thorlabs.com/newgrouppage9.cfm?objectgroup\\_id=10766](https://www.thorlabs.com/newgrouppage9.cfm?objectgroup_id=10766) (Date accessed: 20/07/2023, 2023).
225. Baumann, F.-E. *Laser-sintering powder containing titanium dioxide particles, process for its preparation, and moldings produced therefrom* Aug. 2002.
226. Rao, K. G., Ashok, C. H., Rao, K. V., Chakra, C. S. & Rajendar, V. *Green synthesis of tio2 nanoparticles using hibiscus flower extract in Proceedings of the International Conference on Emerging Technologies in Mechanical Sciences* (2014), 79–82.
227. Pagliero, M., Alloisio, M., Costa, C., Firpo, R., Mideksa, E. A. & Comite, A. *Carbon Black/Polyvinylidene Fluoride Nanocomposite Membranes for Direct Solar Distillation. Energies 2022, Vol. 15, Page 740 15, 740.* ISSN: 1996-1073. <https://www.mdpi.com/1996-1073/15/3/740/htm%20https://www.mdpi.com/1996-1073/15/3/740> (Jan. 2022).



228. Han, D., Meng, Z., Wu, D., Zhang, C. & Zhu, H. Thermal properties of carbon black aqueous nanofluids for solar absorption. *Nanoscale Research Letters* **6**, 1–7. ISSN: 19317573. [https://www.researchgate.net/publication/51500474\\_Thermal\\_properties\\_of\\_carbon\\_black\\_aqueous\\_nanofluids\\_for\\_solar\\_absorption](https://www.researchgate.net/publication/51500474_Thermal_properties_of_carbon_black_aqueous_nanofluids_for_solar_absorption) (2011).
229. Budden, C. L., Lalwani, A. R., Meinert, K. Æ., Daugaard, A. E. & Pedersen, D. B. *Process optimisation of PA11 in fiber-laser powder-bed fusion through loading of an optical absorber* eng. in *Proceedings of the 33rd Annual International Solid Freeform Fabrication (sff) Symposium* (The University of Texas at Austin, Austin, 2022), 75–86.
230. Rhodes, M. J. *Principles of powder technology* XI, 439 S (unknown) (Wiley, 1990).
231. ISO. *Plastics — Determination of tensile properties — Part 2: Test conditions for moulding and extrusion plastics* tech. rep. (International Organization for Standardization, 2012).
232. formlabs. *Layer shifting (SLS)* <https://blog.sciencemuseum.org.uk/nylon-the-creation-of-a-revolutionary-fabric/> (Date accessed: 09/08/2023, 2023).
233. Budden, C. L., Kjer, M. B., Lalwani, A. R., Nadimpalli, V. K. & Pedersen, D. B. *Benchmarking of an Open Architecture Polymer Laser Powder Bed Fusion system* in *Special Interest Group Meeting: Advancing Precision in Additive Manufacturing, September 2023* (Leuven, 2023).
234. Moshiri, M. ; Tosello, G. ; & Mohanty, S. *General rights A new design for an extensive benchmarking of additive manufacturing machines A new design for an extensive benchmarking of additive manufacturing machines*. In *D A new design for an extensive benchmarking of additive manufacturing machines* in *Proceedings of the 18th International Conference of the european Society for Precision Engineering and Nanotechnology* (APA, 2018). [www.euspen.eu](http://www.euspen.eu).
235. Moshiri, M., Candeo, S., Carmignato, S., Mohanty, S. & Tosello, G. *Manufacturing and Materials Processing Benchmarking of Laser Powder Bed Fusion Machines*. [www.mdpi.com/journal/jmmp](http://www.mdpi.com/journal/jmmp) (2019).
236. Moshiri, M., Pedersen, D. B., Tosello, G. & Nadimpalli, V. K. Performance evaluation of in-situ near-infrared melt pool monitoring during laser powder bed fusion. *Virtual and Physical Prototyping* **18**. ISSN: 17452767. <https://www.tandfonline.com/action/journalInformation?journalCode=nvpp20> (2023).
237. Budden, C. L., Grønberg, F., Wolstrup, A. F., Lalwani, A. R., Zsurzsan, T. G., Daugaard, A. E. & Pedersen, D. B. *Simple sensor manufacturing by Laser Powder Bed Fusion of conductive polymer blends* in *euspen's 23rd International Conference & Exhibition, Copenhagen, DK, June 2023* (Copenhagen, 2023).



238. Grønberg, F., Zsurzsan, T. G., Daugaard, A. E., Spangenberg, J. & Pedersen, D. B. Conductive compliant mechanisms: Geometric tuning of 3D printed flexural sensors. *Additive Manufacturing Letters* **3**, 100088. ISSN: 2772-3690 (Dec. 2022).
239. Nguyen, N. P., Behrens, S., Brosda, M., Olowinsky, A. & Gillner, A. Laser transmission welding of absorber-free semi-crystalline polypropylene by using a quasi-simultaneous irradiation strategy. *Welding in the World* **64**, 1227–1235. ISSN: 18786669. <https://link.springer.com/article/10.1007/s40194-020-00913-3> (July 2020).
240. Wudy, K., Greiner, S., Zhao, M. & Drummer, D. Selective laser beam melting of polymers: In situ and offline measurements for process adapted thermal characterization. *Procedia CIRP* **74**, 238–243. ISSN: 2212-8271 (Jan. 2018).
241. Greiner, S., Wudy, K., Wörz, A. & Drummer, D. Thermographic investigation of laser-induced temperature fields in selective laser beam melting of polymers. *Optics & Laser Technology* **109**, 569–576. ISSN: 0030-3992 (Jan. 2019).
242. Schuffenhauer, T., Stichel, T. & Schmidt, M. Experimental determination of scattering processes in the interaction of laser radiation with polyamide 12 powder. *Procedia CIRP* **94**, 85–88. ISSN: 22128271 (2020).
243. AZO Materials. *Optimizing Polymeric Materials with Rheological Analysis* <https://www.azom.com/article.aspx?ArticleID=20979> (Date accessed 30/07/2023, 2021).
244. Mazan, T., Berggren, R., Jørgensen, J. K. & Echtermeyer, A. Aging of polyamide 11. Part 1: Evaluating degradation by thermal, mechanical, and viscometric analysis. *Journal of Applied Polymer Science* **132**. ISSN: 10974628. [https://www.researchgate.net/publication/271589932\\_Aging\\_of\\_polyamide\\_11\\_Part\\_1\\_Evaluating\\_degradation\\_by\\_thermal\\_mechanical\\_and\\_viscometric\\_analysis](https://www.researchgate.net/publication/271589932_Aging_of_polyamide_11_Part_1_Evaluating_degradation_by_thermal_mechanical_and_viscometric_analysis) (May 2015).
245. Berez, J., Saldaña, C. & Woodruff, G. W. *LASER LINE PROFILE SCANNING FOR POWDER BED TOPOGRAPHY MEASUREMENT* in *Proceedings of the 33rd Annual International Solid Freeform Fabrication Symposium – An Additive Manufacturing Conference* (2022), 1039–1051.
246. University of Cambridge. *Polymer Basics: Crystallinity* <https://www.doitpoms.ac.uk/tlplib/polymerbasics/index.php> (Date Accessed 08/08/2023).
247. Waring, S. *Nylon: the creation of a revolutionary fabric* <https://blog.sciencemuseum.org.uk/nylon-the-creation-of-a-revolutionary-fabric/> (Date accessed: 07/08/2023, 2018).

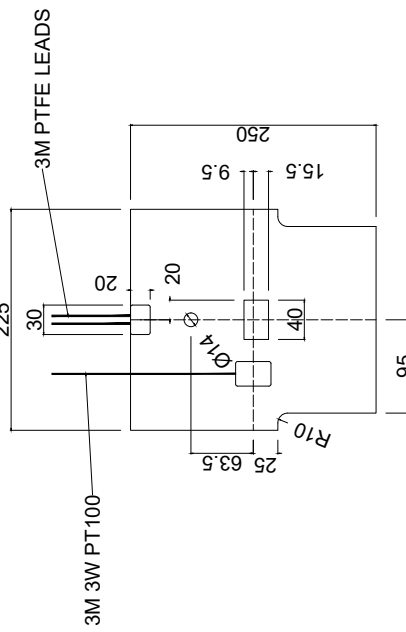
# Appendices



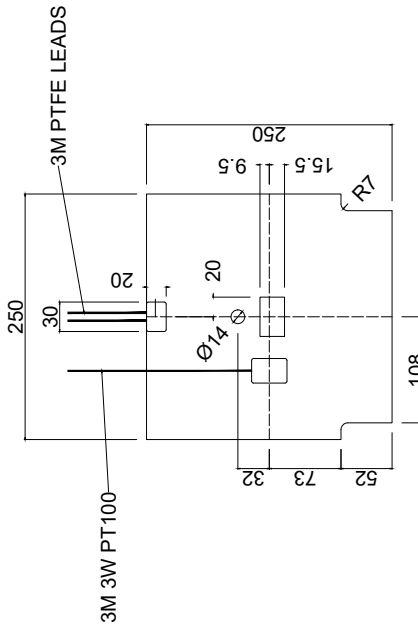
# APPENDIX A

## Technical drawings of the heaters installed in the developed system

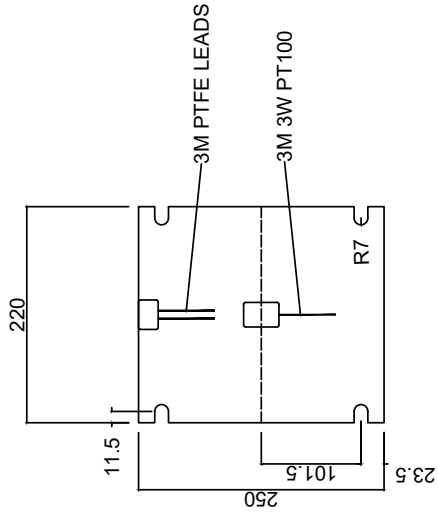
20-2889  
 230V 400W  
 DRAWING SHOWS LEAD EXIT FACE.  
 ADHESIVE ON REAR.



20-2890  
 230V 460W  
 DRAWING SHOWS LEAD EXIT FACE.  
 ADHESIVE ON REAR.



20-2891  
 230V 415W  
 DRAWING SHOWS LEAD EXIT FACE.  
 ADHESIVE ON REAR.



## **APPENDIX B**

# **Chamber Heat Calibration by Emissivity Measurements in an Open Source SLS System**

# Chamber Heat Calibration by Emissivity Measurements in an Open Source SLS System

Christian L. Budden<sup>1</sup>, Kenneth Æ. Meinert<sup>1</sup>, Aakil R. Lalwani<sup>1,2</sup>, and David B. Pedersen<sup>1</sup>

<sup>1</sup>Department of Mechanical Engineering, Technical University of Denmark  
2800 Kongens Lyngby DK

<sup>2</sup> The LEGO Group, 7190 Billund DK

## INTRODUCTION

The goal of this research is to determine the thermal stability of the powder cake produced during the Selective Laser Sintering process. This will be used for process optimisation and verification on a purpose-built Open Architecture Polymer laser powder-bed fusion (L-PBF) system developed at the Technical University of Denmark (DTU). Furthermore, the emissivity of PA11 powder is determined throughout the heating cycle, studying the true temperature readout by means of an infrared (IR) camera (Camera Model – Optris XI400), which is present for process control during build jobs.

The paper presents two experiments. One is focussing on finding the temperature stable build envelope in the build chamber. This is done by using K-type sensors placed in the powder while

heating and cooling the powder cake. And a second experiment is to determine the influence of powder temperature on emissivity, used for non-contact temperature readings done by infrared measurements. This will be used for calibrating the temperature readings with the actual temperature.

## EXPERIMENTAL SETUP

The Open Architecture Polymer L-PBF system at DTU is a rebuilt ProJet 4500 now re-engineered for Selective Laser Sintering materials investigation. The machine has been rebuilt in its entirety, only maintaining the stock mechanical powder handling subsystems, including the powder delivery, powder distribution, and the build piston axis of the machine. The entire system is controlled centrally by a unified systems controller [1], with the capability of controlling both linear motion, laser scan head, and laser power modulation. The chamber temperature control is currently controlled by six PID controllers (RED Lion PXU21A20) each managing one of the heating elements of the system. The heating elements are bespoke to the system and produced to match the layout of the build chamber, with four heating elements placed, one on each side, and one located below the build platform as presented in [Figure 1]. All the heating elements are designed with an energy density of  $0.77\text{w/cm}^2$ , resulting in total heating power of 2.1 kW. This is distributed to the build chamber from the five sides physically in contact with the powder cake. In addition to this, an open side is located on the top of the build chamber. Here two 400W ceramic heaters are placed. These are installed to heat newly distributed powder layers during the build cycle. The resulting heating power achieved on all six sides of the build-up powder cake is in the order of 2.9kW. One PID controller is installed for every heating element, taking the input temperature from a PT100 thermocouple placed on the

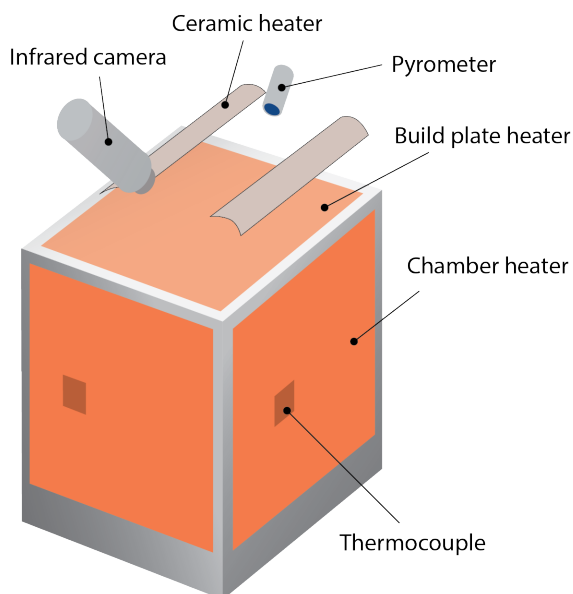


Figure 1. Build chamber with the location and size of the heating elements on each side of the build chamber. The ceramic heaters are shown above the build chamber, along with the pyrometer and IR camera



heating elements as seen in [Figure 1]. To measure the top surface temperature a pyrometer is installed in line with the ceramic heaters. The pyrometer initially has a set emissivity of 0.95, which will be evaluated based on the findings from the experiments conducted. This Pyrometer is used as input for the top heating PID controller.

### MEASUREMENT SETUP

Two separate experiments have been conducted, to investigate the powder cake temperature distribution and the emissivity of plastic powder. The powder used for all experiments was a white PA11 powder [2], used as a ready for production mix.

### TEMPERATURE DISTRIBUTION

Two sensor arrays were designed to locate the K-type thermocouples in the powder cake. The arrays presented in [Figure 2] were placed in the middle of the powder cake having a total thickness of 100 mm. The two experiments were carried out in two separate heating cycles. One is to determine the homogeneity in the entire build chamber, using an array [Figure 2 LEFT] of evenly placed thermocouples along the edges of the build chamber and in the middle. A second is measuring the temperature gradient from the middle of the build chamber to the edges. Using higher sensor density, spanning in a triangle as seen in [Figure 2 RIGHT] from the middle to a corner measuring 1/8<sup>th</sup> of the build area. The approach was inspired by the work of Josupeit, S.

et al [3]. Here they installed sensors that allow for continuous measurement during manufacturing. This research instead focuses on mapping the temperature profile of the bed for verification of the machine. The sensor arrays contain up to 16 K-type sensors, logging the data as a mean every 10 seconds with a sampling rate of 1Hz. The arrays were produced in a plastic frame, to mitigate the risk of thermal conduction, whilst ensuring the position of the sensors was kept. For all experiments, a sensor is placed in the centre of the build plate. Data from this sensor will be used for determining the time of the machine's cooldown time, compared to the cooldown time of the produced parts. The two experiments have been run for 24 hours of heating and 24 hours of cooling, with all heating elements set to the same temperature of 180 °C. Between each heating cycle, the powder was removed and refreshed.

### INFRARED TEMPERATURE READINGS

To measure the influence of temperature on emissivity, an IR camera was used to measure the surface temperature. The IR camera is mounted as seen in [Figures 1 & 5]. The mounting angle might influence the acquired temperature, which is resolved in the IR camera experiment. The temperature change of the powder might influence the emissivity, causing a shift in the readout of the IR camera compared to the actual temperature. The emissivity of the powder during heat up and cool down of the build job was measured for a full heating cycle to correlate with temperature. These heating cycles were only

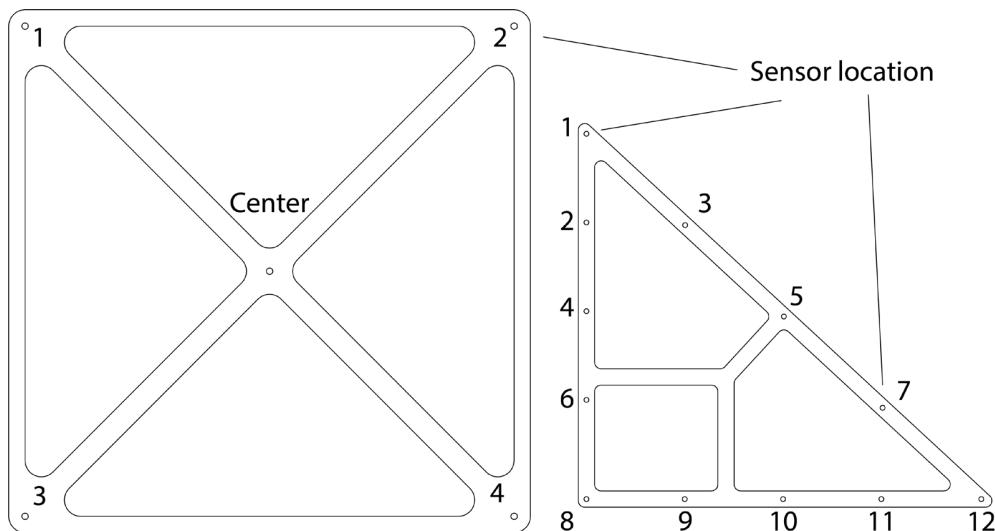


Figure 2. Sensor array one and two. LEFT - The array used for determining the stability towards the sides of the build chamber. RIGHT - The array used for determining the temperature gradient through the powder cake.

using the heating elements physically in contact with the powder, resulting in heating from 5 sides. The IR heaters were not used, to ensure that the measurement was not influenced by the radiation and reflection. However, measurements at the actual build temperature were made and used later for build job temperature observations. The experiment was carried out using a 10mm tall powder cake to shorten the duration of heating before reaching the setpoint temperature. The set temperature was 180 °C, as with the previous experiments, however, the temperature only reached 110 °C as measured by a K-type thermocouple located in the top layer of the powder. This K-type thermocouple was used to determine the measurement error of the IR measurement.

### BUILD ENVELOPE RESULTS

From the heating cycles, it was found that the build envelope of the machine differed from the actual size of the entire build chamber. An accept criteria was set up for the build envelope, ensuring a region of temperature stability and low deviation compared to the setpoint. This accept criteria was set at a maximum deviation of 10°C from the setpoint temperature. A significant temperature variation was observed when moving toward the sides of the chamber as seen in [Figure 3]. The most severe temperature deviation was expected towards the corners. The corners of the build chamber are the least heated and insulated, with an evident gap between the heating elements, as well as no extra insulation. To check the boundary temperatures of the powder cake two thermocouples were placed on the two horizontal surfaces, collecting data from the build plate and the top surface open towards the laser path. Both temperatures were found to correspond to the setting of 180 °C with only a minor deviation as seen in the table below.

	Measured °C	Deviation °C
Bed	179,7	0,3
Top	178,9	1,1
Center	175,4	4,6

A deviation was found when investigating the centre temperatures measured during the experiments. Here the temperature would never reach the desired setpoint, due to thermal losses towards the sides of the build chamber. The thermal loss towards the sides and corners of the build chamber is very clear from the heat map shown in [Figure 3]. The heat map shows the temperature recorded during the experiment. A

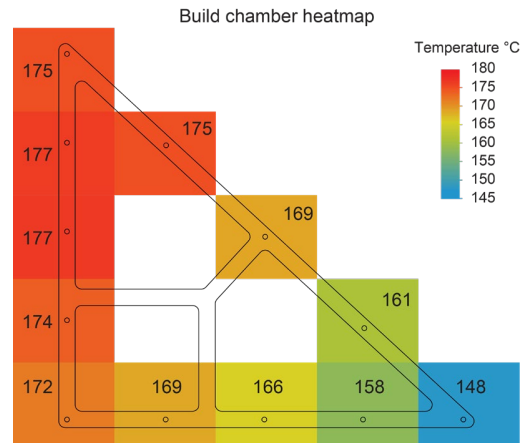


Figure 3. Heat map showing the temperature variation of the build chamber.

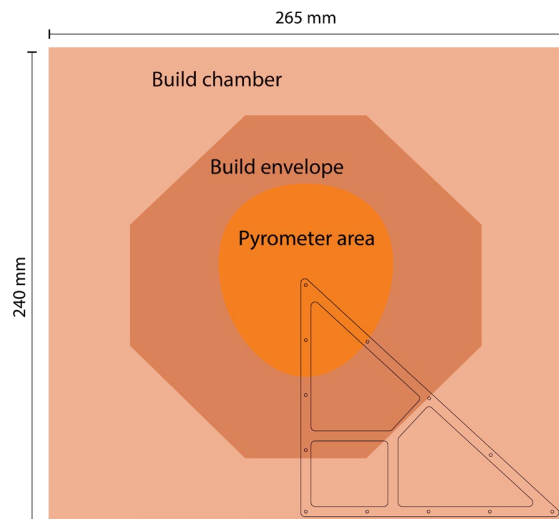


Figure 4. Top view of the build chamber showing the entire build area, the build envelope, based on the findings from the experiments, and the pyrometer measuring area placed in the middle of the build envelope.

large deviation towards the corner is evident in the plot showing the temperature gradient through the powder cake as can be seen in [Figure 3]. Based on the temperature gradient towards the sides of the build chamber, the current setup has a build envelope different from the entire build chamber presented in [Figure 4]. The resulting build envelope ensures small temperature deviations but only uses half of the entire possible build volume. The build envelope would not be round, but instead cut off the corners and stretch towards the sides. This will leave an octagon shape build envelope, based on the current setup and data. However, the exact size for this build envelope will need to be

determined by further investigation, looking into temperature deviation at both higher and lower temperatures. For the current setup, the safe zone for a build job is determined to lie within the boundaries of sensors five and six as seen in [Figure 4]. This build envelope will ensure a minimum temperature of 170 °C during a build job, providing minimum crystallisation before cooling the entire build job when using the PA11 powder investigated in this paper. The octagon shape can be improved both in size and towards a more circular shape, by adding new heaters surrounding the build chamber, as well as better insulation.

### IR MEASUREMENTS IN POLYMER POWDERS

Both the IR camera and the pyrometer rely on accurate infrared thermal measurements. The sensors will be used for process control and monitoring, ensuring that newly distributed layers are heated before sintering with the laser, and for process monitoring and defect detection. For this the actual emissivity for polymer powders, specifically used in the Open Access Polymer L-PBF platform, has been measured during several heating cycles. For polymer powders, a previous study found that Nylon 12 powders have an emissivity of 0.95 [4]. This corresponds well with the pyrometer being fixed at this emissivity, which has proved to provide the correct temperature of the powder top surface as seen above. The pyrometer measures an average surface temperature as shown in [Figures 4 & 5]. The measurement is on a slight angle that extends the area towards the front of the build area as seen in [Figure 5] however, based on data it functions as intended. The IR camera also views the build surface at an angle as seen in [Figure 5]. However, this angling effect is negligible when the angle is above 15° [4], from a view parallel to the build plane. For the current setup, this angle is 48°. The resulting image view can be seen in [Figure 5].

To track the temperature development during the experiments, two different approaches were adopted. First, three pieces of Kapton tape were laid out in the; back, middle, and front of the build surface, considering the camera position. Secondly, two thermocouples were placed in the top layer of the powder. This setup was used for producing the error plot in [Figure 7]. These thermocouples were used for validating the readout of both the pyrometer and IR camera and can be seen in [Figure 9]. The readout of the pyrometer most likely has been influenced by the

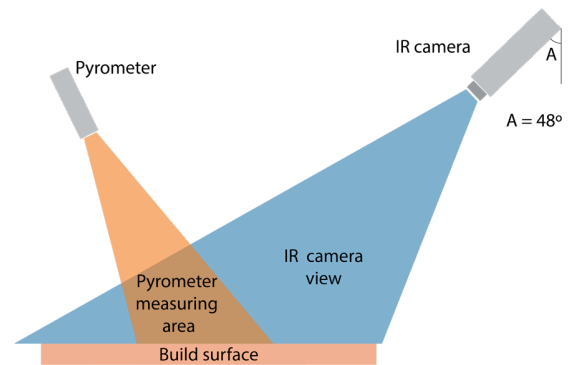


Figure 5. View angle and area for the pyrometer and IR camera in the system. Angle A = 48°

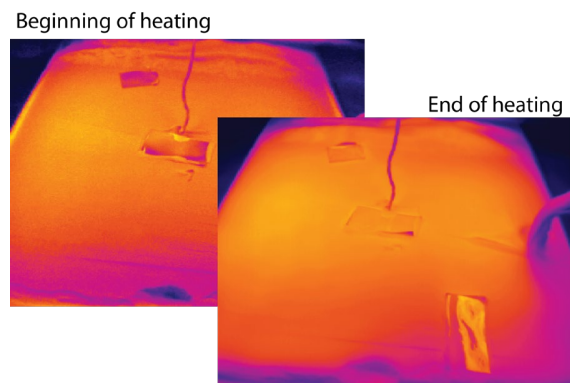


Figure 6. Difference in measured temperature between Kapton tape and powder surface. Top left corner is Kapton showing lower temperature initially.

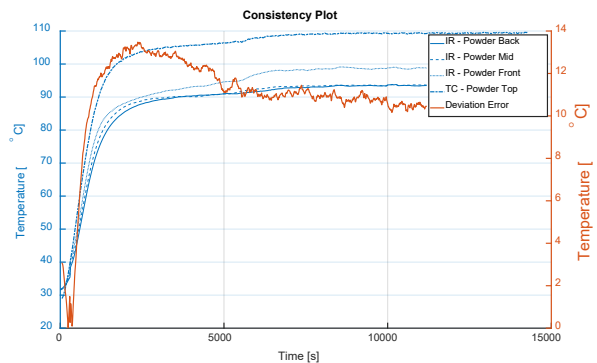


Figure 7. Consistency plot showing the deviation between thermocouple and IR measured temperature

thermocouple wires and Kapton tape placed on the powder cake. However, based on the data obtained by the IR camera, it is expected to show the correct reading, which is further supported by the small deviation between the setpoint and measured temperature, found during the initial heating experiments, as shown above.

The amount of energy emitted from a surface varies with temperature and surface morphology, and it is, therefore, vital to estimate the emissivity for the ability to accurately monitor the process. The emissivity was determined using the following equation (1).

$$\varepsilon_r = \varepsilon_s \frac{T_r^4 - T_a^4}{T_s^4 - T_a^4} \quad (1)$$

Here  $T_a$  is the ambient temperature,  $T_s$  is the absolute surface temperature measured by the thermocouple, and  $T_r$  is the radiative temperature from the measured surface [5]. In the black body method [5] the absolute surface temperature is replaced by the temperature reported by the camera at the black body temperature. The black body is in this case the 3 pieces of Kapton tape placed on the powder surface. The emissivity study found minor changes in the emissivity over the temperature range when heating the polymer powder as seen in [Figure 8]. The shift seen in the low-temperature range is assumedly caused by the Kapton tape heating slower than the powder surface, causing a deviation in the temperature readout. For the emissivity measurements it is assumed that the actual temperature is the same for both bodies. This is also clear when viewing the image data obtained during the experiments, as seen in [Figure 6].

From the experiments, it was found that a small deviation between the temperature measured by the camera and the temperature measured by the thermocouples. As seen in the error plot [Figure 7] a deviation of  $10^\circ$  was found. This error can be caused by several factors in the experimental setup, with the sensor placement and Kapton tape heating being the most predominant. It is expected that the sensor might have shifted during heating since they were not fully restricted

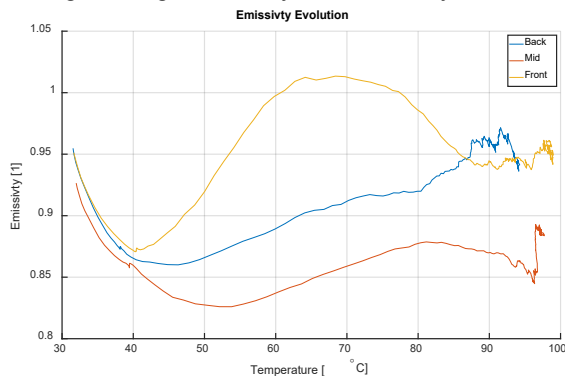


Figure 8. The emissivity vs temperature plot showing initial change to the emissivity.

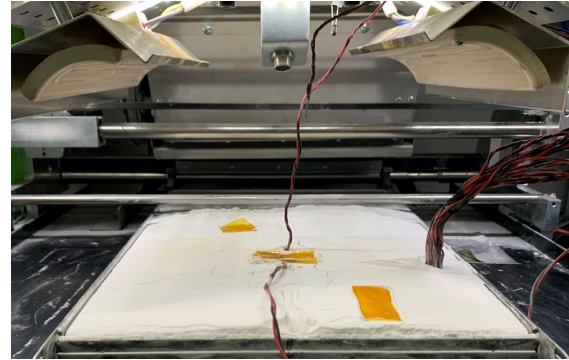


Figure 9. The build surface with the two ceramic heaters shown in the top corners. The pyrometer is seen in the middle top, looking onto the build platform. On the build platform three pieces of Kapton tape are placed as well as two K-type thermocouples.

from movement. Furthermore, the Kapton tape might not have reached the same temperature as the powder simultaneously. To mitigate this error further calibration will be needed. However, the intended purpose of the camera is not to monitor the overall temperature, but rather to monitor the temperature shift caused by the laser processing. For this purpose, an error of  $10^\circ$  is acceptable, seeing that this error can be filtered when comparing heated and molten polymer.

## CONCLUSION

An octagon-shaped build envelope was constructed based on the findings in the heating experiments. This results in a large quantity of powder being used and discarded with every build cycle. Depending on the refresh rate, this will influence the cost of running the equipment. A solution to this is to install better heaters, with better coverage and more insulation covering the entire build chamber.

To improve the experimental setup, a locating mechanism for the K-type sensor array, should be implemented. Ensuring the location in the powder bed, to further enhance the reliability of the results. However, direct contact between the sensor array and the heated wall is also not desirable. The use of plastic suggests low thermal conductivity, which might function even in point contact with the build chamber walls.

The paper presented what the measuring area of the pyrometer looks like, and that it is located within the region of the build envelope, resulting in proper heating of the top layer.

Finally, the paper presented a measurement method for finding the actual emissivity of the polymer powder used in the process, including an

error plot concluding a 10 °C deviation between the thermocouple and IR measurement. This deviation is for the current setup deemed acceptable but can be improved by further experiments.

### **FUTURE WORKS**

To further ensure the powder cake temperature stability, it has been planned to carry out several heating cycles to different temperatures, to see the deviation at both higher and lower temperatures. Another interesting question arose during the experiments, as to whether different materials will react differently in the machine, especially considering the temperatures found with the IR camera. If so, it would mean that the investigation done is to be done for every single new material.

### **REFERENCES**

- [1] Andersen, S. A. (2020). Open Architecture Laser Powder Bed Additive Manufacturing. Technical University of Denmark.
- [2] BASF FORWARD AM. (2022, April 5). Ultrasint® PA11 Polymer Powder for 3D Printers | BASF Forward AM. BASF 3D Printing Materials and Services. Retrieved May 31, 2022, from <https://forward-am.com/material-portfolio/ultrasint-powders-for-powder-bed-fusion-pbf/pa-11-line/ultrasint-pa11/>
- [3] Josupeit, S., & Schmid, H. J. (2016). Temperature history within laser sintered part cakes and its influence on process quality. *Rapid Prototyping Journal*, 22(5), 788–793. <https://doi.org/10.1108/RPJ-11-2015-0166>
- [4] Diller, T. T., Sreenivasan, R., Beaman, J., Bourell, D., & LaRocco, J. (2010). Thermal model of the build environment for polyamide powder selective laser sintering. In 2010 International Solid Freeform Fabrication Symposium. University of Texas at Austin.
- [5] K. Meinert, M. Bayat, D. Pedersen, F. Biondani, V. Nadimpalli. A simple method for estimating the effective emissivity at high temperature, utilizing a black body radiator, Euspen (2021) Copenhagen.



# APPENDIX C

## PA11 - White BASF Ultrasint (TDS)



# Technical Data Sheet

# Ultrasint® PA11

Technical Data Sheet for Ultrasint® PA11

Version No.: 1.3, revised 04/2021

## General information

### Components

**Polyamide 11 powder for Laser Sintering**

### Product Description

Ultrasint® PA11, a bio-based material (castor oil), is an interesting alternative to PA12. Parts produced with this material show a high elongation at break, elasticity and high impact resistance. Typical applications are in environments where high deformations (e.g. film hinges) and/or exposure to special surroundings (e.g. chemical, detergents, oil) may occur. Due to its high ductility, it does not splinter in most crash situations. Ultrasint PA11 can be used for skin contact applications. It is processable on most common LS printers. Parameters for printing will be provided.

Typical applications are:

- Car interior parts
- Bumper components
- Film hinges
- Functional prototypes and spare parts
- Medium-loaded series parts

### Delivery form & warehousing

Ultrasint® PA11 powder should be stored at 15 – 25°C in its originally sealed package in a clean and dry environment.

### Product safety

Mandatory and recommended industrial hygiene procedures and the relevant industrial safety precautions must be followed whenever this product is being handled and processed. Product is sensitive to humid environment conditions. For additional information please consult the corresponding material safety data sheets.

### For your information

Ultrasint® PA11 comes in solid white color. Electrical properties (e.g. volume resistivity, surface resistivity), chemical properties (e.g. resistance against particular substances) and tolerance for solvents are available upon request. Generally, these properties correspond to publicly available data on polyamides.

### Notice

The data contained in this publication are based on our current knowledge and experience. In view of the many factors that may affect processing and application of our product, these data do not relieve processors from carrying out their own investigations and tests; neither do these data imply any guarantee of certain properties, nor the suitability of the product for a specific purpose. Any descriptions, drawings, photographs, data, proportions, weights etc. given herein may change without prior information and do not constitute the agreed contractual quality of the product. It is the responsibility of the recipient of our products to ensure that any proprietary rights and existing laws and legislation are observed.

The safety data given in this publication is for information purposes only and does not constitute a legally binding Material Safety Data Sheet (MSDS). The relevant MSDS can be obtained upon request from your supplier or you may contact Forward AM directly at [sales@basf-3dps.com](mailto:sales@basf-3dps.com).

Technical Data Sheet for Ultrasint® PA11

Version No.: 1.3, revised 04/2021

General Properties	Test Method	Typical Values
Bulk Density / kg/m <sup>3</sup>	DIN EN ISO 60	520
Printed Part Density / kg/m <sup>3</sup>	DIN EN ISO 1183-1	1020
Mean particle size d50 / μm	Laser Diffraction	40-50
Melting Temperature / °C	ISO 11357 (10 K/min)	203
Crystallization Temperature / °C	ISO 11357 (10 K/min)	158
Melt Volume Flow Rate / cm <sup>3</sup> /10min	ISO 1133 (220 °C, 2.16kg)	28

Thermal Properties	Test Method	Typical Values <sup>1</sup>
HDT/A (1.8 MPa) / °C	ISO 75-2	76
HDT/B (0.45 MPa) / °C	ISO 75-2	176
Vicat/A (10 N) / °C	ISO 306	191
Vicat/B (50 N) / °C	ISO 306	177

Skin Contact	Test Method	Typical Value
Cytotoxicity	ISO 10993-5	Pass
In vitro Skin Irritation Testing	ISO 10993-10, OECD Guideline No. 439	Pass
In vivo Sensitization Testing	ISO 10993-10, OECD Guideline No. 429	Pass

Mechanical Properties	Test Method	Typical Values X-direction		Typical Values Z-direction	
		Dry <sup>1</sup>	Cond. <sup>2</sup>	Dry <sup>1</sup>	Cond. <sup>2</sup>
Tensile Strength / MPa	ISO 527-2	52	45	54	46
Tensile Modulus / MPa	ISO 527-2	1750	1100	1800	1250
Tensile Elongation at break / %	ISO 527-2	28	45	24	31
Tensile Strength / MPa	ISO 527-2	31	28	29	26
Tensile Modulus / MPa	ISO 527-2	370	300	420	360
Tensile Elongation at break / %	ISO 527-2	> 150	> 150	51	54
Flexural Modulus / MPa	DIN EN ISO 178	1750	1250	1800	1300
Charpy Impact Strength (notched) / kJ/m <sup>2</sup>	ISO 179-1	5.1	8.3	3.9	4.5
Charpy Impact Strength (unnotched) / kJ/m <sup>2</sup>	ISO 179-1	184	198	85	85
Izod Impact Strength (notched) / kJ/m <sup>2</sup>	ISO 180	6.5	7.7	4.8	5.2
Izod Impact Strength (unnotched) / kJ/m <sup>2</sup>	ISO 180	No break	No break	54	86

 Detailed material data and support for FEA simulations available on request ([sales@basf-3dps.com](mailto:sales@basf-3dps.com)).

1) Measured after drying 14 days at 80°C / vacuum. Water content is about 0.05% acc. to DIN EN ISO 15512

2) Measured after conditioning 14 days at 70°C / 62% r.h. Water content is about 0.9% acc. to DIN EN ISO 15512

All values measured with virgin material.



# APPENDIX D

## PA11 - Black BASF Ultrasint (TDS)

# Technical Data Sheet

# Ultrasint® PA11 black

Technical Data Sheet for Ultrasint® PA11 black

Version No.: 1.2, revised 04/2021

## General information

### Components

**Black Polyamide 11 powder for Laser Sintering**

### Product Description

Ultrasint® PA11 black, a bio-based material (castor oil), is an interesting alternative to PA12. Parts produced with this material show a high elongation at break, elasticity and high impact resistance. Typical applications are in environments where high deformations (e.g. hinges) and/or exposure to special surroundings (e.g. chemical, detergents, oil) may occur. Due to its high ductility and toughness, it does not splinter in most crash situations. Ultrasint® PA11 black is processable on most common SLS printers. Parameters for printing will be provided.

Typical applications are:

- Car interior parts
- Bumper components
- Living hinges
- Functional prototypes and spare parts
- Medium-loaded series parts

### Delivery form & warehousing

Ultrasint® PA11 black powder should be stored at 15 – 25°C in its originally sealed package in a clean and dry environment.

### Product safety

Mandatory and recommended industrial hygiene procedures and the relevant industrial safety precautions must be followed whenever this product is being handled and processed. Product is sensitive to humid environment conditions. For additional information please consult the corresponding material safety data sheets.

### For your information

Ultrasint® PA11 black comes in solid black color. Electrical properties (e.g. volume resistivity, surface resistivity), chemical properties (e.g. resistance against particular substances) and tolerance for solvents are available upon request. Generally, these properties correspond to publicly available data on polyamides.

### Notice

The data contained in this publication are based on our current knowledge and experience. In view of the many factors that may affect processing and application of our product, these data do not relieve processors from carrying out their own investigations and tests; neither do these data imply any guarantee of certain properties, nor the suitability of the product for a specific purpose. Any descriptions, drawings, photographs, data, proportions, weights etc. given herein may change without prior information and do not constitute the agreed contractual quality of the product. It is the responsibility of the recipient of our products to ensure that any proprietary rights and existing laws and legislation are observed.

The safety data given in this publication is for information purposes only and does not constitute a legally binding Material Safety Data Sheet (MSDS). The relevant MSDS can be obtained upon request from your supplier or you may contact Forward AM directly at [sales@basf-3dps.com](mailto:sales@basf-3dps.com).

Technical Data Sheet for Ultrasint® PA11 black

Version No.: 1.2, revised 04/2021

General Properties	Test Method	Typical Values
Bulk Density / kg/m <sup>3</sup>	DIN EN ISO 60	540
Printed Part Density / kg/m <sup>3</sup>	DIN EN ISO 1183-1	1030
Mean particle size d50 / μm	Laser Diffraction	40-50
Melting Temperature / °C	ISO 11357 (10 K/min)	203
Crystallization Temperature / °C	ISO 11357 (10 K/min)	165
Melt Volume Flow Rate / cm <sup>3</sup> /10min	ISO 1133 (220 °C, 2.16 kg)	18

Thermal Properties	Test Method	Typical Values <sup>1</sup>
HDT/A (1.8 MPa) / °C	ISO 75-2	62
HDT/B (0.45 MPa) / °C	ISO 75-2	177
Vicat/A (10 N) / °C	ISO 306	192
Vicat/B (50 N) / °C	ISO 306	175

Mechanical Properties	Test Method	Typical Values X-direction		Typical Values Z-direction	
		Dry <sup>1</sup>	Cond. <sup>2</sup>	Dry <sup>1</sup>	Cond. <sup>2</sup>
Tensile Strength / MPa	ISO 527-2 (23°C)	52	45	52	45
Tensile Modulus / MPa	ISO 527-2 (23°C)	1750	1150	1700	1200
Tensile Elongation at break / %	ISO 527-2 (23°C)	26	42	27	34
Tensile Strength / MPa	ISO 527-2 (80°C)	32	28	28	26
Tensile Modulus / MPa	ISO 527-2 (80°C)	390	330	360	300
Tensile Elongation at break / %	ISO 527-2 (80°C)	> 150	> 150	87	120
Flexural Modulus / MPa	DIN EN ISO 178	1750	1300	1700	1300
Charpy Impact Strength (notched) / kJ/m <sup>2</sup>	ISO 179-1	7.6	11	7.7	11
Charpy Impact Strength (unnotched) / kJ/m <sup>2</sup>	ISO 179-1	193	No break	56	75
Izod Impact Strength (notched) / kJ/m <sup>2</sup>	ISO 180	7.9	9.3	8.0	9.9
Izod Impact Strength (unnotched) / kJ/m <sup>2</sup>	ISO 180	No break	No break	48	63

 Detailed material data and support for FEA simulations available on request ([sales@basf-3dps.com](mailto:sales@basf-3dps.com)).

- 1) Measured after drying 14 days at 80°C / vacuum. Water content is about 0.02% acc. to DIN EN ISO 15512  
 2) Measured after conditioning 14 days at 70°C / 62% r.h. Water content is about 0.8% acc. to DIN EN ISO 15512  
 All values measured with virgin material.





## **APPENDIX E**

# **Process optimisation of PA11 in fiber-laser powder-bed fusion through loading of an optical absorber**

## Process optimisation of PA11 in fiber-laser powder-bed fusion through loading of an optical absorber

Christian Leslie Budden<sup>\*1</sup>, Aakil Raj Lalwani<sup>1,3</sup>, Kenneth Ælkær Meinert<sup>1</sup>,  
Anders Egede Daugaard<sup>2</sup> & David Bue Pedersen<sup>1</sup>

<sup>1</sup>Department of Mechanical and Civil Engineering, Technical University of Denmark,  
Kgs. Lyngby, Denmark

<sup>2</sup>Danish Polymer Centre, Department of Chemical and Biochemical Engineering,  
Technical University of Denmark, Kgs. Lyngby, Denmark

<sup>3</sup>LEGO System A/S, Billund, Denmark

\*Corresponding author: clebu@mek.dtu.dk

### Abstract

Industrial laser processing is rapidly shifting towards fiber lasers with wavelengths between 780nm and 2200nm. This can be largely contributed to the excellent beam properties and, ease of operation. However, for Additive Manufacturing of polymers, CO<sub>2</sub> lasers at wavelengths of 10,6µm are predominantly used. CO<sub>2</sub> lasers provide unmatched energy absorption by the C-H bonds of Polyamide (PA). To remedy this, the current study investigates using a high-power fiber laser (1080nm) for consolidating PA11 mixed with a black optical absorber. Several compositions are produced by mixing commercially available white and black powder. Aiming at finding the optimum optical absorber loading and the corresponding process parameters, allowing the highest possible component fidelity, while achieving the lightest hue of grey possible to allow for later colouring. The experiment is conducted on an in-house developed Open Architecture Laser Powder-Bed Fusion system. The parts are examined through, surface roughness, and mechanical characterisation.

### Introduction

Laser Powder Bed Fusion (L-PBF) is rapidly increasing its popularity in industry. Several materials can be used in the process, with the most predominant materials being polymers, metals, and ceramics. Typically, polymer sintering machines use a CO<sub>2</sub> laser, because polymer bonds react to the wavelength of the laser, leading to heating, sintering, and melting of the polymer [1].

Commercial polymer L-PBF systems like that of EOS and 3DSystems are equipped with CO<sub>2</sub> lasers. However, two main limiting factors in terms of the resolution are the layer thickness (vertical) and the laser beam spot size (lateral). A fiber laser source holds certain advantages over a CO<sub>2</sub> laser. Such as a gaussian beam profile, and a high-power laser, while being a cost-effective solution. Furthermore, the beam delivery system into the scanner via fiber allows for a finer beam spot size, which helps improve the lateral resolution. Another advantage of a fiber laser is the high stability and good beam profile achieved during pulsing. These effects are utilised in the Open Architecture Polymer L-PBF system at the Technical University of Denmark (DTU) by incorporating a fiber laser into a re-engineered Powder Bed Fusion machine, now allowing research for Polymer

Selective Laser Sintering (SLS) materials.

Research in the past has shown that the absorptivity of polymeric materials is very low when attempted to be processed by a fiber laser (1080nm) [1]. Whereas the absorptivity of polymeric materials is much higher when processed with a CO<sub>2</sub> Laser (10,6µm) [1][2][3]. Molecular vibrations of polymeric materials define their optical response to electromagnetic waves at different wavelengths [1]. Organic polymeric materials with aliphatic carbon-hydrogen (C-H) bonds have molecular vibrations in response to electromagnetic waves between 7,5 to 12,5 µm, hence polyamides display high absorptance at 10,6 µm [3]. Since the absorptance for the selected fiber laser is low, most of the energy delivered by the laser is lost in reflectance and transmittance. To improve the absorptance of the powders for CO<sub>2</sub> laser wavelengths, additives such as silicon dioxide (SiO<sub>2</sub>) & titanium dioxide (TiO<sub>2</sub>) are used for polyamide powders [3]. Similarly, work has been carried out to explore the potential of sintering polymers loaded with carbon black as an optical absorber [4][5]. Similar to carbon black any optical absorber (effective at the 1080nm wavelength) theoretically can assist in the consolidation of the powder layer using a fiber laser. This work will explore the last mentioned effect, and how minimising the amount of optical absorber effects the functional production of SLS parts.

### **Experimental methods**

Two kinds of the same PA11 material were used for the experiments. The materials were characterised prior to mixing and laser sintering. To develop the process parameters used during sample manufacturing the individual powders were characterised by, Differential Scanning Calorimetry (DSC), Thermal Gravimetric Analysis (TGA), and powder sizing. These methods inform important aspects of the manufacturing process, the black optical absorber content, and the mixing reliability.

The materials used are the same type of PA11 from BASF Ultrasint<sup>®</sup>. The major difference is that a black optical absorber is added for the one batch colouring this black. The two materials have previously been processed on the Open polymer L-PBF platform developed at DTU. However, with little success due to either too low or too high absorptivity. To mitigate this the two powders have been mixed. The goal is to achieve the lowest black optical absorber loading possible, to have the lightest grey colour of the final parts. Having a light grey colour will in turn open the possibility for direct manufacturing with coloured plastic powders in L-PBF, or easy dying into a desired colour.

DSC analysis has been conducted on both polymer types using the Waters Discovery DSC, to determine the melt and crystallisation temperature. The DSC was done at standard conditions in a nitrogen atmosphere, heating at 10.00°C/min. Heating from 0°C to 230°C, with a subsequent cooling ramp at 10.00°C/min to 0°C. The extracted melting and recrystallisation temperatures have been used for determining the process settings, considering the chamber heating and the final desired melt pool temperature. Based on the DSC curves it was found that the melting temperatures are very close, which is expected to cause the polymers to melt into a homogeneous plastic and not a two-component mix of molten plastic 1 with inclusions of plastic 2. This fully melted plastic part is only expected when the energy absorption in the black part is large enough to obtain and deliver the energy from the laser, onto the white powder, ensuring a fully melted region. The melting and crystallisation temperatures can be seen in Table 1 as well as in Figure 1.

Polymer	Melting (°C)	Crystallisation (°C)
PA11 White	200	159
PA11 Black	200	168

Table 1: DSC results

Based on the results an initial chamber temperature of 185°C was selected, with the top heaters set to 195°C. The resulting temperature for the build job will by these settings be 175°C, as determined by previous experiments [6]. This temperature will ensure that the polymer stays in a molten state and will only crystallise a little before the entire build is done and the machine is set to cool down. The powder cake cools down for a minimum of 12 hours, after which the parts are removed.

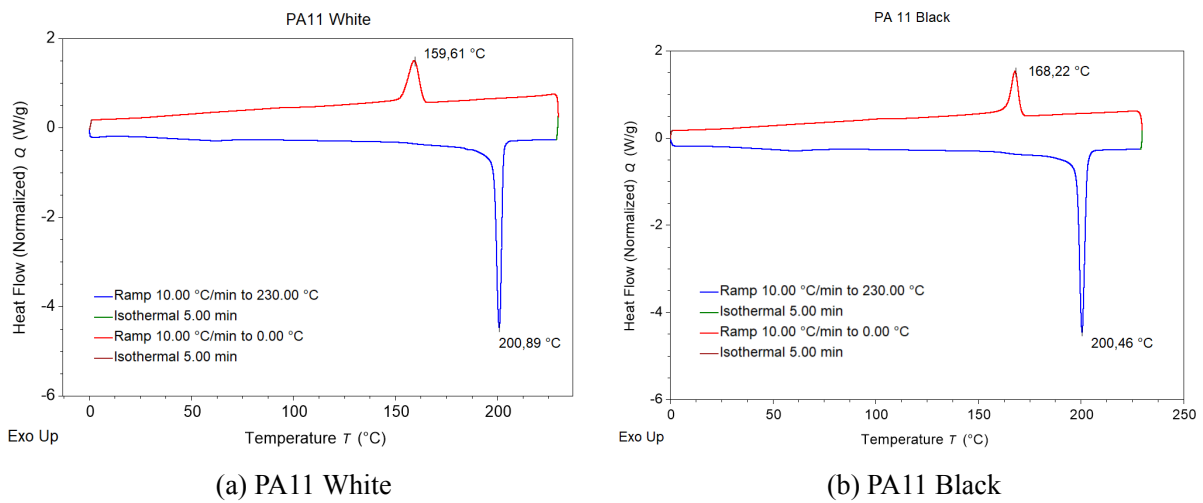


Figure 1: DSC analysis of the two powders used for mixing.

A TGA analysis was carried out to identify the amount of filler in the black PA11 material. It is assumed that the major constituent in the filler is the black optical absorber. The analysis was done on a Waters Discovery TGA showing the composition between the PA11 and filler loading in the powder. The TGA was run at standard conditions in a nitrogen atmosphere, heating the sample at 10°C/min to a final temperature of 800°C. The filler composition has not been explored further since the material is a proprietary blend from BASF.

Figure 2 shows the filler is constituting 6,9wt% and is assumed to be the black part in the polymer blend acting as the optical absorber. Optical absorption of the laser will be aided by the black optical absorber, which even at low filler contents is expected to have a large influence on the final part colour. The test of optical absorption will be determined by the manufacturability of the different batches of powder mixes.

To determine the powder size a Malvern Mastersizer 3000 with the dry dispersion method was used. The powder size will influence the mixing homogeneity and the flow properties of the powders [7]. To ensure that the two powders are alike before mixing separate tests were carried out. The results of the powder sizing can be seen in Table 2.

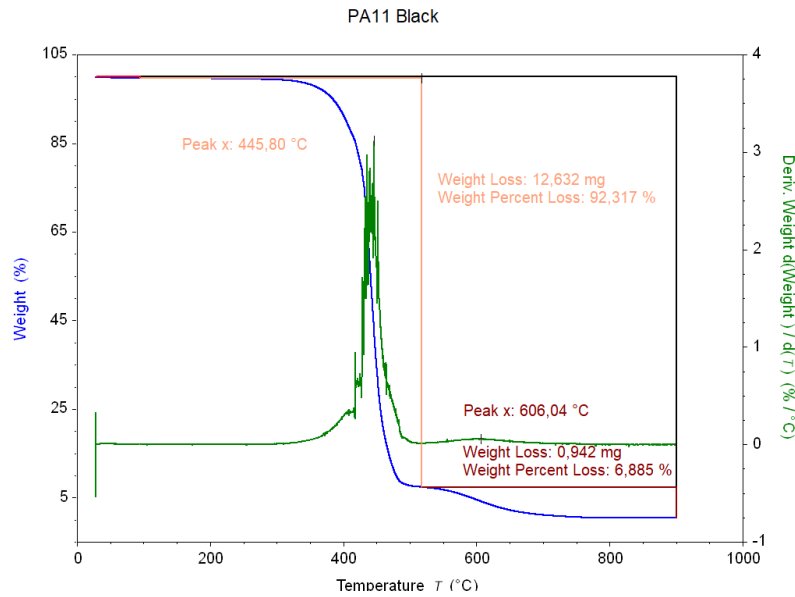


Figure 2: TGA plot for the PA11 Black

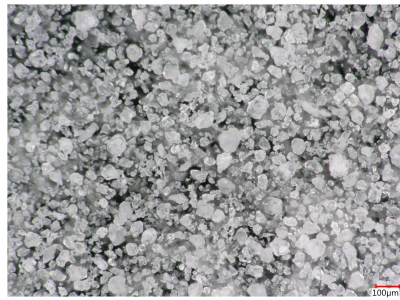
Polymer		PA11 White	PA11 Black
Dv (10)	$\mu\text{m}$	20,3	23,8
Dv (50)	$\mu\text{m}$	44,1	46,7
Dv (90)	$\mu\text{m}$	78,5	79,9
Density (TDS)	$\text{kg}/\text{m}^3$	520	540

Table 2: Powder specification and sizing

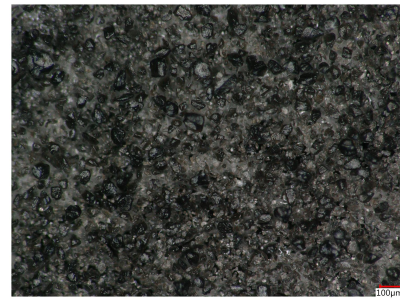
Three different batches of powder have been produced. The batches are White/Black 50/50, 80/20, and a 95/5 batch. Based on the powder properties a tumble mixer was selected. Tumble mixing is suitable when the powders to be mixed are like each other in size, weight, and particle shape [7]. Considering the densities, and powder size are alike according to Table 2, the only difference can be in the powder morphology. This has been investigated by light optical microscopy as shown in Figure 3. Both powders have the same rough and uneven morphology, likely caused by the manufacturing method. This leads to an expectation of complete random mixing between the two powders. A random mixing will ensure a homogeneous mix throughout the batch. The same mixing routine has been used for all batches.

The mixed powders can be seen in Figure 4. The mixing appears uniform, for all batches, with the white hue intensifying between every batch, ranging from W/B 50/50 to 95/5. Based on these results the mixed powders have been used for process optimisation, part production, and testing.

Mixing the powders result in a smaller amount of the black optical absorber ensuring a lighter colour compared to the 100% black powder. The optical absorber loading will for the batches tested be 3,45%, 1,39%, and 0,35% for the W/B 50/50, 80/20, and 95/5 respectively.

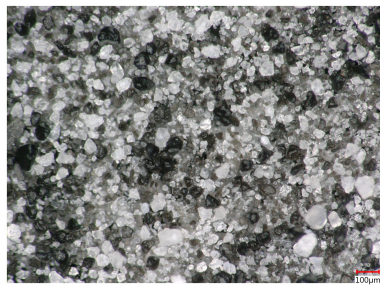


(a) PA11 White morphology

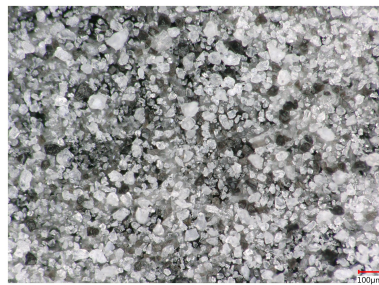


(b) PA11 Black morphology

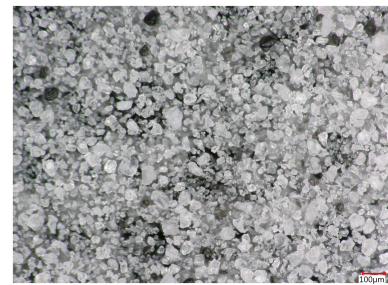
Figure 3: Morphology comparison between the unmixed white and black powder (Keyence optical microscope 200x)



(a) 50/50 W/B morphology



(b) 80/20 W/B morphology



(c) 95/5 W/B morphology

Figure 4: Morphology comparison between the different batches of powder

Test samples were produced on the Open Architecture L-PBF for polymer powders, developed at DTU. The machine is a re-engineered Projet 4500 originally from 3D Systems. The open platform uses the stock powder handling, and build piston axis, with changes to all other subsystems. The machine uses a 300W CW fiber laser source with a 0,2mm spot size [8] to produce the parts. Machine control is achieved by a unified systems controller [9], controlling laser movements and power, as well as the linear motions. Heating for the build chamber is done from all six sides, with heating elements placed on all four sides, and under the build bed, as well as two ceramic heaters placed above the bed. The machine has been developed as a materials investigation platform, challenging the traditional use of CO<sub>2</sub> lasers, by using a fiber laser source. The atmosphere is uncontrolled, causing material degradation, but is not expected to influence the processing capabilities of the machine. The heaters will maintain 180°C in the powder cake build area, ensuring little crystallisation before cool-down. The process is monitored by an infrared camera (Optrix Xi400), to obtain the build bed temperature and ensure steady process control throughout the build. This is currently controlled by operator input during the run-in of new materials. The recoater is a roller recoater, rolling in the opposite direction of the recoater movement, ensuring good packing and distribution of the powder across the powder bed.

The batches of powder used in the process are new introductions to the Open polymer L-PBF platform. Because of this, all batches have required process optimisation for final part quality. The



process optimisation was done by varying the parameters influencing the energy density of the laser equation 1. Here  $P$  is laser power in watts,  $h$  is the hatch spacing of the laser scan tracks,  $s$  is the scan speed, and  $l$  is the layer thickness. Furthermore, the build temperature has been tuned to align with the DSC results.

$$vED = \frac{P}{h \cdot s \cdot l} \quad (1)$$

Several factors influence the final sintering of the powder when varying the energy density. To ensure that complete sintering has been carried out, trials for powder consolidation with different parameter combinations of varying laser power and hatch spacing were assessed.

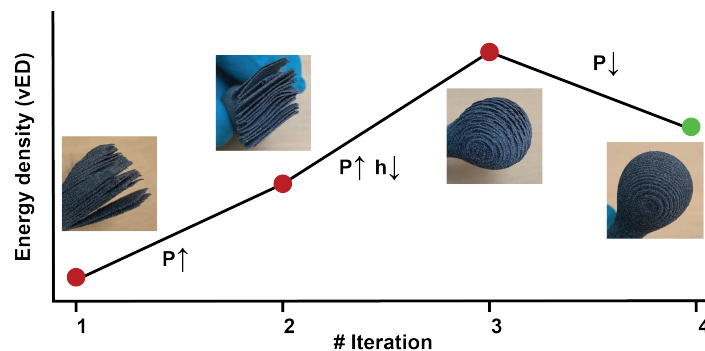


Figure 5: Iterative approach for the process optimisation, here shown for the 50/50 batch

Process optimisation of all batches investigated several different process settings before finding the right fit. Iterative process optimisation was adopted varying the parameters considered by  $vED$ . This process allowed for production of parts at different energy densities, and a conclusion based on the build and sintering quality, as seen in Figure 5. The best fit process parameters were the initial settings used for the next batch. From this baseline, a process optimisation was carried out. For all production runs the temperature settings were kept constant, ensuring a build chamber temperature of 180°C and a top bed temperature of 185°C.

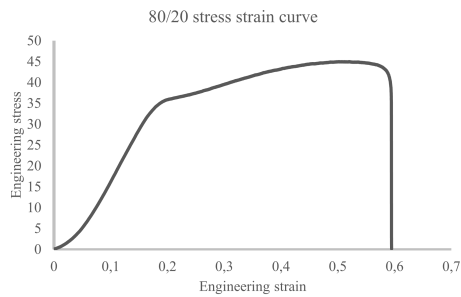
### Part characterisation

The manufacturability of the batches was initially determined in the first step of the process optimisation. Several different parameters were explored. The assessment of process stability was inferred from; the change of colour during laser processing, measurement of melt temperature, the flatness of the part in the bed, and stable recoating.

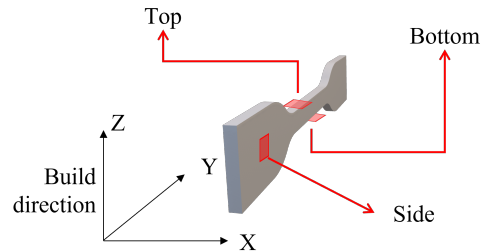
To quantify the different manufacturing strategies and compare the batches, tensile tests and surface roughness measurements were carried out on the final parts. The tensile testing specimens were as per ISO 527-2, design type 5A. In total 6 test specimens were manufactured, 5 for mechanical testing and 1 for surface roughness characterisation. The specimens were built such that the largest cross-section area was along the XY plane, see Figure 6b. The tensile test specimen was characterised using a Mecmesin Multitest-i, with a 1000N load cell. A characteristic curve of the tensile testing



is shown in Figure 6a. The tensile testing results are compared to the supplier datasheet values to determine if the part production is successful. Both the surface roughness and tensile test results are compared between the different batches, to check whether the batches with low optical absorber content can produce comparable parts.



(a) Representation of the typical tensile test for the 80/20 batch.



(b) Tensile test specimen, build orientation and surfaces for characterisation.

Figure 6: Tensile curve and the part build orientation, showing the surface roughness measurement locations

The planar surfaces of the tensile test specimens were used to characterise the surface roughness for varying concentrations of the optical absorber. The data was acquired using a focus variation microscope, Alicona InfiniteFocus G4 and was analysed using SPIP™. The inspection was carried out at a single position on each face of the tensile test specimen, see Figure 6b. The data was acquired over an area of 2,85mm x 2,16mm, with a lateral resolution of 2,2μm, and a vertical resolution of 410nm. The data was processed in SPIP™ to correct for the inclination of the component while measuring, and any curvature of the measured surface. The surface roughness was quantified by extracting the areal arithmetic mean height ( $S_a$ ) as defined in ISO standard 25178-2, see Equation 2.

$$S_a = \frac{1}{A} \iint_A |z(x, y)| dx dy \quad (2)$$

## Results

The initial hypothesis was that lowering the amount of optical absorber would significantly narrow the processing window and produce parts that would show more instabilities and larger deviations considering the mechanical properties. The added expectation was a rougher surface comprised of more adhering particles.

The production of each batch saw a sharp increase in the energy density required for processing the powder. Two parameters from the energy density were kept constant, to allow for variation of the other two. The two constant parameters were the scan speed and the layer thickness. The parameters for each batch including the constant parameters can be seen in Table 3. The scan speed was locked due to limitations of the galvano mirror device, and the controller. While the layer thickness was kept constant, to avoid changes in the material behaviour caused by increasing the

possibility of several powder grains stacked on top of each other. The influence of both scanning speed and layer thickness can be investigated further. The scan tracks were initially determined to benefit from not overlapping. To accommodate this a hatch spacing of  $300\mu\text{m}$  was used. This was done to ensure a low enough energy density, since the equipment cannot go low enough in power, and the speed could not be set any higher. This was eventually minimised to match the spot size of the laser, as the energy density requirement was greater for the batches having more white powder. The top temperature was also subject to change when moving from the 50/50 batch to the 80/20. The temperature change was needed due to curling and warping during the initial layers of production, which was induced by the thermal shock of the laser. The temperature was set to  $5^\circ\text{C}$  higher than for the previous batch, solving the problem.

		50/50	80/20	95/5
Scan speed	mm/s	3000	3000	3000
Layer thickness	$\mu\text{m}$	60	60	60
Hatch spacing	$\mu\text{m}$	300	234	200
Laser power	W	35	35	60
Top temperature	$^\circ\text{C}$	180	185	185
Build temperature	$^\circ\text{C}$	175	175	175

Table 3: Process parameters for the batches of the material tested

An increase in energy density is needed for achieving consolidation of the batches containing small amounts of the optical absorber. The melting and consolidation of the powder were seen to allow the optical absorber to flow out into the entire layer of the part, even when using the 95/5 batch, turning the entire part black internally. The process optimisation proved that sintering powders with a black optical absorber content close to 0,34% are possible while achieving consolidated parts.

When lowering the optical absorber content it is seen that a change in hatch spacing is needed since each black powder particle is spread further apart. A wider hatch spacing with a narrower spot size causes a gap between two scan tracks, which increases the risk of missing a black powder particle completely, causing less energy uptake. The shift is evident between the 50/50 and 80/20 batches, where the same laser power was used, but a significant change in hatch spacing was observed. However, when looking into the parameters of the 95/5 batch the number of black powder particles has been decreased to a point where the chance of hitting a black powder particle (Figure 4) must be optimised. This is done by having the scan tracks adjacent to each other. Processing the 95/5 batch also inferred a large increase in the laser power, due to the low absorptivity of the white powder particles dominating the batch.

The manufactured parts suggest that even lower amounts of the optical absorber can be used when dealing with a fiber laser if the power output and scan speeds can be adjusted accordingly. For the current system, this has not been dealt with further due to the scan speed limitations currently in place. Lowering the optical absorber content could, however, infer that not enough energy is absorbed into the powder, causing the energy to dissipate further into the powder bed. This energy dissipation into the powder bed has previously been seen to cause large instabilities of the desired

geometry of the parts.

Verification of the mechanical properties was used for determining the part quality, in terms of the consolidation between layers, and the overall manufacturing stability. There was a slight deviation between the batches, with the 80/20 batch showing the best mechanical properties. The mechanical properties of the parts are determined by the melt zone and how much the white powder has melted, as well as the layer-to-layer consolidation. Both are controlled by the energy absorption in the powder, as well as the rheological properties. The two constituent powders have not been tested for their rheological properties but are expected to start flowing even though the shear in the process is very low. This flow of the black molten polymer was observed during manufacturing. The flow caused by melting the black powder will allow for it to surround the white particles and provide heat for either melting or fusing them. The results presented in Figure 7 suggest that the 80/20 batch is the best batch produced, providing good mechanical properties even, when compared to the datasheet values from the supplier. This is contributed to the flow and relatively high content of the black particles in the mix, allowing for proper melting of the parts during production.

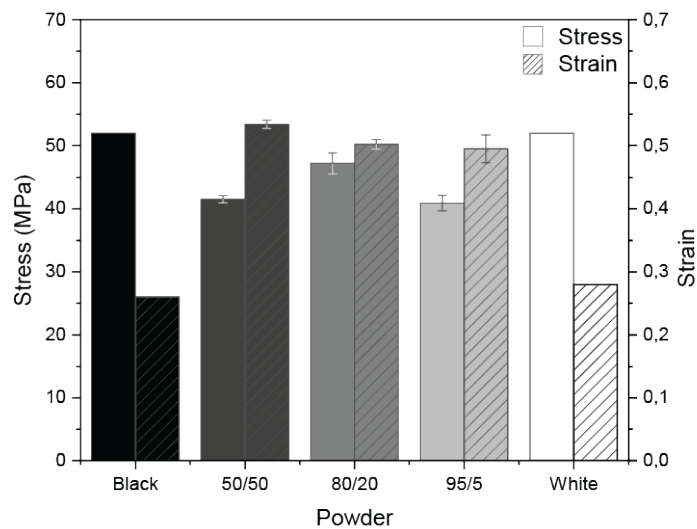


Figure 7: Engineering Stress and strain results for varying Black to White powder ratio concerning supplier datasheet (White Black)

The parts produced from the 95/5 batch showed comparable results to those of the 50/50 batch, leading to the conclusion that even lower optical absorber levels could be used to produce parts. These parts would be expected to show comparable, if not slightly lower mechanical properties, but at a much lighter grey colour. The strain results from the tensile tests proved that the parts behave differently from the datasheet values. The deviation in mechanical properties is attributed to the machine used for production not having an inert and dry atmosphere during manufacturing, causing moisture uptake in the manufactured parts. The moisture ingress during the manufacturing process cannot be avoided due to the limitations of the current machine setup. This moisture uptake will for PA11 cause a hydrolysing effect, leading to chain scission and a change in both the tensile

strain and strength [10][11]. This effect can also be the influencing factor, as to why the stress levels for the manufactured parts were lower than the datasheet values found. The effect of the optical absorber content on mechanical properties is still unexplored.

The surface roughness,  $S_a$ , characterised for the varying mixing ratios of black to white powder is shown in Figure 8. From the three faces characterised, the surface roughness for the XZ plane (vertical) was found to be the highest. This can be attributed to the caterpillar effect which can be a function of the layers and the layerwise scan track rotation. The waviness profile of the caterpillaring effect (see Figure 9a & 9d) has a period of  $300\mu\text{m}$  which is equivalent to 5 layers of  $60\mu\text{m}$  each, i.e. every 6 layers there is a formation of the bulge in the lateral dimension. This can be mitigated by optimizing with contour process parameters for the individual mixtures.

The surface roughness for the top and bottom surface was significantly better as the scan tracks would bring the entire layer to a melt. Even though the bottom face was built on the powder bed directly, it is almost equivalent to that of top face. The almost similar  $S_a$  values are representative of well identified process parameters for the mixtures used.

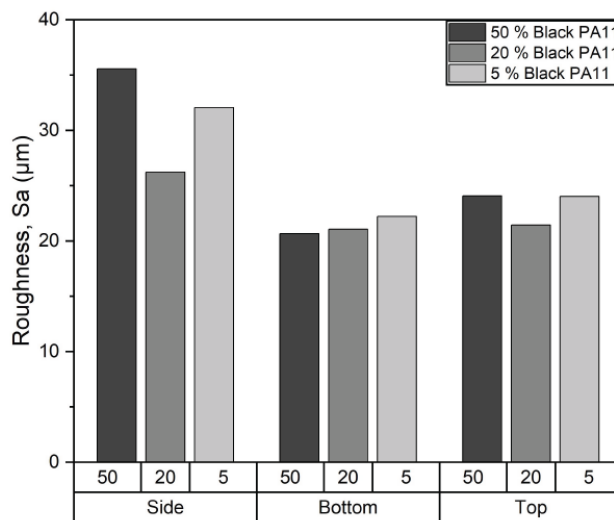


Figure 8: Surface roughness,  $S_a$ , for varying mixing ratios

Just like the powder particles being stuck in the black molten matrix discussed above, the surface roughness is also typically caused by powder particles sticking to the side of the parts. These powder particles are not fully molten due to too low energy but will adhere to the surface of the underlying molten matrix, typically causing the surface roughness to be a function of the size of these powder particles.

The 80/20 batch overall had the most uniform surface roughness. The comparison of areal plots between the 80/20 to the 95/5 batch can be observed in Figure 9. The side faces for both show the caterpillaring effect (in the form of lines along X in the XY plane) mentioned above. In general, when comparing all three faces, it is evident that the texture of the faces is relatively the same with the difference being that the 95/5 mix consists of more satellite powder particles sintered along the walls. The results presented are comparable to that of industrially manufactured and post-processed

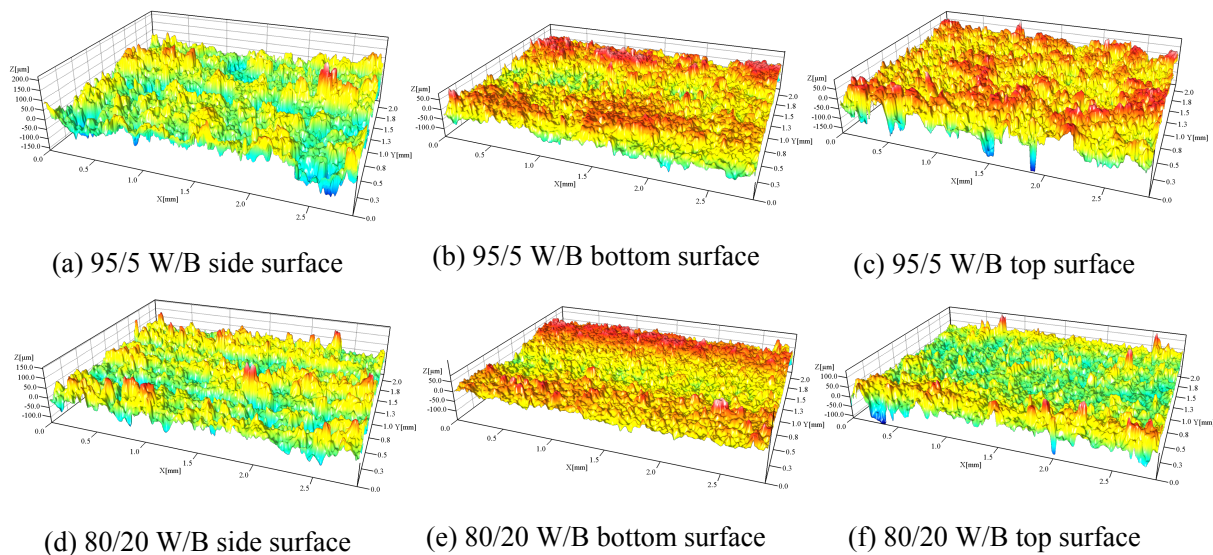


Figure 9: Surface comparison of parts with lower content optical absorber

PA12 SLS parts [12]. To process the 95/5 batch the laser power (effectively the energy density) was scaled up to compensate for the low optical absorber content, hence possibly dissipating more energy along the walls. Indicating the need for a further study into optimising the parameters and identifying the benefits/losses in functionality going lower or higher in optical absorber content.

### Conclusion

Several ratios of white and black powder were mixed and manufactured successfully on the Open Architecture Polymer L-PBF system developed at DTU. All the batches processed showed mechanical properties comparable to the supplier data sheets. Reducing the optical absorber (as a function of the mixing ratio) was successful considering the manufacturing of parts. The parts produced showed both mechanical and surface roughness characteristics comparable to results found in the literature. The conclusion is therefore two-fold; 1. The batch processed to the highest quality by the measures in this investigation was the 80/20 mix. 2. Depending on the final part requirement it is possible to go as low as 0,34% optical absorber while producing parts with good surface finish, and functional mechanical properties. The study proved that it is feasible to manufacture parts with low amounts of optical absorber while using a fiber laser at 1080nm wavelength. The investigation was carried out in an uncontrolled atmosphere, and for future work, it is desired to test the capabilities in a controlled N<sub>2</sub> atmosphere, as well as the influence on the final part properties. The current hue of the parts shows potential for post-colouring. The study suggests that optical absorber content can be lowered further, however, this can lead to detrimental effects of over-sintering the parts. By lowering the optical absorber content further, it will be possible to achieve lighter colours when developing the process. To make a precise estimate of by how much to reduce the optical absorber content, the optical properties of both black and white PA11 powder will be characterized for the near-infrared wavelength and its role in the consolidation mechanics will be explored in the future work.

## References

- [1] Nikolay K Tolochko et al. “Absorptance of powder materials suitable for laser sintering”. In: (). URL: [http://www.mcbup.com/research\\_registers/aa.asp](http://www.mcbup.com/research_registers/aa.asp).
- [2] J. P. Kruth et al. “Lasers and materials in selective laser sintering”. In: *Assembly Automation* 23.4 (2003), pp. 357–371. ISSN: 01445154. DOI: [10.1108/01445150310698652](https://doi.org/10.1108/01445150310698652).
- [3] Manfred Schmid. “LS Materials: Polymer Properties”. In: *Laser Sintering with Plastics* (2018), pp. 65–99. DOI: [10.3139/9781569906842.004](https://doi.org/10.3139/9781569906842.004).
- [4] Siddharth Ram Athreya, Kyriaki Kalaitzidou, and Suman Das. “Processing and characterization of a carbon black-filled electrically conductive Nylon-12 nanocomposite produced by selective laser sintering”. In: *Materials Science and Engineering A* 527.10-11 (2010), pp. 2637–2642. ISSN: 09215093. DOI: [10.1016/j.msea.2009.12.028](https://doi.org/10.1016/j.msea.2009.12.028). URL: <http://dx.doi.org/10.1016/j.msea.2009.12.028>.
- [5] N. Woicke, T. Wagner, and P. Eyerer. “Carbon assisted laser sintering of thermoplastic polymers”. In: *Annual Technical Conference - ANTEC, Conference Proceedings* 7.January 2005 (2005), pp. 36–40.
- [6] Christian L Budden et al. “Chamber Heat Calibration by Emissivity Measurements in an Open Source SLS System”. In: *Summer Topical Meeting: Advancing Precision in Additive Manufacturing - ASPE-euspen, conference proceedings*. 2022.
- [7] Martin J Rhodes. *Principles of powder technology*. Wiley, 1990, XI, 439 S (unknown). ISBN: 0471924229, 9780471924227.
- [8] MaxPhotonics. *MAXMaxphotonics Co.,Ltd*. URL: <http://en.maxphotonics.com/product/18.html>.
- [9] Sebastian Aagaard Andersen. *Open Architecture Laser Power Bed Additive Manufacturing*. 2020.
- [10] John Moalli, Society of Plastics Engineers, and N Y Plastics Design Library Norwich. *Plastics failure : analysis and prevention*. Ed. by John Moalli. Plastics Design Library, 2001, Online–Ressource (IV, 341 S) (unknown). ISBN: 008095054x, 081551865X, 081551865x, 1282011391, 1591242509, 1884207928, 9780080950549, 9780815518655, 9781282011397, 9781591242505, 9781884207921.
- [11] Pierre Yves Le Gac et al. “Yield stress changes induced by water in polyamide 6: Characterization and modeling”. In: *Polymer Degradation and Stability* 137 (2017), pp. 272–280. ISSN: 18732321, 01413910. DOI: [10.1016/j.polymdegradstab.2017.02.003](https://doi.org/10.1016/j.polymdegradstab.2017.02.003).
- [12] M. Launhardt et al. “Detecting surface roughness on SLS parts with various measuring techniques”. In: *Polymer Testing* 53 (Aug. 2016), pp. 217–226. ISSN: 01429418. DOI: [10.1016/J.POLYMERTESTING.2016.05.022](https://doi.org/10.1016/J.POLYMERTESTING.2016.05.022).





## **APPENDIX F**

# **Benchmarking of an Open Architecture Polymer Laser Powder Bed Fusion system**

## Benchmarking of an Open Architecture Polymer Laser Powder Bed Fusion system

Christian L. Budden<sup>1</sup>, Magnus B. Kjer<sup>1</sup>, Aakil R. Lalwani<sup>1</sup>, Venkata K. Nadimpalli<sup>1</sup>, and David B. Pedersen<sup>1</sup>

<sup>1</sup>Technical University of Denmark, Institute of Civil and Mechanical Engineering, Denmark

clebu@dtu.dk

### Abstract

This study aims to benchmark a fibre laser powered Open Architecture Polymer Laser Powder Bed Fusion (LPBF) system, which has been developed to offer complete process control. It enables researchers to investigate the process and materials development for the Polymer laser powder bed fusion process by providing control over critical parameters during the additive manufacturing process. To verify the solution, a benchmark study was conducted to investigate the system's capabilities. The investigation involved manufacturing a known benchmarking geometry that challenges the polymer powder additive manufacturing process. The results indicate that the Open Architecture Polymer LPBF system can reproduce the benchmarking geometry successfully. The findings of this study demonstrate the potential of the Open Architecture Polymer laser powder bed fusion system for research and development in the field of additive manufacturing.

Open-source, laser powder bed fusion, L-PBF, open-architecture, polymer, Selective laser sintering, sls

### 1. Introduction

Additive manufacturing of plastic components employs various methods, with laser powder bed fusion of polymers being one of the most widely used. It selectively melts polymer powder layer-wise with a laser to create 3D objects. An Open Architecture laser powder bed fusion system for polymers has been developed to enhance user control and allow research into fibre lasers. Traditionally, CO<sub>2</sub> lasers were used for polymer

**Table 1** Process parameters used to manufacture the benchmark

powder processing, but this work implements an optical absorber in a powder mix to enable consolidation using a fibre laser. [1-4]

This work presents the capabilities of a laser powder bed fusion system for polymers developed at the Technical University of Denmark by producing a benchmark geometry with intricate details and complex geometries. The work is part of a joint collaboration with the authors of benchmarking of an open architecture metal laser powder bed fusion system. This work utilises the same method and benchmarking geometry, with the major difference being the material and processing system presented in the work.

### 2. Methodology

The benchmark geometry was manufactured on the Open Architecture polymer laser powder bed fusion system developed at the Technical University of Denmark [2]. The system utilises a fibre laser with a spot size of 150 µm. The system is a repurposed 3D Systems binder jetting machine (Projet 4500) now capable of laser powder bed fusion of polymers.

	Feedrate	Power	Hatch	Layer
Hatch	3000mm/s	55W	150µm	40µm
Contour	1500mm/s	35W		

#### 2.1. Benchmark manufacturing

The benchmark was manufactured using a blend of white and black PA11 Ultrasint polymer powder from BASF. The powder mix consisted of 95% white powder and 5% black powder, as detailed in a previous publication [2]. The process parameters utilised are listed in Table 1. The manufacturing strategy involved hatch and contour scanning, with a 10-second temperature stabilisation period after each recoating.

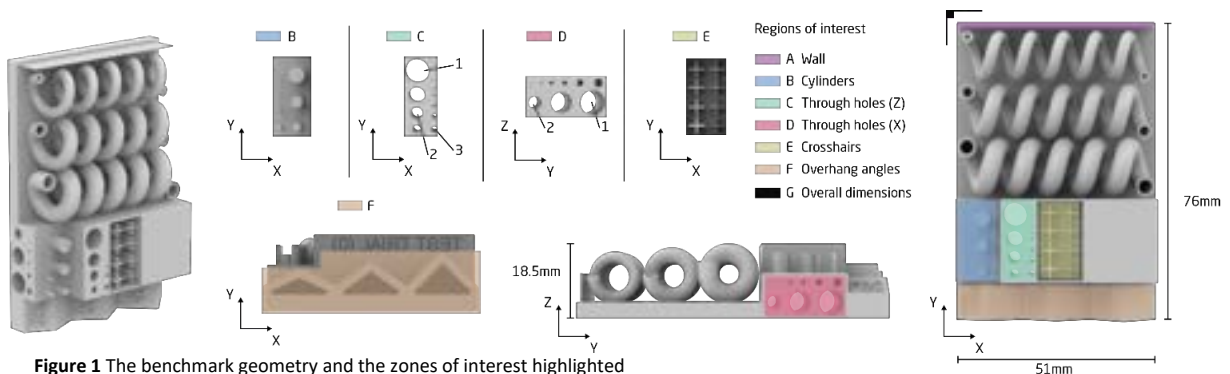


**Figure 1** The benchmark geometry and the zones of interest highlighted

	A	A1	A2	B	C	C1	C2	D	D1	D2	E	F	G1	G2
Insp.														
Feat.				1	1.5			2						
$\mu$ [mm]	0.66	6.32		5.61	2.68			5.50	2.47				76.44	50.55
$\sigma$ [mm]	0.0093	0.0085		0.0009	0.0028			0.0022	0.0063				0.0003	0.0003
Nom. [mm]	0.3	7		6	3			6	3				76	51
$\Delta$ [mm]	0.364	-0.683		-0.394	-0.315			-0.503	-0.525				0.438	-0.455
$\Delta$ [%]	121.2	-9.761		-6.573	-10.52			-8.389	-17.51				0.576	-0.892
R [mm]	-	-		0.226	0.197			0.4063	0.3271				-	-
$\sigma$ R [mm]	-	-		0.002	0.001			0.0015	0.0266				-	-

Table 2 Featured inspected visually (ie. A) features measured by DeMeet (ie. A1)



Figure 2 Benchmark geometry

Originally designed for metal powder bed fusion [3], [4], the benchmark geometry was reconfigured and modified for polymer powder laser processing. The entire geometry was shelled to a thickness of two mm, and holes were incorporated into the large flanges to minimise bloating and reduce gas entrapment. None of the benchmark features were modified during this adaptation. The build job was created using Netfabb Premium (Autodesk, USA), and the geometry was shrinkage compensated by 2% in both the X and Y directions, based on a trial run of the geometry with no compensation included. The Netfabb build file was then converted to a custom G-code-inspired syntax compatible with the system controller.

## 2.2. Benchmark measurements

The benchmark components underwent evaluation on two tracks. Firstly, an overall inspection was conducted to identify the minimum feature within each geometrical category (Figure 2) and detect possible surface defects. Secondly, selected features were measured using a DeMeet 220 (Schut Geometrical, Netherlands), 3D CNC coordinate measuring machine to compare their dimensions with the CAD file's nominal values. The parts were inspected in their as-printed state, with only loose powders removed prior to measurement.

## 3. Results

The manufactured parts demonstrated the system's capability to produce mm-sized features with expected accuracy. Visual inspection and measured results are presented in Table 2, where green indicates passed features and red indicates missing or damaged features. The inspection window shows the minimum feature size of failed geometries, reflecting the system's capabilities, considering the material and process. Measured features, including mean ( $\mu$ ), standard deviation ( $\sigma$ ), nominal parameter (nom.), absolute ( $\Delta$ ) and relative ( $\Delta$ ) deviation, roundness (R), and roundness standard deviation ( $\sigma$ R), are shown below the inspected features. The wall (A) was structurally stable but oversized, which was clear from the mean of A1. Cylinders (B) were within an expected range, with a minimum feature size of 1 mm. Z-direction holes (C) exhibited roundness issues due to uncontrolled part growth in the heated build environment. X-direction holes (D) showed decreased roundness, resulting in oval-shaped holes. Crosshairs (E) were all present, and overhang angles (F) displayed good capabilities without surface defects. Overall dimensions (G) closely matched nominal values, correlating with the utilised shrinkage factor but lacking full compensation. The Z direction lacked shrinkage compensation, exacerbating the oval effect for features perpendicular to it. The system successfully produced intricate details in geometry.

## 4. Analysis

The benchmark geometry was reproduced successfully, showcasing many of the fine intricate features. The system could

not reproduce all the pillars in B with the breakdown level being less than 1.5mm. The majority of the holes were well formed in both the X and Z direction. The minimum feature size for the through holes travelling the length of the part is 2mm for X and 1.5mm for Z. Enhancing the thermal process control of the build volume temperature and homogenising the black optical absorber, can improve the results further, which is planned for future work.

## 5. Summary and conclusion

The benchmark component was produced successfully, producing the majority of the intricate features. Despite the low energy absorption in the polymer at fibre laser wavelengths. The smallest features were impossible to produce due to the process and material limitations. For robust features to be produced by polymer laser powder bed fusion, larger features are needed in order to consolidate the powder particles. Laser irradiation in very small areas leads to too little energy delivery, not melting the particles fully. Aided by the very high energy density required for consolidating the major geometries. This, in conjunction with large wait times between successive scanning in small feature areas, cause the minimum feature size to be in the mm range. The mechanism is inverted for holes with small holes growing over because of too high heat intensity in this area, not leaving behind unsintered particles. The main hypothesis of utilising a fibre laser to obtain finer detail resolution is not fully met. However, it is clear that fine details can be produced, with a potential for further optimising the material and optical absorber.

## References

- [1] T. Wohlers, I. Campbell, O. Diegel, R. Huff, J. Kowen, and W. A. (Firm), *Wohlers report 2023: 3D printing and additive manufacturing global state of the industry*. Wohler Associates Inc., Fort Collins, CO, 2023.
- [2] C. L. Budden, A. R. Lalwani, K. Æ. Meinert, A. E. Daugaard, and D. B. Pedersen, "Process optimisation of PA11 in fiber-laser powder-bed fusion through loading of an optical absorber," *Proceedings of the 33rd Annual International Solid Freeform Fabrication (sff) Symposium*, pp. 75–86, 2022.
- [3] M. Moshiri, G. ; Tosello, and S. Mohanty, "A new design for an extensive benchmarking of additive manufacturing machines," *Proceedings of the 18th International Conference of the European Society for Precision Engineering and Nanotechnology*, 2018.
- [4] M. Moshiri, D. B. Pedersen, G. Tosello, and V. K. Nadimpalli, "Performance evaluation of in-situ near-infrared melt pool monitoring during laser powder bed fusion," *Virtual Phys Prototyp*, vol. 18, no. 1, 2023, doi: 10.1080/17452759.2023.2205387/SUPPL\_FILE/NVPP\_A\_2205387\_SM5236.DOCX.



## **APPENDIX G**

# **Simple sensor manufacturing by Laser Powder Bed Fusion of conductive polymer blends**

## Simple sensor manufacturing by Laser Powder Bed Fusion of conductive polymer blends

Christian Leslie Budden<sup>1</sup>, Frederik Grønberg<sup>1,2</sup>, Anders Frem Wolstrup<sup>3</sup>, Aakil Raj Lalwani<sup>1,4</sup>, Tiberiu Gabriel Zsurzsan<sup>3</sup>, Anders Egede Daugaard<sup>5</sup>, and David Bue Pedersen<sup>1</sup>

<sup>1</sup>Department of Civil and Mechanical Engineering, Technical University of Denmark, Kgs. Lyngby, Denmark

<sup>2</sup>Bjørn Thorsen A/S, Hellerup, Denmark

<sup>3</sup>Department of Electrical and Photonics Engineering, Technical University of Denmark, Kgs. Lyngby, Denmark

<sup>4</sup>LEGO System A/S, Billund, Denmark

<sup>5</sup>Department of Chemical and Biochemical Engineering, Technical University of Denmark, Kgs. Lyngby, Denmark

Corresponding author: [clebu@dtu.dk](mailto:clebu@dtu.dk)

### Abstract

The efficacy of manufacturing conductive plastic components by the Material Extrusion (MEX) method has been shown previously by Grønberg et al. [1]. To increase the effectiveness of additive manufacturing of these sensors a study utilising Polymer Laser Powder Bed Fusion (L-PBF) technique has been undertaken. The study investigates; the conductive networks created during manufacturing and the influence of processing parameters on the conductivity of the parts. The test specimen has been manufactured on the Open Architecture Polymer L-PBF system developed at the Technical University of Denmark. Utilising the capability of full-scale process control, and the implemented high-power fiber laser to achieve consolidation of the powder. The feedstock material has been designed to allow high energy absorption at the fiber laser wavelength (1080 nm), and thermal properties to comply with the L-PBF process. A conductive network manufactured by the Polymer L-PBF process is demonstrated. The parts produced have been tested by measuring the material's conductivity at the initial unaltered state, and further investigated by SEM micrographs to conclude on the stability of the manufactured parts.

### 1. Introduction

This work presents the current state of Additive Manufacturing (AM) of flexible polymer parts, which show conductivity, by Polymer Laser Powder Bed Fusion (PL-PBF). PL-PBF is a method of AM, processing powdered polymer into parts, by selectively sintering a geometry layer by layer using a mirror-guided laser beam [2]. Utilising the PL-PBF technology allows for building 3D parts without support structures or other unwanted attached geometries. The parts can be post-processed depending on the desired finish but can be used directly from production with minimum post-processing. PL-PBF can be used for direct manufacturing of wearable sensors, which fit perfectly for the individual, where a close fit will benefit the sensor's capabilities.

Athreya et al. (2009) [3], conducted a study on the manufacturing of conductive polymer parts from the PL-PBF process and successfully manufactured conductive parts made from a blend of PA12 and Carbon Black. Athreya et al. (2009) [3], investigated the effect of coating PA12 with a nanoparticle carbon black powder to produce a conductive PA12 part. The conductivity was for the case of PA12 coated by carbon black by five orders of magnitude. The study also concludes that no significant change in the crystalline morphology was observed.

The present research has been conducted as a proof-of-concept for consolidating a powdered flexible polymer blend composite into electrically conductive parts. A blend of a conductive polypropylene with a high loading of carbon black, and a flexible thermoplastic polyolefin elastomer, is developed for the study. The work consists of developing the polymer blend composite with consideration towards the PL-PBF process

requirements, micronisation of the polymer pellets and qualifying this powder. As well as investigating the electrical conductivity of these parts. The study uses two different process parameter approaches for the production of parts, which will be used to conclude the influence of these process parameters, on the conductivity of the parts.

### 2. Materials and Methods

The experiments considered several factors for defining the efficacy of producing conductive parts by PL-PBF. The materials were developed and produced to align with the process capabilities of the Open AM machine. The production process was designed for the specific powder, with two separate process parameter sets developed. Furthermore, the electrical conductivity of the parts produced was tested to conclude the effect of process parameters.

#### 2.1. The Open AM PL-PBF setup and parts produced

The conductive test specimen was manufactured on the Open Architecture PL-PBF system developed at the Technical University of Denmark [4]. The Open Architecture allows complete control of the processing parameters, including; scanning speed and strategy, as well as control of the chamber heating. The system uses a high-power fiber laser (1080nm), contradictory to an industrial system using a CO<sub>2</sub> laser (10,6μm). The fiber laser allows for better laser tuning and a gaussian beam profile, with a high energy absorption into the black constituent of the powder [3,5]. The parts produced on the system were a 10mmx50mm rectangle, produced as a single layer. The single-layer approach was selected for the proof-of-concept for manufacturing consolidated parts, that show conductivity, from

a material designed for PL-PBF. The parts are produced in the atmosphere without saturation of inert gas.

## 2.2. Material development

A conductive polymer blend composite consisting of 60/40 wt% Cabelec CC6057 conductive concentrate from Cabot Corporation with a Conductive Carbon Black content of 40% (MFI 1g/10min 230°C/5kg), and Vistamaxx 6502 from ExxonMobil (MFI 45g/10min 230°C/2,16kg), respectively was compounded for the study. Cabelec CC6057 was chosen for its ease of handling and good electrical conductivity (~9,0\*10<sup>2</sup> Ω/sq, according to the datasheet). Vistamaxx 6503 was selected for its flexibility and compatibility with the conductive concentrate. Both materials showed a promising thermal processing window for PL-PBF. The compounding of the conductive polymer blend composite was performed on a Thermo Fisher Eurolab 16XL Twin Screw Extruder with a set of medium shear mixing screws with an output of 2 kg/h at 75 RPM. The temperature profile of the extruder was, from the die: 200-200-200-200-200-200-170-130-80°C. The Cabelec 6057 was dried at 80°C in a hot air dryer for at least 12 hours ahead of processing. The extrudate was cooled in a water bath and subsequently pelletised and dried to remove any water from the cooling bath.

From the pelletized material, a powder was produced. The Powder was made by Cryogenic ball Milling using a Retsch CryoMill, running at -196°C with 2 minutes of cool-down time and 30-second intervals of grinding and cooling, respectively. The powder obtained was sieved, and the fraction below 96µm was used for part production. The powder was quantified by laser diffraction using the Malvern Panalytical Mastersizer 3000 with the dry cell attached.

## 2.3. Process development for SLS

An understanding of the processing capabilities of the powder is developed based on the DSC analysis of the conductive polymer material. The DSC scan was carried out at standard conditions in a nitrogen atmosphere, with a heating rate of 10.00°C/min from temperatures of -95°C to 230°C followed by a cooling down to -95°C at the rate of -10.00°C/min. The measured melting and recrystallisation temperatures are used for determining the process settings. The DSC analysis reported exhibits both the initial heating curve as well as the cooling curve, traditionally not reported. However, for the purpose of process development for SLS these curves show the most dominant characteristics considered.

The baseline for fundamental process variables such as laser power and scan speed was based on feedback via thermal imaging in the system during pilot experiments to consolidate polymer powder using single-layer line scans. The process optimisation followed the method of varying one influential parameter and keeping the remaining constant, as suggested by Singh, et. Al. [5,6] A homogeneous part achieved by well-consolidating powder and true to the original geometry was the visual qualitative metric used to iteratively optimise the process parameters when fusing single-layer area scans. For process development, initial experiments were carried out using 50mm line scans followed by 10mm x 10mm area scans and finally, 10mm x 50mm area scans, i.e. identical to the test part geometry.

## 2.4. Conductivity qualification

To accurately measure the conductivity of the samples, a 4-wire (4W) measurement is preferred. The 4W measurement injects current through a set of contacts (Force) and measures voltage through a separate set of contacts (Sense). This

separation between the Force and Sense contacts means that any contact resistance should be bypassed and hence the intrinsic resistance of the samples can be measured directly. A Keithley 2450 SourceMeter was used for the measurements. Each sample was measured 50 times, roughly 2 seconds apart. The mean of those 50 measurements was used for the conductivity calculation, which is done with the following equation:

$$\sigma = \frac{l}{RA}$$

Where  $\sigma$  is the apparent conductivity,  $l$  is the distance between the sense contacts,  $A$  is the cross-sectional area of the sample and  $R$  is the mean resistance described above.

## 3. Results

Several methods are used to determine the conductivity and possible sensor capabilities of the parts. The parts are quantified by microscopy providing additional information on the level of consolidation of the powder. These efforts are described below. All parts were allowed to condition in an open atmosphere for at least one week before the investigation of part stability and electrical conductivity.

### 3.1. Material production and qualification

A DSC analysis was carried out to indicate the process parameters of the material. The elevated chamber temperature was selected based on a DSC scan of the material as seen in Figure 1. The DSC analysis showed the primary material melting peak at 167°C, along with a small endothermic shoulder at 33-55°C. These are the other components of the designed polymer, providing the characteristics of the flexible conductive polymer part. The analysis also shows the crystallisation temperature of the main constituent polymer, at 128°C.

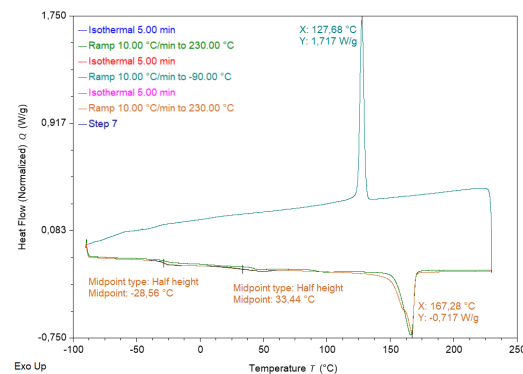


Figure 1 – DSC analysis of the PL-PBF tailored material

### 3.2. Powder characteristics

The processed powder was analysed by light optical microscope (LOM) and Scanning Electron Microscopy (SEM), to determine the morphology of the powder particles. Due to the nature of cryogenic ball milling, the main constituent of the powder is oblong flakes, as seen in Figure 2. These flakes cause issues in the spreadability of the powder, due to the adhesion and interlocking of the particles. This was evident in the heated process parameter test, where large agglomerates would disturb the powder bed. The agglomeration is further aided by the Vistamaxx component turning soft and sticky at the process temperatures. The powder contains a large number of small particles. The small particles are highlighted by the red circles in the SEM picture showing the variation in particle size. These particles also influence the agglomeration of the powder.

The powder particle sizes for the fine and coarse powders were analysed to have a D50 of 72,6 ± 0,182 µm and 290 ± 4,63



µm respectively. As seen from Figure 3 the fine powders include a fraction of very fine (<10µm) particles which add to the agglomeration of powders and hence a lower cut-off from the final powder will be carried out in powder production for future investigations.

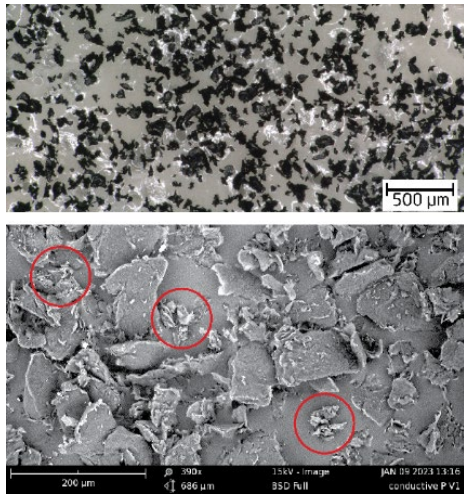


Figure 2 – Powder particles. Large flakes and smaller particles. Top 100x LOM picture. Bottom 390x SEM picture.

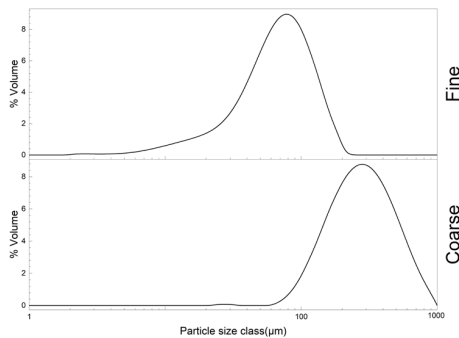


Figure 3 – Particle size curve of the manufactured powder. Fine is the sieved powder used for part manufacturing. Coarse is the discarded portion after sieving.

### 3.3. Process parameters

The process parameters developed for producing conductive parts were different by the chamber temperature, which is a key parameter of PL-LBF. The chamber temperature setting has a large influence on the laser power input required to achieve consolidation of the part. The level of internal stress is also reduced by elevating the chamber temperature minimising the risk of warpage and curling during laser scanning. The chamber temperature was set to 130°C for the heated sample manufacturing and left unheated for the other parameter set resulting in 20°C in the build chamber.

The elevated chamber temperature was selected based on a DSC scan of the material, as seen in Figure 1. The process window for the material proved to be rather large, extending from melting at 167°C to recrystallisation at 128°C. Vistamaxx softens at a temperature of around 50°C, according to the datasheet. The two polymer phases seem to be only partially miscible as seen from the small shoulder in the DSC around 50°C. This shoulder indicates the glass transition of the material. Thus, a small part of the Vistamaxx could be softening, causing a very sticky powder to be formed at elevated temperatures. Based on this, the preheating setting was chosen. The temperature setting allowed for minimal shrinkage during processing, while not producing a consolidated matrix from the entire powder cake.

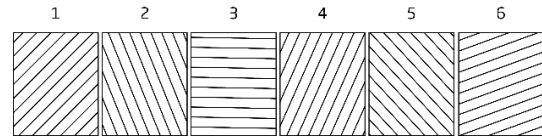


Figure 4 – scan strategy per scan pass from scan one to six

The process optimisation developed two process parameter sets for the two trials. The process parameters are seen in Table 2, showing the main difference in scanning speed. The resulting energy density is also presented in the Table, showing a reduction of 1/3 of the energy input between the unheated and heated run. This lower energy input still ensured consolidated parts that maintained dimension, during processing and after cooling to room temperature. The parts were produced by scanning the same part 6 times while rotating the scan direction 67 degrees. This variation in the scan direction is seen in Figure 4. This ensures consolidated parts while minimising the risk of unsintered particles or areas.

Table 1 – Process parameters

		Unheated	Heated
Scan Speed	mm/s	2000	3000
Power	W	30	30
Scan rotation	Degrees	67	67
Hatch spacing	µm	150	150
Scan repetitions		6	6
Energy density	J/mm <sup>2</sup>	0,1	0,066

The production of parts was done in the atmosphere, leading to possible moisture ingress. The atmosphere is considered not to be problematic. The constituent materials are not prone to hydrolysis or other degradation caused by moisture uptake from the atmosphere. Furthermore, the powder is handled with minimised contact with the atmosphere before part manufacturing.

### 3.4. Part Characteristics

The parts manufactured showed large variation between the two process parameter sets. The unheated parts exhibited shrinkage and geometric variation compared to the intended size.

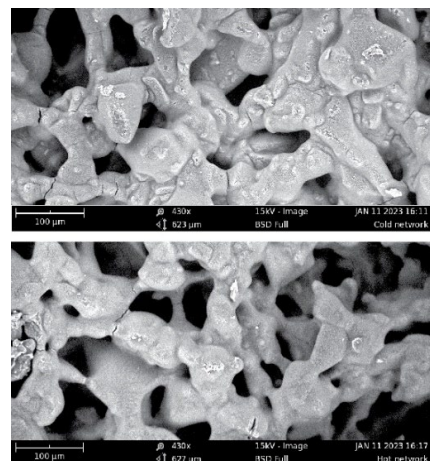


Figure 5 – SEM image of the laser-processed plane of the parts showing the comparison of the two networks for unheated (top) and heated (bottom)

The unheated parts were thinner than the heated ones with an average thickness of 373µm and 674µm, respectively. The variation in thickness is caused by energy penetrating deeper into the heated samples due to the lower loss of energy in the

initial powder layer, due to the increased temperature of the powder cake. The melting effect on the unheated and heated samples is also evident in the SEM picture in Figure 5 showing a smooth surface with less evidence of the powder particles in the heated sample compared to the unheated one. The melting behaviour and flow of the particles into a smooth network point towards the heated sample experiencing the melting of both polymers, with time above crystallisation long enough to flow. Where the tendency of the unheated sample points to only melting of one of the components. This is evident by the shape retention with the unheated part network resembling the powder structure.

### 3.5. Conductivity

The results from the conductivity measurement can be seen in Tables 2 and 3 for the heated and unheated samples respectively. Five samples were tested for each, however, one of the unheated samples tore completely before the measurement could be done.

The unheated samples were relatively consistent with samples B, C and D having similar apparent conductivity. Sample A, while having the highest conductivity overall, is assumed to be an outlier. The heated samples are more inconsistent. Sample A and B are very similar, as is sample C and E, but the two pairs are quite different from each other as well as sample D.

The measurement was done with crocodile clips. The cables used outweigh the samples and it is possible that the measurements were influenced by the strain put on the sample by the cables. Additionally, any tears in the samples due to the strain will have a significant influence on the measured resistance and conductivity.

**Table 2: Heated samples**

Sample	Resistance [kΩ]	Area [mm <sup>2</sup> ]	Length [mm]	Conductivity [mSm <sup>-1</sup> ]
A	71,37	6,7	24,0	49,9
B	66,81	6,7	24,0	53,3
C	158,7	6,7	25,5	23,9
D	109,2	6,7	24,0	32,6
E	141,8	6,7	25,1	26,2
Avg/ std	109,6 / 41			37,2 / 13,6

**Table 3: Unheated samples**

Sample	Resistance [kΩ]	Area [mm <sup>2</sup> ]	Length [mm]	Conductivity [mSm <sup>-1</sup> ]
A	101,3	3,0	23,32	77,1
B	132,8	3,0	21,08	53,2
C	137,5	3,0	20,97	51,1
D	133,2	3,0	22,63	56,9
Avg / std	126,2 / 16,7			59,6 / 11,9

### 4. Analysis

The parts manufactured were initially expected to be dense and not show porosity, however during the investigation of the parts, it was clear that the sintering process developed a network-like sponge. This sponge structure has a large influence on the structural integrity and the conductivity of the parts. The sponge structure develops due to the process not allowing the flow of material into the voids during the scanning. The material exhibits a high zero shear viscosity, which is known for most polymers [7]. Highly loaded composites typically show an increase in viscosity, with the carbon black loading known to cause this. The effect is evident when comparing the MFI of the two miscible polymers, with a significantly higher MFI reported for the carbon black loaded polyolefin compared to the

Vistamaxx. This high viscosity causes the powder particles to stay in place even when molten due to the limited external forces, besides gravity acting on the powder. From the SEM pictures, it can be seen that the flow behaviour is improved in the heated samples with a smoothed surface of the network.

The conductivity of the parts is influenced by the network structure. The apparent conductivity for the unheated samples is higher than for the heated samples. However, both process parameters created parts with large variations, proving that the powder, packing and process should be further optimised. The higher conductivity of the unheated parts can be due to the Vistamaxx polymer having a lower viscosity allowing a flow of the material and creating a network that is more ductile causing a better conductivity in the network after the parts have been handled in the measurement setup. The flow behaviour and optimisation of the process and powder are planned for future experiments.

### 5. Conclusion

Manufacturing of parts which show conductivity when measured using the 4W approach was successful. From these parts, a simple sensor function can be expected. However, from the network structure seen by SEM pictures, it is clear that the manufacturing process needs to be optimised. This includes consideration of the material and the zero shear viscosity, and the powder manufacturing, making a more uniform and less flaky powder. As well as finding an even more suitable set of process parameters.

The two parameter sets both proved viable for producing parts. The result is conflicting with the heated samples showing the highest geometric and structural stability, with an internal network that has been smoothed during manufacturing. These samples, however, also show the lowest conductivity with the standard deviation being more than 1/3 of the average apparent conductivity. The unheated samples were showing a better average apparent conductivity with a smaller standard deviation in the measurements. These parts were highly irregular, showed large shrinkage and a not fully melted network.

### References

- [1] Grønberg, F., Zsurzsan, T. G., Daugaard, A. E., Spangenberg, J., & Pedersen, D. B. (2022). Conductive Compliant Mechanisms: Geometric tuning of 3D printed flexural sensors. *Additive Manufacturing Letters*, 100088.
- [2] Redwood, B., Schöffner, F., & Garret, B. (2017). *The 3D printing handbook: technologies, design and applications*. 3D Hubs
- [3] Athreya, S. R., Kalaitzidou, K., & Das, S. (2010). Processing and characterization of a carbon black-filled electrically conductive Nylon-12 nanocomposite produced by selective laser sintering. *Materials Science and Engineering a*, 527(10-11), 2637–2642. <https://doi.org/10.1016/j.msea.2009.12.028>
- [4] Budden, C. L., Meinert, K. Æ., Lalwani, A. R., & Pedersen, D. B. (2022). Chamber Heat Calibration by Emissivity Measurements in an Open Source SLS System. In *2022 ASPE and euspen Summer Topical Meeting* (pp. 180 - 185). American Society for Precision Engineering.
- [5] Singh, S., Sharma, V. S., Sachdeva, A., & Sinha, S. K. (2013). Optimization and analysis of mechanical properties for selective laser sintered polyamide parts. *Materials and Manufacturing Processes*, 28(2), 163–172. <https://doi.org/10.1080/10426914.2012.677901>
- [6] Budden, C. L., Lalwani, A. R., Meinert, K. Æ., Daugaard, A. E., & Pedersen, D. B. (2022). Process optimisation of PA11 in fiber-laser powder-bed fusion through loading of an optical absorber. *Proceedings of the 33rd Annual International Solid Freeform Fabrication (Sff) Symposium*, 75–86.
- [7] Mills, N. J. (1993). *Plastics: microstructure and engineering applications* (pp. XI, 377 S. (unknown)). E. Arnold.



*Remember, kids, the only difference between  
screwing around and science  
is writing it down.*

*Alex Jason - Ballistics expert*

*Made famous by: Adam Savage*

DTU Construct

Koppels allé 404  
2800 Kongens Lyngby

[www.construct.dtu.dk](http://www.construct.dtu.dk)

978-87-7475-762-7